

THE UNIVERSITY OF ASTON IN BIRMINGHAM

ANALYSIS OF THE PARTICLES PRODUCED

BY SADDLE FIELD ION SOURCES

Thesis submitted for the Degree of

DOCTOR OF PHILOSOPHY

by

M. KHORASSANY (BS.C., MS.C.)

Department of Physics

July 1977

- 8 AUG 1978

219563

537.56 KHD

ACKNOWLEDGMENTS

In this Thesis it is appropriate to express my sincere thanks to my supervisor, Dr. R.K. Fitch for his continual help and encouragement throughout the different periods of this work.

Thanks are also due to Professor T. Mulvey for much helpful advice and also to Professor S.E. Hunt for providing the facilities in his Department.

I would like also to acknowledge and express my gratitude to Mr. K. Mahmoud, the Vacuum laboratory technician, Mr. H. Arrowsmith and other staff in the Physics Workshop for their help in construction of the various parts of the apparatus.

My acknowledgments are also due to the National University of Iran, Teheran, Iran, and the Ministry of Science of Iran for supporting me during these studies.

SUMMARY

"Analysis of the particles produced by saddle
field ion sources"

Mohammad Khorassany

Ph.D - 1977

A review of the literature concerned with the production of ion beams is given and the development of saddle field ion sources and their importance in relation to other devices is also discussed.

In this work two forms of the saddle field ion source, one with cylindrical and the other with spherical geometry, have been studied for argon, nitrogen and helium and a comparison between them has been made in terms of their characteristics and applications.

It has been confirmed that in both sources there are three principal modes of operation - the oscillating, transition and glow modes. These have been explained in terms of the mean free path for electron-molecular collisions inside the source and its relation to the dimensions of the source and show that the source efficiency is greatest in the low pressure oscillating mode.

A retarding field energy analyser has been developed to measure the energy distribution of the ions. The results show that the energy spectra of both sources are dominated by a high energy peak which arises from ions being accelerated through a potential equal to that between the saddle point and the cathode. Lower energy ions are also produced but these are mainly confined to the edges of the ion beam. The proportion of these low energy ions increases as the mode changes from the oscillating to the glow mode.

The energetic neutral content of the beam has been studied using an electrostatic analyser. These experiments indicate that the percentage of energetic neutrals can vary from 10% to 80% with different gases and modes of operation. These results have been confirmed by etching copper films and are explained in terms of a charge exchange process between a fast ion and a slow neutral occurring inside the source.

Key words: discharge, ion, ion source, neutral, vacuum.

CONTENTS

	<u>Page</u>	
<u>CHAPTER 1</u>	<u>DEVELOPMENT OF ION SOURCES</u>	
1.1	Introduction	1
1.2	Properties and requirements of ion sources	2
1.3	General classification of ion sources	5
1.3.1	Hot cathode sources	5
1.3.2	Cold cathode sources	11
1.3.3	Radio frequency sources	13
1.3.4	Special type of ion sources	13
1.4	Limitation of existing ion sources	15
<u>CHAPTER 2</u>	<u>THEORY AND APPLICATIONS OF THE OSCILLATOR</u>	
2.1	Introduction	21
2.2	Theory of the oscillator	22
2.3	Applications of the oscillator as vacuum gauges, detectors, and source of ultra violet radiation	26
<u>CHAPTER 3</u>	<u>DEVELOPMENT OF SADDLE FIELD ION SOURCES</u>	
3.1	Cylindrical source	29
3.2	Spherical source	35
3.3	Ion energy distribution	36
3.4	Application of saddle field ion sources and discussion	39

CHAPTER 4

EXPERIMENTAL ARRANGEMENT AND DESCRIPTION

OF THE ION SOURCES

4.1	The cylindrical source	42
4.2	The spherical source	44
4.3	Vacuum system and experimental procedure	46
4.3.1	Vacuum system	46
4.3.2	Electrical circuit	51
4.3.3	Principle of the source operation	52
4.4	Development of the Faraday collector	56

CHAPTER 5

SOURCE CHARACTERISTICS AND MODES OF OPERATION

5.1	Introduction	60
5.2	Characteristics of the ion sources	60
5.3	Modes of operation	72
5.4	Ion source efficiency	78
5.5	Discussion	86

CHAPTER 6

ION ENERGY DISTRIBUTION

6.1	Introduction	90
6.2	Description of the analyser	91
6.3	Energy distribution measurements	94
6.4	Discussion	113

	<u>Page</u>
<u>CHAPTER 7</u> <u>MEASUREMENTS OF ENERGETIC NEUTRALS IN THE</u>	
<u>SADDLE FIELD ION SOURCES</u>	
7.1 Introduction	116
7.2 Design of the analyser	118
7.3 Experimental results	121
7.4 Etching of thin film by energetic neutrals	134
7.5 Discussion	134
 <u>CHAPTER 8</u> <u>CONCLUSIONS AND SUGGESTIONS FOR FUTURE WORK</u>	 144
 APPENDIX 4.2/1	 148
APPENDIX 4.2/2	149
APPENDIX 5.2/3	150
APPENDIX 5.2/4	152
APPENDIX 5.3/5	157
APPENDIX 5.3/6	160
APPENDIX 6.3/7	162
 LIST OF FIGURES	 164
 LIST OF SYMBOLS	 169
 REFERENCES	 173

CHAPTER 1

DEVELOPMENT OF ION SOURCES

1.1 Introduction

Any process which removes an electron from atom by imparting energy greater than the first ionisation potential of the atom produces an ion, and this action is called ionisation. As a result of ionisation, usually a group of ions, electrons and unionised atoms (neutrals) will exist together, and this is referred to as a plasma when the number of ions and electrons are equal.

An ion source produces and accelerates ions to the required intensity and energy for the particular application. In fact it is generally difficult to extract ions from a plasma region, so the properties of the source should be such that the required number and type of ions can be extracted. It is also important that the source should be stable in operation for in some applications, such as ion etching, the source must be run for long periods. In the same application, it is also sometimes desirable that the ions should have a broad energy spectrum, in order to provide differential etching of the sample.

Although ion sources have been in use for a considerable time, it is only in the last two or three decades that there has been significant progress due mainly to the advances in electronics and vacuum technology. The main requirements of any ion source are (a) the capability of producing the appropriate ions, (b) a vacuum system to produce the necessary pressure which may range from 1 torr to 10^{-7} torr, depending upon the particular application and

(c) a facility to accelerate and focus the ion beam. Some of these aspects will be discussed in this chapter together with the development of the different types of ion sources.

Early experiments on charge particle accelerators by J.J. Thompson and F.W. Aston (1912-1920) led to the development of Nier's mass spectrometer and ion source for analytical purposes using positive and negative ions. However, real progress and improvement in ion beam devices began with the birth of nuclear physics in about 1930. Thus the energies of the particles have changed from a few 100 eV in the Thompson accelerator to several GeV in the recent machines. For example the energy required in ion implantation usually does not exceed 0.5 MeV, but energies greater than 1 MeV are needed for studies in Rutherford backscattering.

The method by which the plasma and resulting ion beam is formed varies in different sources and the electrons which ionise the molecules or atoms should preferably move in a helical trajectory to increase the ionisation efficiency.

Of course many of the ions used in ion implantation are solid ions, and some of the materials that we need to use are corrosive, so that this adds to the complexity of the source.

In order to place certain ions at the desired depth in the target, we need to consider the design of the source, to select the appropriate ion species. Thus numerous problems exist in designing ion sources and the method of overcoming these will be discussed in the next section.

1.2 Properties and requirements of ion sources

The ion source is one of the most important parts of, for example, an accelerator and its function is to provide the required

type of ion beam. Thus the requirements of the ion source must be considered in relation to the particular application.

During the early development of ion sources the design and assembly has been influenced by the availability of appropriate materials for the electrodes and insulators and also the associated power supplies. Thus any assessment of progress in this technology must take into account how those technical aspects have gradually been solved. Of course it is difficult to state the precise requirement and particulars of all types of ion sources in use today, so the intention is to describe certain general points and techniques of ion source design.

As the ionisation process results from electron impact with atom or molecule, the source of the electrons in ion source construction is a very important consideration. Thus the cathode material is an important parameter in ion source technology. The function of the cathode is to provide electrons either by thermionic emission or secondary electron emission during ion bombardment. In the case of thermionic cathodes the operating temperature and hence the cathode work function is the main consideration but in cold cathode devices, the secondary electron yield at the cathode is important. Furthermore the cathode is one factor which determines the life and stability of operation of the source.

Another important aspect in source design is the material used for the insulators. In many cases the optical quality and stability of the ion beam depends on the ability of the insulator to stand at high voltages (Hamilton)¹. The insulators which are used in any source must have not only a reasonably high insulating factor, but they should also be sufficiently soft to be machinable, quick to outgas and easy to clean if they become contaminated.

The properties of the anode material are less important but must be designed to provide the required accelerating field. In many sources, considerable power is dissipated at the anode so that in some sources water cooling of the anode may be essential.

The manner in which the ions are produced and extracted varies in different sources. In order to obtain the maximum degree of ionisation, the electrons should have a long path length, so that they are not collected too quickly by the anode. For this purpose many sources use a magnetic field to coil up electrons into a spiral path but a few sources use an electrostatic configuration to cause the electrons to oscillate. Thus in both cases the source can be operated at a reduced pressure. Any reduction in source pressure is an advantage as this reduces contamination of the specimen during ion bombardment and scattering of the ion beam by the residual gas in the experimental chamber.

It is also often necessary for the source to produce a well collimated beam, preferably without the addition of a complex system of extraction and focusing electrodes.

Perhaps the most important property of any ion source is its ability to produce a beam of ions at the required intensity, energy and charge state. The current density in, for example, ion cleaning in ultra high vacuum may be only a few $\mu\text{A cm}^{-2}$ whereas in large sputtering systems current of several A cm^{-2} may be required. In a mass spectrometer the ions will need to have a very small energy spread, but in ion etching it may be advantageous to use a large energy spread. The charge state of the ion is not always important, but multicharged ions are injected into some types of accelerators.

Finally, all sources will have a finite operating life which will depend upon the type and construction of the source. One such

limitation may be due to the eventual failure of the thermionic cathode. On the other hand in cold cathode devices it is quite common for the source to deteriorate due to the gradual contamination of the electrodes and insulators from the vacuum pump fluids. Thus this factor may ultimately influence the type of source used when it is necessary to have a stable beam of ions for a long period of time.

1.3 General classification of ion sources

There are now a large number of different type of ion sources available, each having its own characteristic design, properties and applications. It is thus rather difficult to classify them in any special way, but an attempt has been made in this section to discuss the most important types in four main groups, namely, hot cathode, cold cathode, radio-frequency and special types of ion sources.

1.3.1 Hot cathode sources

1 - Electron impact ion source

The electron impact source was one of the earliest devices and was first described by Bleackney² and Nier³. This source, which produces a low energy spread, and reasonably intense ion beam, has found many uses in mass spectrometry. It consists simply of cathode, anode, filament, repeller and extractor electrodes. Electrons are produced at the filament and accelerated into the ionisation chamber with an energy exceeding the first ionisation potential of the atoms. A magnetic field is applied to make the electrons oscillate as they traverse the ionisation region. The ions are extracted by making the repeller a few volts positive and the extractor a few volts negative. The ion energy is about 70-100 eV, and the source operates at about 10^{-4} Torr, and gives a beam current of only 10^{-9} A with 0.5 eV energy spread. By increasing the source pressure to 5×10^{-4} Torr and using a higher emission

current the ion beam may be increased to about 10^{-7} A but the energy spread increases to 2-3 eV when the ions are at an energy of about 500 eV.

2 - Duoplasmatron ion source

One of the most common thermionic or hot cathode ion sources that has been widely used and developed is the duoplasmatron ion source. The duoplasmatron was first described by Ardenne⁴ in 1956 and has since been used as an intense source of high energy ions for various ion bombardment studies. Ions in this source originate by collision of electrons emitted from a filament with atoms or molecules, and the ion beam emerges from a hole in the anode. A schematic diagram of this source is shown in Fig. 1-1.

The duoplasmatron consists mainly of an anode, cathode intermediate and extractor electrodes, a filament and a magnetic field in the anode region. The latter is produced by a solenoid to constrain the electrons and also restrict the formation of ions to a small volume. The source normally operates at a pressure between 10^{-2} - 10^{-3} Torr and produces a beam current of 1 to 15 μ A, at an energy of about 50 keV. The energy spread of the ions is only 5-10 eV. Illgen⁵ showed that any increase in magnetic confinement causes an increase in the energy spread of the ions. The source has been further developed by Masic et al⁶ and Wilson and Brewer⁷. This device has the advantages that (a) it can be used for both gas and solid ion production, and ion currents of up to 1 mA for Cu and O₂ are reported and (b) any corrosive elements are not in contact with the main parts of the source. A disadvantage of this source is that when it is used for solid ions the insulators in the extraction region become coated and this leads to breakdown. The rapid development of these heavy ion sources has enabled beams of

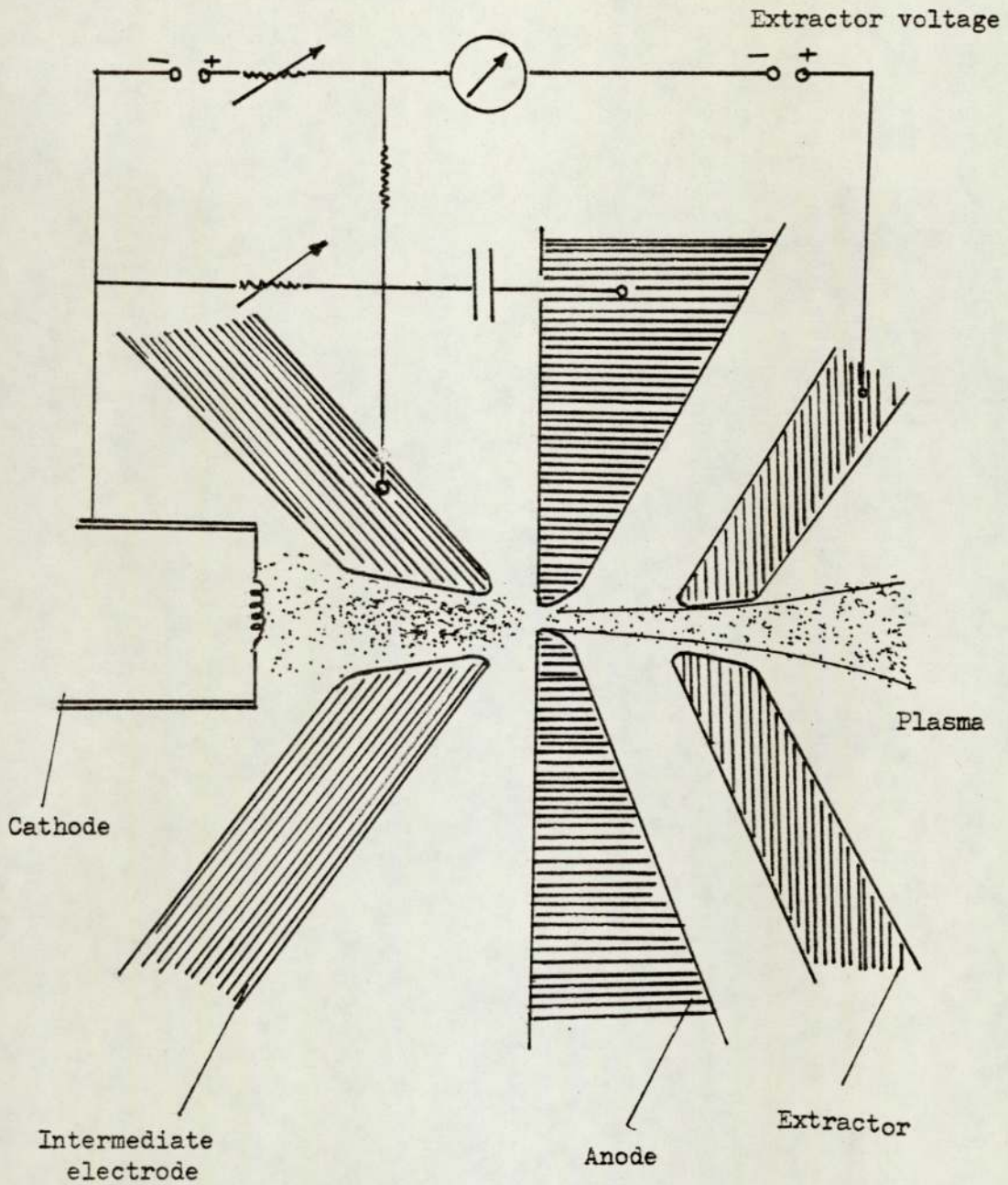


Figure 1.1. Schematic diagram of a duoplasmatron showing the intermediate electrode which confines the discharge between cathode and anode and the extractor which accelerates ions from the plasma cap projected through the anode aperture.

multiply-charged ions of almost all elements to be available for solid state physics research. An illustration of these sources is the

Penning ionisation gauge type ion source (PIG) which was designed by Bethge et al⁸. A PIG type cold cathode source developed by Bennet et al⁹, consists of an extractor electrode, magnetic coil, cooling system, anode cylinder, cathode and anti-cathode. (Bamann et al)¹⁰

A simplified diagram of this source is shown in Figure 1.2.

The source with a few kV discharge voltage, produces 1-4 mA beam current, with about 60-80 eV energy spread. Winter and Wolf¹¹ produced a continuous multiple ion beam for rare gases up to 75 μ A beam current. The gas flow and magnetic field in this source can vary without affecting the discharge current

Duoplasmatron ion source can produce negative ions by reversing the polarity of the extractor. In fact, they accept appropriate atoms and attach one or a few electrons and thus emit negative ions. These sources are particularly useful in tandem accelerators.

3 - Electromagnetic isotope separator ion source

This highly developed source was first used by Freeman¹² and it is a high resolution electron impact ion source for isotope separation. A magnetic field is applied parallel to the filament, which together with the field produced by the filament causes the emitted electrons to travel in a spiral path and increase the ionisation rate. This source produces solid ions, and the heat generated from a heater and filament inside the source is sufficient to vapourise the material in a crucible placed near to the filament, and thus the source does not need a separate oven to evaporate the metal. An advantage of this source is that the beam can be focused by a sector magnet without the need of any ion optics.

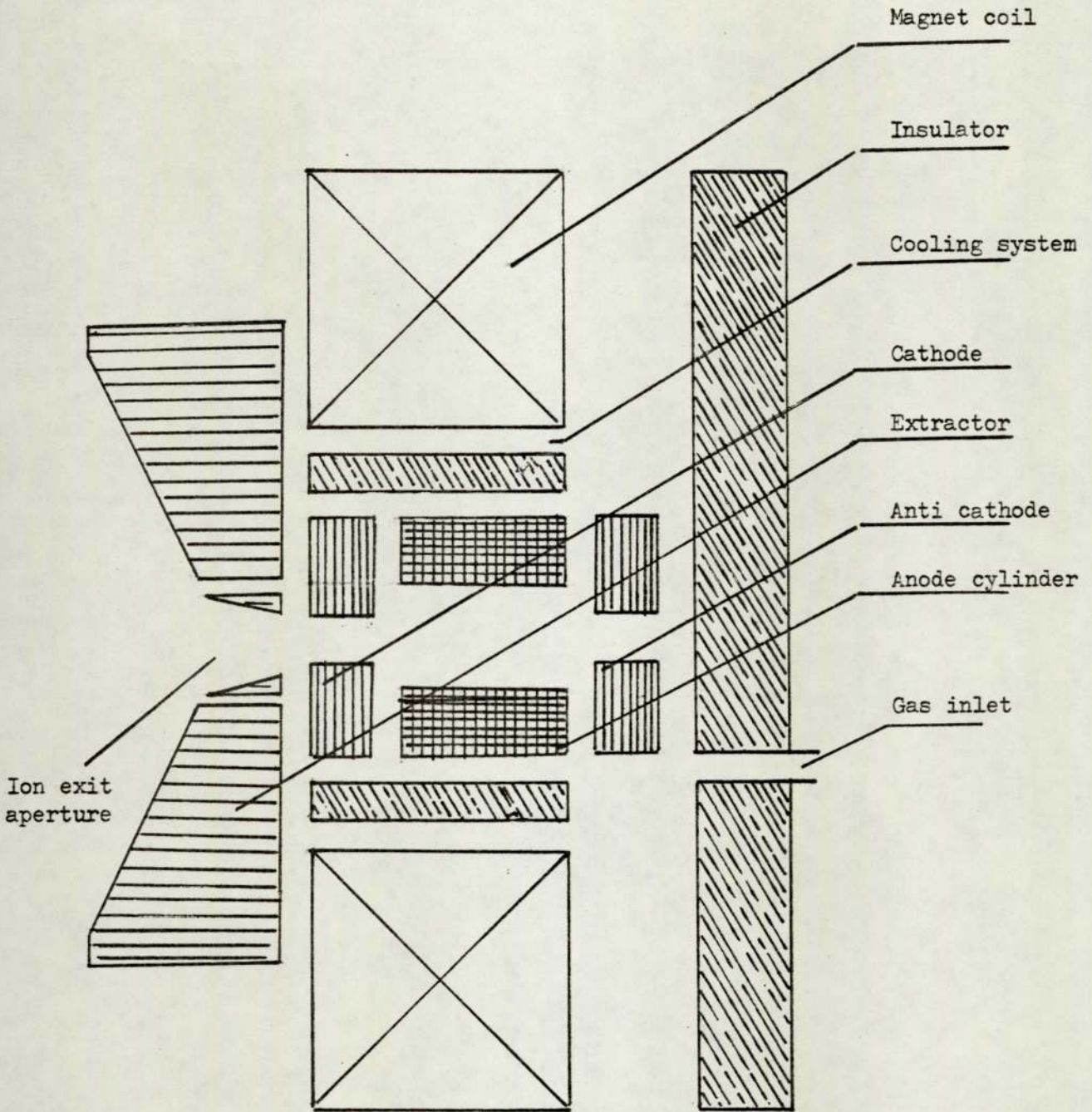


Figure 1.2. Schematic diagram of the PIG-type ion source.

4 - High yield low pressure ion source

This ultra high vacuum source which operates at a pressure less than 10^{-5} Torr was used to produce mass analysed beams by Kornelsen¹³. The source operates in a system having a background pressure of about 4×10^{-11} Torr and the energy range of the ions is 100 eV-10 keV with 10^{-7} A beam current. A schematic diagram of this source is shown in Figure 1-3.

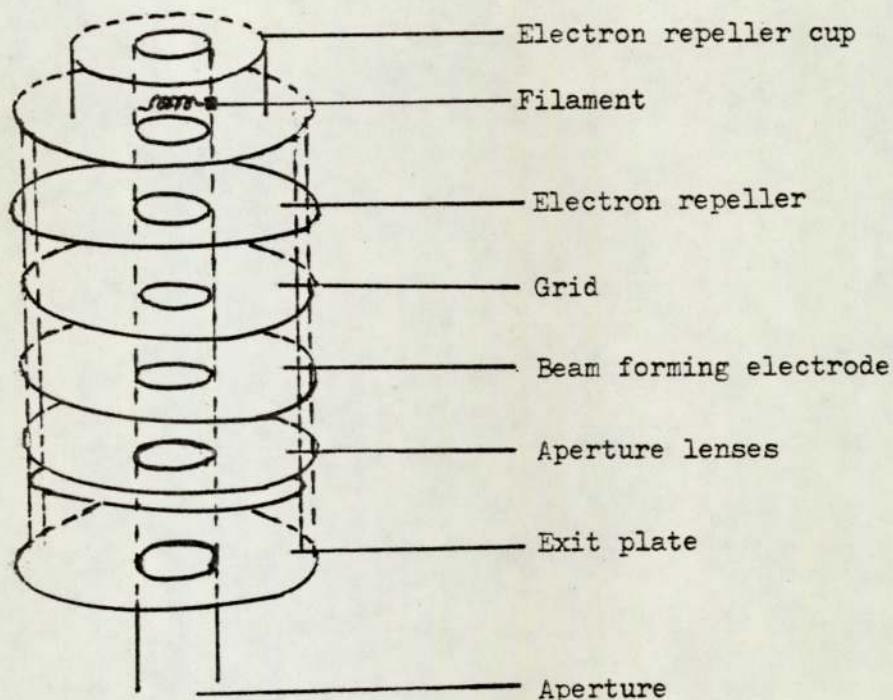


Figure 1.3. A diagram of the high yield low pressure ion source.

Its main components are the filament, electron repeller grid and beam forming electrode. The ions are extracted from an aperture in the beam forming electrode and ionisation occurs by electron bombardment.

5 - Low voltage arc source

This source is applicable in isotope separation of small quantities of materials. The discharge is maintained between the

heated filament and an anode, as illustrated in Figure 1-4.

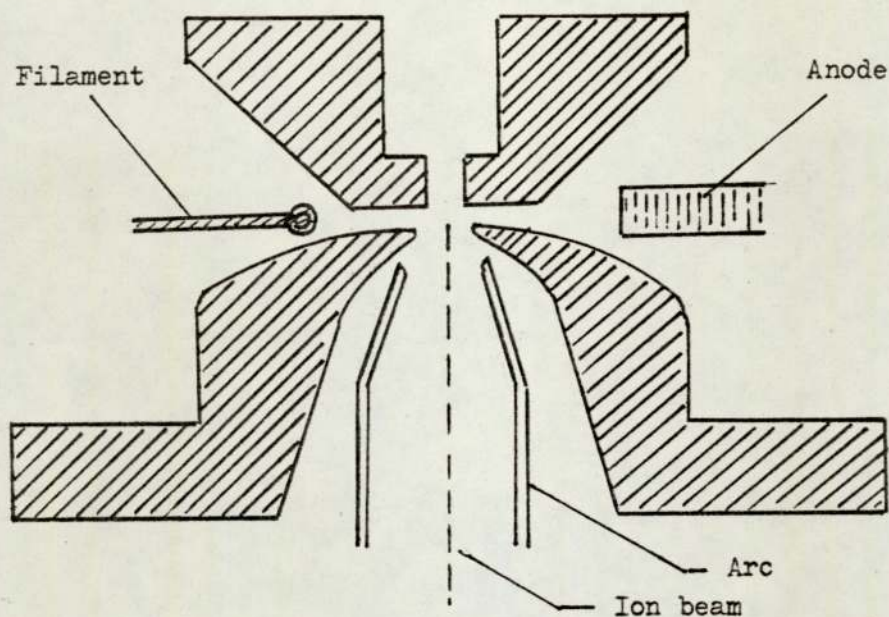


Figure 1.4. Low voltage arc source.

A suitable magnetic field is applied and thus the operating pressure of the discharge can be slightly reduced. This arc source produces an ion beam current of 100-200 μA with about 0.2 eV energy spread. It operates at 2×10^{-3} Torr and the beam forming voltage is around 100 V. This device, which can produce solid ions, was developed by Koch¹⁴.

1.3.2 Cold cathode ion sources

These sources operate essentially on the principle of the Penning ionisation gauge and no thermionic cathode or filament is used. A magnetic field is often used and an electrostatic field is sometimes added to extract the ions.

1 - Mercury pool cathode discharge source

The mercury pool cathode discharge was first used by Fetz¹⁵. This source is basically a low voltage arc discharge, which uses a mercury pool cathode. The mercury vapour can be frozen out and the source produces noble gas ions. An interesting development of the

mercury pool system has been used by Stuart¹⁶. In his modified system the main discharge is constricted by a magnetic field. The main discharge current is normally between 2-5 mA with 30 V between the anode and cathode giving about 5 mA cm^{-2} ion current density.

2 - Oscillating discharge source

This source consists of a hollow cylinder as anode and two plane circular cathodes. A magnetic field is applied parallel to the axis of the anode, thus restraining any electron to oscillate in a helical path between the anode and cathode. Ions can be extracted through a small aperture in one of the cathodes. The source is basically a modified form of the Penning gauge and has no filament. It operates at a discharge voltage of 7.5 kV & pressure of 10^{-3} to 10^{-4} Torr and produces a beam current of more than 1 mA and an energy spread of 25 eV. The oscillating discharge source was developed by Barnett et al¹⁷ and he used it for controlled ion bombardment experiments because of its wide energy spread. Cobic et al¹⁸ described a type of this source using a filament and has successfully applied it to solid materials.

3 - Glow discharge ion source

This simple glow discharge ion source which was developed and used by Crockett¹⁹, produces gas ions useful for etching biological applications. R.G. Livesey, a colleague of Crockett designed a parallel plate analyser of this type of source and used it to measure the energy distribution of ions. The source operates with a discharge voltage of a few kV and a pressure of about 10^{-4} Torr. It consists essentially of an anode, cathode and the beam emerges from a hole in the cathode disc.

1.3.3 Radio frequency sources

A radio frequency ion source was first used by Thonemann et al²⁰. In this device ionisation does not rely on either a thermionic device or the cold cathode method. In an R.F. ion source ionisation takes place by collision produced by coupling the gas discharge tube with a radio frequency tuned supply. It consists of a glass tube surrounded by a radio frequency coil. The source produces gas ions better than solid ions. In order to constrain the ions near to the exit aperture, a magnetic field is used and the electric field from the positive potential of few kV on the anode moves the ions towards the exit aperture. ~~Eubank~~ et al²¹ developed this source and constructed an r.f. source up to 15 mA of hydrogen ion current. The r.f. ion source can produce about 10 mA of ion current with 20-100 eV energy spread at 10^{-2} - 10^{-3} Torr. This source is useful for high energy bombardment and production of proton beams. It is particularly useful when bombarding insulating materials as there is no problem with charge build up on the specimen as is often the case with D.C. sources.

1.3.4 Special type of ion sources

Many other types of ion sources which operate on quite different principles to those discussed so far have been described in the literature and some of those will be discussed.

1 - Surface ionisation source

This source does not rely on energetic collision between electrons and atoms. If an atom with a low ionisation potential is desorbed from a surface with a high work function it may come off more like a positive ion than a neutral atom, as a result of it losing an electron at the surface. The heated surface, which is

called hot ioniser, thus produces an energetic beam of ions. A simple diagram of this source is shown in Figure 1.5.

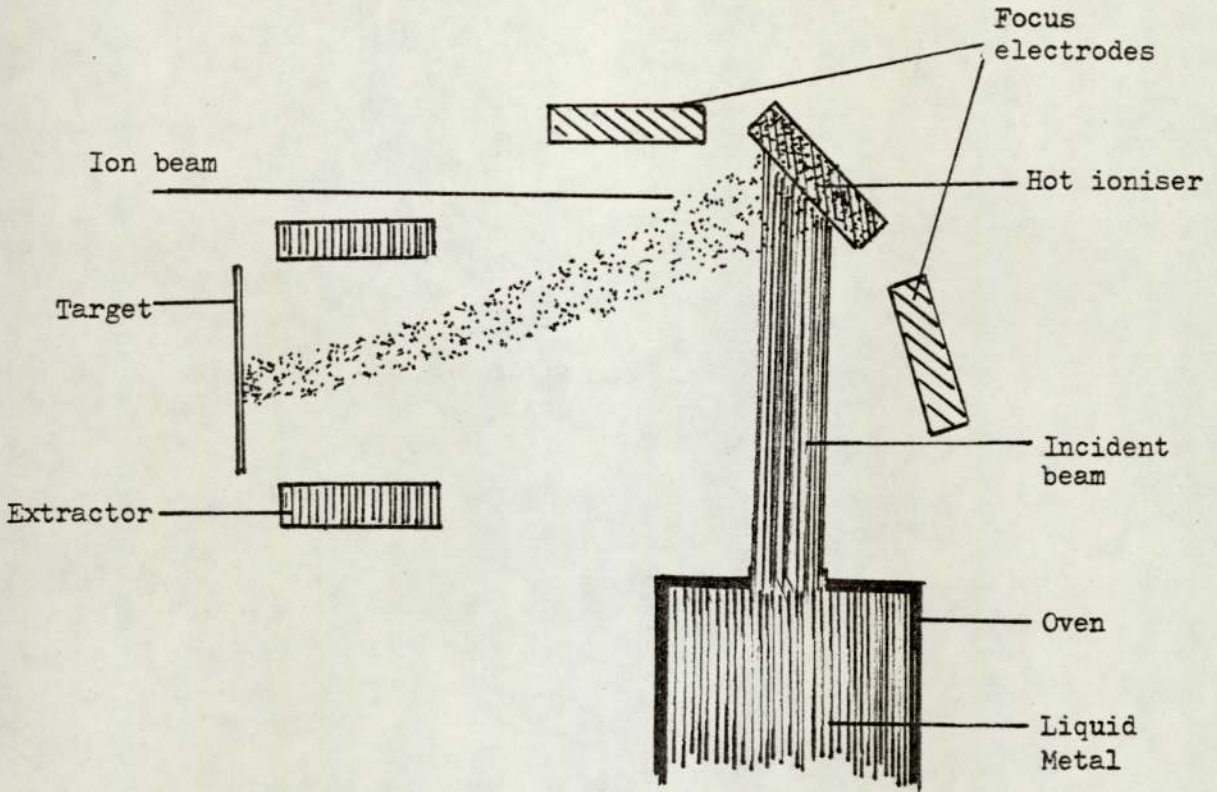


Figure 1.5. Schematic diagram of the surface ionisation ion source.

This ion source does not need any gas and is thus suitable for ultra high vacuum applications. The main parts of this ion source are; an oven to produce the incident atoms, the hot ioniser, focusing and accelerating electrodes. Hague et al²² developed this source using Platinum and Iridium as the ioniser surface.

2 - Vacuum spark ion source

Dempster²³ developed and used the vacuum spark ion source for demonstrations of isotopic formation, and since then, this source has been established by Craig et al²⁴ as being suitable for chemical analysis of solid materials. The spark ion source operates in a high voltage of 50-100 kV, together with a radio frequency supply applied between the electrodes. The source pressure is about 10^{-6}

Torr and produces a very intense ion beam with a current density of about 100 A cm^{-2} . Its energy spread is between 100-1000 eV and the beam current 10^{-10} A. Consequently, due to the small beam current this source is not suitable for clean surface studies and has found most use as a source for mass spectrometry. Also as this source produces an energy spread of about 1000 eV it is not recommended for ion surface interactions.

3 - Thermal ionisation source

This source produces energetic beams on the same basis as that described for the surface ionisation ion source. In fact there are two methods of heating the material to form ions in this source. One uses an ordinary single filament on which the sample is placed, and the other is a multiple filament arrangement, where the sample is evaporated from one filament heater and is ionised by the other. In operation all the filaments are operated at the same potential. The disadvantages of this source are (a) the rapid fluctuation in source intensity and, (b) the need for replacement of sample material. Tyrell et al²⁵ developed this source and used a combination of ionisation and electron bombardment ion source.

1.4 Limitation of existing ion sources

In recent years there has been a considerable increase in the application of ion beams. Furthermore, some of these applications, such as ion thinning of specimens for electron microscopy and ion implantation of semiconductors, have extended into the commercial field. It is now well accepted that there are areas where special advantages are to be gained using ion beams in preference to other techniques. In this section particular problems related to the existing ion sources and also factors limiting the performance of particular ion beam systems are discussed.

Different applications, of course, require some particular value of ion beam current and energy. For example, in surface studies ion beams of $1 \mu\text{A} - 1 \text{mA}$ and $5-200 \text{keV}$ energy, in sputtering $100 \mu\text{A}-10 \text{mA}$ with $1-10 \text{keV}$ beam energy and in surface analysis $1-10 \mu\text{A}$ current at $10 \text{eV}-20 \text{keV}$ beam energy, are the usual values (Hurley)²⁶. Consequently, in application of ion beams the limiting factors in the performance of the ion beam system which may comprise an ion source, extractor, focusing and accelerating electrodes, mass separator, target facilities and beam transportation, should be studied. The design of the ion beam system always relates in detail to its application. Fig. 1-6 shows a typical ion beam system and its requirements as an example.

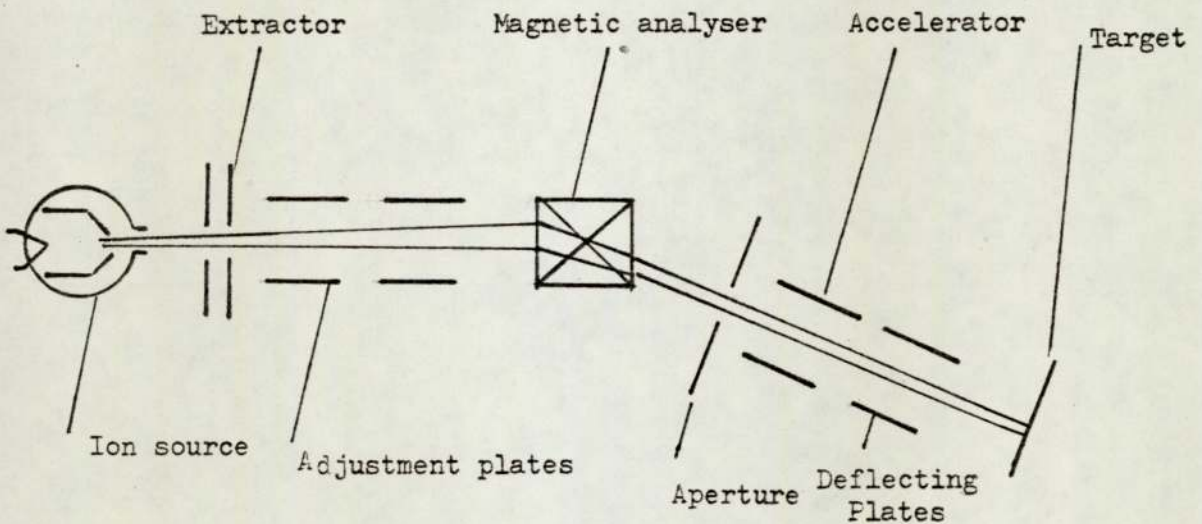


Figure 1.6. Typical ion beam system

The quality of the emerging beam permits comparison between different ion sources. The production of a low emittance source and high brightness ion beam is limited by several factors.

(a) required beam density -

To obtain the optimum performance of the source and provide

the required ion beam density may be difficult. For example a low current density is needed to minimise radiation damage but on the other hand an intense beam may be required at a target placed a considerable distance from the source.

(b) Momentum dispersion -

Ion particles are not uniform and they disperse because of their various momenta and also ions with the same charge repel each other, so that the ion beam diverges (Taylor)²⁷. At high pressures charge exchange and secondary electron ionisation causes a significant dispersion of the ion beam at the extractor aperture, and produces ions with different energies which will be restrictive in certain applications. Therefore the ion beam must be focussed and accelerated towards the target and in a simple system a pair of electrodes may be sufficient to accelerate and focus the beam.

(c) Mass separation -

In some applications some species of ions are unwanted. However ions of the same energy but different mass cannot be separated by a D.C. electrostatic device and one must use a magnetic analyser or alternating electric field as in the quadrupole analyser. Thus separation of the ion beam into its component masses can be achieved.

(d) Beam transport and control -

This is another aspect which limits application of ion beams and generally it is necessary to minimise contamination of the target from the vacuum pump fluid.

In spite of these limitations in ion beam production and in various applications, many studies of ion bombardment phenomena have been carried out in which much of the work has been of a basic nature and designed to learn more about sputtering and various

ionic and electronic emission process. It is perhaps only since about 1950 that applications of various ion bombardment process became of importance. For example it is possible to ion etch all types of materials, whereas chemical etching is often difficult and is limited to certain materials. Furthermore ion bombardment can be carried out at any selected temperature which is necessary with materials in which the temperature range is restricted. Normally there is no contamination of the surface with ion bombardment, but sometimes gases such as oxygen are used in reactive sputtering.

In ion bombardment the energetic ion impinges on the surface and removes atoms, without disturbing the other atoms (Hawkins)²⁸. The yield is usually of the order of one atom per ion and thus this process is very suitable for removing one or a few atomic layers. In fact the etching process is one in which the energy of the incident ion is transferred to the bombarded atom; This can cause the atom to be ejected when (a) the energy transferred to the atom in the collision process exceeds the binding energy of atom and (b) when the momentum imparted to the atom is such that the atom is directed away from the surface. If the ion energy is less than a few keV then only the first few atomic layers of material are involved (Gloersen)²⁹.

The process of removal of atoms, during ion bombardment is often called sputtering and early experiments on sputter ion etching showed that at high pressures, if the mean free path of sputtered particles is less than the distance from target to the collector, some of the liberated atoms diffuse back to the surface after collision with gas molecules. These particles are either resputtered or buried underneath the subsequent returning particles. However, in ion beam etching it may be required that (a) the energy spread of the ions should be small, (b) the gas pressure or source

pressure must be such that the mean free path of sputtered particles and ions is large compared with the source dimensions and (c) the beam current density, d_i , must be high and the background pressure surrounding the target P_b should be low. Thus the best condition

is $\frac{d_i}{P_b} > 10^8$, where d_i is in $\mu\text{A cm}^{-2}$ and P_b in torr (Pleshivtsev)³⁰.

The etching yield also depends on the incident angle. Gloersen showed as the angle of incidence of the incoming beam is increased away from normal to the surface, the sputter yield increases at first and reaches a maximum for an angle of about 45° and then decreases. Of course this angle is for a certain target and few hundred^{eV} to one keV ion energy. The most interesting experiments to determine the variation of sputtering yield in different conditions have been carried out by Wehner³¹. However Wehner and Gloersen³¹ showed that the angle of maximum incidence varies with target material, ion species and ion energy. Figure 1-7 shows the variation of angle of incidence as a function of sputtering yield (atom/ion) for Hg^+ ions and at different energies by Wehner, (a) with 800 eV and 200 eV ion energies and (b) with 200 eV ion energy and various targets. The maximum yield for Argon ion bombarding a copper target is reported at approximately 75° by Tsong et al³².

The example of ion etching has been used to illustrate the nature of the requirements that any particular application imposes on the ion source. More recently there has been considerable interest shown in ion etching carried out in-situ in the specimen chamber of scanning and transmission electron microscopes and this has placed further restrictions on the type of ion source that can be used. Under these conditions it is necessary that the source should operate at low pressure without the need of a magnetic field which would effect the electron beam. It is also preferable that

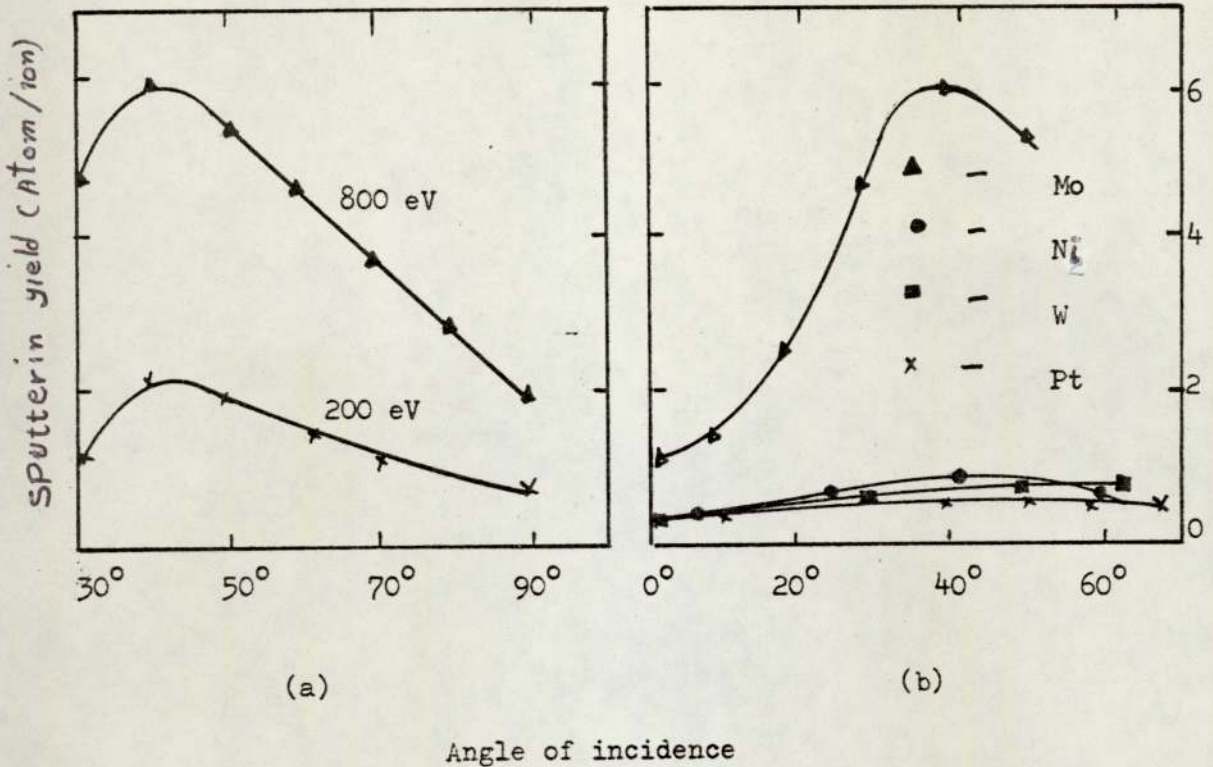


Figure 1.7. Variation of sputtering yield with angle of incidence for Hg^+ ions with (a) 800 and 200 eV ions using Ni target and (b) for 200 eV using various targets.

the source should be small, but still produce an intense beam of ions without the complexity of additional extracting and focusing electrodes.

The sources already discussed in section 1.3 do not readily meet all of these requirements but a new type of ion source which is very suitable for these applications has recently been developed from the idea of McIlraith³³, for an electrostatic charge particle oscillator. This source is the main subject of this thesis and its present developments and properties will be discussed in the next chapter.

CHAPTER 2

THEORY AND APPLICATION OF THE McILRAITH OSCILLATOR

2.1 Introduction

In 1966 McIlraith³³ found that a ball released on a stretched rubber sheet, into which a vertical pair of rods had been pressed, oscillated for a long time. These observations gave him the idea how to make charged particles of one sign oscillate within a limited volume by means of an electrostatic field alone. This arose during his investigation of electron paths in an x-ray tube by means of the rubber model, and he found that the ball follows a path which is very similar to that followed by an electron released at the corresponding point in the electric field. Thus the ball passes between the rods many times before finally colliding with one of them. The trajectory of the ball on a rubber model and hence the electron path in an evacuated device with two rods at a positive potential depends on the position from which the ball or electron is released.

Figure 2.1 shows examples of electron trajectories caused by a pair of equally charged poles. He also stated that the type of motion may occur in the gravitational field of stars where the asteroids could be held in oscillatory motion between the stars. The theory, use and development of the McIlraith idea is given in this chapter.

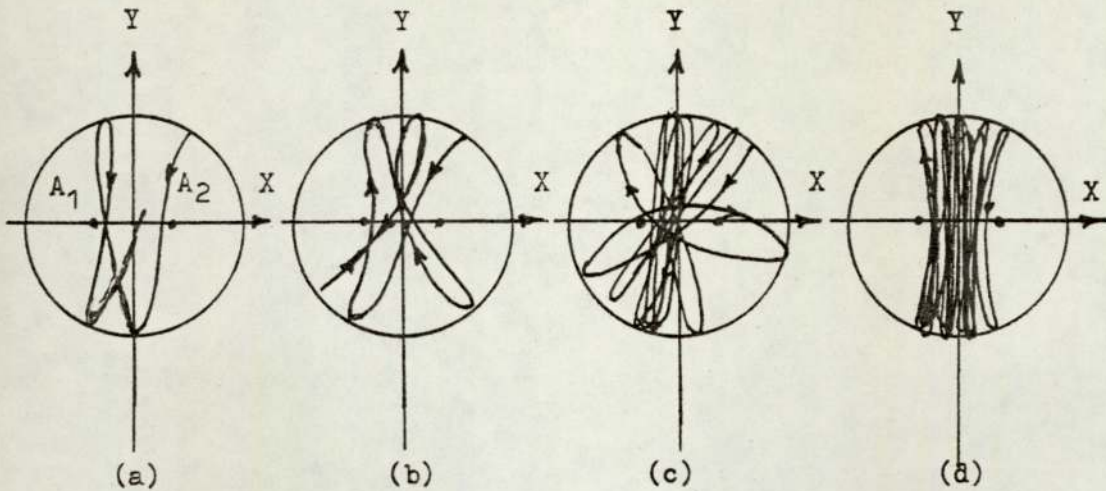


Figure 2.1. Examples of particle trajectories caused by a pair of equally charged poles.

2.2 Theory of oscillator

McIlraith showed that in a corresponding electrical model comprising a pair of positive charged parallel rods surrounded by a conducting cylinder, an electron oscillates between the rods and follows a very long oscillatory path which usually passes between the electrodes. This assumes that the electron does not lose any energy by radiation.

At low pressures the oscillating particle must travel a very long distance in order to collide with other particles or gas molecules to provide the necessary degree of ionisation and hence maintain the discharge. For example if the pressure is 10^{-5} Torr McIlraith showed that each electron will travel about 5 km. The particle trajectories are of two types - stable and unstable. In the case of a stable trajectory the oscillating particle passes between the two electrodes and in the unstable trajectory it orbits around them. However in the stable oscillation the electron will be collected by one of the poles after an appreciable length of time depending on the pressure. In this case the electron starts from rest inside the region R (Fig. 2.2), and those released

outside of R have unstable trajectories.

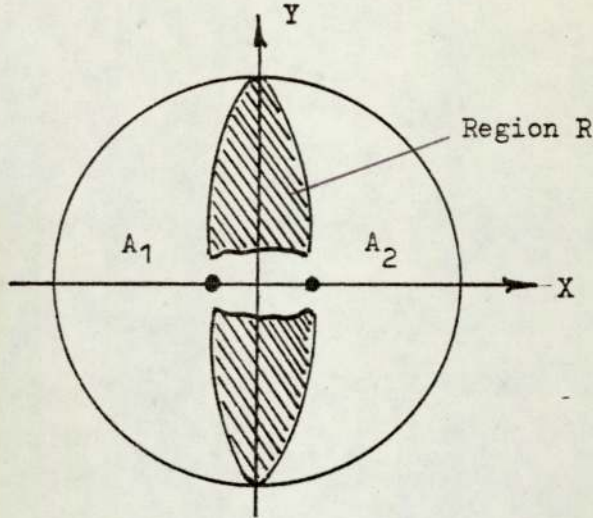


Figure 2.2. Region R, in which the stable trajectories start.

Thus during operation the source of electrons should be inside the region R. Figure 2-3 shows (a) stable and (b) unstable electron paths.

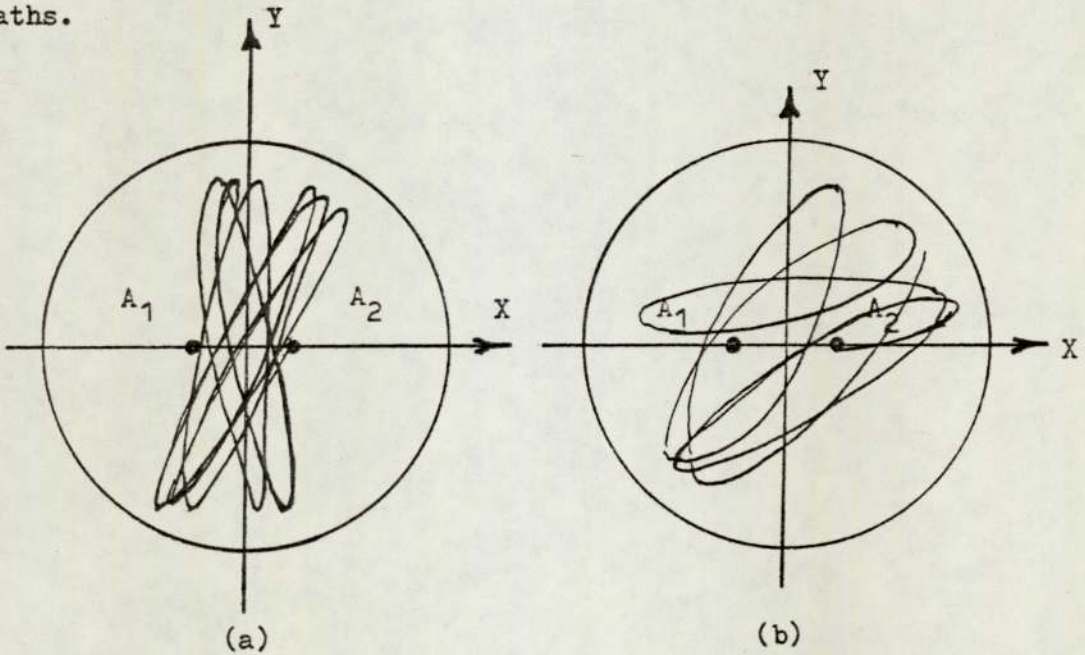
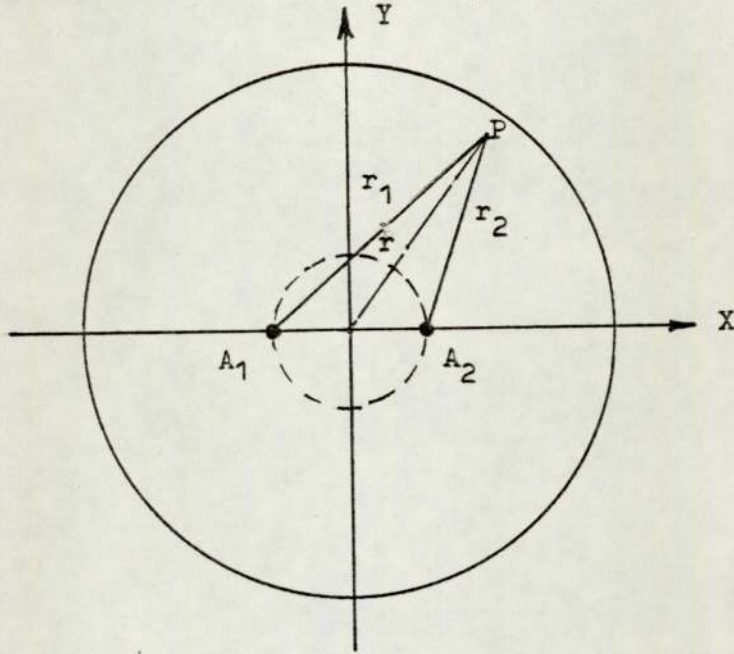


Figure 2.3. Different electron trajectories inside a saddle field ion source (a) stable and (b) unstable trajectory.

McIlraith showed that the electric field has a saddle point at the origin O between the two anodes A_1 and A_2 . In fact Möllenstedt³⁴ as early as 1949 described a type of saddle point field electrostatic

analyser for the first time, but no one appears to have made use of his idea. Although the saddle point is a point of unstable equilibrium, the electrons can oscillate through it in stable trajectories along the y axis of the oscillator, and lines of force curve in the vicinity of the origin O. McIlraith investigated the trajectories followed by a charged particle within the oscillator using computing techniques. As a result the potential and the electric field was calculated for a point, P.



He showed that the potential at P is given by:

$$V_p = V_{xy} = q \ln \frac{d^4}{r_1^2 + r_2^2}$$

or

$$V_p = q \ln \frac{d^4}{(y^2 + (x-d)^2)(y^2 + (x+d)^2)}$$

where 2d is the distance between anodes. The electric field along the axes E_x and E_y are found by differentiating V_p with respect to

x and y. In this case:

$$E_x = \frac{4qx(x^2+y^2-d^2)}{(y^2+(x-d)^2)(y^2+(x+d)^2)}$$

$$E_y = \frac{4qy(x^2+y^2+d^2)}{(y^2+(x-d)^2)(y^2+(x+d)^2)}$$

It is obvious that for $x = 0$ (particle on the y axis) and also for $x^2 + y^2 = d^2$ (particle on the circle with A_1A_2 as its diameter), the electric ^{field} component E_x is zero. Outside this circle E_x is directed away from the y axis and inside E_x is towards the y axis, but the force F_y on the electron is always towards the x axis.

From the two above equations, E_x and E_y , then

$$\frac{E_x}{E_y} = \frac{y}{x} = \frac{y^2 + x^2 - d^2}{y^2 + x^2 + d^2}$$

Thus at large distances for r_1 and r_2 , that is for $y^2 + x^2 > d^2$ when the particle is outside of the circle of A_1A_2 , the field lines radiate from the saddle point at O, and the accelerating force on the electron will be towards the saddle point.

Owing to the long paths followed, each oscillating electron has a large number of elastic collisions with the gas molecules before collection by the anode. According to whether the collisions are elastic or inelastic between the electron and the neutrals, if the electron energy is higher than the ionisation potential of the neutral, the neutral will be ionised, and with the large electron path a high density plasma can be produced even at the low pressure.

If we assume that i_e is the initial electron current which starts the oscillation, then the electron can ionise N_i pair of

ions before being collected by one of the anodes. Therefore $(N_i + 1)$ electrons will strike the anode, and N_i ions bombard the cathode. Thus $K N_i$ secondary electrons will be emitted where K is the secondary electron coefficient which depends on the type and energy of the ions and cathode material, and N_i depends on the electron energy, pressure and type of gas.

It should also be mentioned that during this process neutral atoms and sputtered ions are emitted from the cathode so that the cathode target can produce neutral particles or cause recombination of ions and secondary electrons. As a result of this electron transition from higher to lower energy levels photons will also be emitted. Now in the next ionisation process between the two poles $(N_i + 1)$ electrons will cause $N_i(N_i + 1)$ electrons and $N_i(K N_i)$ ions and so on in the third and fourth collisions etc.

Therefore,

$$\frac{i_c}{i_e} = (N_i + 1) + (N_i + 1) K N_i + (N_i + 1) K^2 N_i \dots\dots\dots$$

$$\text{or } i_c = i_e (N_i + 1) (1 + K N_i + K^2 N_i \dots\dots\dots K^n N_i)$$

where i_c is the ion current. This is due to the primary electron ionisation, and the effect of secondary electrons from the anodes due to the high accelerating field is ignored.

2-3 Application of the oscillators

The high ionisation efficiency of the oscillator has lead to some important applications and these will be now briefly discussed.

1 - Vacuum gauges

A thermionic ionisation gauge based on the charged particle oscillator was first discussed by Fitch et al³⁵. The gauge

consisted of a cylindrical collector surrounding the anodes, and a V-shaped tungsten filament protruding through a hole in the cathode wall to inject electrons towards the saddle point between the anodes. The maximum sensitivity of the gauge was about $7 \times 10^4 \text{ Torr}^{-1}$, and due to this high sensitivity and low emission current it was suitable for pressure measurement in the ultra high vacuum region.

However full advantage cannot be taken of this high sensitivity, as most of the x-rays generated at the anode are intercepted by the ion collector, and thus the low pressure limit was not much better than the Bayard-Alpert gauge.

Atkinson et al³⁶ largely overcame this problem by using a series of rods in place of the solid cylindrical collector. This design not only reduced the collection of x-rays but also eliminated unwanted electron trajectories arising from electrons orbiting around the anodes. The gauge produced a directed beam of ions and thus the remaining x-ray current could be eliminated by deflecting the ion beam onto a collector which was shielded from the x-rays. With this device the x-ray limit was estimated to be about 10^{-12} Torr but it was only tested down to about 10^{-10} Torr .

2 - Molecular beam detector

Another significant application of the charged particle oscillator is as a molecular beam detector. This detector was originally suggested by McIlraith based on his oscillatory particle idea, and later in a practical form described by Peggs et al³⁷. In this device the molecular beam passes through a band of oscillating electrons emitted from a hot filament and is detected by measurement of the resultant current of ions. The sensitivity of this detector to a molecular beam of argon was about 6 Torr^{-1} . The detector is designed to measure molecular velocity distributions when used with

a time of flight molecular beam system. This velocity distribution was calculated from the shape of the detected pulse. This detector has also been used for determination of the scattering patterns for Ar, N₂ and He on a stainless steel target.

3 - Source of vacuum ultra violet radiation

Burget et al³⁸ have recently developed a new type of source of ultra violet radiation based on the principle of the McIlraith oscillator. The source was operated as a cold cathode discharge at a pressure of about 10^{-5} Torr. He obtained intense emission lines from helium, neon and argon ions and suggested that this device is a convenient windowless photon source of He II (304 and 256 Å) and Ne II (461 and 462 Å) for photoelectron spectroscopy. Furthermore the number of emission lines of the ions of argon and neon make it a useful source for photoionisation experiments when used in conjunction with a monochromator.

At present the most important application of the McIlraith oscillator is as a source of positive ions. This source is now available commercially and has already been used in a variety of applications. The development of this source will therefore be discussed in some detail in Chapter 3.

CHAPTER 3

DEVELOPMENT OF SADDLE FIELD ION SOURCES

It is clear from the previous chapter that the McIlraith oscillator can maintain a cold cathode discharge at low pressures without a magnetic field, or thermionic source of electrons. It was therefore suggested by McIlraith in 1969 that some fraction of the ions produced in the discharge could be allowed to escape through an aperture in the cathode without serious perturbation of the discharge and this idea led to the development of the saddle field ion sources.

Two forms of these sources have now been produced using either cylindrical or spherical geometry and the development of these will now be given.

3.1 Cylindrical source

The first version of this source was described by Fitch et al³⁹. It consisted essentially of two tungsten wires 0.3 mm, diameter symmetrically disposed about the axis of a stainless steel cathode 20 cm. long, and 5.4 cm internal diameter, and the ions were allowed to escape through an aperture milled midway along the cylinder. In this source the end-plates were made of copper or stainless steel mesh held at cathode potential, so that the pressure inside the source was assumed to be the same as the chamber pressure, and the anodes were spring loaded to prevent them from bowing. The source was operated with 6-10 kV at below 10^{-3} Torr producing about $300 \mu\text{A cm}^{-2}$ beam current density.

Figure 3.1 shows the current density of positive ions for this source when the collector was moved parallel to the plane of the

anodes and at right angles to the axis of the cylinder.

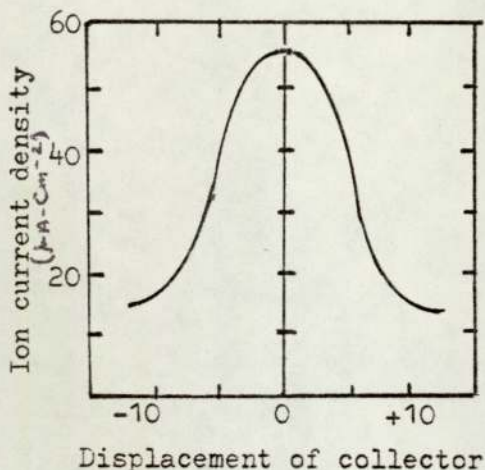


Figure 3.1. Variation of ion current density due to the collector position.

The usefulness of this source was assessed by etching a specimen of OFHC copper placed normal to the ion beam. However the disadvantage of this source was the thin anode wires were easily burnt out as they were heated by electron bombardment.

The operational characteristics of an ion source similar in construction to the above mentioned one, was designed and used by Mukherjee⁴⁰. This source was mostly used for neon and argon ions at about 10^{-4} - 10^{-1} Torr.

Later the performance of a twin anode oscillator was described by Rushton et al⁴¹. The source was operating between 10^{-5} - 10^{-3} Torr and up to 16 kV and 10 mA tube current. Figure 3.2 shows the discharge characteristics of this source at various pressures. They showed that, when operating the source either as a cold or hot cathode discharge, the performance of the oscillator was influenced by the earth's magnetic field. That is the source operated at a lower pressure when the cathode cylinder was horizontal compared with the case when the cylinder was vertical. This was because the horizontal component of the earth's field is less than the vertical component.

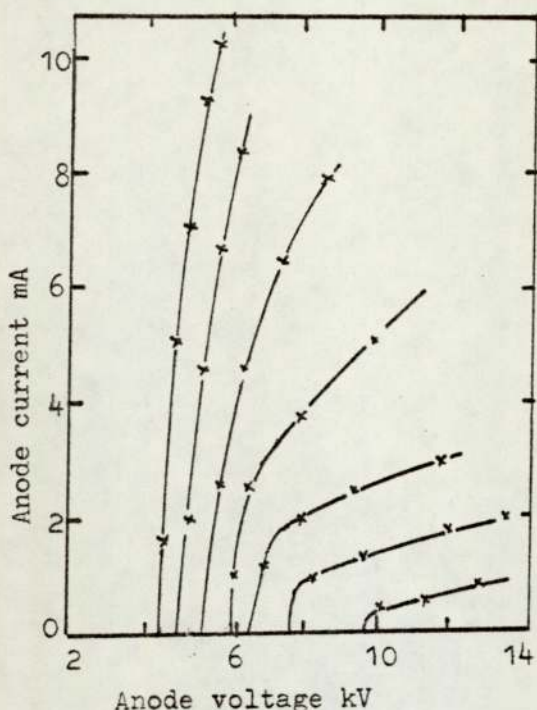


Figure 3.2. Cold cathode discharge characteristics

They also determined the variation of the tube current with anode separation and found there is no discharge when the anode separation is 4 mm or less, but the source performance and hence the beam current for 5-6 mm centre to centre anode separation was at a maximum. They also showed that the anode diameter has only a very small effect upon the source performance and thus larger diameter anodes could be used. As a result further developments were made by Fitch and Rushton⁴². This source was operated at a pressure of about 5×10^{-4} Torr with 10 kV anode voltage, producing a broad energy spread ion beam of about $100 \mu\text{A cm}^{-2}$ density suitable for etching conducting and non-conducting samples. The performance of this source compared to the previous ones, was improved by the use of tungsten rod anodes that did not burn out due to electron bombardment.

Two modified forms of these sources, multiple beam and wide beam, were designed and developed by Fitch et al⁴³. They showed that the saddle field geometry could be extended to any even number

of anodes within the cylinder to provide a number of ion beams to etch different samples under identical conditions at the same time. On the other hand the wide beam source which employed a rectangular cross-section for the cathode could be used to etch relatively large areas of specimen. They also showed during operation when the anodes get hot that the specimen being etched is heated by thermal radiation from the anodes as well as due to the ion bombardment. In order to overcome this problem and also permit the source to be operated for a long time, the anodes were water cooled (Dahriwal)⁴⁴. The water cooled source was found to be more stable during prolonged periods of operation due to the elimination of the build up carbon contamination on the anodes.

In 1972 Rushton et al⁴⁵ injected gas directly into the source as suggested by Franks⁵¹. They were therefore able to operate this source at higher pressures without causing electrical breakdown in the experimental chamber. As a result of calculating the efficiency of the source, defined as $\frac{I_B}{I_T}$, as a function of pressure Rushton et al⁴⁶ suggested that there were three main modes of operation, namely the glow mode, transition mode and oscillation mode. Figure 3.3 shows variations of ion source efficiency for argon ions with chamber pressure.

In order to estimate the uniformity of the ion beam they used a Faraday cage containing a small entrance aperture. Figure 3.4 (a) and (b) shows the variation of the beam density as the Faraday cage was displaced parallel to the source axis for oscillation and transition modes respectively.

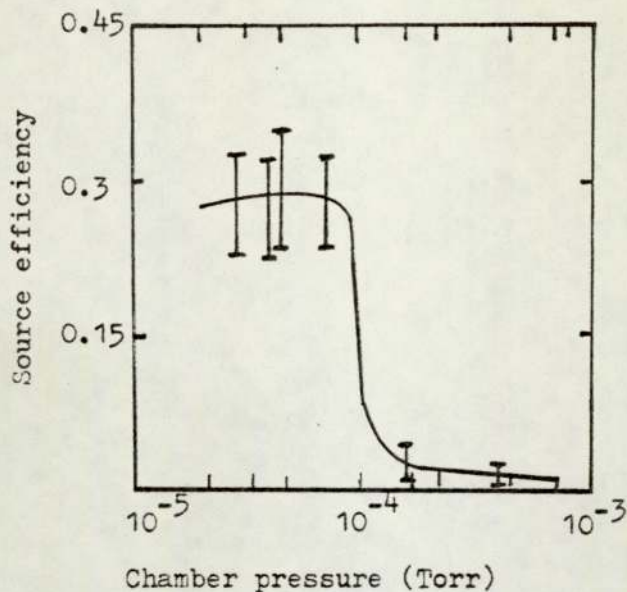
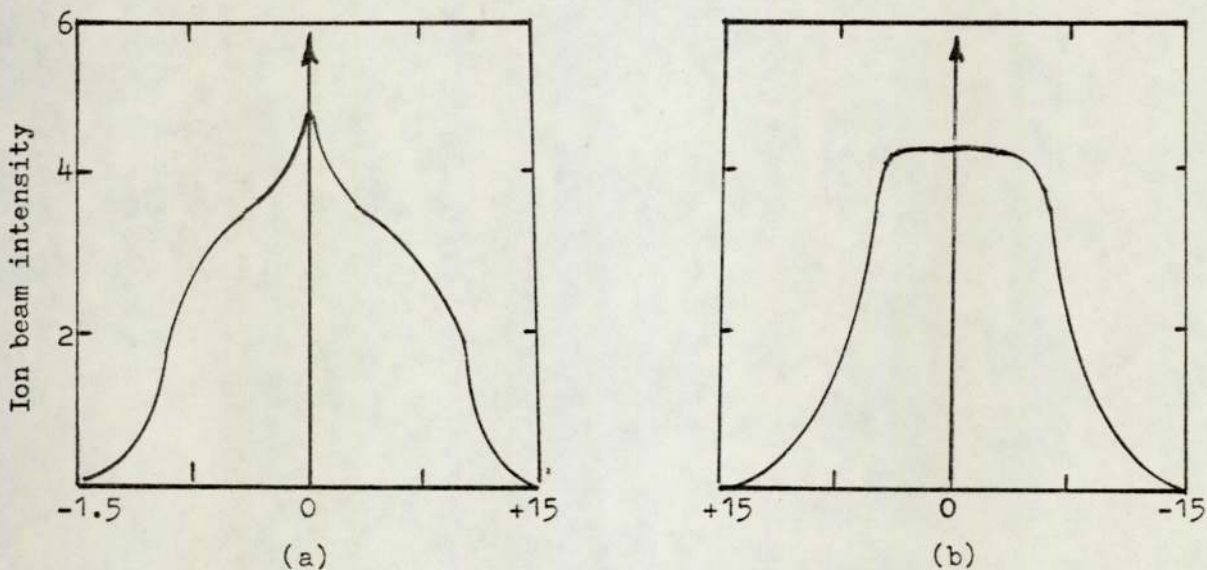


Figure 3.3. Ion gun efficiency at different pressures.



Displacement of the collector relative to the aperture

Figure 3.4. Ion beam density at (a) oscillating mode and (b) transition mode.

Ghander⁴⁷ investigated these modes by measuring the change of voltage and the beam current on a function of pressure for a constant anode current and a typical condition reported by him is shown in Figure 3.5 for argon. In addition to the three principal modes discussed above he claimed that there were also other modes one of which he called the non-uniform plasma mode.

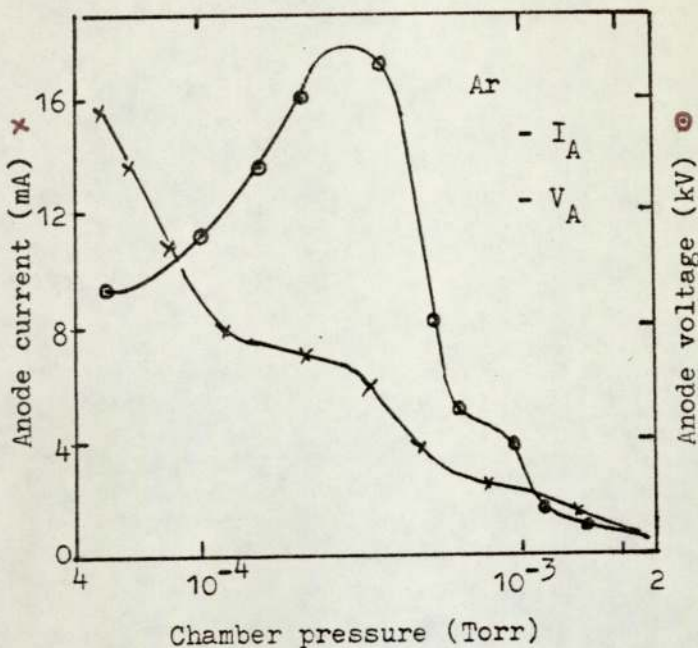


Figure 3.5. Modes of operation for a cylindrical source with 5 mm aperture.

In further development Rushton et al⁴⁸ injected electrons into a source with a tungsten filament inserted through a small hole in the cathode wall. The beam current obtained in this source was comparable with that obtained with a similar source of the cold cathode type, but it could be operated at lower voltages and pressures. The resulting ion beam was therefore of lower energy and thus produced less heating of the sample during ion bombardment and consequently less structural damage of the specimen. This type of ion gun is more suitable for such applications as Auger spectroscopy. Clark et al⁴⁹ used a source with cooling of the anode and cathode to investigate the charge state of argon, nitrogen, helium and hydrogen ions using a magnetic analyser. They showed that for argon, nitrogen, helium and hydrogen, the predominant ions were Ar^+ Ar^{++} N^+ He^+ H_2^+ , but higher charge states were seen with increasing source power.

A further improvement was made to the source by using a small chimney on the ion exit aperture to reduce the field distortion and this together with a focusing electrode (Ghander and Fitch)⁵⁰,

produced a well collimated ion beam, and hence a higher beam intensity and also increased the total ion beam current by extracting more low energy ions from the source.

3.2 Spherical source

In the cylindrical source the diameter of the source is relatively large, even when narrow and fine beams are required and sometimes it is necessary to focus the emerging ion beam. Furthermore with the cylindrical geometry there is a saddle line along the axis of the cylinder, and consequently it is necessary to terminate the electric field with end plates at cathode potential. This produces undesirable end-effects.

However, it has recently been shown by Franks⁵¹, that the saddle field configuration need not be confined to cylindrical geometry. He showed that if the cathode is made spherical and the anode rods are replaced by a ring anode, then the saddle line becomes a saddle point and the end effects are eliminated. In 1972 Franks⁵¹ described and designed a saddle field ion source of spherical geometry by making the cathode from two aluminium hemispheres, and the anode from a stainless steel annulus. In order to retain the true spherical geometry, he added two guard rings at earth potential placed either side of the anode. These were isolated from the anode by four ceramic insulators and the ion beam emerged through a hole in the cathode. A schematic diagram of this source is shown in Figure 3.6 (a). In a later version he simplified this by using tubular cathodes as shown in Figure 3.6 (b) to assimilate the spherical field.

Later on Ghander⁴⁷ showed how the characteristics were effected by variation of the anode hole diameter, and he showed that as the anode hole diameter is decreased the saddle point potential increases. He therefore determined the appropriate anode hole diameter in the

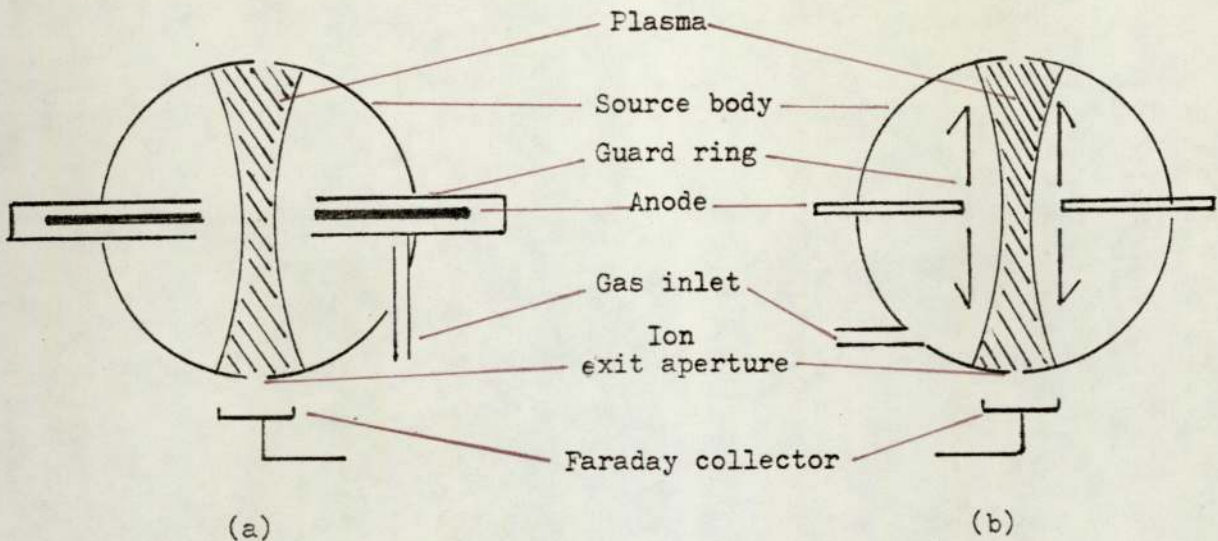


Figure 3.6. Schematic diagrams of previous and recent spherical ion sources same way as Rushton⁴¹ did to optimise the anode separation in the cylindrical source.

One of the later designs of the spherical source produced by Ion Tech Ltd., is the subject of part of this thesis, and the characteristics and specification of this source will be discussed in the next chapter.

3.3 Ion energy distribution

The energy distribution of the ions produced by any ion source is an important feature which may ultimately determine if the source is suitable for a particular application. However at present there has not been much satisfactory work done on the energy measurement of the ions produced by the saddle field ion sources.

The first attempts at energy measurements on the cylindrical source were made by Rushton⁴⁵ using a simple retarding field energy analyser. This method proved to be rather unsatisfactory due to the type of retarding plate and ion collector used. He also found that with this analyser it was difficult to find the characteristics of high energy ions due to the instabilities in the system arising from electrical breakdown in the experimental chamber.

Franks⁵² used an electrostatic analyser with a cylindrical ion source. He found one main peak in the energy spectrum and a few low energy peaks which varied with source geometry, type and pressure of the gas and tube voltage.

Ghander⁴⁷ used a similar type of parallel plate to the one used by Rushton, but with two stainless steel meshes of 40% transparency instead of the two plates, and he also used a small conical copper Faraday collector. He applied the retarding voltage to the grid near to the source and connected the other grid to earth potential to protect the collector from the accelerating field due to the retarding grid. He used this system to determine the energy distribution for both cylindrical and spherical ion sources in different conditions and with various gases. For example he found many peaks with nitrogen for the cylindrical source and noticed that the highest energy peak was also the most intense peak. Figure 3.7 (a) shows the variation of voltage with ion collector current, and 3.7 (b) shows the variation of the number of ions per unit energy $N(E)$ with ion energy (E).

The main points to note about these experiments are:-

- (1) There is a sudden fall of i_c with V_R changing from 0 to 0.5 kV and at $V_R = 0$, $\frac{di_c}{dV_R} > 0$, which implies that many of the ions have very low or almost zero energy, and this is not shown in the Figure 3.7 (b).
- (2) The experimental points have been recorded at large intervals of V_R .
- (3) The number and width of the peaks in different experimental conditions change.

(4) It was difficult to produce any model of the source which could explain this complex energy distribution.

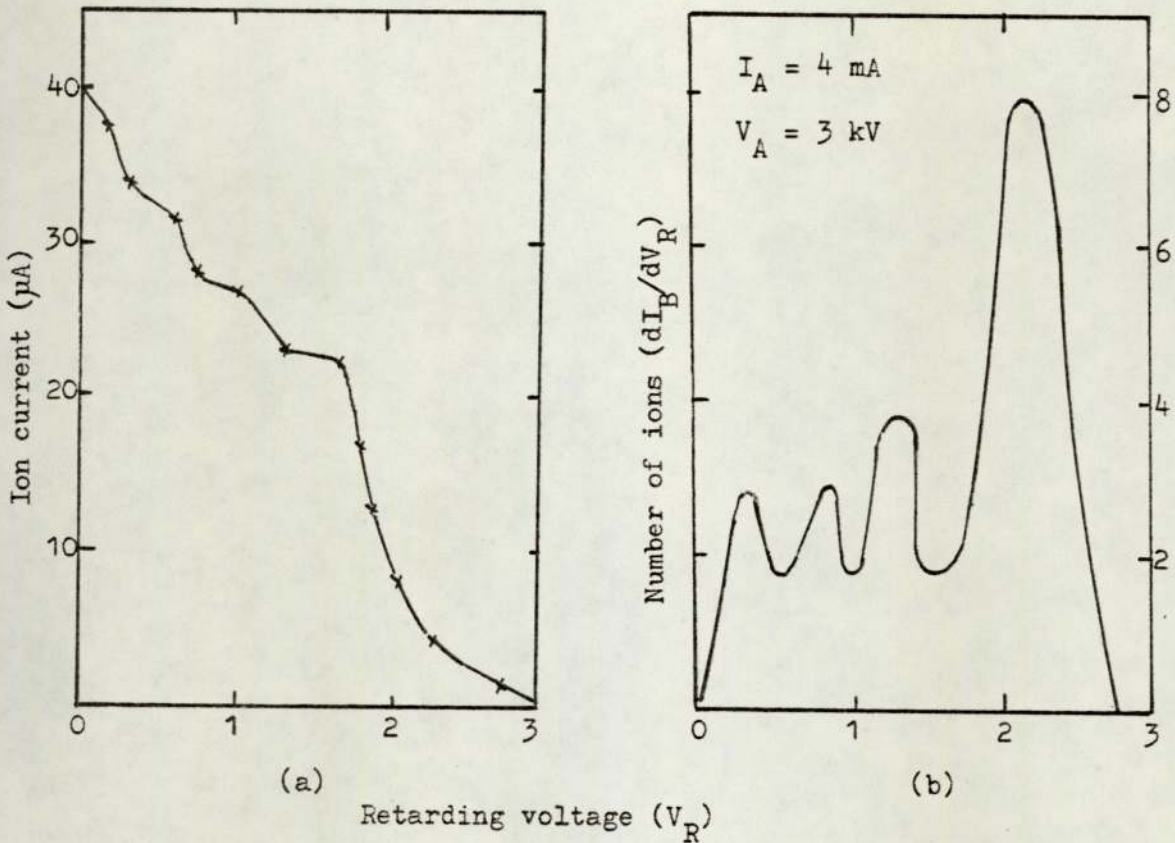


Figure 3.7. Ion energy spectrum for a cylindrical source using nitrogen.

By using a spherical source with the same analyser, Ghander showed that the energy spectra contained one main high energy peak and also a number of lower energy peaks. The high energy peak had the energy equivalent to about 85% of anode voltage and a half width of 0.25 kV. Thus the resolution of his energy analyser was (the smallest measurable difference in energy of particles by the analyser) when the tube voltage is 6 kV was

$$\frac{\Delta E}{E} = \frac{2 \times 0.25}{6 \times 0.85} \approx \frac{1}{10}$$

Once again the results were not very satisfactory and they were difficult to interpret.

Franks and Ghander⁵³ used the spherical source with the above-

mentioned analyser. They observed one high energy peak with a 1.5 mm aperture diameter for argon ions, but multiple peaks obtained when the exit aperture was enlarged to about 6 mm diameter. They claimed that the multiple peaks appeared because different energy ions originate from different locations within the source.

Swamathan et al⁵⁴ measured the ion energy produced by a cylindrical source incorporating thermionic electron injection. The ion beam was allowed to enter a double focusing mass spectrometer of the Mattauch-Herzberg geometry with electrostatic and magnetic analyser. They did the experiment for anode voltages of about 1.5 kV or less and in all experiments they found two distinct peaks - one a high and the other at low energy.

It is evident from the above discussion that there is considerable disagreement between the energy spectra, reported from these earlier measurements. Thus one of the main purposes of this work was an attempt to produce some reliable information of the energy distribution of the ions produced by the cylindrical and spherical ion sources.

3.4 Application of saddle field ion sources and discussion

Controlled removal of materials in ion beam etching and ion cleaning is an important technique, which has been developed in parallel with the development of ion sources. However a disadvantage of existing ion sources is that they must be run at relatively high pressures in order to obtain sufficient current density that is necessary for different applications. In addition the actual size and even construction of some sources may be rather restrictive. However, the saddle field ion sources are particularly useful for this purpose as they operate at relatively low pressures without the need of a magnetic field and because of their small size

they can be easily inserted inside the vacuum chamber. These sources which have been continuously developed since 1970 have now found many uses such as part of a beam analysis apparatus for cleaning the specimens and high power versions may be used for sputtering purposes.

Fitch and O'Shea⁴³ used a cylindrical source for etching and thinning specimens by scanning electron microscopy (S.E.M). They showed that an ion beam of about $100 \mu\text{A cm}^{-2}$ removed in one hour 0.85 mg of material from an O.F.H.C. specimen of area 0.09 cm^2 .

Ghander et al⁵⁰ used the cylindrical source with about 1.6 mA - cm^{-2} current density to etch a sample of copper sheet of 0.06 mm thickness, and reported that the etching was about $7 \mu\text{mh}^{-1}$. Later Franks et al⁵³ used the spherical geometry source with about 1 mA cm^{-2} current density for copper ion thinning. He showed that both the cylindrical and spherical sources are compatible with ultra high vacuum equipment and may be used for cleaning surfaces prior to analysis by Auger electron spectroscopy (A.E.S) or electron spectroscopy of chemical analysis (E.S.C.A).

Dahriwal et al⁵⁵ etched the enamel and the dentine of human teeth with a cylindrical source to reveal artefacts when examined by scanning electron microscopy.

Also two improved cylindrical and spherical ion sources for in situ ion etching in the scanning electron microscopy were used by Dhariwal⁴⁴. He showed steps produced on a copper film shielded by aluminium foil, and also measured the temperature of a tooth enamel during bombardment and the growth of cones on tooth enamel, copper, ceramics, dental amalgam, araldite, annealed copper, soft and hard biological materials by these sources.

Clark et al⁴⁹ showed that these sources were suitable for small

accelerators and Professor M.W. Thompson⁵⁶ mentioned that they might be useful for ion implantation.

There are several other applications currently in use at this University. For example, the cylindrical source is in use in uniform specimen thinning for the transmission electron microscopy (T.E.M) in the Metallurgy Department and also in the field emission laboratory to remove the oxide layer from a titanium target in high voltage breakdown experiments (S. Mohindra et al)⁵⁷, and removal of oxide layers from aluminium samples in ellipsometry in the thin film laboratory (Rehal et al)⁵⁸.

It is thus evident that the saddle field ion sources are already useful and have been applied with a considerable degree of success. These sources have several advantages over other sources such as their relatively simple construction and operation, easy cleaning, high resolution and efficiency and suitability for conducting and non-conducting materials. Their small size makes them advantageous in ion bombardment in a variety of experiments in physics and biology. However if further progress is to be made with these sources it is essential to have a better understanding of the manner in which the discharge operates and to have more reliable information about the nature and type of the particles they produce. These aspects have been the main object of this present work which will be described in the following chapters.

CHAPTER 4

EXPERIMENTAL ARRANGEMENT AND DESCRIPTION OF THE ION SOURCES

In the experimental work described in this thesis two forms of the saddle field ion sources have been used. The cylindrical source was designed and made in this department, whereas the spherical source was purchased from Ion Tech Ltd and modifications to this were made where necessary.

4.1 The cylindrical source

This source consisted mainly of a stainless steel cylinder of internal diameter 25 mm and length 75 mm surrounding two tungsten anode rods of 1.5 mm diameter and a centre to centre separation of 5 mm which is the optimum spacing as determined by Rushton et al.⁴⁵. A schematic diagram of this source is shown in Figure 4.1. In order to prevent the electrons drifting out of the cylinder two separate stainless steel end caps held at cathode potential and containing the insulators and anodes were used. The insulators were ceramic bushes of diameter 22 mm and thickness 5 mm situated in the end caps such that the anodes were symmetrically disposed around the cylinder axis. The anodes were only a loose fit in the insulators to allow for thermal expansion. In the first design the insulators were made from special machinable ceramic under the trade name of "Ceramtec". The major problem with this material was that it is soft and brittle, so that in the later design a machinable glazed ceramic manufactured by McGeoch was used which proved to be much more satisfactory. The ion exit aperture was made from a flat stainless steel disc fixed on the cathode cylinder to give an aperture of length 3.5 mm and diameter 5 mm. The gas was admitted directly into the source via

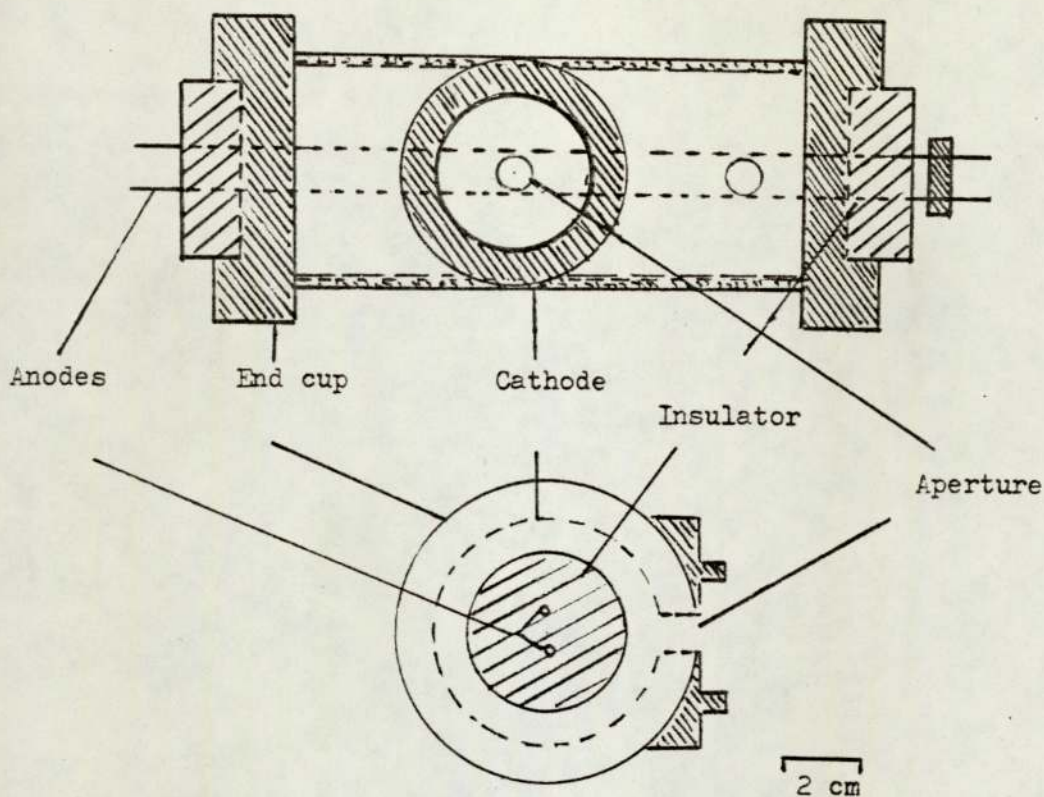


Figure 4.1 - The cylindrical ion source.

a stainless steel tube of diameter 5 mm and in order to prevent disturbing the emerging ion beam the gas inlet tube was situated near to one end of the cylinder. The size of the ion exit aperture could be varied by using two stainless steel discs with apertures 2 and 3 mm diameter positioned on the main aperture.

Another cylindrical source with exactly the same size and construction was modified so that it was possible to rotate the aperture around the cathode cylinder in order to monitor different parts of the beam. A schematic diagram of the modified aperture is shown in Figure 4.2.

The circular aperture has been replaced by a rectangular slot cut in the cathode perpendicular to its axis and extending from an angle of -10° to $+40^{\circ}$ as shown in the diagram. A twin ring of width about 10 mm and internal diameter 28 mm containing two holes 3 and 5 mm in diameter was held in position over the slot. By rotating

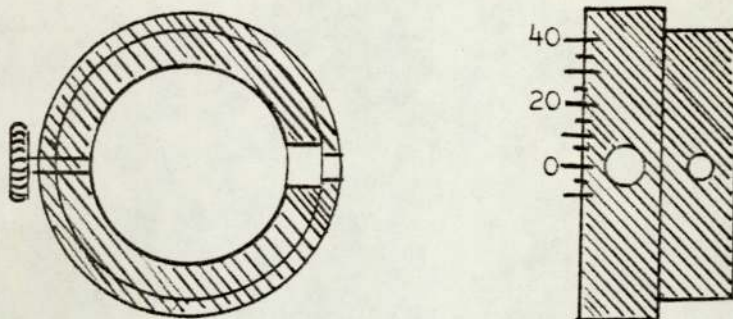


Figure 4.2. Rotating aperture ring.

the ring around the slot either of these holes could be positioned at the required angle, with respect to the central position.

Figure 4.3 shows an end-on view of cylindrical source including the anodes and ion exit aperture and shows the potential distribution and lines of force inside the source.

A diagram of the source was painted onto resistance paper by using a conducting paint, and the painted electrodes were energised by a Servomax field plotter. The equipotentials were expressed as the percentage of the anode voltage (V_A), and the saddle field line occurred at 80 - 90% of V_A .

4.2. The spherical source

In the first design of the spherical source Franks supported an anode ring between two guard rings at earth potential. However the source used in this work was a more recent design by Ion Tech Ltd., (B 11 source). A schematic diagram of this source is shown in Figure 4.4.

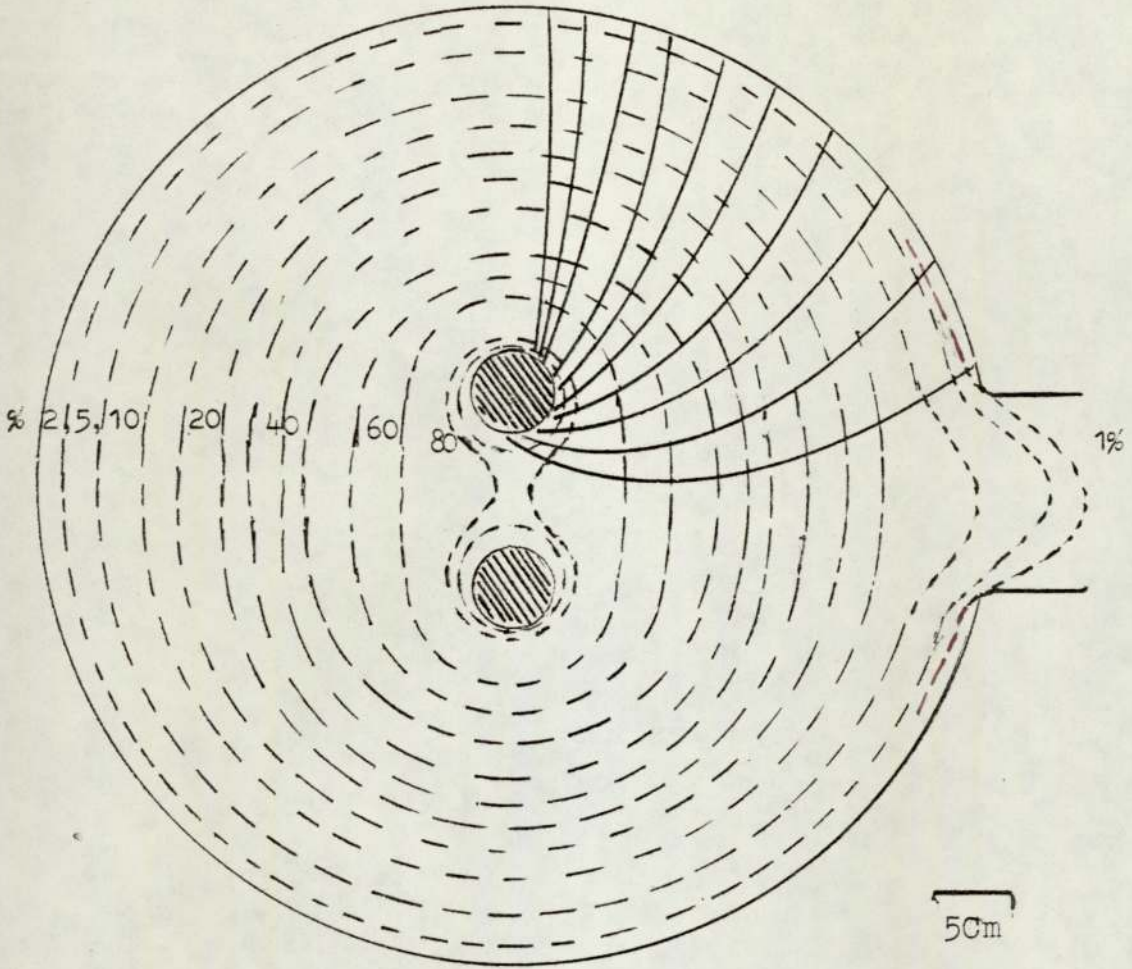


Figure 4.3. End on view of the cylindrical ion source showing the potential distribution.

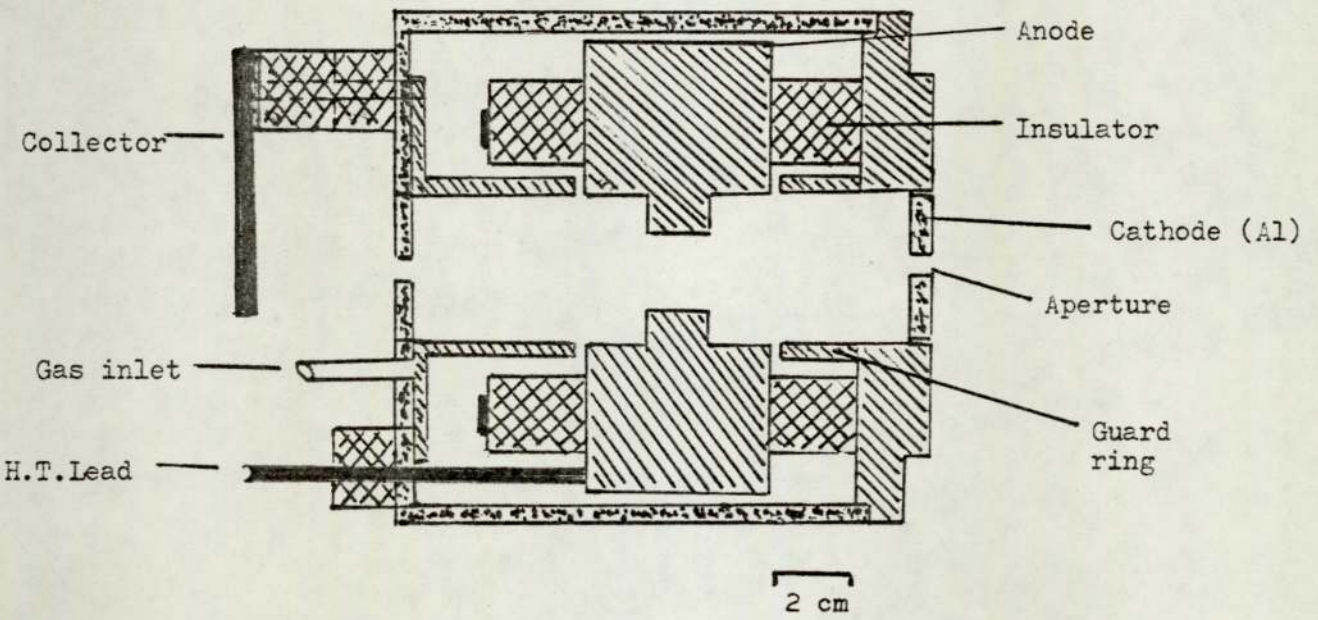


Figure 4.4. Fine beam ion source.

In this device the spherical configuration is produced by using two stainless steel cylinders length 8.5 mm and diameter 10 mm spaced either side of the stainless steel anode of aperture diameter 5 mm and thickness 7 mm. The ends of two cylinders are closed with two aluminium cathode discs of diameter 10 mm and thickness 1.5 mm. The ion beam is allowed to escape through 1.5 mm diameter holes in each disc. The insulators in this source were all made from a glazed ceramic material, and the whole assembly including the H.T. lead to the anode and gas injection tube are enclosed in an outer cylindrical Duralumin body. A nickel plate is placed opposite one of the apertures in order to monitor the ion beam. In this source in order to monitor different parts of the beam, various cathode discs with apertures, 0.55, 0.75, 1 and 2 mm in diameter were used. In addition other discs were used with apertures set at distances of 0.55, 0.75 and 1 mm off from the centre position in order to monitor the edges of the beam.

A cross sectional diagram of the source was painted on the resistance paper and is shown in Figure 4.5. The diagram shows the equipotentials in the spherical source. The saddle point field was found at about 70 - 80% of the anode potential. Of course it is realised that this technique is only approximate with this type of three dimensional geometry.

Photographs of the above mentioned sources are shown in Figure 4.6.

4.3 Vacuum system and experimental procedure

4.3.1 Vacuum system

In all the experimental investigations a conventional high vacuum system was used and a photograph of the system showing the

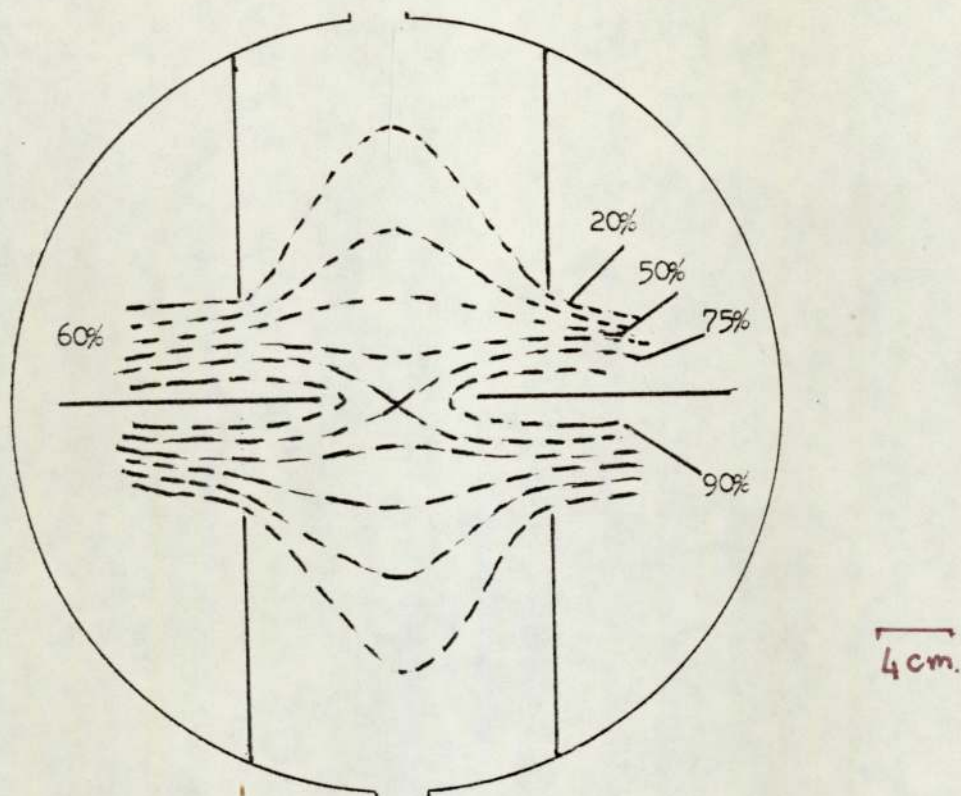


Figure 4.5. End-on-view of the spherical source showing the potential distribution.

experimental chamber and the associated electrical and gas supplies is given in Figure 4.7.

The system consisted of combination of a rotary pump with ultimate pressure about 1×10^{-3} Torr (after gas balast) and a water cooled oil diffusion pump using Santovac 5 fluid. This sytem gives an ultimate vacuum of less than 10^{-6} Torr. Santovac 5 was used because it is more resistant to decomposition in the presence of a high voltage discharge and is fairly chemically stable, non corrosive and non toxic at normal operation and temperature. The vacuum chamber was a stainless steel cylinder of internal diameter 12" and volume approximately 35 litres. The chamber contains two flanges carrying six high voltage connections, and three glass

Figure 4.6. Photographs of the cylindrical
and spherical ion sources

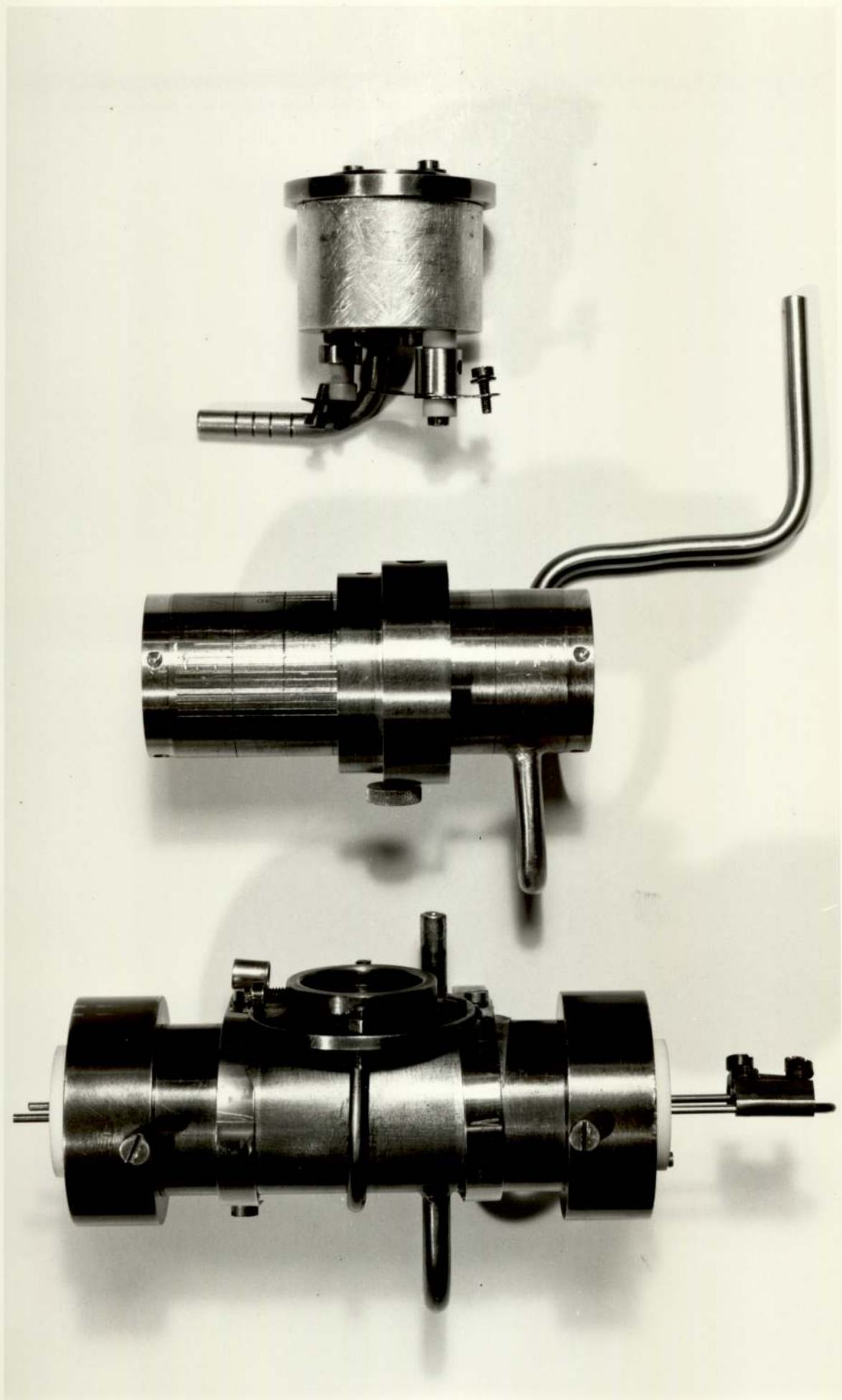
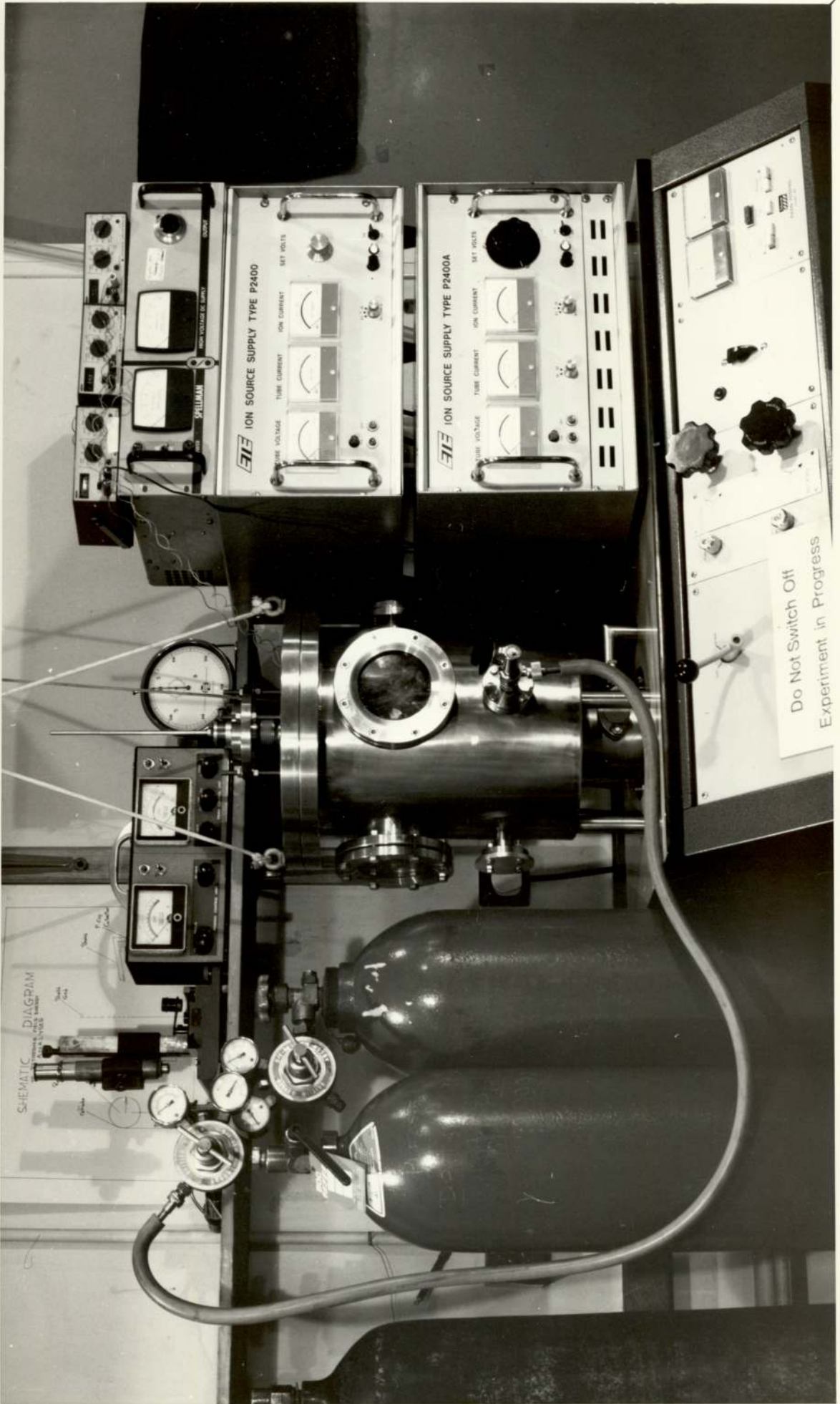


Figure 4.7. The photograph of the
experimental chamber and gas
supplies.



SHEMATIC DIAGRAM

Do Not Switch Off
Experiment in Progress

EIE ION SOURCE SUPPLY TYPE P2400

EIE ION SOURCE SUPPLY TYPE P2400A

viewing windows. The gas could be admitted to the source by a needle valve through a P.T.F.E. tube and the chamber pressure was measured by a Penning gauge covering the range 9×10^{-7} to 3×10^{-2} Torr. The Penning gauge was chosen for this work because although it is generally thought to be not very accurate it is more robust at high pressures compared to an ionisation gauge and also it was found that the reading with an ionisation gauge was affected by stray ions from the ion source. It was thus felt necessary to calibrate the Penning gauge for nitrogen against the McLeod gauge. Figure 4.8 shows the calibration of the Penning gauge against the McLeod, at 10^{-4} - 10^{-2} Torr for nitrogen and the calibration factor from this curve was obtained 0.97. Similar

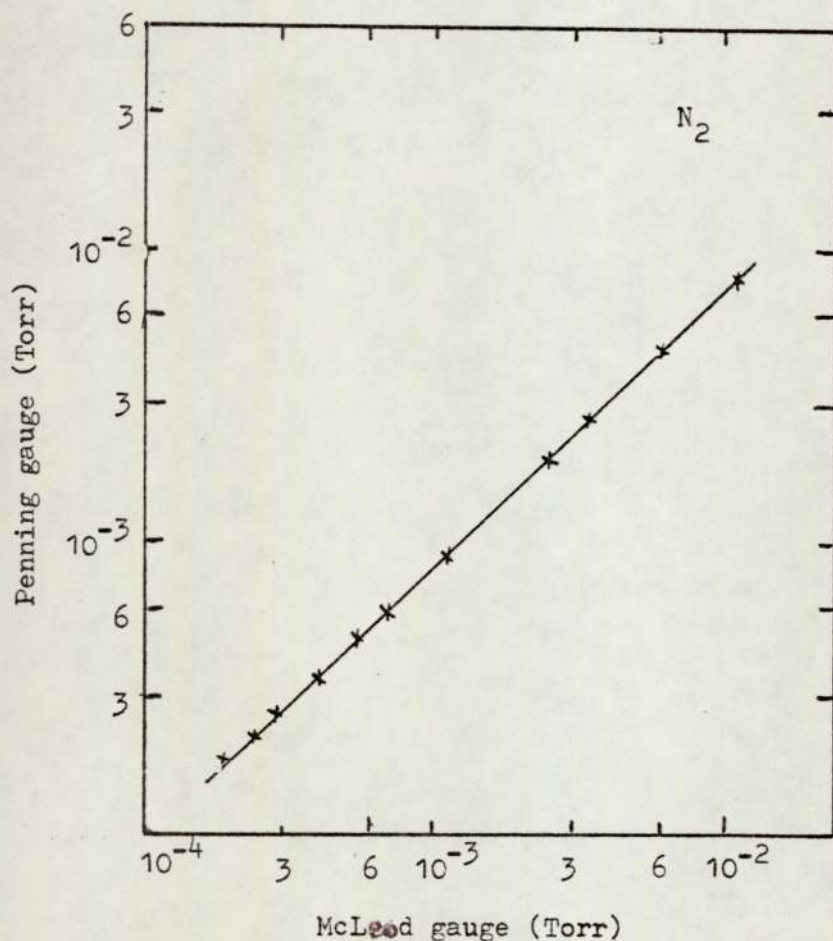


Figure 4.8. Calibration of the Penning gauge against the McLeod gauge using nitrogen.

experiments enabled the Penning gauge calibration for the argon and helium to be found, the calibration factors being 1.41 and 0.21, which compares well with the published values for this gauge of 1.4 and 0.18. Therefore the true pressure (P_t) was calculated from equation

$$P_t = \frac{P_g}{K}$$

where P_g is the gauge reading and K is the calibration factor.

It was also necessary to know the effective speed of the diffusion pump to be able to calculate the pressure inside the source. Thus the effective speed of the diffusion pump was measured by the constant volume method relative to the rate of rise of pressure as a function of time, and for argon gas it was found to be 90 l. sec^{-1} (Appendix 4.2/1).

Therefore the source pressure (P_s) was calculated from a knowledge of the chamber pressure, P_c , effective speed of the diffusion pump (S_E) and the gas conductance of the ion exit aperture (C), as is given in appendix 4.2/2.

4.3.2 Electrical circuit

A schematic diagram of ion source and its associated circuit is shown in Figure 4.9. A voltage stabilizer power supply capable of providing 50 mA at 20 kV was used and the anode voltage and current were measured with two moving coil instruments built in the power supply. The ion beam was collected by an earthed Faraday cup which is described in detail in section 4.6, and the ion beam current was measured by a multirange three-digit microammeter with an accuracy of 0.5%. In some experiments when it was necessary to keep the anode current constant a current stabilized power supply was used.

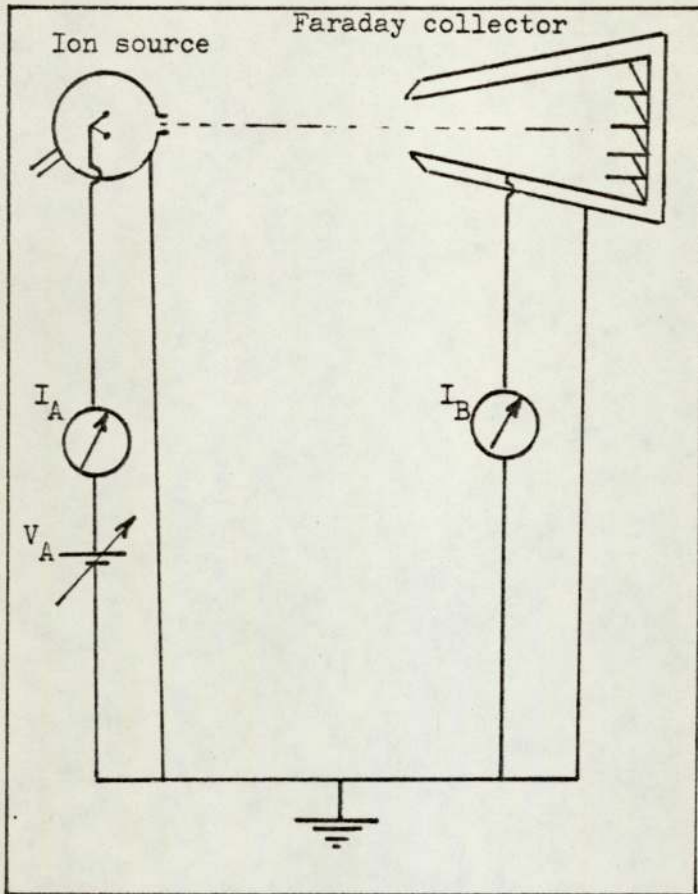


Figure 4.9. Electrical circuit for the ion current measurements.

4.3.3 Principle of the source operation

The cylindrical source with 5 mm aperture operates in the range of about $4 \times 10^{-3} - 7 \times 10^{-5}$ Torr chamber pressure. Typical operation conditions were 0.2 to 8 kV anode voltage (V_A) and approximately 0.4 - 6 mA anode current (I_A). At an early stage the ceramic insulators had been identified as a problem causing the instability when operating at tube currents more than 4 mA or tube voltage over 7 kV. Another problem limiting the source operation and running time, was due to the breakdown occurring across the insulators and anodes after using for about 10 hours. It was due to the build up of sputtered cathode material on the insulators and anodes, and some carbon deposition presumably caused by the vacuum pump fluids. An X-ray analysis of this deposit showed that it

mainly consisted of stainless steel, carbon, and argon (when argon gas was used). Figure 4.10 shows the electron micrograph of this deposit on the insulator and anodes.

An attempt was made to overcome these problems in order to operate the source more efficiently and for a longer time, and this was eventually achieved by using a glazed ceramic and very high purity gas. As a result it was possible to operate the source for as long as 20 hours without the need for cleaning. However in all experiments with this source it was found necessary to operate it at high power for about 30 minutes before starting the measurements in order to outgas the source and ion clean the cathode.

The operating pressure of the spherical source with two 1.5 mm ion exit apertures was at about 1×10^{-3} to 1×10^{-5} Torr. Typical operating conditions were about 0.5 to 7 kV anode voltage and 0.2 to 12 mA anode current. One of the ion beams was collected by a simple collector, so that the source could be continuously monitored during operation independently of the nature of target or collector. A problem limiting the source operation was breakdown due to the black contamination on the insulators and cathodes, and a widening of the ion exit aperture in the aluminium cathode discs due to sputtering causing a rapid increase in source pressure, and hence a deterioration in performance and efficiency of the source. Figure 4.11 shows two micrographs of aluminium discs (a) when the aperture was widened after about 10 hours source running, and (b) the black contamination on the cathode. This was overcome by replacing the aluminium discs with stainless steel discs. The source had to be cleaned after about 15 hours, and experiments showed that the time required for outgasing the insulators and cathode ion cleaning in this source was about 10 minutes.



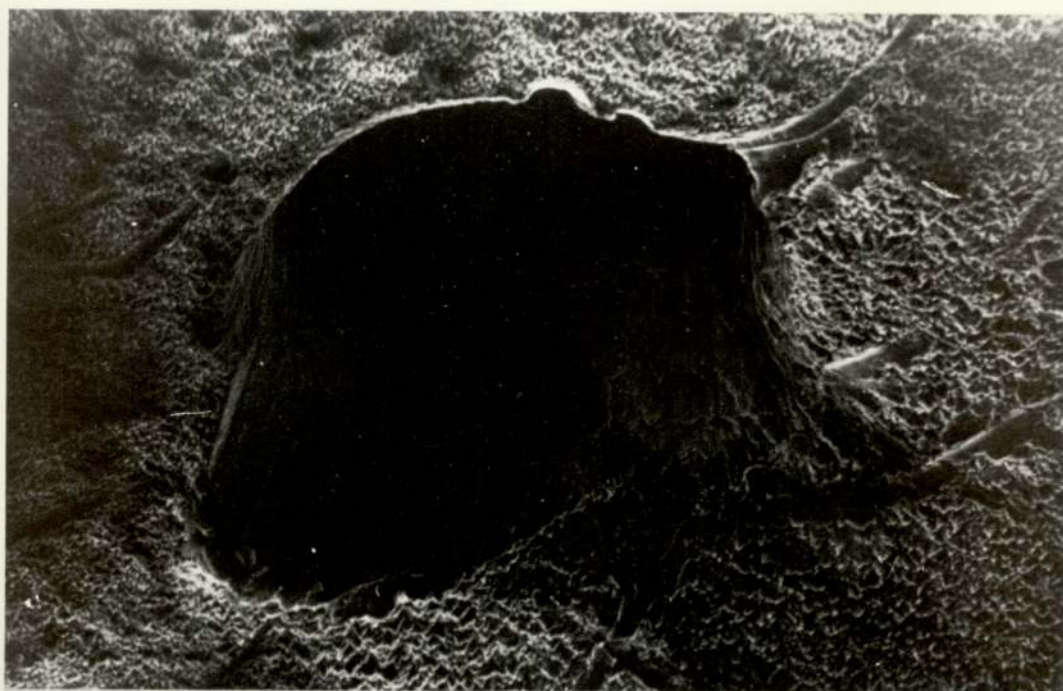
(a)

2.00X



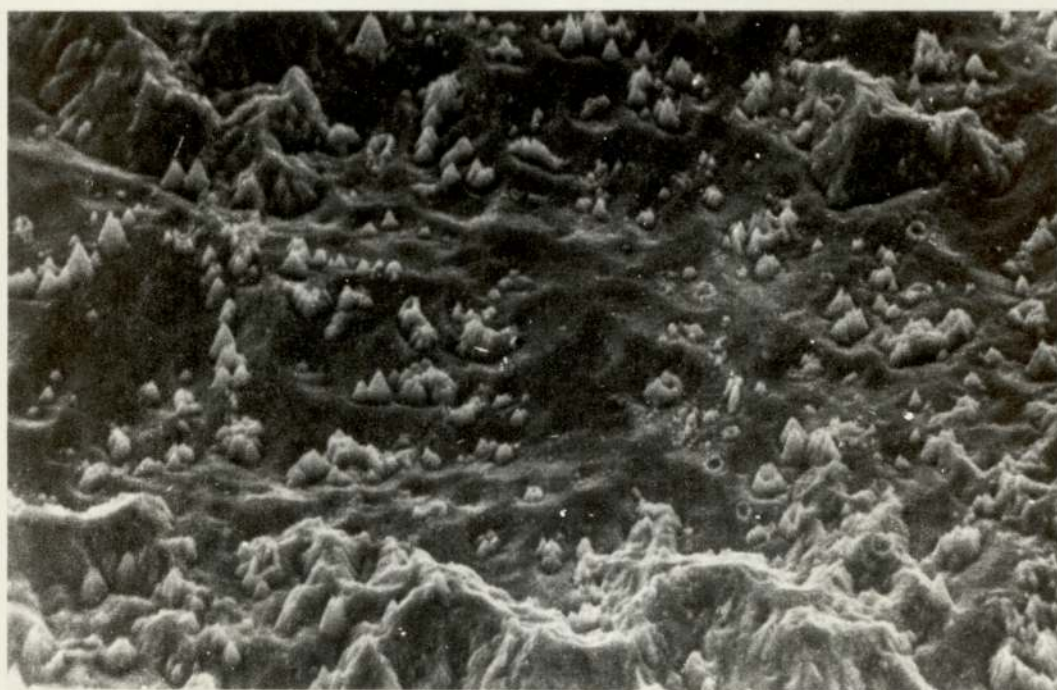
(b)

Figure 4.10. Electron micrographs of carbon deposit on (a) ceramics and (b) anodes in the cylindrical source.



(a)

200X



(b)

Figure 4.11. Electron micrographs of cathodes in the spherical source.

4.4 Development of the Faraday cup collector

In much of the initial work with these ion sources a simple flat plate or a small Faraday cup collector of Ni or some other metal was used as the ion collector. Consequently the effect of the yield of secondary electron on the collector material and also the necessity of a trap for secondary electrons was not always taken into account.

For example Rushton⁴⁵ used a small cylindrical Faraday cup with a relatively small entrance aperture, and Ghander⁴⁷ used a V-shaped unshielded copper collector. It was therefore decided to design and test a collector to;

- (a) have less yield of secondary electron emission
- (b) to be efficient at retaining the secondary electrons, and
- (c) have a relatively large entrance aperture to admit the total ion beam at a distance relative to the beam divergence.

In studying the effect of collector material on yield, Arifov and Rakhimov⁵⁹ obtained a linear relation between the secondary electron emission coefficient and the work function and showed that the yield decreases as the work function increases. Later Arifov et al⁶⁰ showed that as the work function of ion collector material increases, the secondary electron emission due to the ion bombardment decreases. Therefore in this present work nickel metal was used for the collector because of its high work function (5.24 eV) and relative ease of construction. Furthermore an attempt was made to design a collector whose shape was such that it was efficient at retaining the secondary electrons. Each design was tested by monitoring the residual collector current due to the secondary electrons produced by energetic neutrals present in the beam. During these measurements the positive ions were removed

from the beam by deflecting them with a grid held at a positive potential, and placed between the ion source and the collector as will be described in detail in Chapter 6. The residual current was called the "neutral" current.

Six designs of collector were used and tested. One was a flat nickel plate and the last five are shown to scale in Figure 4.12.

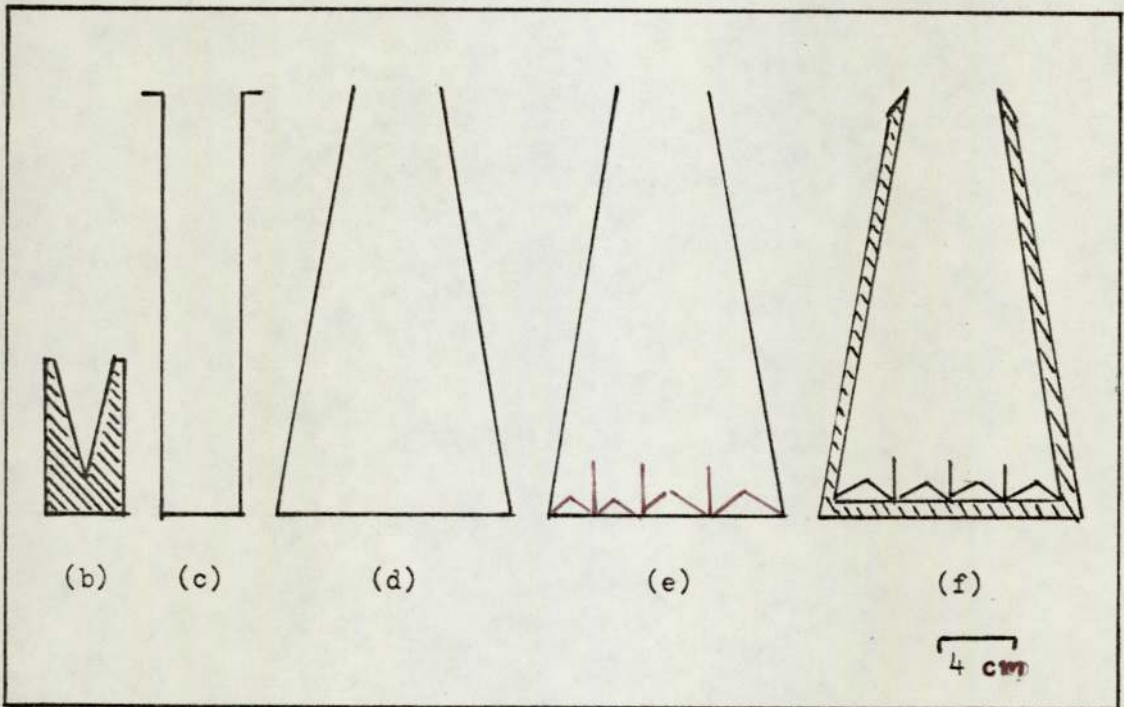


Figure 4.12. Schematic diagram of the different ion beam collectors.

The results of these measurements are summarised in Table 4.1 which shows the neutral current for all six collectors using the cylindrical source with a 5 mm aperture under different operating conditions.

TABLE 4.1

Variation of "neutral" current for
different collectors using the cylindrical source

Operating conditions		"neutral" current - μA					
V_A kV	I_A mA	(a)	(b)	(c)	(d)	(e)	(f)
4	2	3.6	1.4	0.7	0.40	0.25	0.10
5	2	3.0	2.0	0.65	0.30	0.10	0.10
6	2	2.4	0.6	0.41	0.30	0.10	0
5	3	7.0	2.4	1.40	0.60	0.40	0.20
6	3	5.2	3.6	0.30	0.40	0.20	0
7	3	3.9	1.7	0.3	0.2	0.10	0

The flat nickel plate collector (a) as expected has the highest "neutral" current which is as much as 25% of the collector current. Collector (b) - the one used by Ghander⁴⁷ - is a V-shaped copper collector of aperture diameter 25 mm and length 50 mm and was more efficient than the flat plate but still the "neutral" current was over 15% of the total current. Collector (c) is a cylindrical nickel collector of length 125 mm and entrance aperture 27 mm which is slightly more than the maximum ion beam divergence at 70 mm from the source. Table 4.1 shows that "neutral" current has reduced to about 7% of the total beam current. Thus in spite of the high length to diameter ratio, secondary electrons were still escaping from this collector. Therefore a conical shape of base diameter 78 mm, but

the same length and aperture as for collector (c) was designed as shown in Figure 4.12d. This collector showed further reduction in the "neutral" current which was now about 3.5% of the collector current. In an attempt to reduce the secondary electron current still further, a few nickel plates of about 25 x 50 mm were welded inside the cone, perpendicular to the larger base of the same size collector as shown in Figure 4.12(e). The results showed that the residual current was now reduced to about 2% of the beam current

The final collector (f) was the same as collector (e) except that an earthed screen was constructed around the collector as shown in Figure 4.12(f). The "neutral" current was seen to have been reduced even further and varies from 0-1% of the total beam current. This additional improvement was due to the elimination of any collection of low energy and reflected ions in the experimental chamber.

The table also shows that at constant I_A the "neutral" current reduces with increasing V_A . It will be shown later in Chapter 7 that this is due to a decrease in the percentage of neutrals in the beam as V_A is increased.

Therefore in experiments described in the remaining chapters collector (f) was used to measure ion currents.

CHAPTER 5

SOURCE CHARACTERISTICS AND MODES OF OPERATION

5.1 Introduction

The discharge characteristics for both the cylindrical and spherical ion sources were studied with argon, nitrogen and helium gases. Before the characteristics were recorded the system was pumped down to a pressure of about 10^{-6} Torr and the chamber was filled to the nearly atmospheric pressure with the particular gas and again evacuated. This flushing procedure was repeated several times in order to reduce the partial pressure of the residual gases in the chamber. The sources were operated for sometime and outgassed before taking measurements. If these precautions were not taken, it was difficult to obtain reproducible results. Furthermore reproducibility was found to be better if measurements were taken as the pressure was decreased rather than increased. However at each value of pressure variations of V_A with I_A were obtained by measuring I_A when V_A was decreased.

5.2 Characteristics of the ion sources

A - Cylindrical source

The characteristics obtained for the cylindrical source were of the same form as those produced by Rushton⁴⁵ and Ghander⁴⁷ using a similar design of ion source but with various geometries of ion exit aperture. The usual forms of current voltage characteristics were taken for Ar, N₂ and He.

Figure 5-1 indicates the variation of the anode current, I_A , and anode voltage, V_A , for various pressures using a 5 mm diameter aperture. The range of pressures given in these curves show that the

measurements were taken for 10^{-3} Torr down to 8×10^{-5} Torr. It was not possible to extend this range because at higher pressures gas breakdown occurred in the chamber and at lower pressure breakdown occurred across the insulators. The linearity of the curves especially for anode voltages over 3 kV and less than 8 kV indicates a stable operation of source in which it was possible to take I_A up to 8 mA. The results showed that it was not possible to operate the source at a threshold voltage of less than 0.5 kV or more than 14 kV. Figure (5-2) shows the corresponding curves for nitrogen from 1×10^{-3} Torr to 6×10^{-5} Torr chamber pressure. Taking into account the gauge calibration factors 1 and 1.4 for nitrogen and argon respectively, it can be seen that the source operates over a wider range of pressure for nitrogen. Variation of the ion beam current, I_B , is plotted against I_A at different pressures for argon and nitrogen and are shown in Figure (5-3) and (5-4) respectively. For both gases the curves fan out from the origin and show that the slope increases as the pressure decreases. However between 4×10^{-4} Torr to 9×10^{-5} Torr for argon, and 2×10^{-4} Torr to 8×10^{-5} Torr for nitrogen, the experimental points lie on one curve. This shows that below a given pressure (4×10^{-4} Torr for Ar and 2×10^{-4} Torr for N_2) the ion current is constant for all pressures at a fixed value of I_A , whereas above these pressures the ion current decreases when I_A is constant.

These characteristics imply that at lower pressures the oscillating electrons are effectively confined to a narrow region between the anodes, whereas at higher pressures the electrons are not oscillating so effectively and the corresponding electron path lengths are relatively small. Furthermore the ion beam density, defined as the number of ions in unit volume of the source, varies

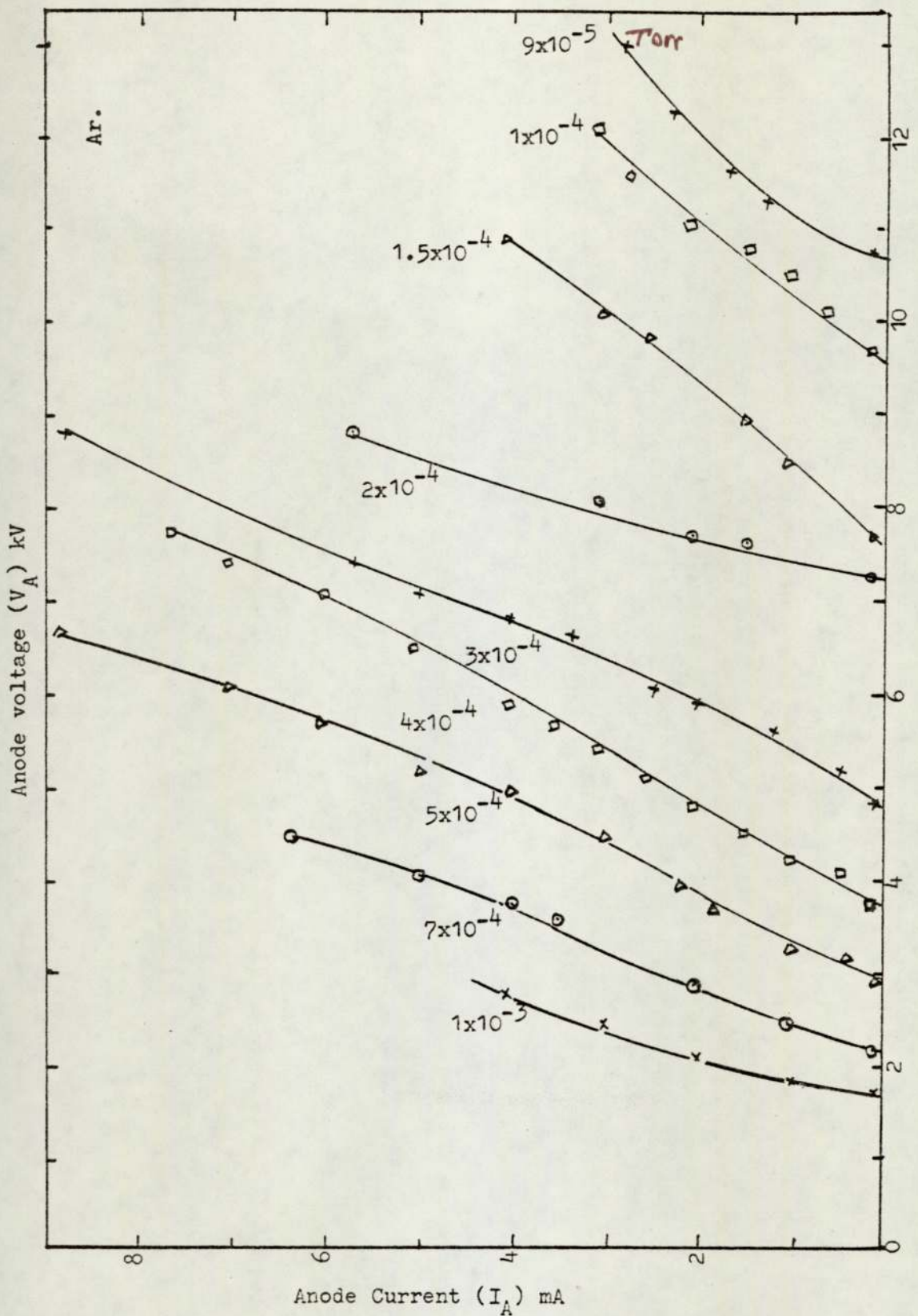


Figure 5.1. Variation of anode current with anode voltage for the cylindrical source with 5mm aperture using argon.

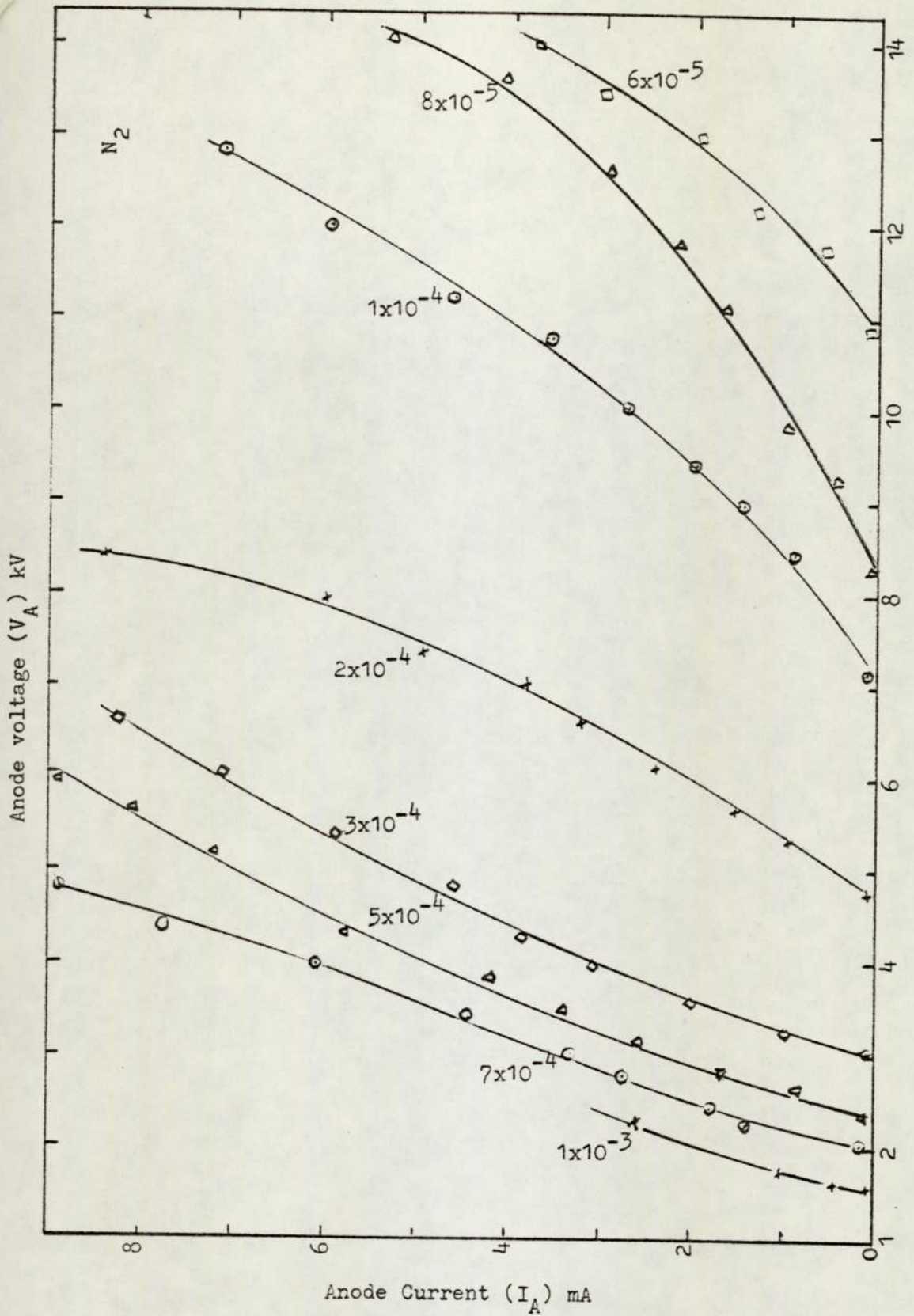


Figure 5.2. Variation of anode current with anode voltage for the cylindrical source with 5 mm aperture using nitrogen.

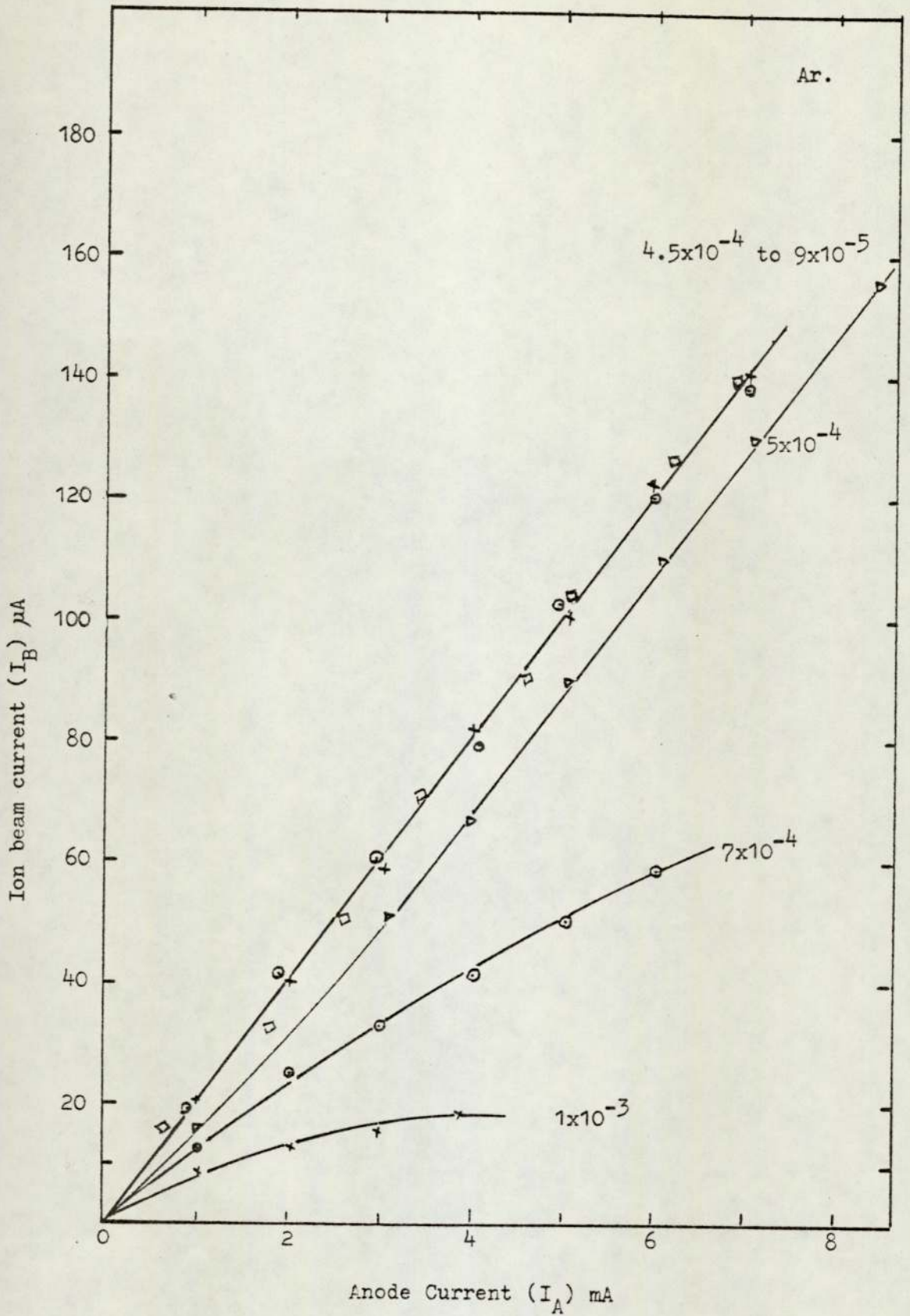


Figure 5.3. Variation of ion beam current with anode current for the cylindrical source with 5 mm aperture using argon.

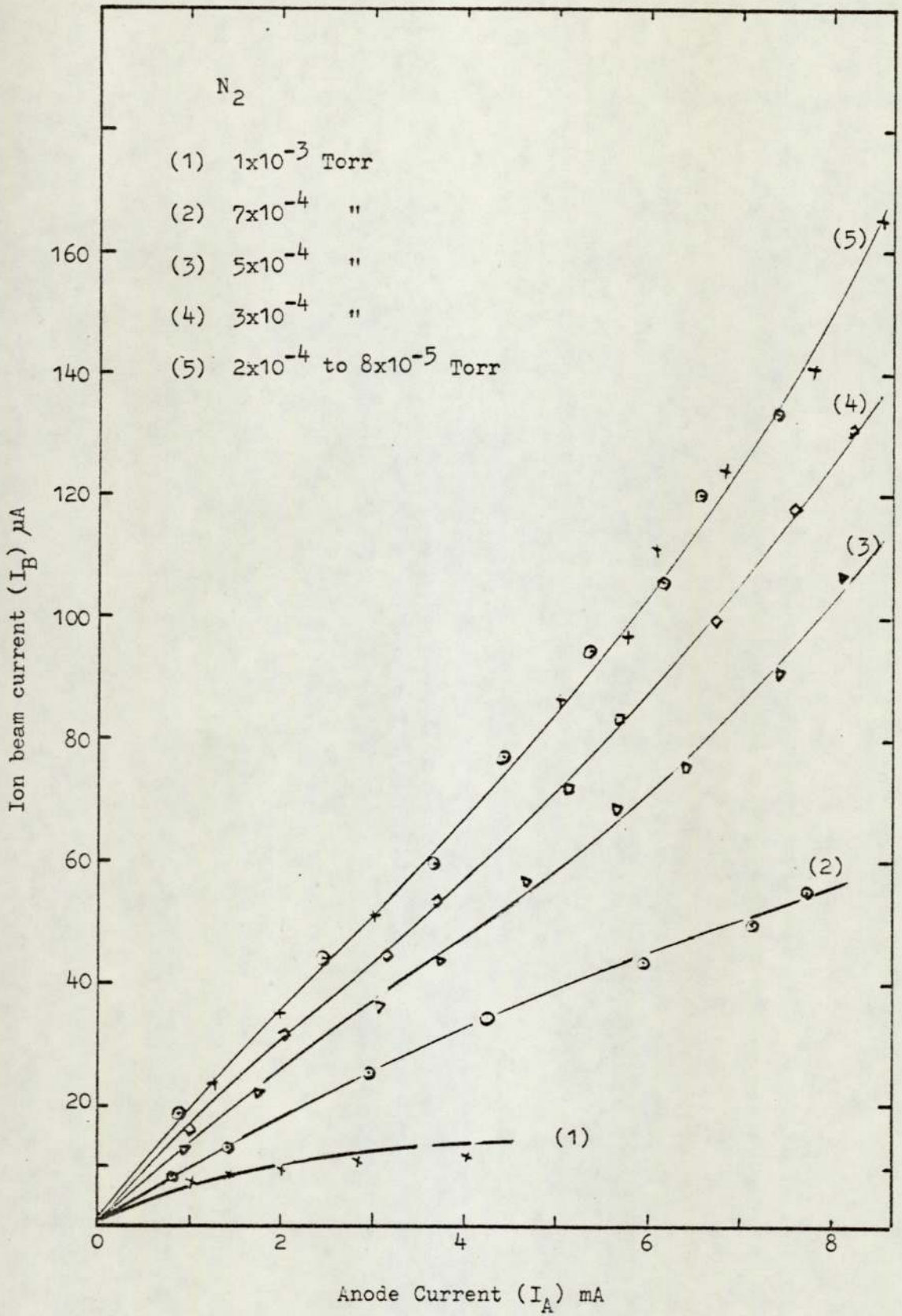


Figure 5.4. Variation of ion beam current with anode voltage for the cylindrical source with 5 mm aperture using nitrogen.

in different parts of the plasma and thus the intensity of the extracted beam at different parts relative to the central aperture changes. Figure 5-5 shows the variation of the average ion beam intensity for Ar at different radial positions of a 5 mm aperture using the adjustable aperture as described in section 4-2.

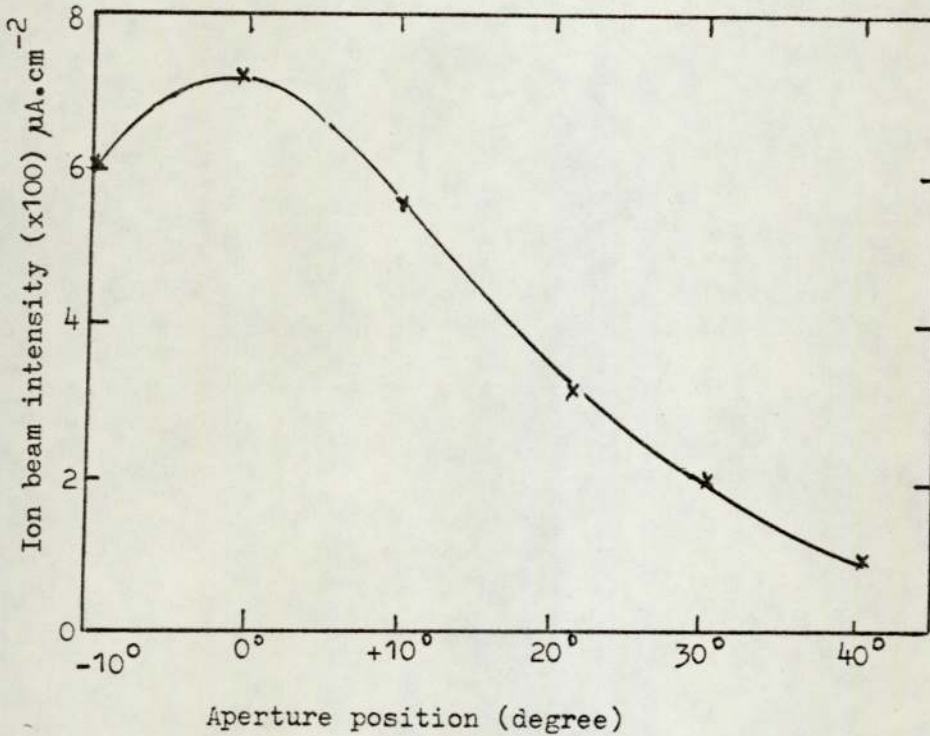


Figure 5-5. Angular distribution of the ion beam emerging from a 5 mm aperture using the cylindrical source for argon.

This curve shows that the ion beam is maximum at the central position, and decreases at either side of it. Furthermore it is appropriate to express the ion beam current as a function of input power at different chamber pressures. A set of these curves for this source with a 5 mm aperture and using argon gas is given in Figure (5-6). The same family of curves for nitrogen is given in appendix 5.2/3. These characteristics show that for a given value of power, higher beam current can be obtained by selecting different values of pressure. For example the maximum ion beam current of about 200 μA with 100 W input power is at 3×10^{-4} Torr chamber pressure.

B - Spherical source

The variation of anode voltage, V_A , with anode current, I_A , for the spherical source with two 1.5 mm apertures using argon gas at various chamber pressures is shown in Figure (5-7). Figure (5-8) also shows the change of ion beam current, I_B , with anode current at the same conditions. These characteristics show that the source operates from 2×10^{-5} Torr up to about 1×10^{-3} Torr. It was thought that a higher ion beam current could be obtained by using a larger ion exit aperture, or that the source performance would be better with a smaller aperture and hence lower pressure. However neither was found to be the case. With the larger aperture a greater fraction of ions are extracted but the source performance deteriorates due to the increased distortion of the field in the region of the aperture (Dhariwal⁴⁴). On the other hand when very small apertures are used and therefore the perturbation of the field is negligible the increased performance of the source is not sufficient to compensate for the reduced fraction of ions extracted. In addition using these extreme sizes of aperture, reduces the operating range of the source.

However this source with two 1.5 mm apertures at 4×10^{-5} Torr pressure produced an ion beam of about 2.7 mA cm^{-2} which was greater than the largest value of about 1.4 mA cm^{-2} recorded for the cylindrical source. The curves show that the source operates from a minimum voltage of a few hundred volts up to about 9 kV but its performance is more effective between 1.5 to 7kV or from 4×10^{-5} Torr to 3×10^{-4} Torr chamber pressure.

Nevertheless it was extremely difficult to use the source at higher pressures than 10^{-3} Torr or lower than about 2×10^{-5} Torr due to breakdown in the chamber or across the insulators respectively. Figure (5-8) also shows that in spite of very high anode current at

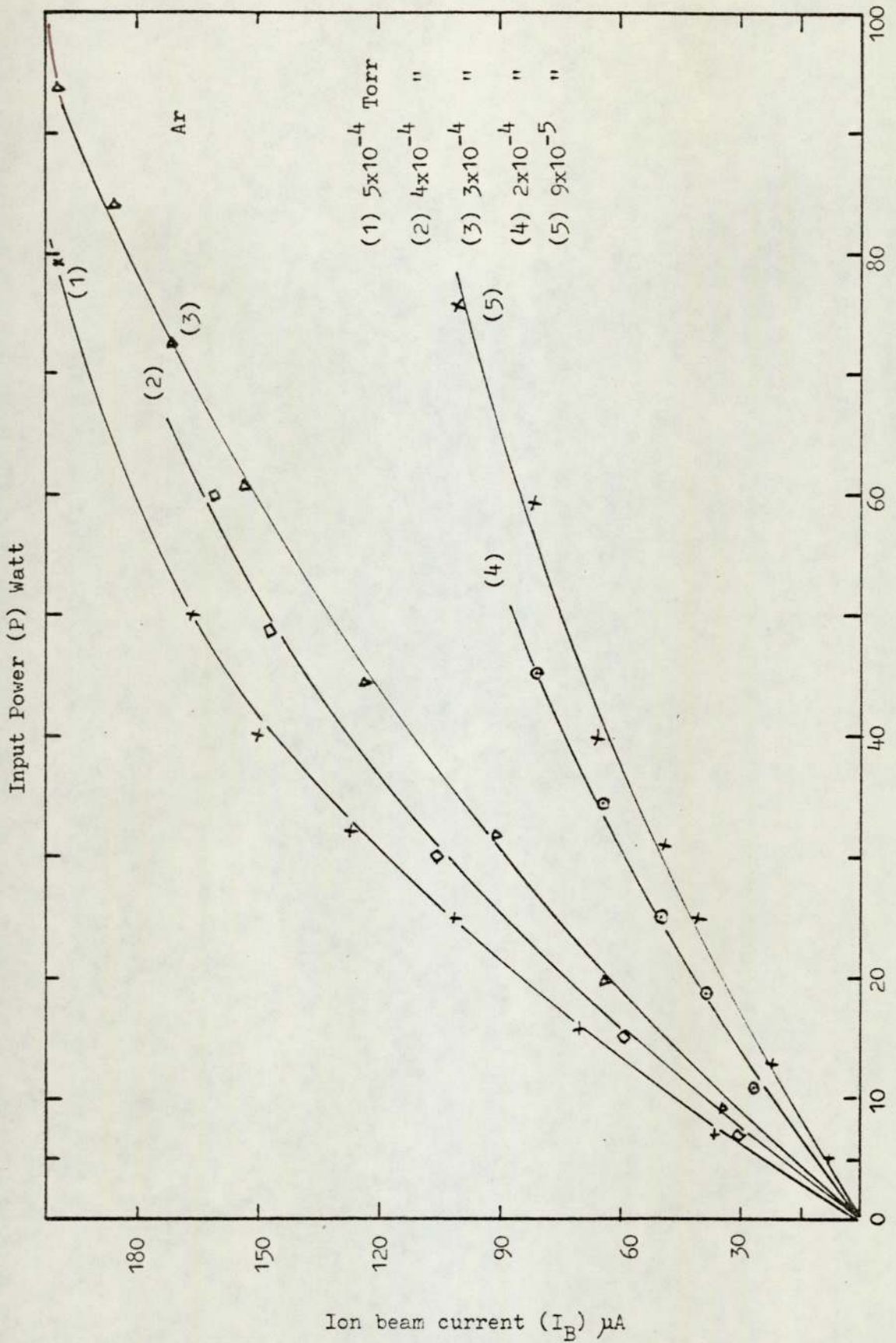


Figure 5.6. Variation of ion beam current with the input power for the cylindrical source with 5 mm aperture using argon.

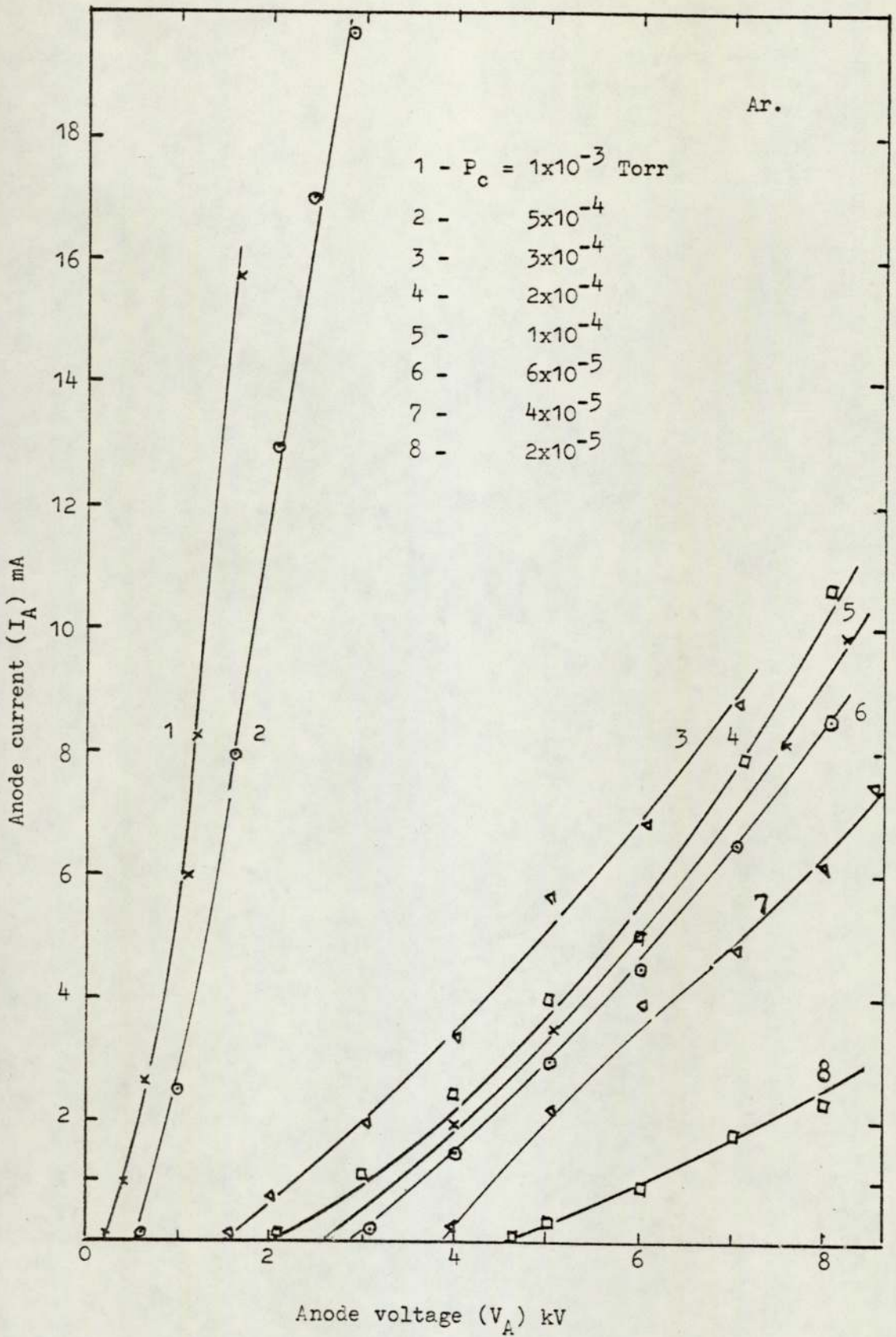


Figure 5.7. Variation of anode current with anode voltage for the spherical source with 1.5 mm aperture using argon.

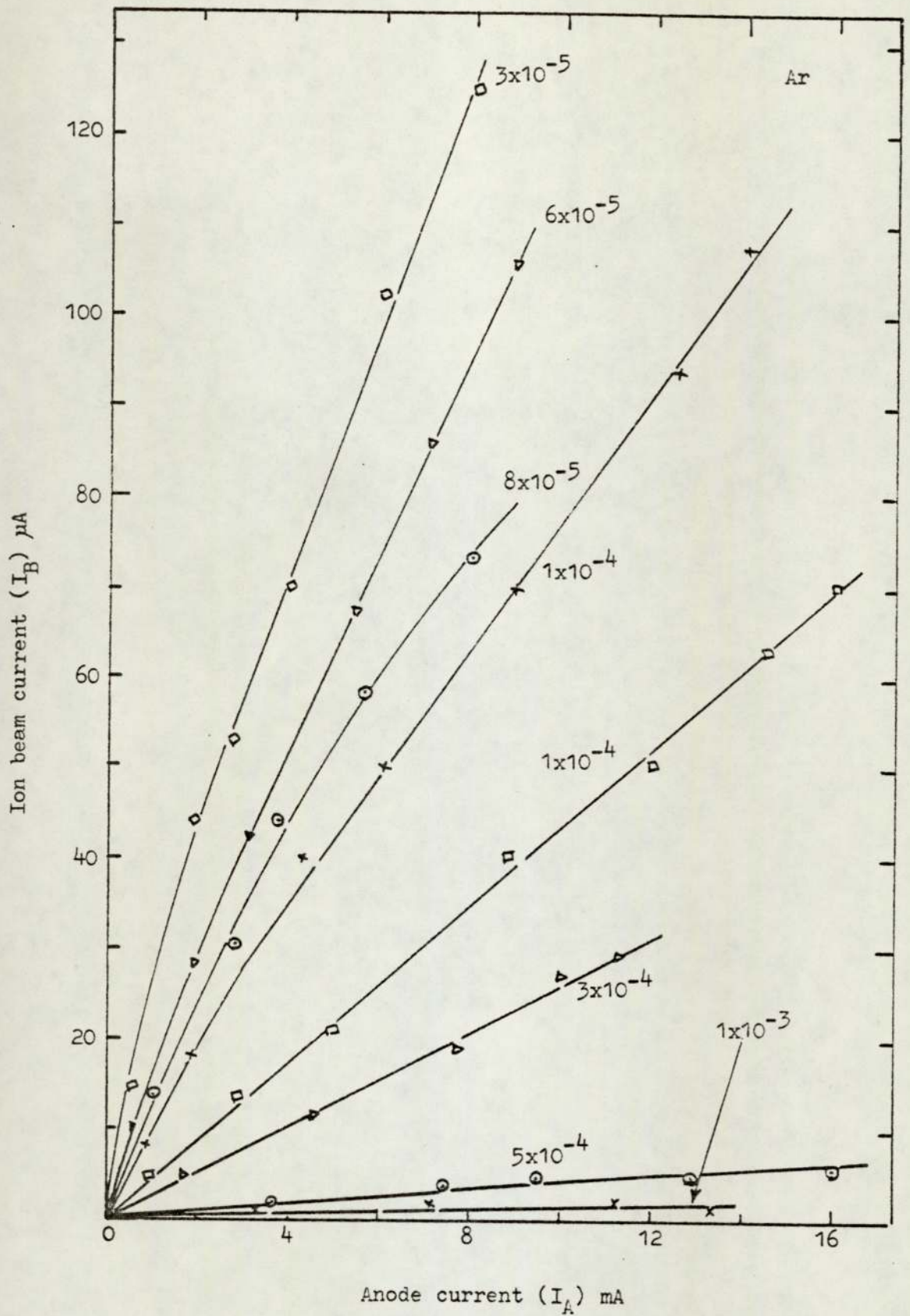


Figure 5.8. Variation of ion beam current with anode current for the spherical source using argon.

5×10^{-4} Torr, the ion beam current was less than 10% of the maximum current at low pressures. The corresponding curves using nitrogen and helium are given in appendix 5-2/4.

A glance at the figures 5.7 and 5.8 shows that they are similar to those for the cylindrical source and it is possible to say that the dispersion of the curves between 1×10^{-4} Torr to 4×10^{-5} Torr is more than in other regions of pressure. Consequently the density of the ions inside the source is not uniform, thus variation I_B relative to I_A , $\frac{dI_B}{dI_A}$, varies for different positions of the aperture. Figure (5-9) shows the variation of the ion beam intensity emerging from a 0.75 mm aperture at angles of 3° , 3.5° and 7.5° with respect to the central position, at $V_A = 5$ kV and $I_A = 2$ mA.

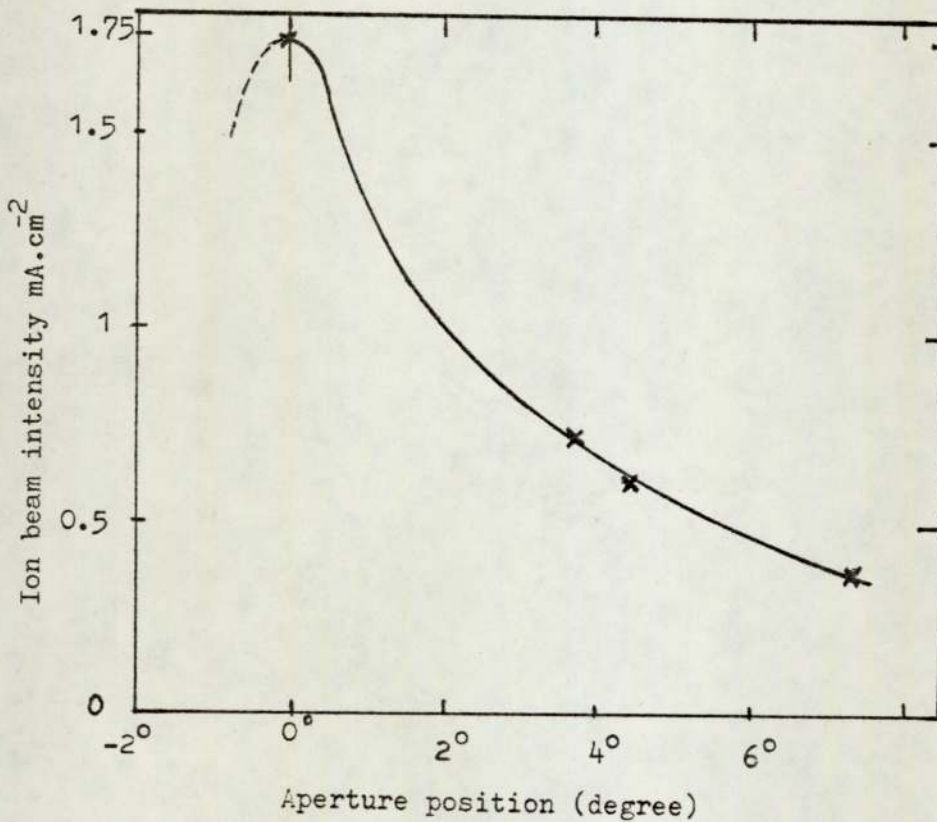


Figure (5-9). Angular distribution of the ion beam intensity of the spherical source with 1.5 mm apertures for argon.

Figure (5-10) shows the discharge input power of this source using argon. These curves show that the source with a low beam current, for example of about 10 μ A, at the highest chamber pressure requires a high power of about 80 watts, whereas in the cylindrical source this value of power occurs at a low pressure and high beam current of 100 μ A. Also these curves show that to produce a given beam current, this can be obtained at different source powers.

5.3 Modes of operation

It has already been reported that the modes of operation have been investigated by Fitch et al⁴³, and Ghander⁴⁷ for the cylindrical source with circular and rectangular apertures, but there was a significant difference between their results. In the latter work the results were difficult to interpret and in fact they were different for different gases and apertures. An attempt has thus been made to operate these two sources in various conditions, size of aperture and using several gases in order to clarify these problems.

A - Cylindrical source

The variations of both ion beam current and the anode voltage with the chamber pressure for the cylindrical source are shown in Figure 5.11 and Figure 5.12 using argon at constant anode currents of 1, 3 and 5 mA. Figure 5-11 shows that the beam current is constant from the lowest pressure of 8×10^{-5} Torr up to about 5×10^{-4} Torr, for all curves. The anode voltage in this range of pressure decreases from about 14 kV down to 2 to 4 kV in a very smooth manner as shown in Figure 5.12. This range of operation is characterised by a high ion beam current and can be referred to as the "oscillating mode", because it is feasible to say that in this range of pressure almost all electrons effective in ionisation oscillate with a long path length. However a sudden decrease of

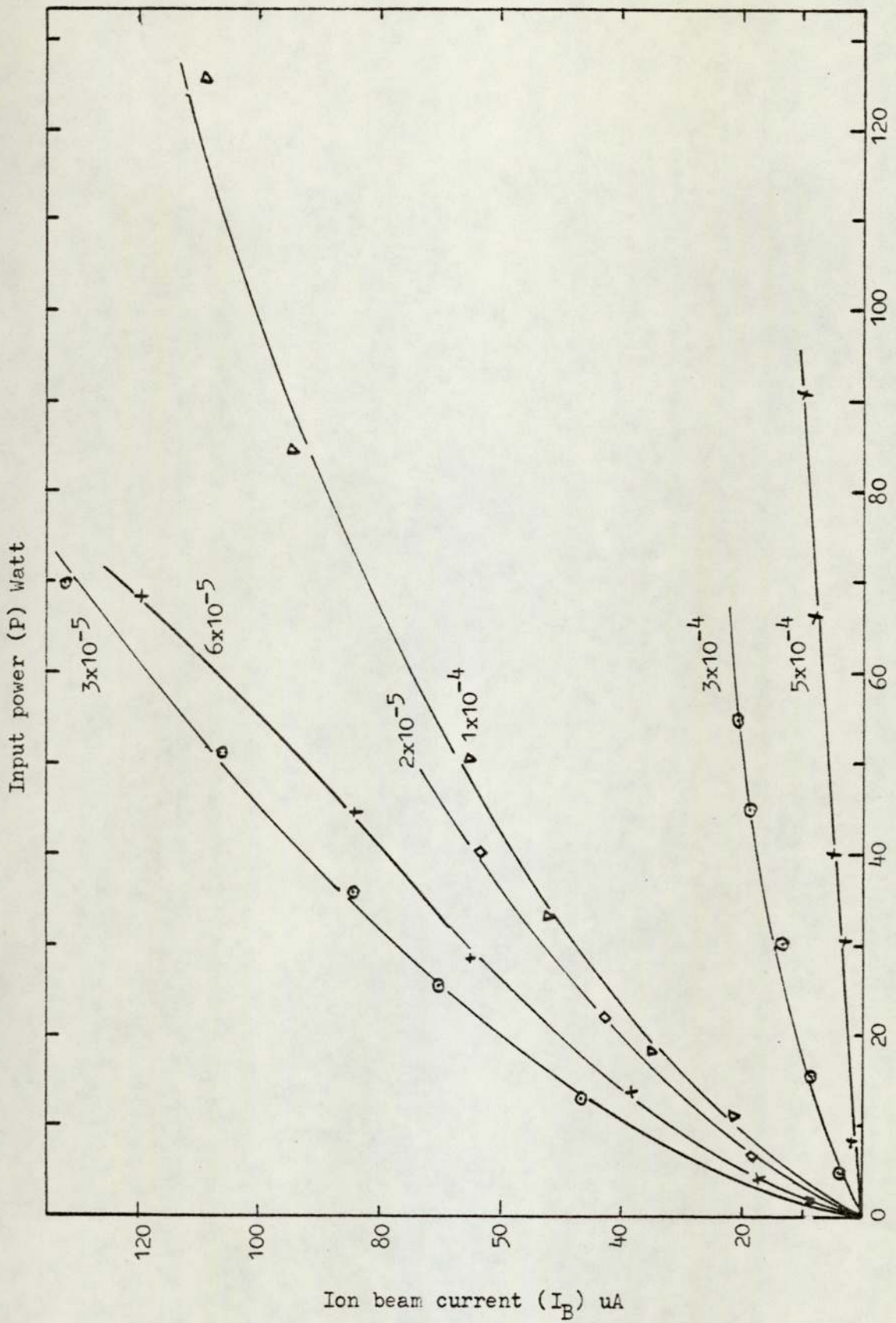


Figure 5.10. Variation of input power with ion beam current for the spherical source with 1.5 mm aperture using argon.

the ion beam current occurs as is illustrated in Figure 5.11, when the pressure increases from 5×10^{-4} Torr to 1 to 1.5×10^{-3} Torr, especially at the higher anode currents. The corresponding anode voltage drops from only 3 to 1 kV. In this range of pressure the mean free path of the electrons is still long enough for a moderate degree of ionisation relative to the previous mode. Thus their motion will not be confined to oscillating between the anodes and the source performance changes very rapidly. This range is called "transition mode". Furthermore at pressures higher than 1.5×10^{-3} Torr the ion beam current does not exceed more than a few μA . At this chamber pressure the voltage is considerably reduced and never more than 1 kV. This is due to the fact that at this high pressure the electrons will not be able to produce a high rate of ionisation due to their small path length. This condition of source operation is called the "glow discharge mode". Similar curves to those shown in figures 5.11 and 5.12 have been obtained for different apertures and some of these are given for nitrogen and helium in Appendix 5.3/5.

In order to get a better appreciation of these modes of operation, a cylindrical source was modified to incorporate a pyrex glass insulator in place of the ceramic one. The discharge could thus be viewed at various operating pressures. The photographs in figure 5.13 show three particular cases, (a), (b) and (c), which have been taken at pressures corresponding to the "oscillating", "transition" and "glow" modes. It can be seen that in the "oscillation" mode the discharge is well confined between the two anodes, whereas in the "transition" mode the discharge has spread out considerably. In the final photograph, (c), the discharge is distributed over nearly all the volume when it is in the "glow mode".

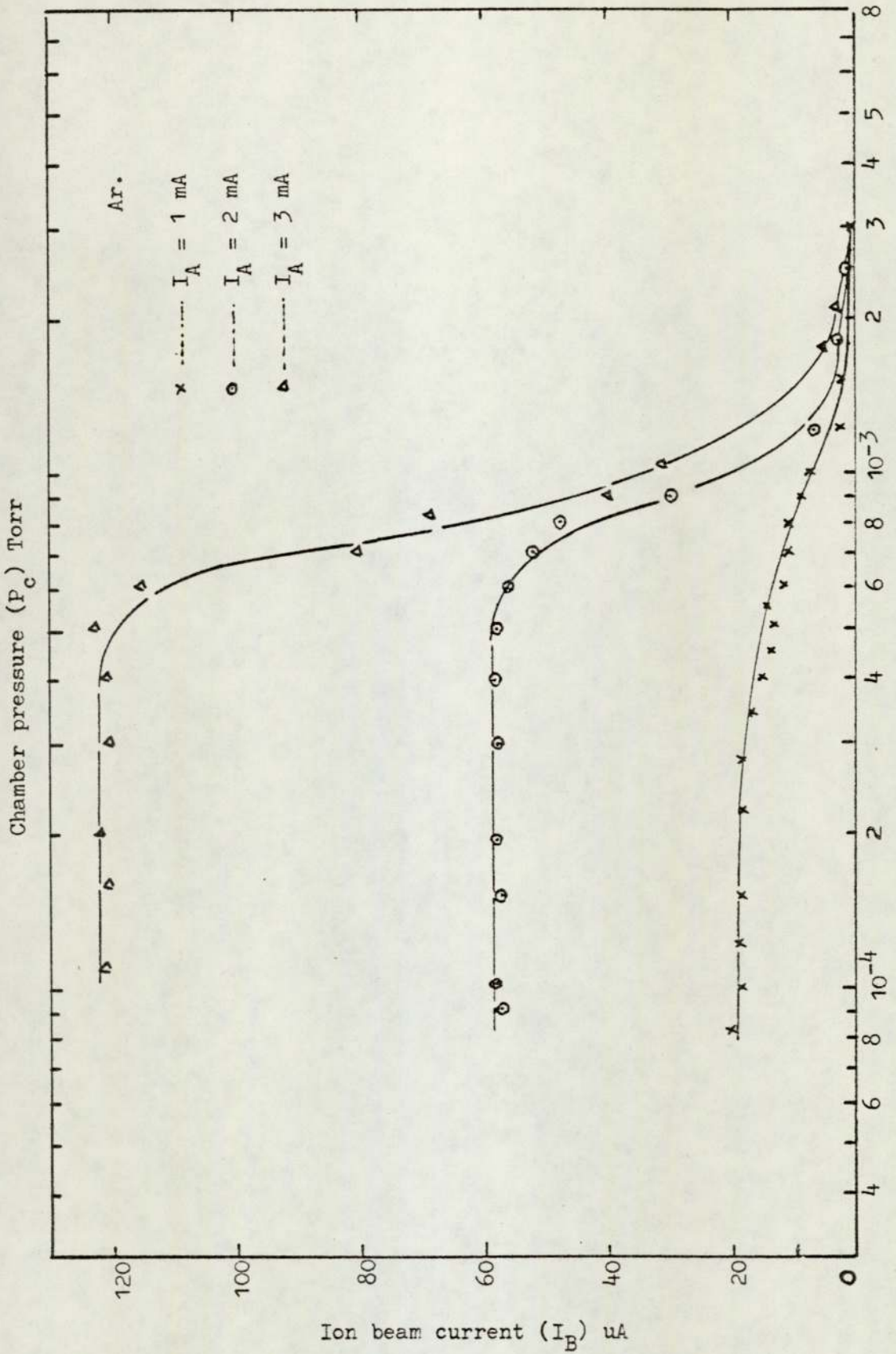


Figure 5.11. Variation of ion beam current with chamber pressure for the cylindrical source using argon.

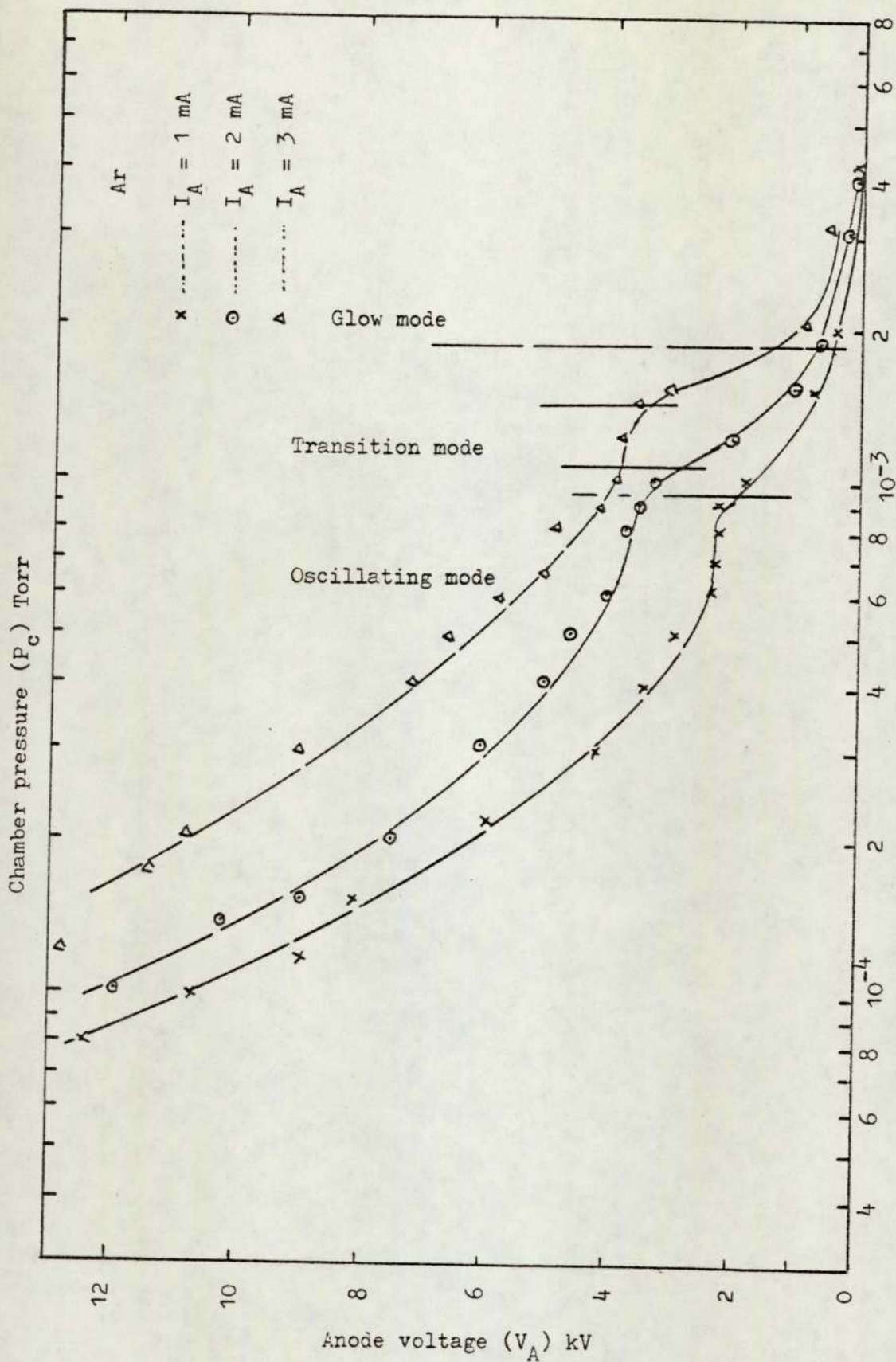


Figure 5.12. Modes of operation for the cylindrical source using argon.

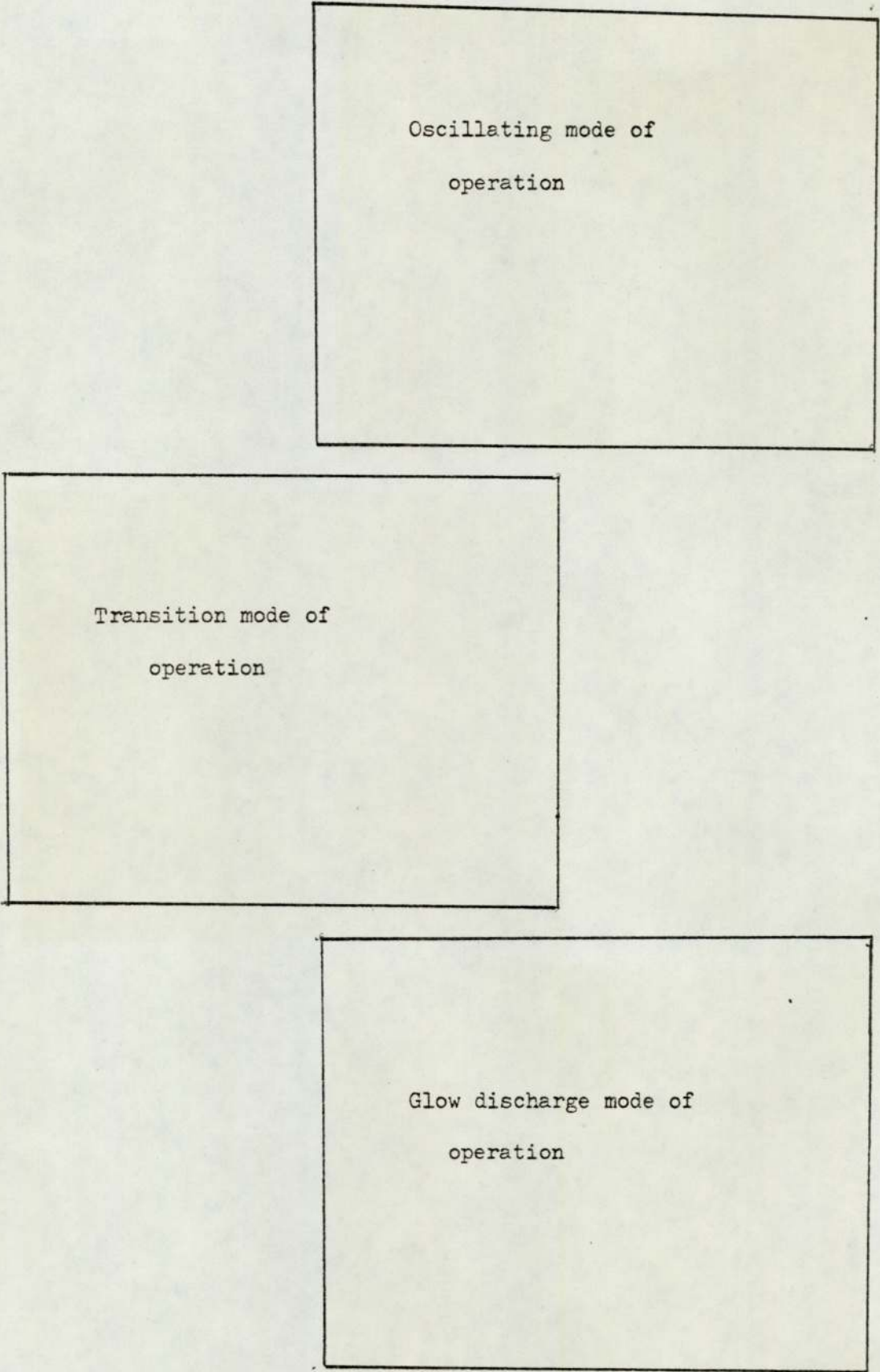
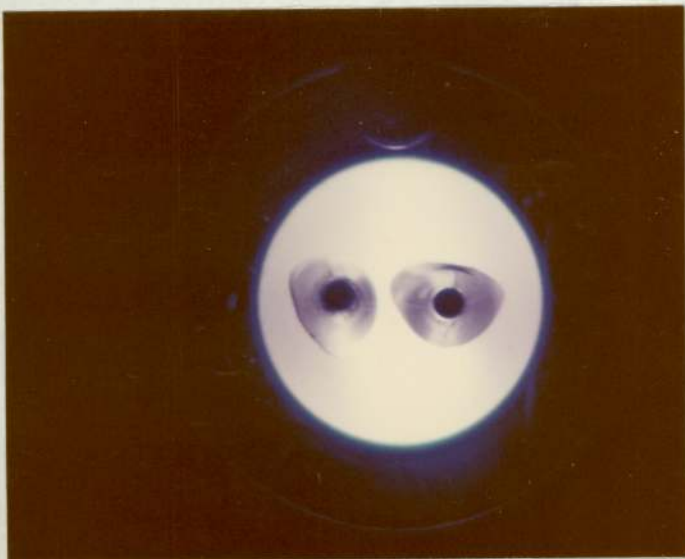
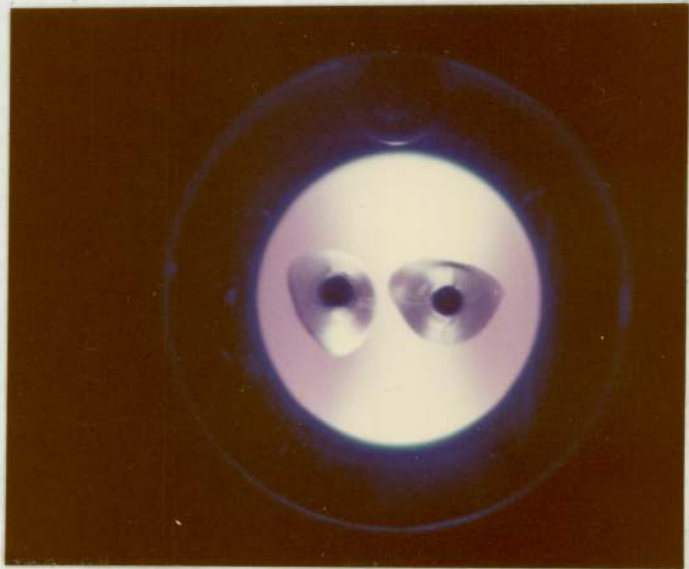
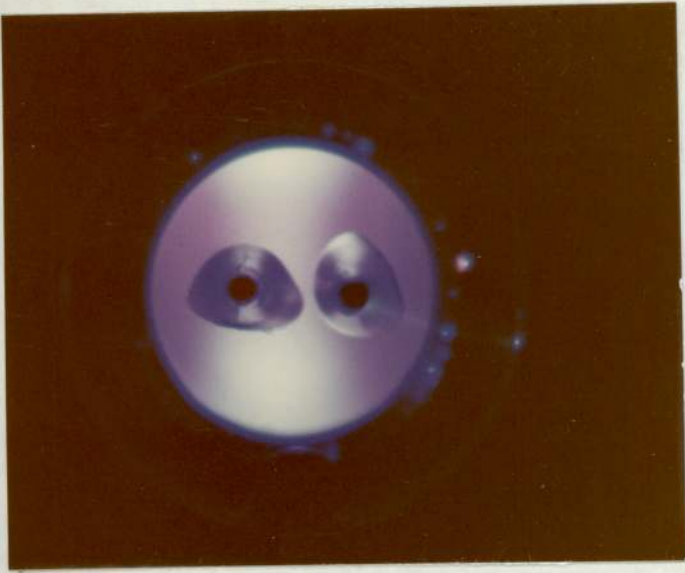


Figure 5.13. Three different modes of operation



B - Spherical source

The existence of various modes in the spherical source, with two 1.5 mm ion exit apertures using argon gas, was inspected by studying the variation of the ion beam current and discharge voltage with chamber pressure at constant anode current of 1, 2, 4 and 6 mA as shown in Figures 5 - 14 and Figures 5 - 15. These curves indicate that from the lowest pressure of source operation with the anode current constant, the ion beam is first constant and then diminishes by about 80% at a pressure of about 2×10^{-4} Torr. This is the "oscillating mode" and figure 5.15 shows the corresponding variation of anode voltage which first falls and then remains nearly constant until a pressure of about 2×10^{-4} Torr, (Figure 5-15). At higher pressures, the slope of the curves in Figure 5.14 slightly changes and the ion beam current falls to about 2.5% of the maximum value at a pressure of 3×10^{-4} approximately. In this region the anode voltage falls rapidly to about 1 kV and this is called "the transition mode". At still higher pressure the beam current decreases to about 2½% of the maximum value and the anode voltage is now only a few hundred volts in the "glow" mode.

The modes of operation of this source under the same conditions but using helium are given in Appendix 5-3/6.

5.4 Ion source efficiency

In all ion sources it is important to consider not simply the actual ion beam current, but also the efficiency of the source in producing that current. One such criterion for assessing this is to determine the current efficiency (ϵ_1) defined as the ratio of the ion beam current to the source current (I_B/I_A). This makes it possible to choose the ideal condition for operating the source. The efficiency, ϵ_1 of both sources was measured for a constant

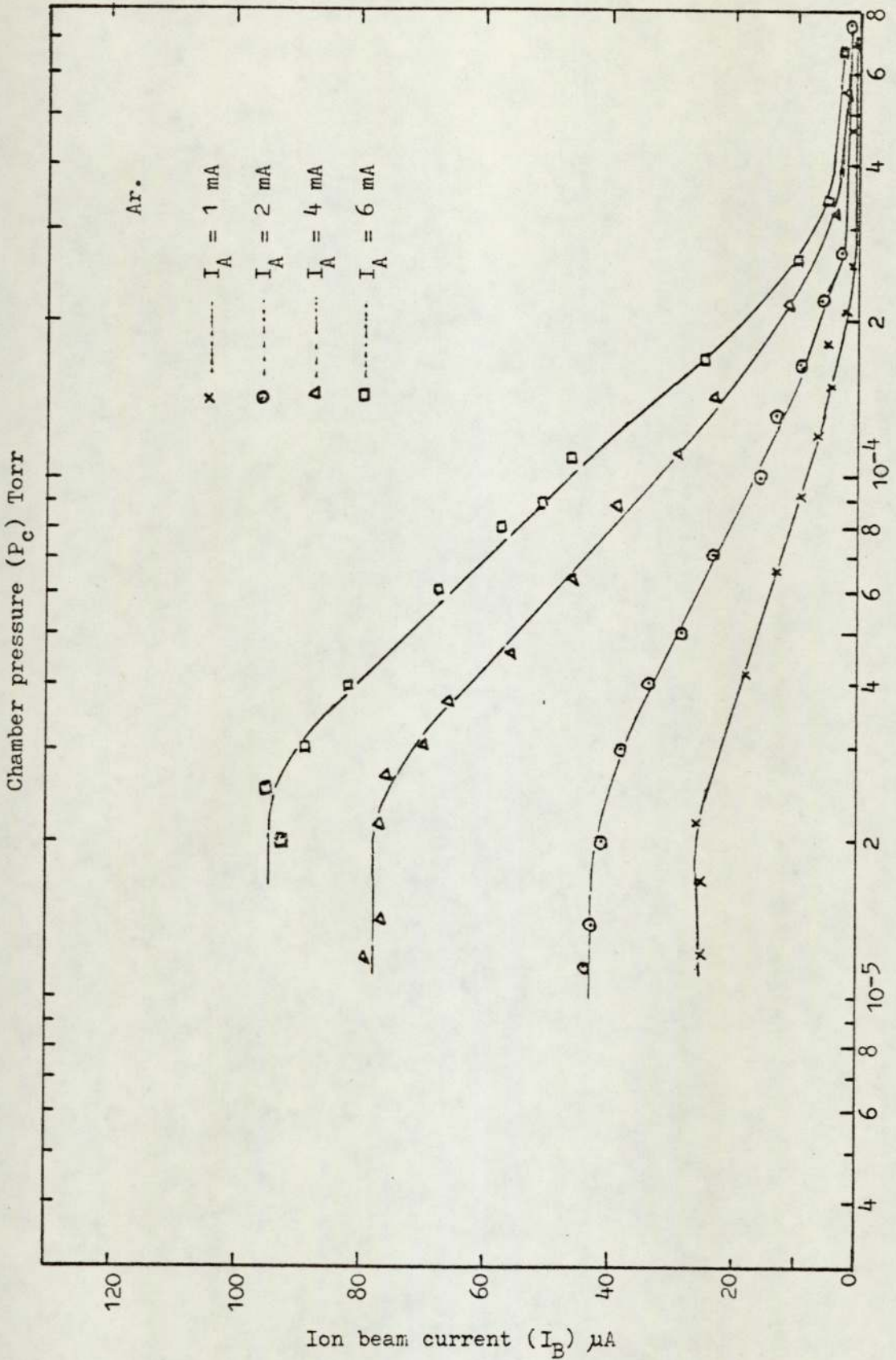


Figure 5.14. Variation of ion beam current with chamber pressure for the spherical source using argon.

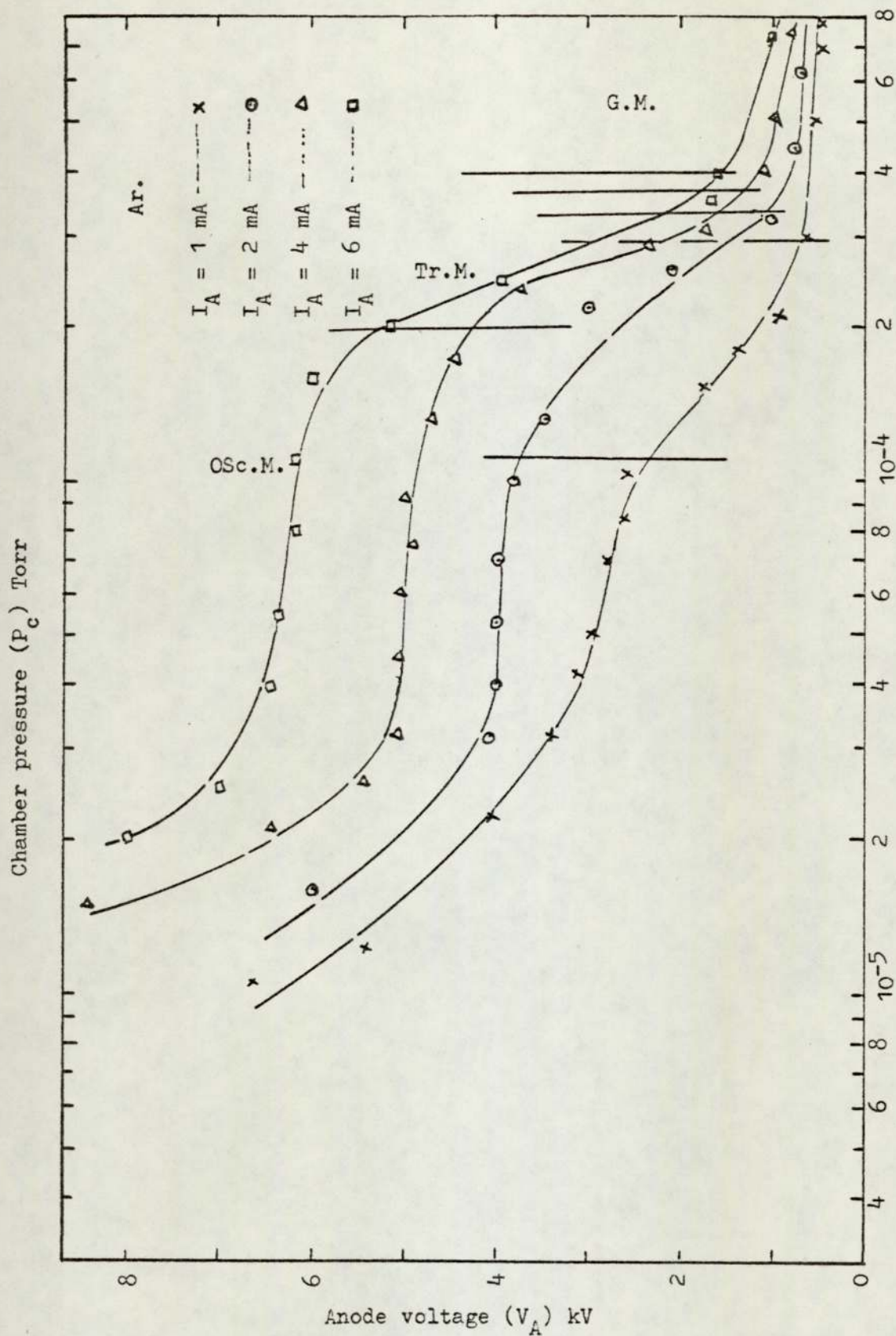


Figure 5.15. Modes of operation for the spherical source using argon.

distance between the collector and aperture. Figure (5-16-a) shows the variation of ϵ_i against pressure for the cylindrical source with 2 and 5 mm ion exit apertures, and Figure (5-16-b) shows the corresponding curve for the spherical source with two 1.5 mm apertures. Both curves were obtained using argon. The bars give the range of efficiency for various values of V_A at a given pressure. As the curves show it is possible to say that the efficiency is constant when the source is operating in the oscillating mode. At higher pressures corresponding to the glow discharge mode the efficiency is very low, whereas at intermediate pressures (in the transition mode) the efficiency diminishes rapidly as the pressure increases. This reduction in current efficiency is more pronounced with the cylindrical source than with the spherical source. After taking into account the difference in size of the ion exit apertures the efficiency of the spherical source is approximately five times that of the cylindrical source.

An alternative approach is to consider the power efficiency, ϵ_p , of the source defined as the ratio of the ion beam current to the input power of the source - i.e. $\epsilon_p = \frac{I_B}{V_A I_A}$. Figure 5.17 (a) and (b) show the variation of ϵ_p against the chamber pressure for both sources using argon gas. The curves show that the power efficiency (ϵ_p) is at maximum when the cylindrical source is operating at 5×10^{-4} Torr and the spherical source at 3×10^{-5} Torr. These pressures correspond to the region between the oscillating and transition modes.

However these maximum values of ϵ_p in both curves are nearly the same, but in fact it is greater in the spherical source as the effective area of its ion exit aperture is about five times smaller than the exit aperture's area of cylindrical source.

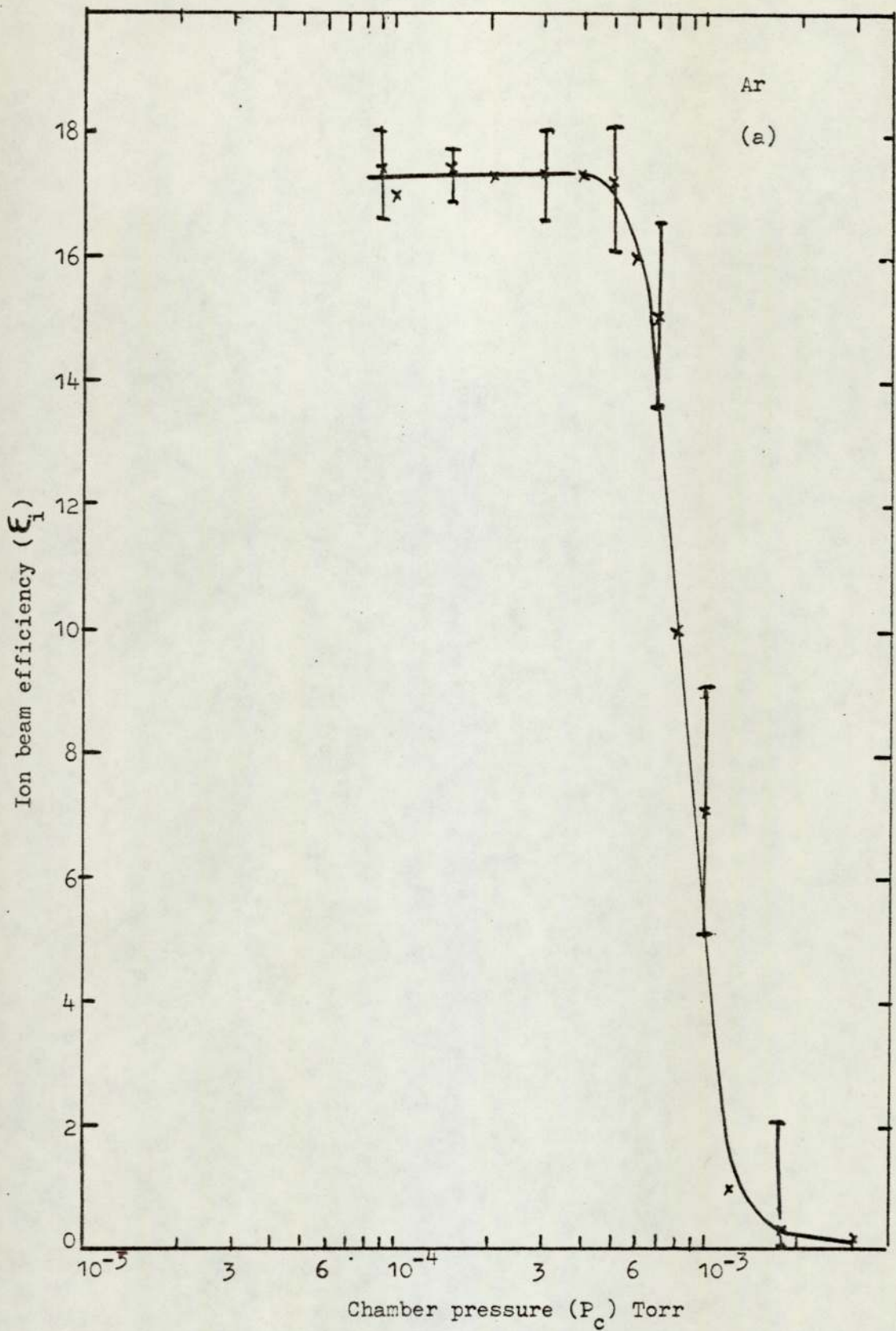


Figure 5.16a. Variation of ion beam efficiency with the chamber pressure using argon for the cylindrical source.

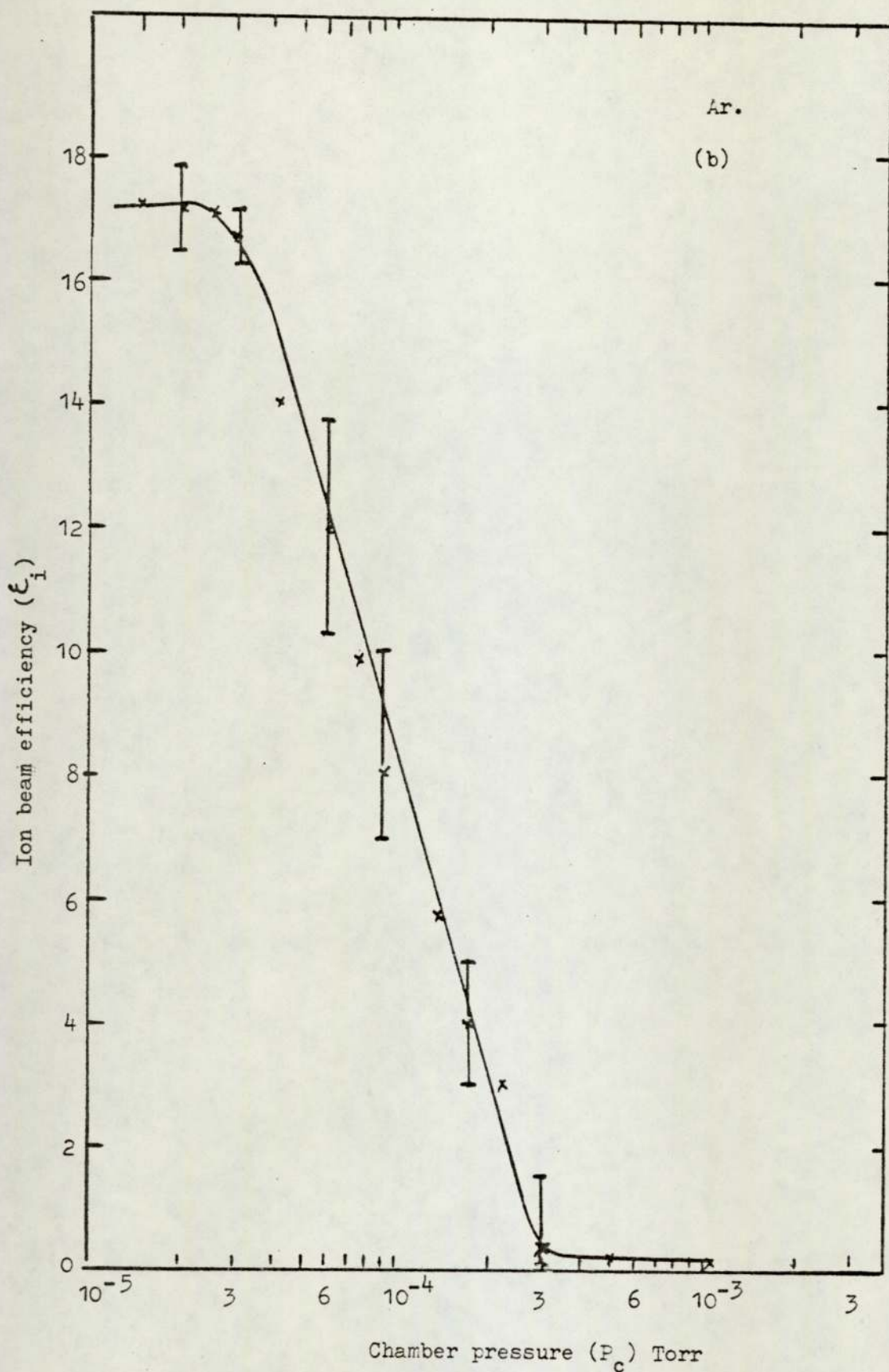


Figure 5.16b Variations of ion beam efficiency with the chamber pressure using argon for the spherical source.

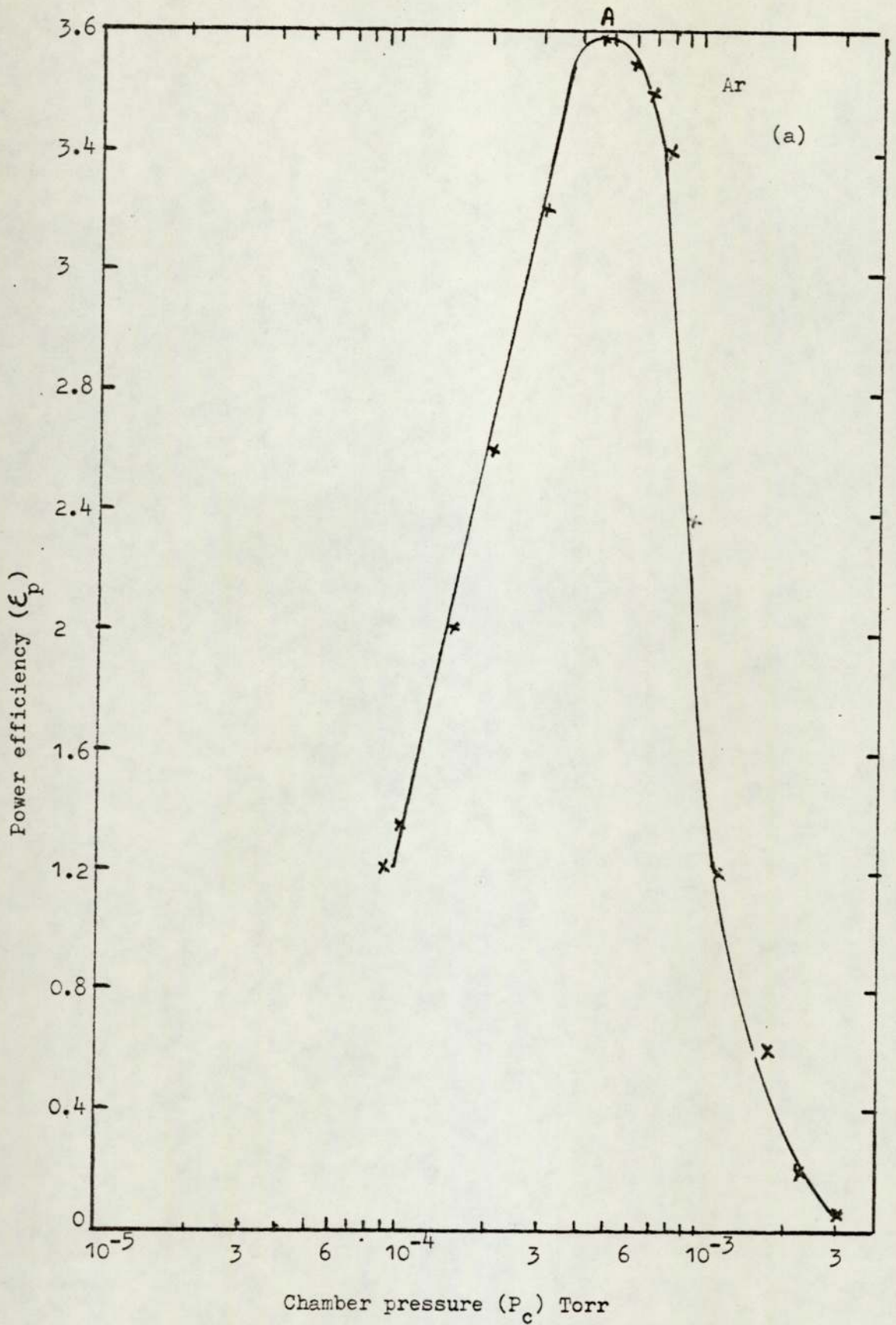


Figure 5.17a. Variation of the power efficiency with chamber pressure using argon for the cylindrical source.

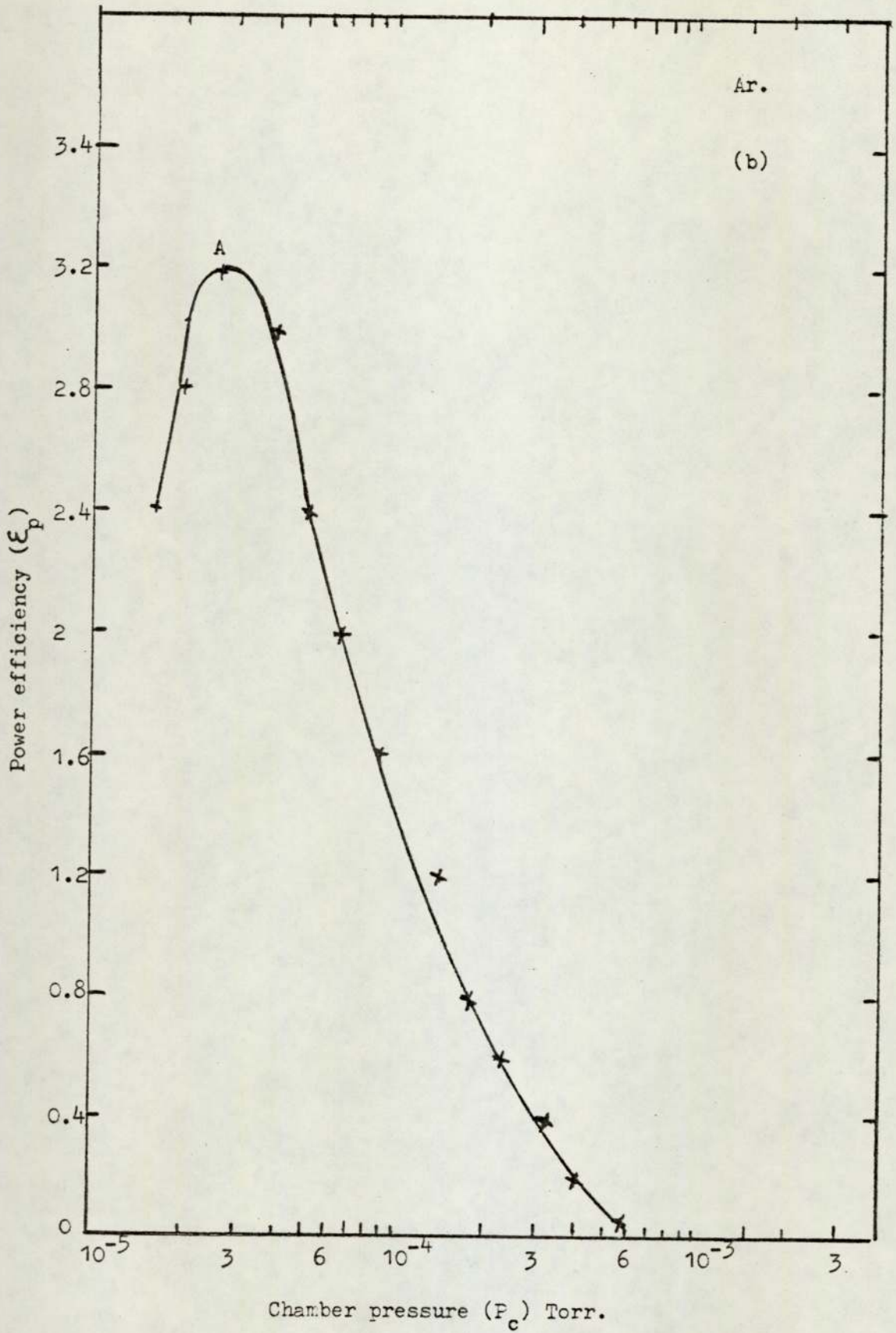


Figure 5.17b. Variation of the power efficiency with chamber pressure using argon for the spherical source.

5.5 Discussion

Experiments and measurements with the two ion sources using different gases and conditions of size and position of the apertures have provided useful information about the beam divergence, ion beam current density, ion source efficiency, characteristics and modes of operation.

The main reason for the ion beam divergence can be understood from figures 4.3 and 4.5 which show the equipotentials and lines of force in both sources. The electric field distortion is shown more clearly with the cylindrical source. This field distortion causes deflection of the ions especially near the edges of the aperture as is shown in figure 5.18. This was verified by etching a thin film of copper using the cylindrical source with a 5 mm circular aperture.

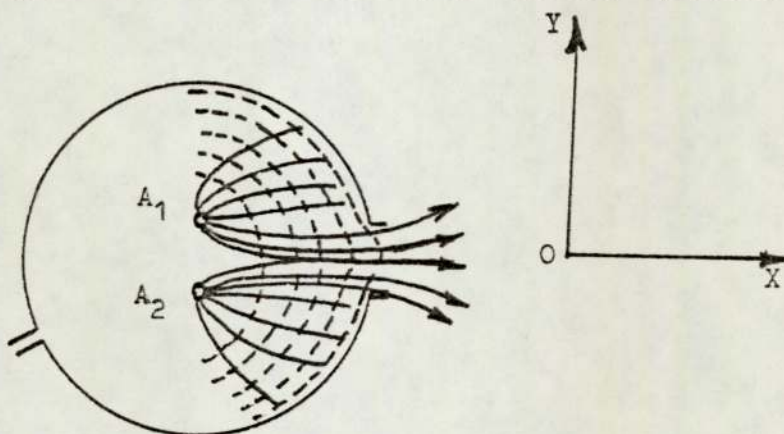


Figure 5.18. The shape of the lines of force and the equipotentials near the aperture.

The etched region showed that the beam diverges into an elliptical shape with the major axis in the Y direction. The length of the major axis was more than four times greater than the aperture diameter (22 mm). A similar experiment with the spherical source showed that the beam divergence is almost equal in both directions, due to the axial symmetry of the spherical source as is shown in Figure 4.4. Therefore the emerging ion beam is more uniform with this source.

The modes of operation have been found to be similar for all gases using both sources. They show clearly three distinct regions, namely the 'oscillating mode', 'transition mode' and 'glow discharge mode'. These mode characteristics have the same general form as that reported using a different technique by Fitch et al⁴³, and do not show the more complex characteristics as given by Ghander⁴⁷.

The complexity of the latter are believed to be due to the unsatisfactory collector used by Ghander and described in section 4.4. However it has been found that the transition mode occurs at different chamber pressures for argon, nitrogen and helium. This was recognized as being mainly due to the differences in gauge sensitivity, conductance of the apertures, effective speed of the diffusion pump and variation of ionisation cross section for different gases.

Thus if these factors are taken into account the true source pressure of argon and helium at the transition mode is about the same as that for nitrogen. Of course if the results for nitrogen are taken, no corrections are required due to the gauge sensitivity, pump speed and conductance across the aperture. Table 5.1 given below shows for both sources the mean chamber pressure (p_{CT}) at the transition mode, the ratio of the source pressure to the chamber pressure $\frac{p_{ST}}{p_{CT}}$, the source pressure (p_{ST}) and the corresponding mean free path for electron molecular collision for nitrogen (λ_e) together with the approximate radius of each source.

The ratio $\frac{p_S}{p_C}$ was calculated assuming molecular conductance for the aperture. The mean free path, λ_e , was calculated from the equation;

$$\lambda_e = \frac{1}{n \cdot \sigma}$$

	Cylindrical source	Spherical source
P_{CT} - Torr	6.5×10^{-4}	1.4×10^{-4}
$\frac{P_{ST}}{P_{CT}}$	35	190
P_{ST} Torr	2.3×10^{-2}	2.7×10^{-2}
Source radius cm.	1.3	1.2
λ_e - cm	1.6	1.4

Table 5.1. The source pressure, and electron molecule mean free path at the transition mode for both sources.

where n is the number of molecular per cm^3 inside the source and α is the maximum total collision cross section of electrons with molecules which is about $9 \times 10^{-16} \text{ cm}^2$ for nitrogen for electron of energy 100 eV.⁶¹ The table shows that the transition mode occurs when the λ_e is about the same as the radius of the source. This agreement is rather better than anticipated because of the uncertainties in the values of n and α . This makes it possible to put forward a model to explain the behaviour of the source at all pressures.

At high pressures λ_e is less than the source radius, therefore many of the electrons collide with the gas molecules before being collected by the anode either as an elastic collision or an inelastic

impact, followed by ion formation. Thus a small degree of ionisation occurs and a low voltage glow discharge resulting in a small ion beam current is formed. As the pressure reduces from the glow mode to the transition mode λ_e is about the same as the source radius, and a sudden increase in anode voltage and also ion beam current occurs. In this situation the discharge is rather unstable as the increased ionisation arises from both electrons orbiting around and oscillating between the anodes.

With a further reduction in the pressure, λ_e increases resulting in the stable oscillating mode in which the oscillating trajectory of the electrons are confined to a well defined region between the anodes. In this region as the pressure decreases, the anode voltage first remains fairly constant but the beam current increases while the anode current is constant. This is particularly noticeable with the spherical source. The increase in ion beam current can be explained as being due to a narrowing of the oscillating region. However at a still further reduction of pressure it is necessary to increase the anode voltage to maintain a constant anode current and the ion beam current remains constant.

This model also explains why the current efficiency ϵ_i is maximum and constant in the low pressure region of the oscillating mode for both sources. In the beginning of this region, labelled A on figures 5.11, 5.14, 5.16 and 5.17, the power efficiency (ϵ_p) reaches a maximum value when the discharge has just been confined to its limit. Thus there is no obvious advantage in operating the source at lower pressures as the beam current remains constant unless it is necessary to have a more energetic beam of ions.

CHAPTER 6

ION ENERGY DISTRIBUTIONS

6.1 Introduction

It has already been pointed out in Section 3-4 that there has been considerable disagreements between the energy spectra from the few energy analysis measurements of the sources. In the present work an initial attempt was made to repeat Ghander's measurements, for example those given in figure 3.7, using his analyser and ion source, but increasing the resolution by recording the ion beam current at much smaller intervals of V_R . The main consequence of this was that the energy spectra did not contain more than two, but poorly resolved peaks. Thus it was decided to study the possibility of using a different energy analyser from one of the many types now in use which are described in an excellent review of this subject by Steckelmacher⁶². However different types of energy analysers have been recognised as valuable diagnostic tools for studying the behaviour of charged particles and ion beams, and the literature on this subject is rather extensive. Parallel plate energy analysers can be considered adequate for the low energy particles with narrow energy spread and this has been put in use recently to investigate the energy distribution of charged particles and ions produced by various sources, especially the retarding field analyser utilizing high transparency grids which is a relatively well known instrument. Therefore in the present work which imposed certain restrictions on the analyser, such as freedom for magnetic field and use of a large entrance aperture, it was decided to use a retarding field analyser similar to that used by Ghander, but with the main emphasis placed

on improving the grid and the ion beam collector.

6.2 Description of the analyser

The analyser employs two parallel grids placed between the ion source and the collector. The charged particles are assumed to enter into the electrostatic field produced by a retarding potential, V_R , with kinetic energy $E = eV$, where V is the accelerating voltage on the ions, and the ions are retarded or reflected by the retarding field. The current, I_B , shown by the collector denotes that for $V > V_R$ some of the particles (ions) can pass the potential barrier and when $V < V_R$ they will be repelled. It is possible to say, if the ion beam is monoenergetic the variation of collector current, I_B , as a function of V_R will be as shown in Figure 6.1a⁶³. However if the ions are not all incident normally to the retarding field, the variation of collector current will be as shown in figure 6.1b, which gives the appearance of a relatively broad energy spread.

Other factors which must be taken into consideration include:

- (a) - The problem of whether all the particles of sufficient kinetic energy reach to the collector?

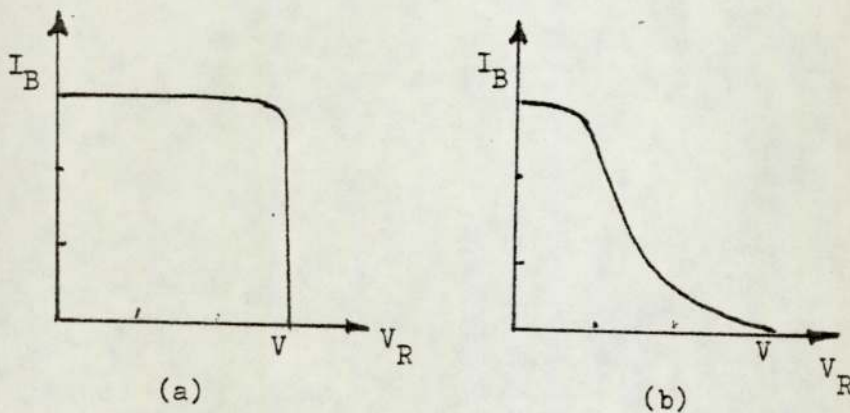


Figure 6.1. (a) Ideal $I_B \rightarrow V_R$ characteristic for monoenergetic particles, (b) $I_B \rightarrow V_R$ characteristic for high divergent beam of monoenergetic ions.

Author KHORASSANY, M

Title Analysis of the particles produced by saddle field ion sources

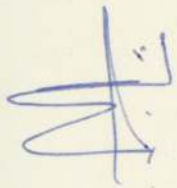
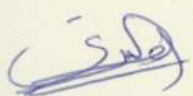
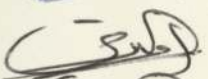
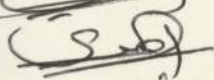
Award Ph.D.

BLD 21069/77
Date of Award 1977

CONSULTATION OF THESIS

I undertake not to publish or use information derived from this thesis without the consent in writing of the author.

Thesis For Use In The Library Only

Signature	Address	Date consulted	Return checked by
	65 WARREN RD.	15.5.80	M
	B. 8 physics	21/7/1980	R
	physics	22 nd 7/80	
	physics	9 th 9/80	
K.S.Ali	physics	18/4/83	
K.S.Ali	physics	25/7/83	

and (b) on arrival at the collector some of the ions may not be retained.

Now it is shown that charged particles hitting a surface produce secondary electrons and the number of these electrons is a function of the incident energy. Simpson⁶³ also showed that the reflection coefficient of the ion beam collector is a function of the incident energy and depends also on the nature of the particles and the collector materials. These effects were shown by the flat plate and the collector used by Ghander as discussed in detail in section 4.4. Thus it was clearly recognised that a way to minimize this effect in an improved analyser was to change the collector to a Faraday type cage, so that the secondary electrons after a few reflections are retained.

A further improvement of the energy analyser was made by replacing the stainless steel mesh grids of 40% transparency with two double grids which had a much larger transparency but at the same time provided a reasonably uniform field. These grids were made by winding 0.1 mm diameter tungsten wire round an aluminium frame of 5 mm thickness such that the grid was 40 x 40 mm with the wire spaced at about 1.8 mm and the two grids were thus 5 mm apart. The dimensions of these grids were such that they should have a transparency of about 98%. In practice due to some misalignment of the grid wires, the transparency was found to be about 90%. Two grids were used - one (G_R) for the retarding potential, and the other was the shield grid, G_S , which shielded the collector from the positive field due to G_R .

The collector current I_B was recorded with a digital meter as a function of retarding voltage in 50 - 100 V intervals, and the corresponding energy spectrum was obtained by differentiating these

curves. It is known that these sources produce a significant proportion of energetic neutrals which are of course unaffected by the retarding field, but can still produce secondary electrons at the collector. Thus the efficiency of the collector at retaining the secondary electrons could be assessed by recording the collector current with V_R greater than the anode voltage V_A . It was found that under these conditions the escape of secondary electrons contributed to always less than 3% of the I_B depending upon the anode voltage as was given in Chapter 4, Table 4.1.

A schematic diagram of the energy analyser showing the source and collector is shown in Figure 6.2.

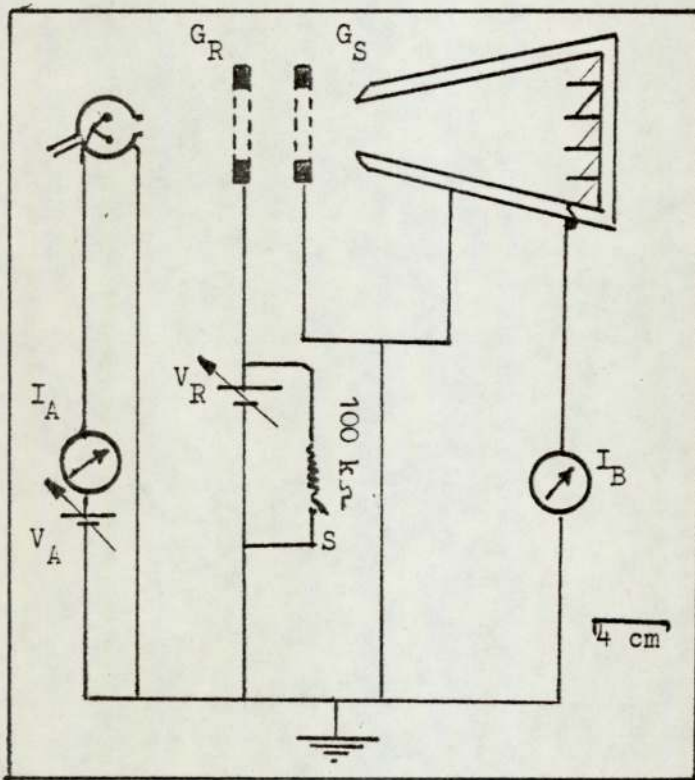


Figure 6.2. Schematic diagram of the energy analyser.

In these measurements the two power supplies used for V_A and V_R were earthed, and in order to make measurements at V_R between 0 and about 1 kV - depending upon the pressure - it was necessary to

switch in a 100 k Ω resistor in parallel with the power supply. This was necessary because at low value of V_R the current in the retarding grid generated a voltage across the input impedance of the power supply.

6.3 Energy distribution measurements

In the energy distribution measurements, variations of ion beam current I_B as a function of retarding voltage V_R for both sources have been investigated. These experiments were done over a wide range of pressure from the glow mode to the oscillating mode using argon, nitrogen and helium and various size of apertures. The corresponding energy spectra - $N(E)$ against E - were also given and are discussed below.

A - Cylindrical source

The variation of I_B with V_R for the cylindrical source was recorded at different chamber pressures (P_c) and anode voltages (V_A). Figure 6.3 shows four of these measurements with a central aperture of 5 mm in diameter using argon for $V_A = 1, 3, 4.5$ and 6 kV at a constant anode current of 3 mA between 1.5×10^{-3} Torr to 2.5×10^{-4} Torr. These curves were unlike those of Ghander⁴⁷ as the first part of the curve is flat indicating the absence of very low energy ions. The corresponding energy spectra of these curves are shown in Figures 6.4 and 6.5. In these measurements it was noticed that all curves at different pressures are very similar, having two distinct peaks between 0.30 to 2 Kev for the first peak and 0.9 to 4.25 Kev for the second peak. These peaks occur at a range of about 30-40% and 70-80% of the anode voltage respectively. These curves also showed that the height and width of the peaks, which indicate the number of ions at a given energy, are affected by the pressure. As

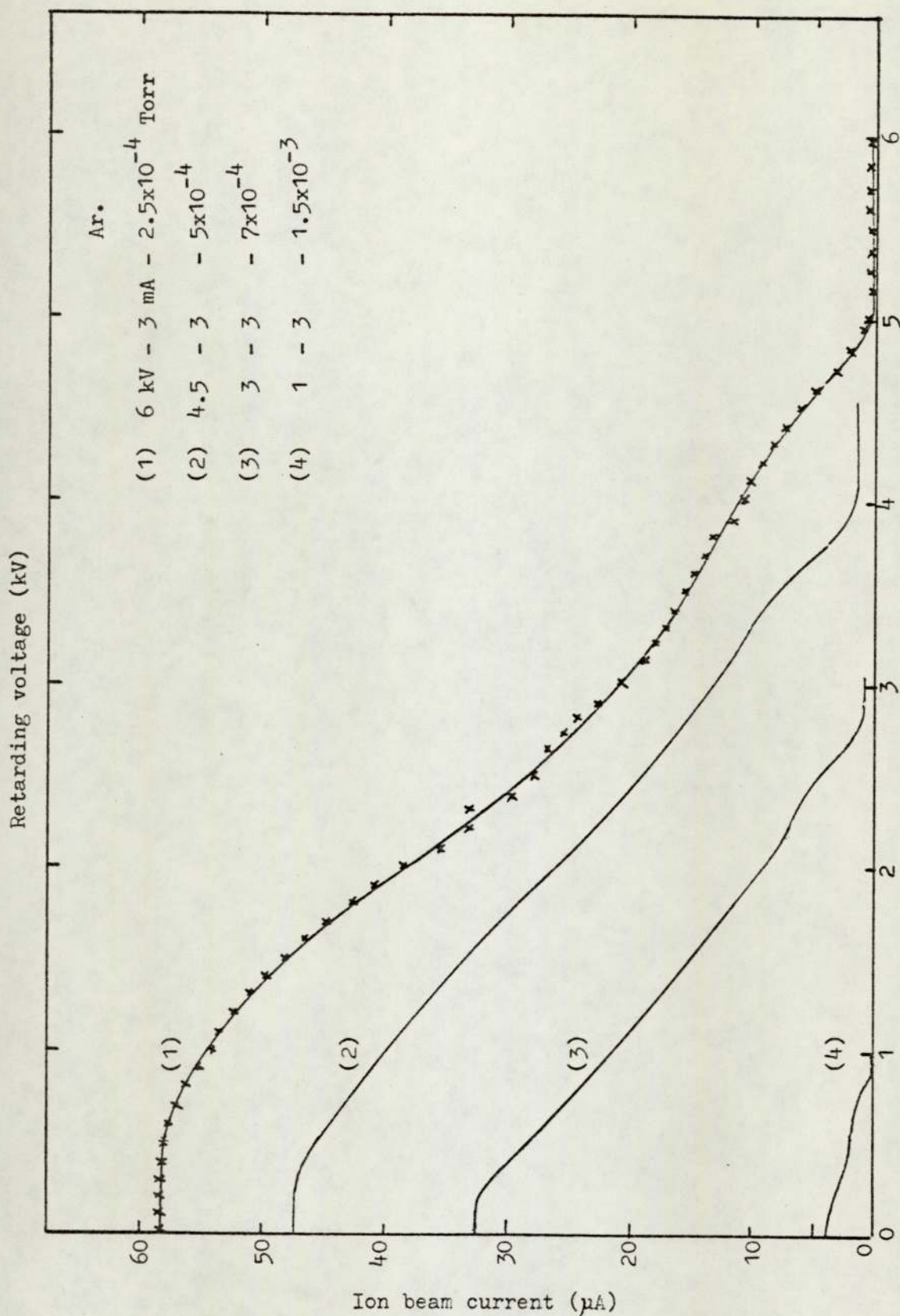


Figure 6.3. Variation of ion beam current with the retarding voltage for cylindrical source with 5 mm aperture using argon.

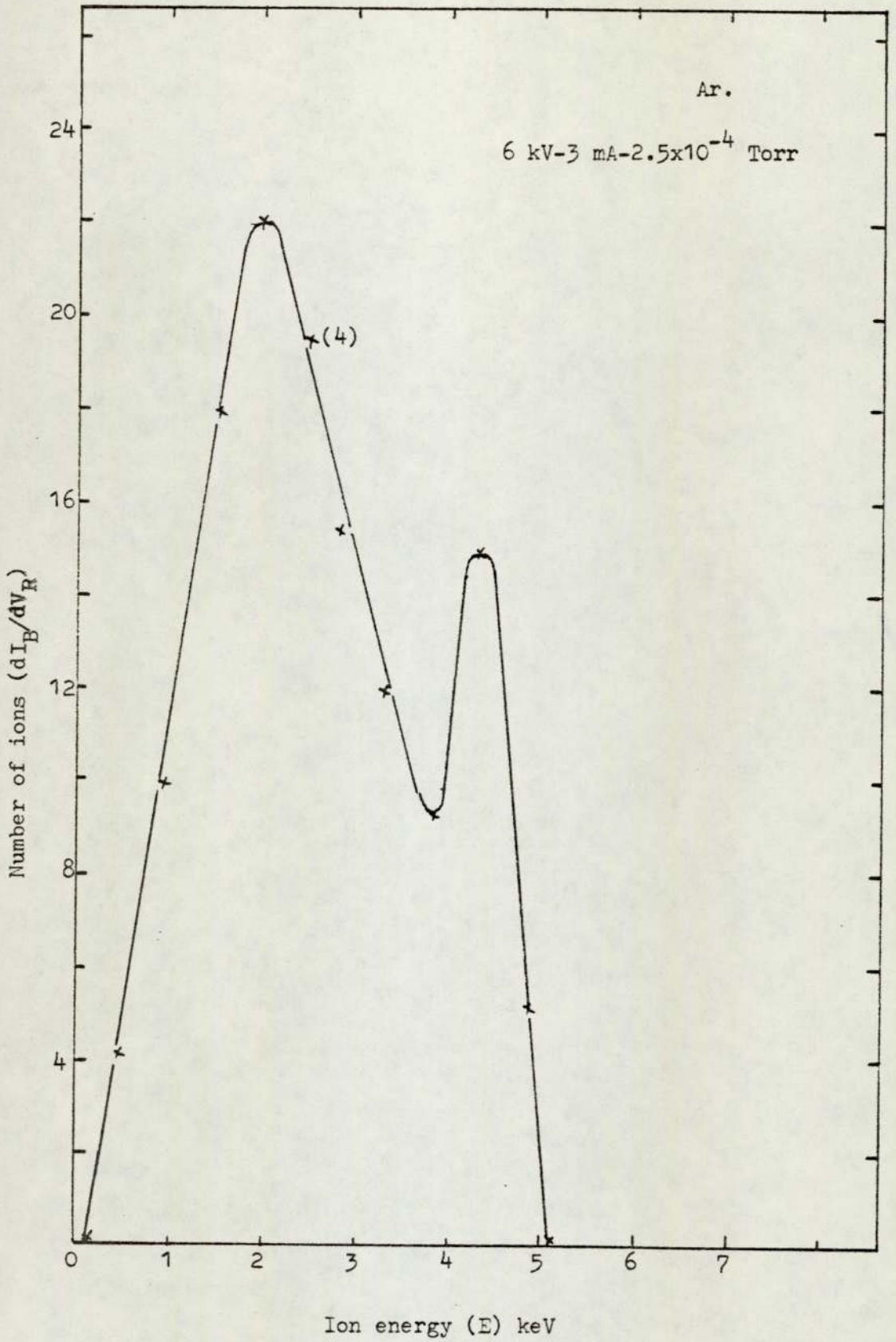


Figure 6.4. Ion energy distribution from the cylindrical source with 5 mm aperture using argon.

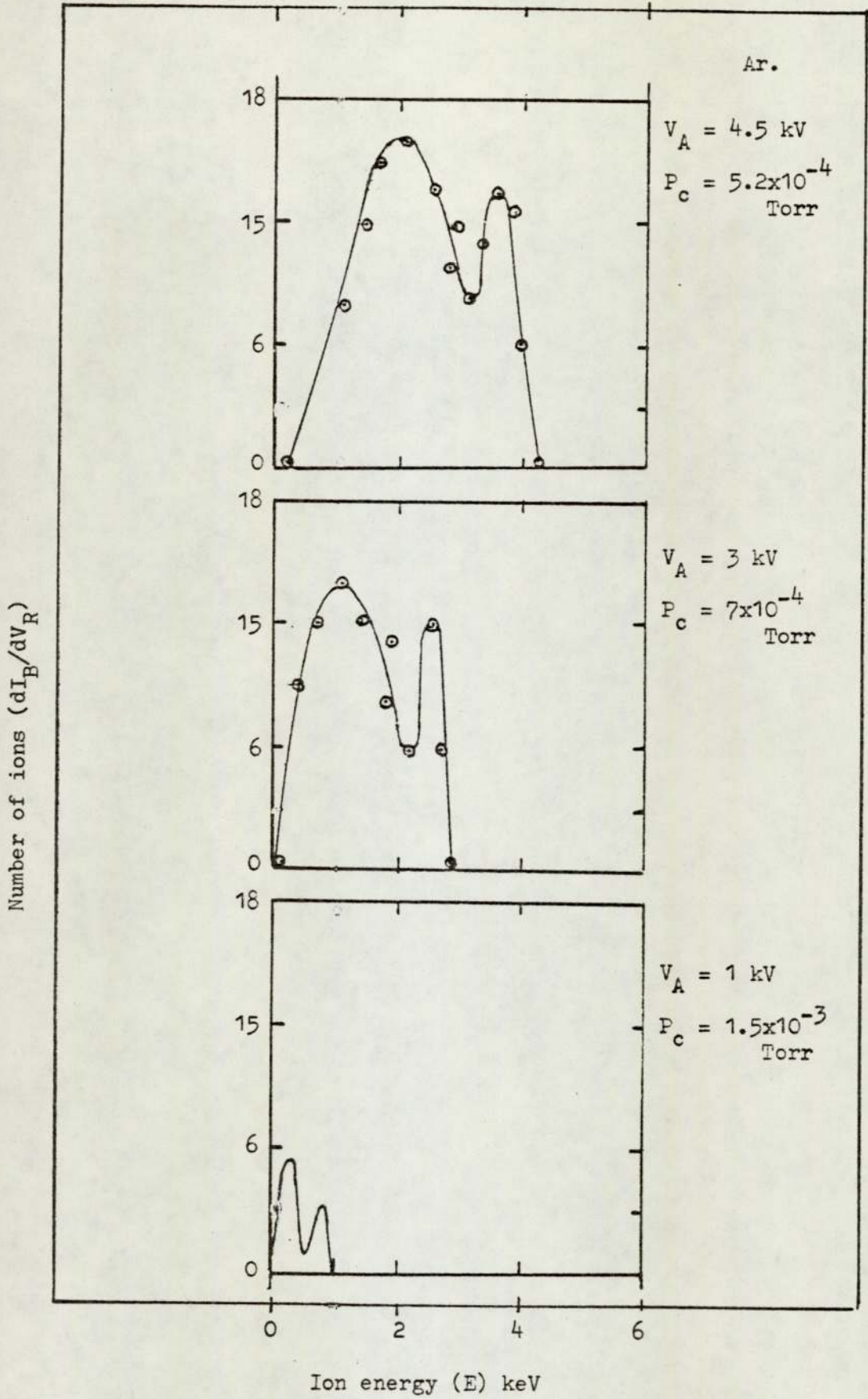


Figure 6.5. Ion energy distribution from the cylindrical source at 3 mA anode current using argon.

figures 6.4 and 6.5 show, at constant anode current the ratio of the high energy ions to the low energy ions decreases as the pressure increases. Table 6.1 shows that for all results taken for argon with anode voltages in the range 1 - 9.6 kV and for anode currents in the range of 0.6 - 3mA the energy peaks always occurred at about 30-40% and 70-80% of the anode voltage

$P \times 10^{-4}$ Torr	V_A kV	I_A mA	V_1 kV	V_2 kV	$\frac{V_1}{V_A} \%$	$\frac{V_2}{V_A} \%$
15.0	1.0	3.	0.3	0.80	30	80
6.8	3.0	3.0	1.0	2.50	33	83
6.0	4.0	2.2	1.6	3.1	40	77
5.2	4.5	3.0	2.0	3.5	42	74
4.0	5.0	3.0	2.0	4.0	40	80
3.6	5.5	2.8	2.2	4.0	40	74
2.5	6.0	3.0	2.2	4.5	37	75
2.1	6.5	3.0	2.0	4.5	31	70
1.7	7.0	2.0	2.5	5.5	36	78
1.3	8.0	2.0	2.5	6.0	31	75
0.8	9.0	1.0	3.5	6.3	39	70
0.64	9.6	0.6	3.5	7.0	30	73

Table 6.1. Variation of energy peaks with the pressure and anode voltage at different anode current with a 5 mm aperture using argon.

Further experiments with this source using nitrogen and helium in the same conditions showed that these gases behave very similar to argon and two peaks were always obtained. The energy curves for nitrogen at 3, 4.5 and 6 kV anode voltage, 3 mA anode current and

from 6×10^{-4} to 1.8×10^{-4} Torr are given in Figure 6.6. A similar curve for helium at 6 kV and 3 mA is also given in Figure 6.7. These curves also show that the two low and high energy peaks always occur at 30 - 40% and 70 - 80% of V_A as was found for argon.

Different experiments showed that the width of the peaks, which show the energy spread of the ions, is less in the high energy peak than the low energy peak, and also the full width at half maximum (FWHM) (ΔE) in all curves and different gases is larger in the lower energy peak.

In further measurements the energy spectra of different intensity ion beams emerging from various aperture positions of this source, as was explained in section 4.2, was obtained using a 5 mm aperture⁶⁴. Figures 6.8a to 6.8f show the energy spectra using argon for $V_A = 5$ kV and $I_A = 3$ mA at angular positions of -10° to $+40^\circ$ with respect to the central position at 0° . The corresponding curves at angular positions -10° to $+20^\circ$ for nitrogen are given in appendix 6-3/7. It is clear from these figures that in all cases two well defined peaks were obtained and the proportion of high energy ions is much greater at the central position shown in Figure 6.8b, and decreases when the aperture is moved either side of the central position. The similarity of figures 6.8a (-10°) and 6.8c ($+10^\circ$) demonstrates that the aperture was correctly placed in the central position in Figure 6.8b. These experiments also showed that the number of the ions in both peaks, which occur at about 40% and 80% of V_A , diminishes to about 5% of the maximum at the extreme position ($+40^\circ$). Table 6.2 shows position of the first and second peak relative to V_A . The different pressure and anode voltage at a tube current of 3 mA.

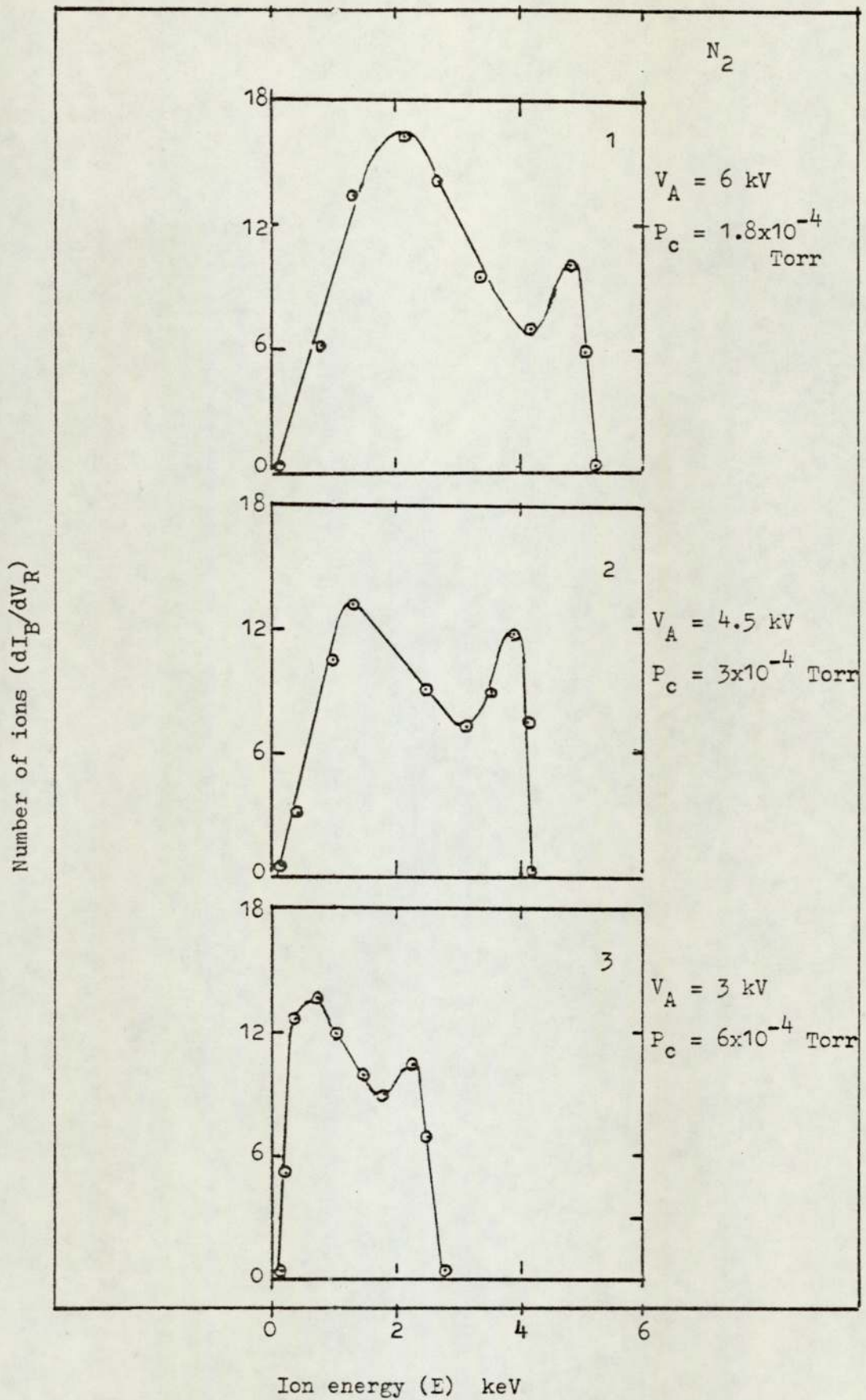


Figure 6.6. Ion energy distribution from the cylindrical source at 3 mA anode current using nitrogen.

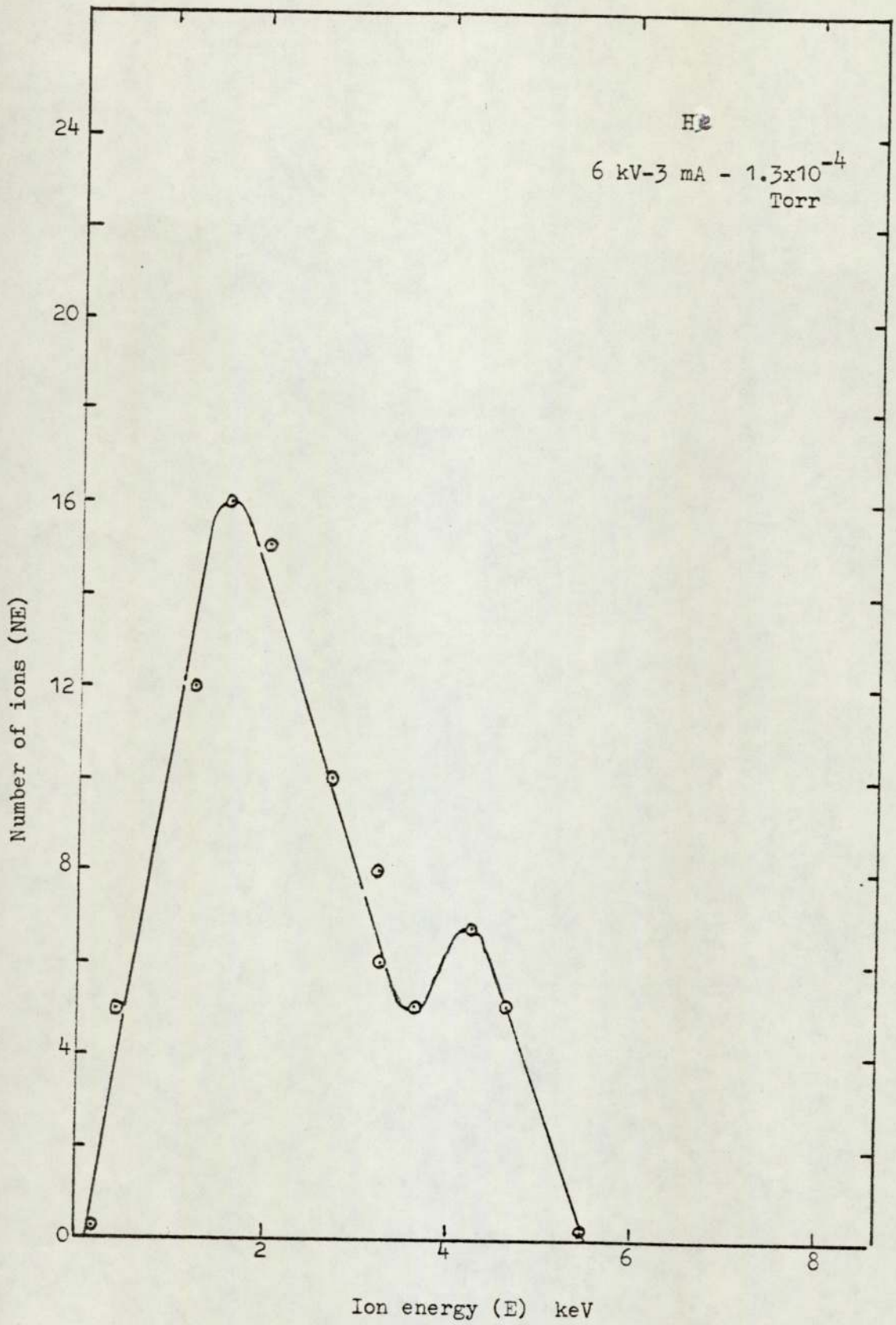


Figure 6.7. Ion energy distribution from the cylindrical source with 5 mm aperture using helium.

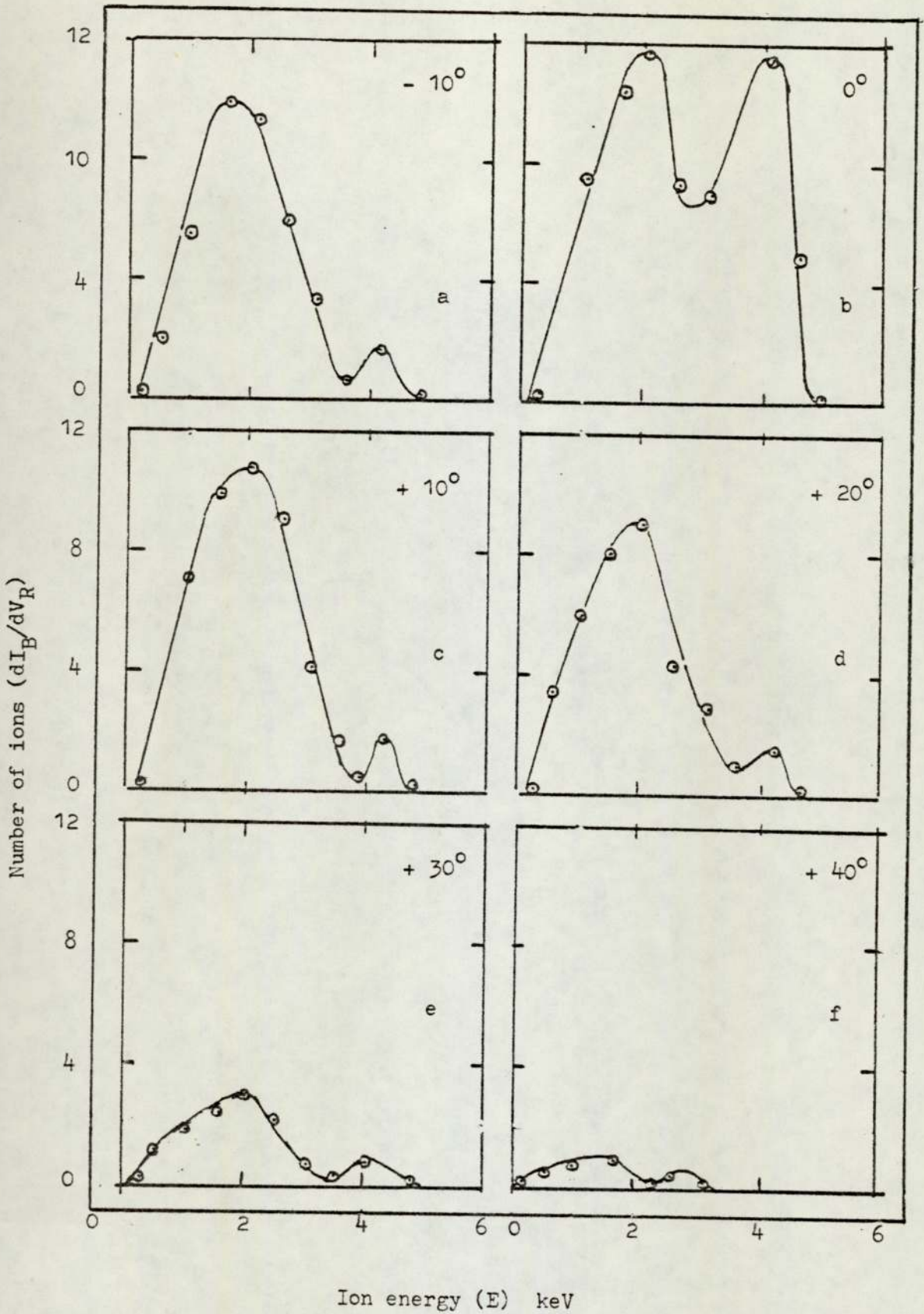


Figure 6.8. Ion energy spectrum for argon with the cylindrical source using 5 mm aperture at different angular positions at $V_A = 5\text{ kV}$, $I_A = 3\text{ mA}$.

Angular position	$P \times 10^{-4}$ Torr	V_A kV	$\frac{V_1}{V_A}$ %	$\frac{V_2}{V_A}$ %
-10	2.5	4	37.5	85.0
	1.3	5	36.0	82.0
	0.85	6	33.0	81.5
0	2.8	4	30	80.0
	1.5	5	40	80.0
	0.95	6	33	80.0
+10	2.0	4	37.5	90.0
	2.2	5	40.0	86.0
	1.4	6	33.0	83.0
+20	3.0	4	37.5	90.0
	1.5	5	42.0	84.0
	1.0	6	33.0	72.0
+30	1.8	4	36.2	85.0
	0.85	5	40.0	84.0
	0.95	6	33.0	83.0
+40	2.6	4	25.0	53.0
	1.5	5	30.0	64.0
	0.9	6	33.0	58.0

Table 6.2. Variation of the energy peaks for different angular positions of the aperture.

The variation of ion energy in different angular positions is also shown in Figure 6.9 which indicates the percentage of the ions having energies greater than 60% of V_A , estimated from the appropriate current on the $i_c \rightarrow V_R$ curves for $V_A = 5$ kV and $I_A = 3$ mA.

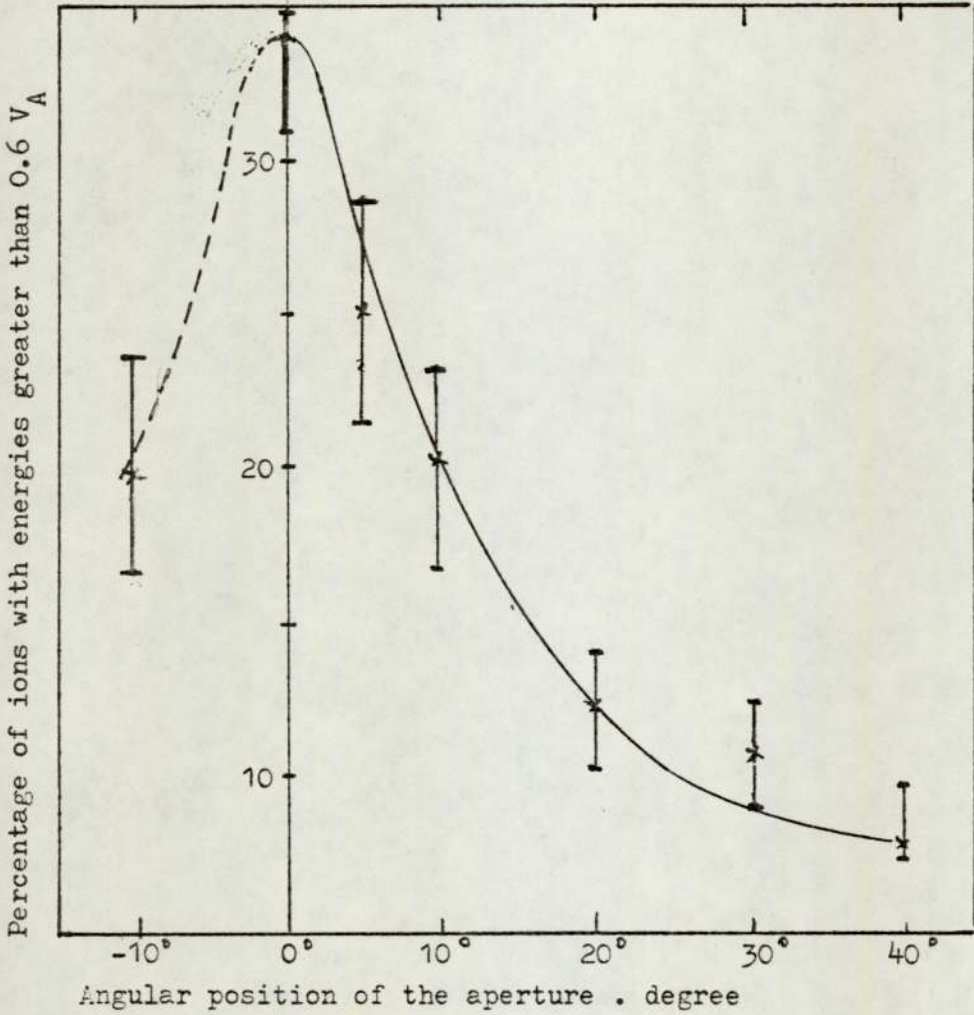


Figure 6.9. Variation of the percentage of ions having energy greater than $0.6 V_A$ with angular position of the aperture.

Measurements showed that when using a smaller aperture of 2 mm, the flat part of $I_B \rightarrow V_R$ curve does not appear even at high voltages. An example of this is shown in figure 6.10, for $V_A = 6$ kV and $I_A = 3$ mA at $p_c = 10^{-4}$ Torr using argon.

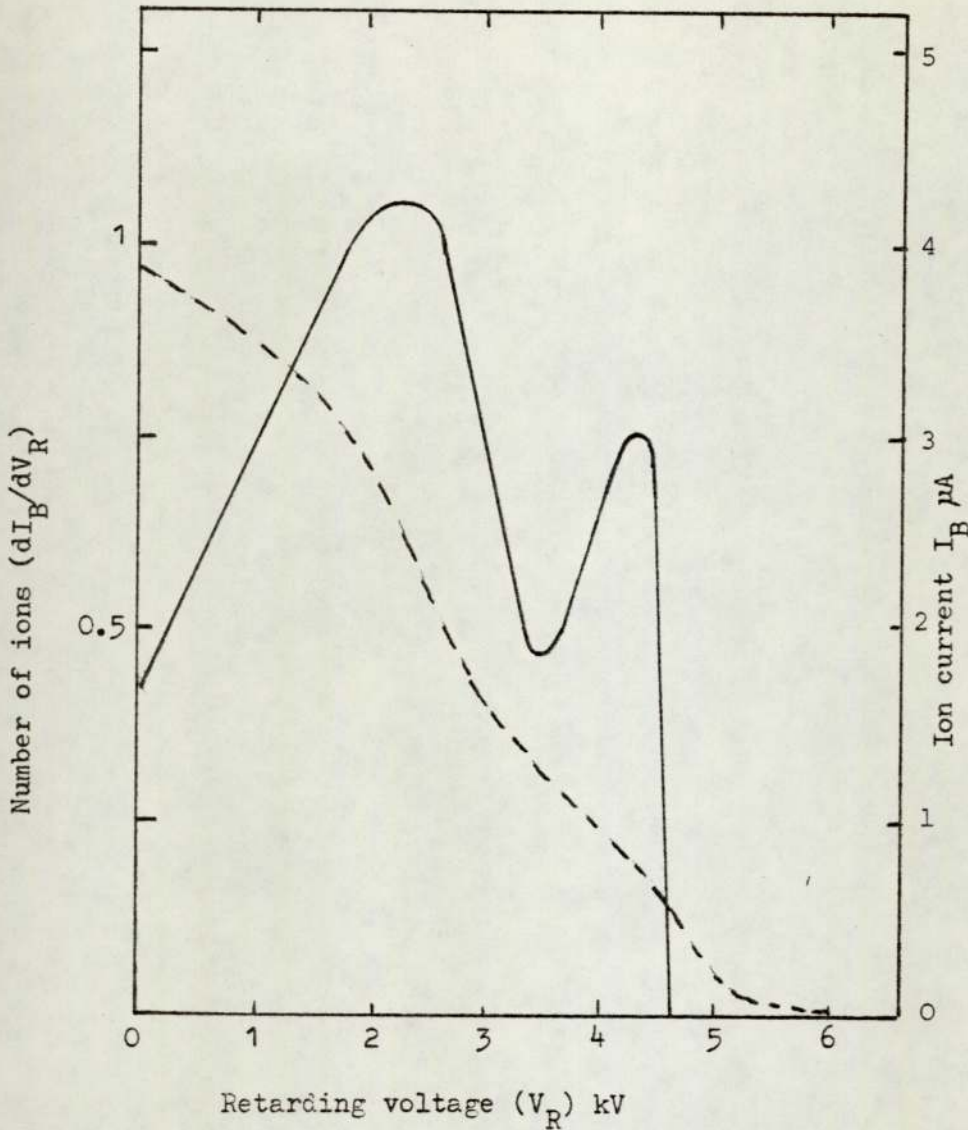


Figure 6.10. Variation of ion beam current with retarding voltage and corresponding energy spectra for a 2 mm aperture using argon at 1×10^{-4} Torr.

This is thought to be due to a reduction in the aperture size which gives an increase in the source pressure (P_S) from 1×10^{-2} Torr for the 5 mm aperture (Figure 6.3) to 2.4×10^{-2} Torr for the 2 mm aperture (Figure 6.10) due to the smaller conductance. This effect also can be seen in Figure 6.3 curve number 4 at 1 kV anode voltage and 1.5×10^{-3} Torr using a source pressure of 6×10^{-2} Torr.

B - Spherical source

In a similar way the energy distribution of the emerging ion beam from a 1.5 mm aperture in the spherical source was measured for a wide range of pressures and using argon, nitrogen and helium. Figure 6.11 shows some of these measurements using argon from 3×10^{-4} Torr to 8×10^{-5} Torr at $V_A = 4, 5, 5.5$ and 6 kV and $I_A = 2$ and 3 mA. The corresponding energy spectra are given in Figure 6.12 and 6.13. It is obvious that the ion energy spectra obtained by this source is very different from that of the cylindrical source and it shows only a high energy peak at 3.4, 4, 4.2 and 4.6 keV in a range of 75 - 80% of V_A , which is superimposed on a broad low energy background. This low energy part does not contribute much to the total number of ions. Different experiments showed that the height of the peak which corresponds to the high energy ions is affected by pressure and anode current. Thus with reference to the figures 6.12 and 6.13 curves 1, 2 and 4 at constant anode current but different pressures show that, number of high energy ions diminishes to about 10% when pressure, P_c , increases from 8×10^{-5} Torr to 3×10^{-4} Torr which corresponds to a change of mode of operation. Also curves 2 and 3 at the same pressure but different anode current show that the height of the peak reduces to half at lower anode current (Curve 2). Further experiments using nitrogen and helium showed similar results for $I_A = 2$ mA with $V_A = 5$ kV and $P_c = 4.5 \times 10^{-5}$ Torr for nitrogen, and with $V_A = 2.5$ kV and $P_c = 4 \times 10^{-5}$ Torr for helium which are given in figure 6.14. The high energy peaks for the nitrogen and helium at 3.2 and 1.8 keV respectively occurred between 65 - 75% of V_A .

However figures 6.12 to 6.14 show that the ratio of FWHM to the maximum width (MW) of the energy peak ($\frac{\Delta E}{E}$) and also the range of the low energy ions (the flat part) at constant anode current decreases with the increase in pressure. The energy distributions of the ions

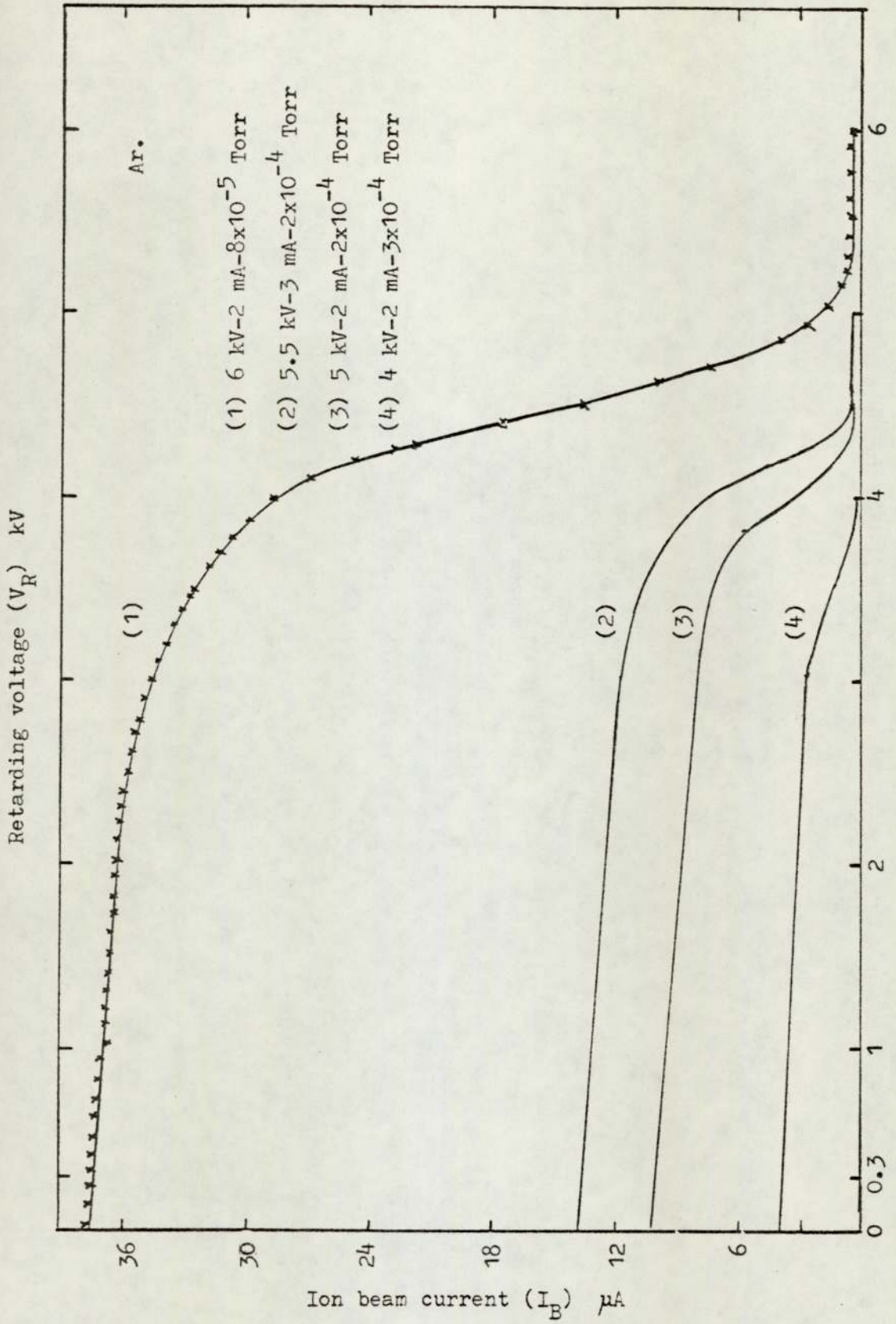


Figure 6.11. Ion beam current against the retarding voltage for the spherical source using argon.

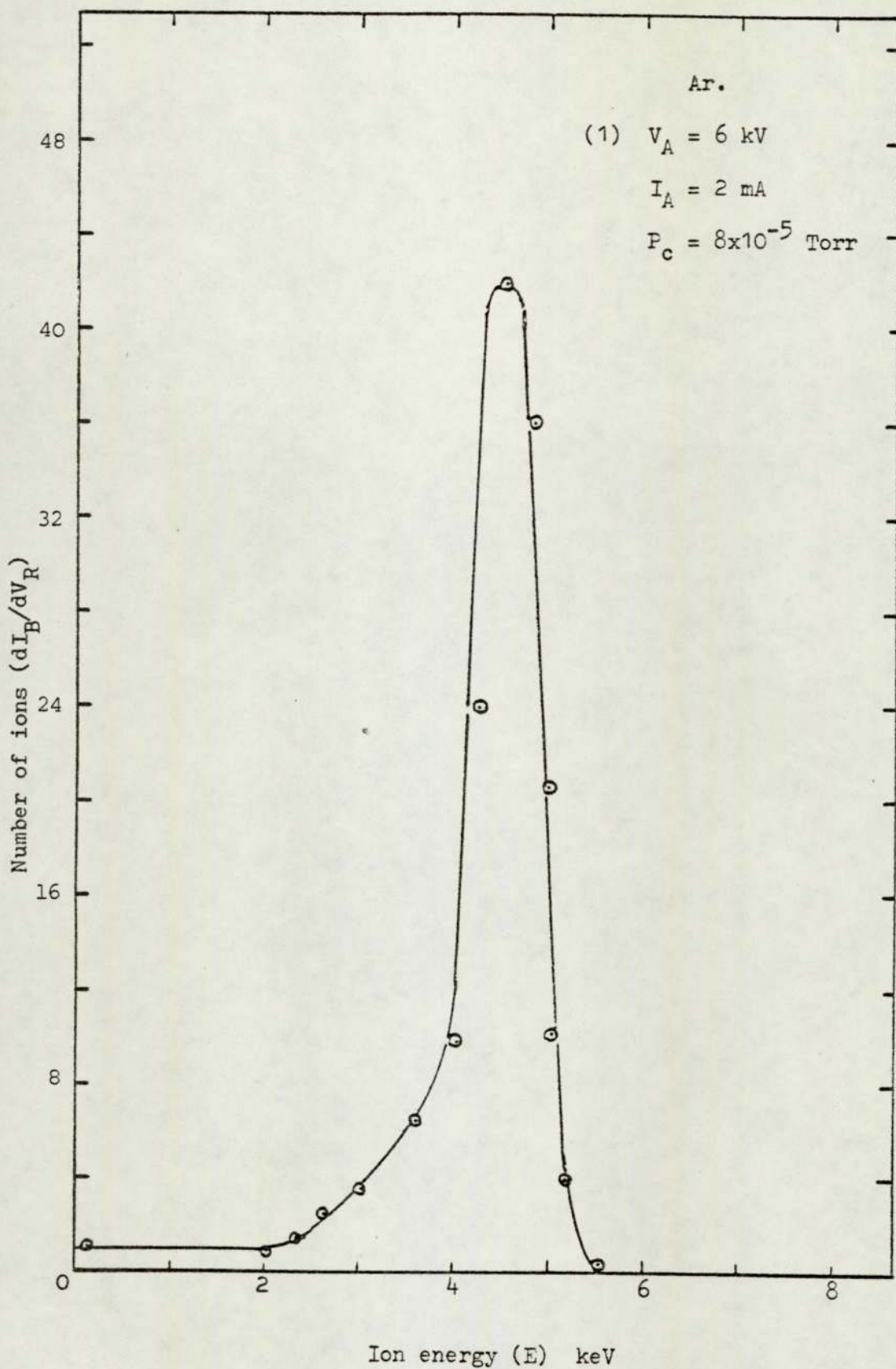


Figure 6.12. Ion energy spectrum for the spherical source using argon.

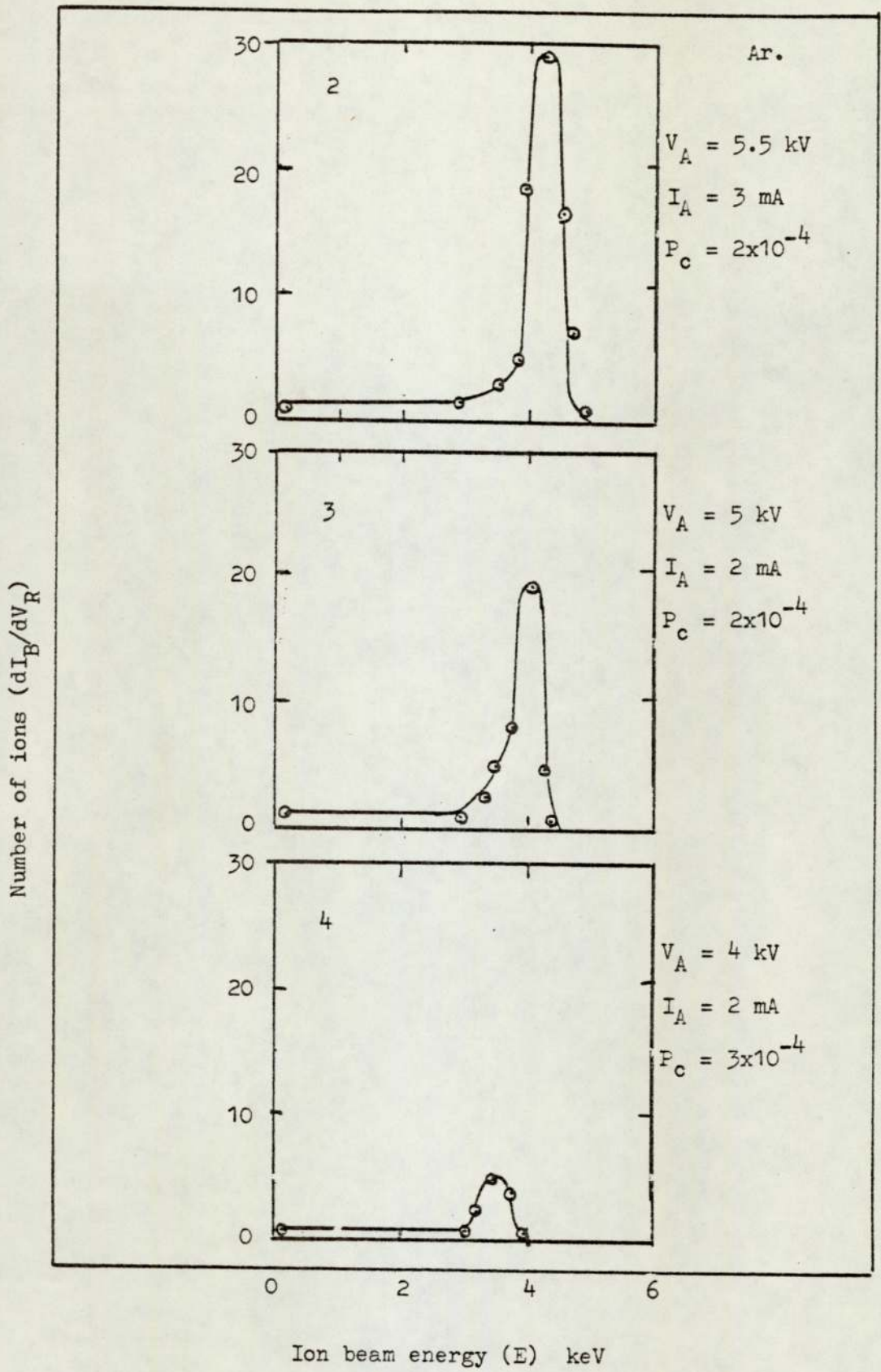


Figure 6.13. Ion energy spectrum for the spherical source using argon.

at angular positions of 4, 4.5 and 7.6° with respect to the central position with a 1 mm aperture at $V_A = 5$ kV and $I_A = 2$ mA, using argon are given in figure 6.15a to 6.15d. It is clear from these figures that the number of high energy ions is much greater at the central position shown in figure 6.15a. This number decreases when the aperture is changed from the central position. These experiments showed that the height of the peak at 4.1 keV for the central aperture reduces by about 95% when the operation is at 7.6°. This effect also is shown in Figure 6.16 showing the ions having energy greater than 60%.

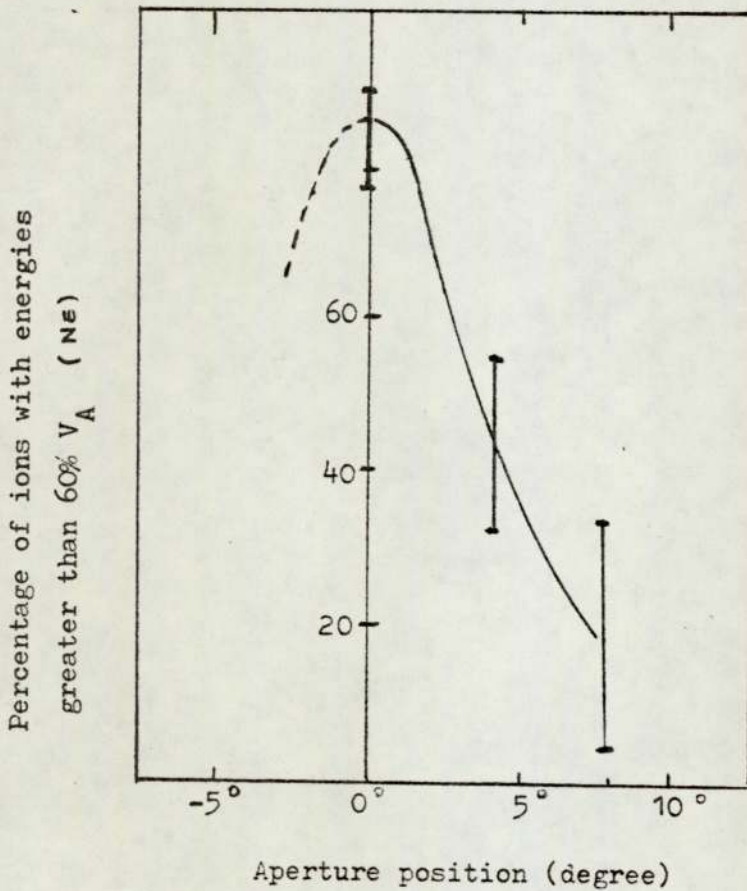


Figure 6.16. Variation of the percentage of ions having energy greater than $0.6 V_A$ with angular position of aperture.

This figure indicates that the high energy ions are much more confined to the central position of the beam than with the cylindrical source.

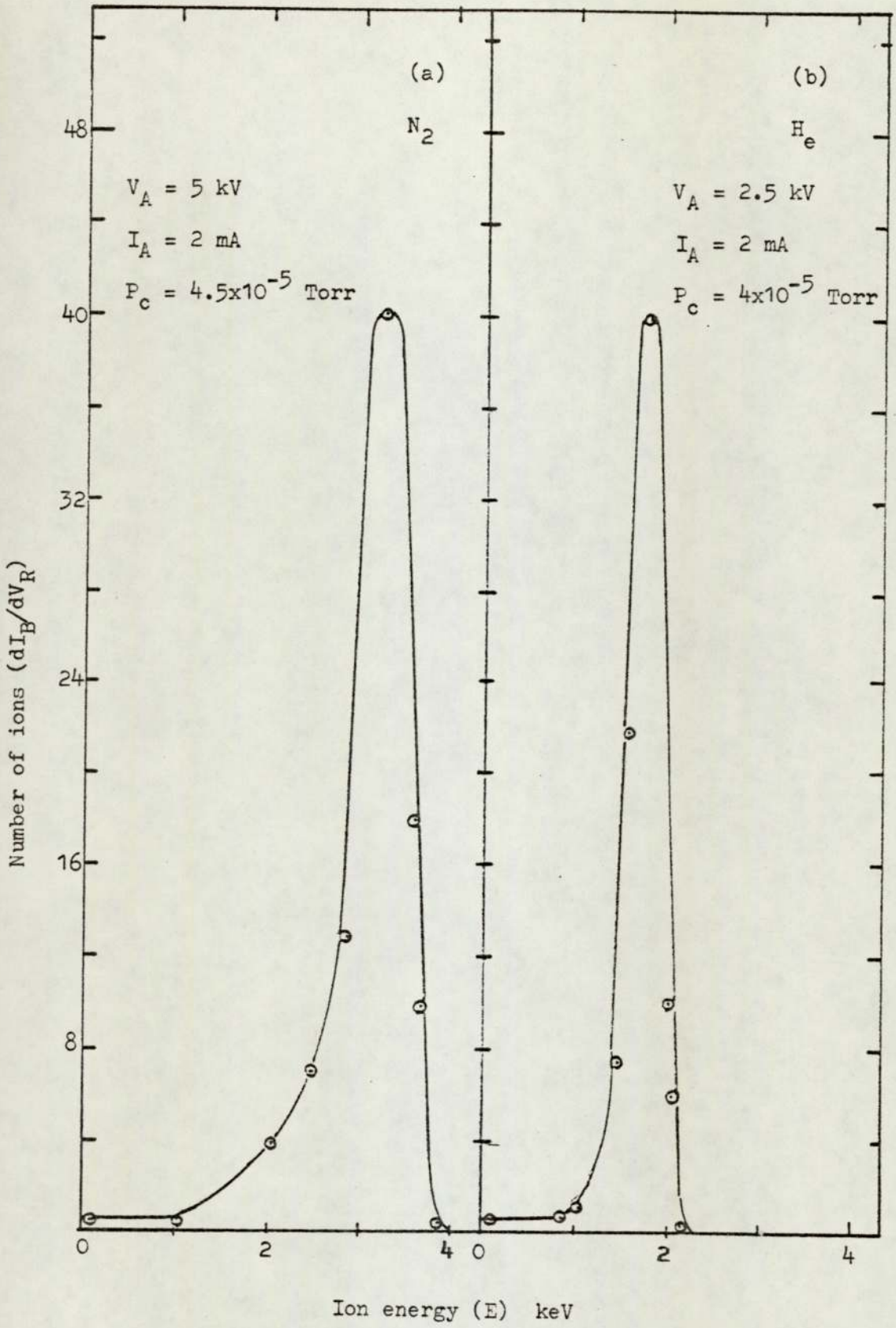


Figure 6.14. Energy spectrum for the cylindrical source using (a) nitrogen and (b) helium.

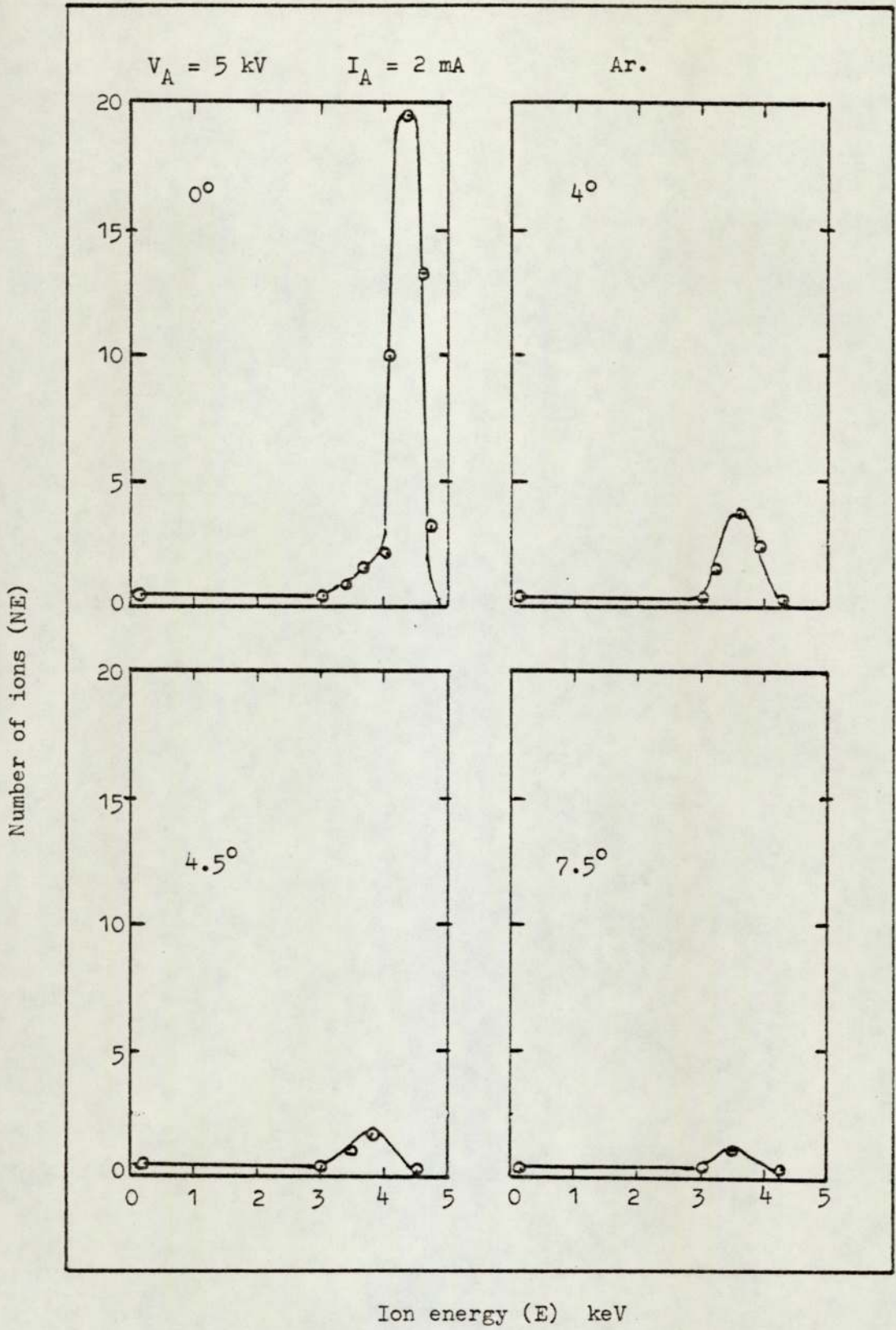


Figure 6.15. Ion energy spectrum for argon with the spherical source using 1 mm aperture at different angular positions.

Further measurements also showed that the number of high energy ions decreases when using a smaller aperture. Figure 6.17 shows the energy distribution curves for 0.55, 0.75 and 1 mm aperture at 2 mA anode current and 5 kV anode voltage. As with the cylindrical source this corresponds to a change of mode of operation.

6.4 Discussion

The energy spectra obtained in these measurements for the cylindrical source are mainly characterised by two distinct peaks at about 35 and 75% of V_A for all pressures as investigated with argon, nitrogen and helium. No evidence has been produced to indicate the presence of any additional peaks as found by Ghander⁴⁷. Present results are much more similar to those obtained by Swaminathan et al⁶⁵ using an ion source with a thermionic source of electrons whereas the present measurements were taken with the normal cold cathode source. The confidence in the present results is justified by the nature of the $I_B \rightarrow V_R$ curves where in general, when V_R is near to zero, a flat part in the curve appears which increases as the anode voltage increases, indicating the absence of very low energy ions. When $V_R > V_A$ the ion beam current is near to zero showing that the Faraday collector is fairly efficient at retaining the secondary electrons. In fact this residual current in the collector which is not always zero varies for different conditions and has been found to be greater at higher pressures or lower voltages. The high energy peak coincides with the saddle field potential between the anodes and this implies that the plasma which is maintained inside the source is at this potential. Thus the majority of ions gain this equivalent amount of energy from the field. This is most noticeable in the centre of the emerging ion beam which is as a result of electrons oscillating in the most stable configuration along the Y axis of the

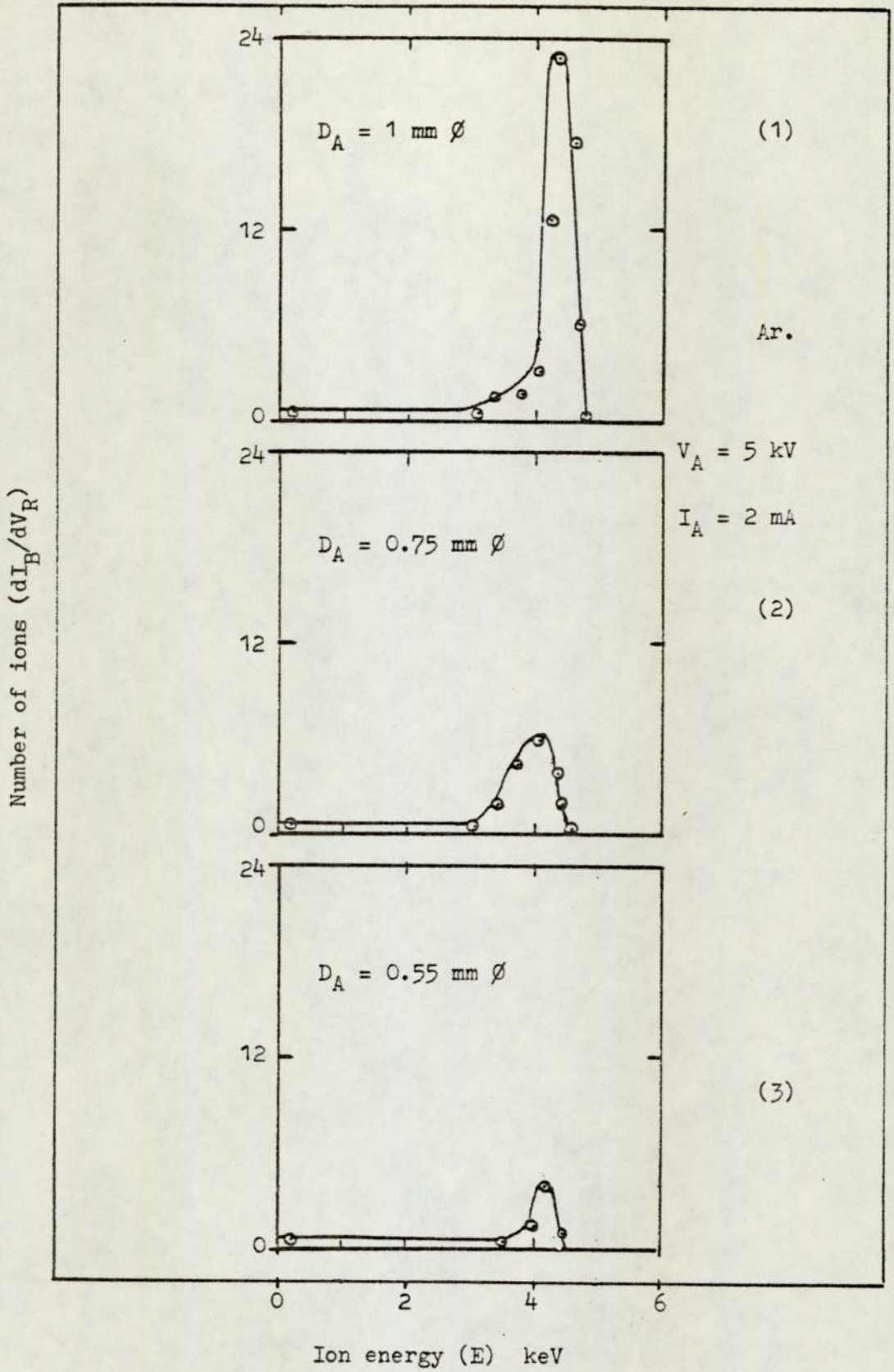


Figure 6.17. Ion energy spectrum for argon with the spherical source using different size of apertures.

source. However the presence of the low energy peak and the increased proportion of the low energy ions when the extracted ions are at the edges of the beam suggests that plasma is weak and thus there is a potential gradient across the plasma along the X axis.

In the spherical source the spectra for all gases and pressures are dominated by a single peak appearing at the saddle point potential. This is in agreement with Franks and Ghander⁵³ but no evidence has been found for a number of small peaks that they have reported. It is thought that these differences are due to the more satisfactory design of the grids and Faraday collector used in the present work. In this source the proportion of low energy ions also increase at the edges of the ion beam. The high energy ions are much more confined to the central region and this is believed to be due to the axial symmetry of the design of the spherical source, in which the end-effects of cylindrical source have been eliminated.

In both sources the percentage of the low energy ions increases as the pressure increases and with the spherical source there is a background of low energy ions extending down to a few eV. This can be explained in terms of the modes of operation in which one important effect is the increase in the production of the energetic neutrals as the source pressure increases. These results and their consequence will be discussed in the next Chapter.

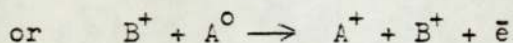
CHAPTER 7

MEASUREMENT OF ENERGETIC NEUTRALS IN THE
SADDLE FIELD ION SOURCES

7.1 Introduction

Recently Dahriwal et al⁶⁶ used a saddle field spherical ion source in the specimen stage of a scanning electron microscope for ion etching and applied it to a variety of materials. They observed that the source could be used with electrically insulating materials as well as conductors, and suggested that this was due to the presence of energetic neutrals in the emerging ion beam.

These sources are expected, as all other plasma devices, to produce energetic neutral particles. It should be mentioned that in the majority of these experiments the ion beam production inside the source is restricted to the electron atom collision rather than ion atom collision. However it is possible to say that ionisation is followed usually by



Therefore in order to assess the ion beam quality and determine the ratio of ions to neutrals in the extracted beam two main problems must be considered;

- (a) The formation of the ion beam by extraction from a plasma source and,
- (b) The neutralisation or recombination of the ion beam or charged particles.

The latter process mostly takes place when an ion and electron collide at low pressures. Thus they have a finite probability of recombining into neutral atoms. In this process in order to conserve momentum, a third body must be presented. If this third body is an emitted photon, the process is called radiative recombination and if it is a particle the process is called three-body recombination. It is due to the fact that ionisation inside the ion source in all conditions, especially when the pressure is high, cannot be perfect and some unionised but energetic atoms escape from the aperture.

Moreover the ion beam is expected to contain ions and neutrals, but it is also possible to say that a small percentage of low energy electrons, produced by ions hitting the edges of the aperture, leave the source. These electrons can combine with some of the ions to increase the number of energetic neutrals in the ion beam. This process can be shown by:



where A_F^0 is the energetic neutral.

However in these cold cathode ion generators in spite of the possibility of creating both singly and doubly charged ions using argon or nitrogen⁴⁹, only singly charged ions have received attention in the present work. In the next section experiments will be described in which an attempt has been made to determine the neutral content of the beam as a function of pressure and anode voltage for various gases. This is important because there has been little published work on this subject and the only information at present available is contained in a commercial publication by Ion Tech Ltd., for the spherical source but no details of the experimental methods used are given.

7.2 Design of the analyser

An electrostatic analyser has been designed and developed which involved a determination of the secondary electron coefficient of the collector materials in order to measure the proportion of energetic neutrals in the beam produced by both types of saddle field ion sources using argon, nitrogen and helium. The analyser consisted essentially of two nickel plates P_1 and P_2 which were used when it was required to deflect the ion beam and two different collectors. One was a flat nickel plate and the other was the Faraday collector as described in Chapter 4 which is known to be reliable at retaining the secondary electrons produced by energetic neutrals and ions. The analyser was designed to deflect the emerging ion beam in an electrostatic field when a positive and negative voltage was applied to the side plates (P_1 and P_2) as Figure 7.1 shows:

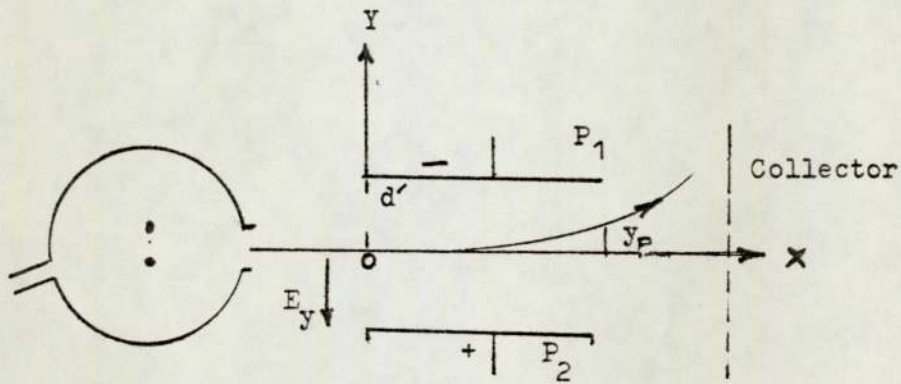


Figure 7.1. The basic ion deflecting system.

The equation of motion for a singly charged particle in this field shows that the deflection (y_p) of the ion at an energy eV_A due to the potential differential of the deflector plates, $V_D = (V_2 - V_1)$ is;

$$y_p = \frac{x_p^2}{4d'} \cdot \frac{V_D}{V_A} \quad \dots\dots 7.1$$

where x_p is the length of the deflector plate and $2d'$ is the distance between them.

The two deflector plates, 4 cm in length and 3 cm apart, were about 1.2 cm away from the source to prevent electrical breakdown between the source body which was earthed and plates. This distance was also close enough to enable the secondary electrons produced at the aperture to be collected by the positive plate and hence minimise the electron-ion recombination. The deflecting voltages were produced by negative and positive polarity power supplies. Three digital meters connected to the deflecting plates and collector could show the alignment of the analyser. The simple diagrams of source and the analyser showing the three various arrangements for ion and neutral measurements are given in Figures 7.2a, b and c.

Assuming singly charged ions, in Figure 7.2a using the Faraday collector and with $V_D = 0$, the current i_1 indicates the number of ions. In Figure 7.2b $V_D = 0$ but the Faraday collector was replaced with a flat nickel plate and thus the collector current, i_2 , indicates the ion current and the current equal to the secondary electrons produced by the energetic neutrals and ions. In the Figure 7.2c with the same arrangement as 7.2b but $V_1 = +\frac{1}{2} V_A$ and $V_2 = -\frac{1}{2} V_A$, the collector current, i_3 , is equivalent to the secondary electrons produced by the energetic neutrals. The following equations represent these three situations;

$$i_1 = n_+ e \quad \dots\dots 7.2$$

$$i_2 = n_+ e + kn_+ e + kn_0 e \quad \dots\dots 7.3$$

$$i_3 = kn_0 e \quad \dots\dots 7.4$$

where n_+ and n_0 are the number of positive ions and neutrals respectively, e is the electron charge and k is the secondary

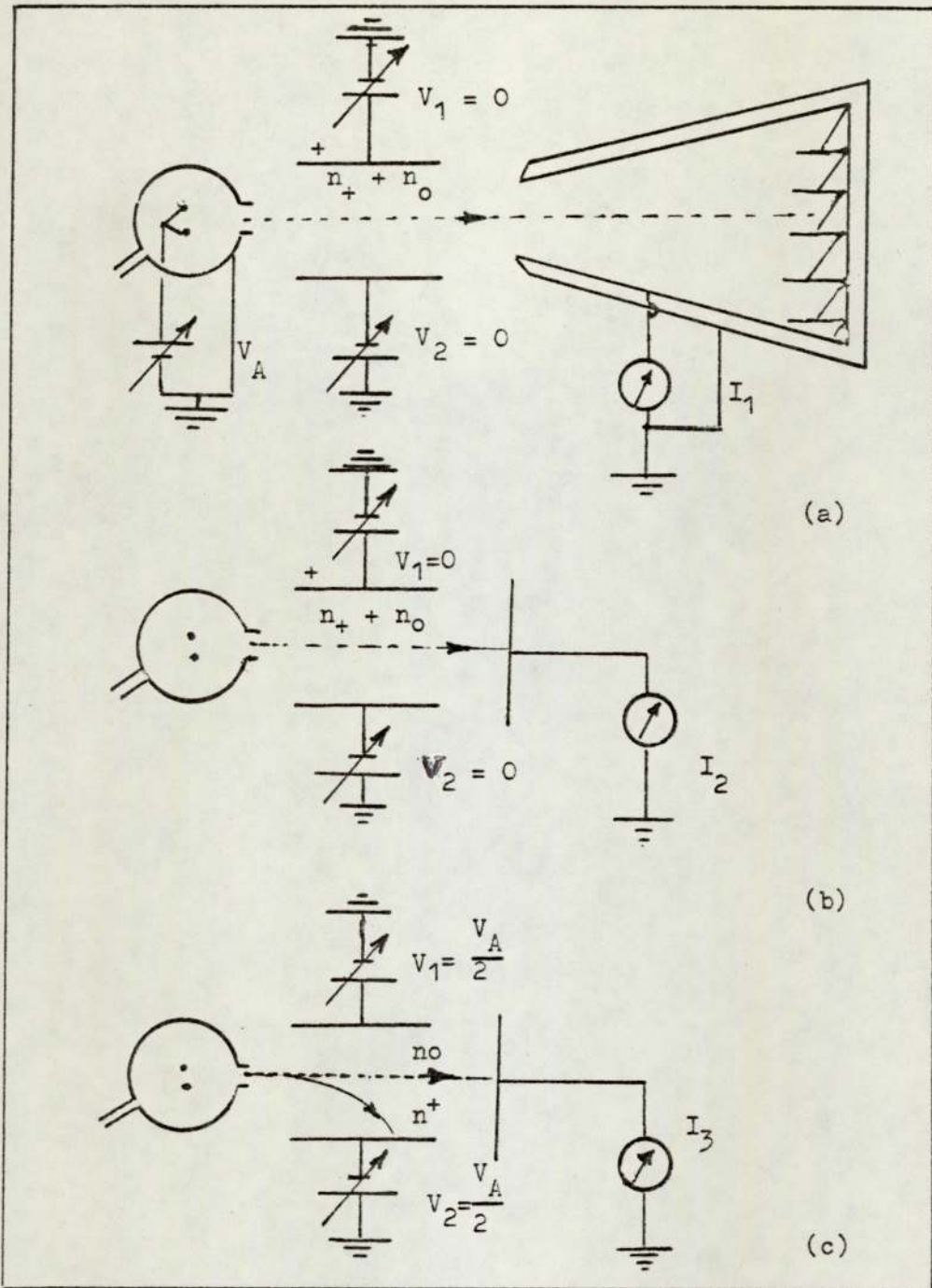


Figure 7.2. The three arrangements of the analyser.

electron coefficient assumed to be equal for ions and neutrals of the same energy. Thus by knowing the currents i_1 , i_2 and i_3 the percentage of the neutrals (N_0) and secondary electron coefficient (k) for different values of V_A and different chamber pressures, P_c , can be obtained by the following equations:

$$N_o = \frac{n_o}{n_o + n_+} \times 100 \% \quad \dots\dots 7.5$$

$$k = \frac{i_2 - i_1 - i_3}{i_1} \quad \dots\dots 7.6$$

7.3 Experimental results

a - Cylindrical source

Variations of i_1 , i_2 and i_3 with V_A and P_c at constant anode current I_A were recorded with a 5 mm aperture for the cylindrical source using argon, nitrogen and helium. Figure 7.3 shows variation of (k) obtained from above measurements with V_A for $I_A = 1, 2$ and 3 mA. The figure shows that as the V_A and hence the ion energy increases, k also increases reaching a maximum value at about 0.7. The error bars show the k values with respect to the measurement accuracy calculated from equation 7.6. Experiments showed that the error bars are greater at lower V_A or higher P_c . These large uncertainties were expected considering the limitation of the method and the likely variations of the condition of the collector surface during measurements. However the k values, as expected, do not depend upon the value of I_A . The corresponding curves using nitrogen and helium are given in Figure 7.4a and b. These curves also show that B is independent of I_A and increases with increasing V_A .

Variation of the percentage of neutrals (N_o) with V_A and therefore with P_c at constant $I_A = 1, 2$ and 3 mA using argon is given in Figure 7.5 and corresponding curves for nitrogen and helium are shown in Figure 7.6 a and b. These curves show that N_o increases when V_A decreases and thus when P_c increases. The figures also indicate that the percentage of neutrals for helium, especially at

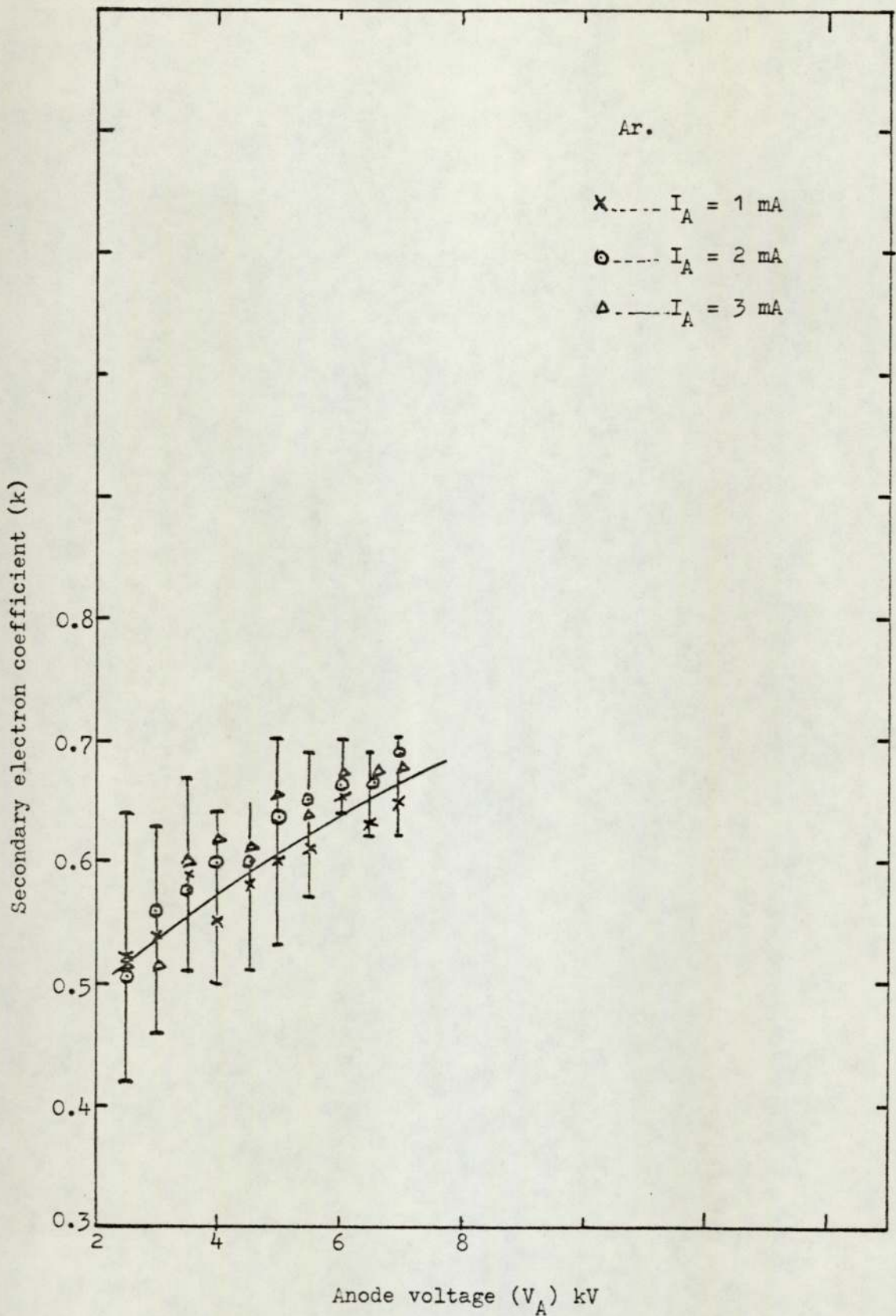


Figure 7.3. Variation of the secondary electron coefficient with anode voltage for the cylindrical source using argon.

lower V_A is much more than that for nitrogen and argon. The number of ions (n_+) at different V_A for argon, nitrogen and helium at 1, 2 and 3 mA are given in figures 7.7 and 7.8 a and b respectively. This number for all three gases increases first at lower V_A and then remains constant for further increase of V_A . It is clear from these curves that the number of ions are more constant for argon than for nitrogen and helium. However it can be said that N_0 and n_+ both depend on I_A and are greater for higher anode currents.

In order to compare these results for various gases, variation of k , n_+ and N_0 for different V_A and P_C using argon, nitrogen and helium at a constant anode current of 3 mA are given in Table 7.1

b - Spherical Source

The collector current changes with V_A and P_C in three arrangements at constant anode current I_A was measured with a 1.5 mm ion exit aperture in the spherical source using argon, nitrogen and helium. Figure 7.9 shows the k values obtained for this source with different values of V_A when $I_A = 1, 2$ and 3 mA. This figure shows that the k values increase when V_A increases, but does not change considerably when I_A varies from 1 to 3 mA as the error bars show. It is possible to say that the secondary electron coefficient in this relatively high source pressure in comparison with the cylindrical source is independent of I_A . Figure 7.10 a and b show the corresponding curves using nitrogen and helium showing that the k values increase more with increasing V_A than they do for argon.

Figures 7.11, 7.12a and 7.12b show percentage of neutrals obtained from argon, nitrogen and helium respectively. Experiments showed that the percentage of the neutrals is much higher at low V_A and they vary from about 70% at $V_A = 2$ kV to less than 20% when $V_A = 7$ kV.

Gas	$P \times 10^{-4}$ Torr	V_A kV	k	N_o %	n_+
Ar	6.2	3	0.50	37	29.5
	5.5	3.5	0.60	35	45
	4.0	4	0.62	26	46
	3.0	4.5	0.60	20	47
	2.2	5	.66	16	47
	1.5	6	.67	17	46
	0.95	7	.68	14	47
N ₂	2.7	3	0.74	38	37
	1.8	3.5	0.80	28	39
	1.4	4	.86	26	42
	1.2	4.5	.92	27	47
	0.8	5	.94	26	49
	0.7	6	.93	23	46
	0.5	7	1.0	20	47
He	2.2	3	.72	39	23
	1.8	3.5	.77	33	26
	1.5	4	.73	26	30
	1.2	4.5	.69	21.5	32
	1.0	5	.72	20	33
	0.85	6	.75	18	35
	0.65	7	.84	16	36

Table 7.1 Variation of k, N_o and n_+ with V_A and P_c using argon, nitrogen and helium with cylindrical source for $I_A = 3$ mA

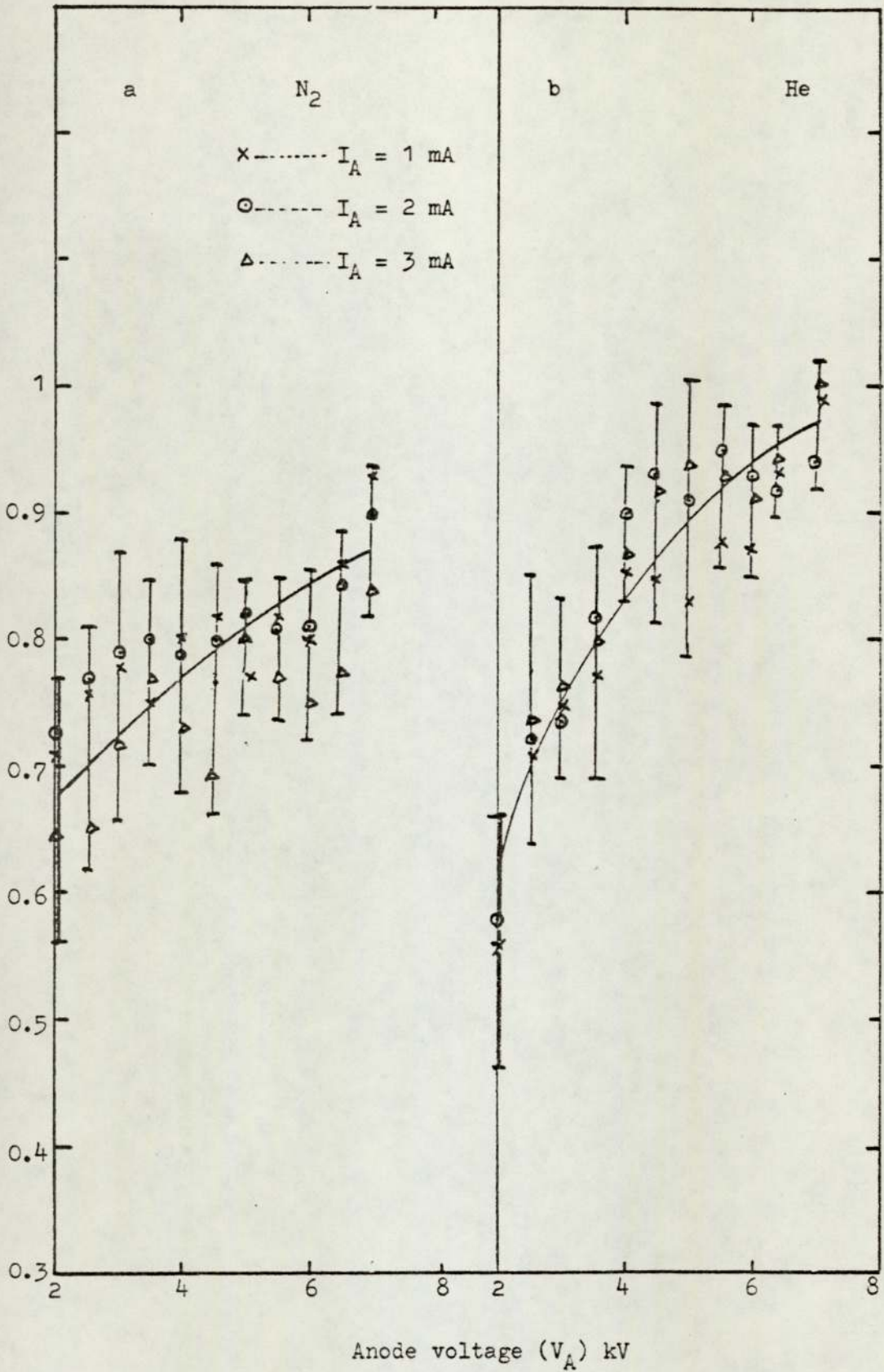


Figure 7.4. Variation of secondary electron coefficient with anode voltage for the cylindrical source using nitrogen and helium.

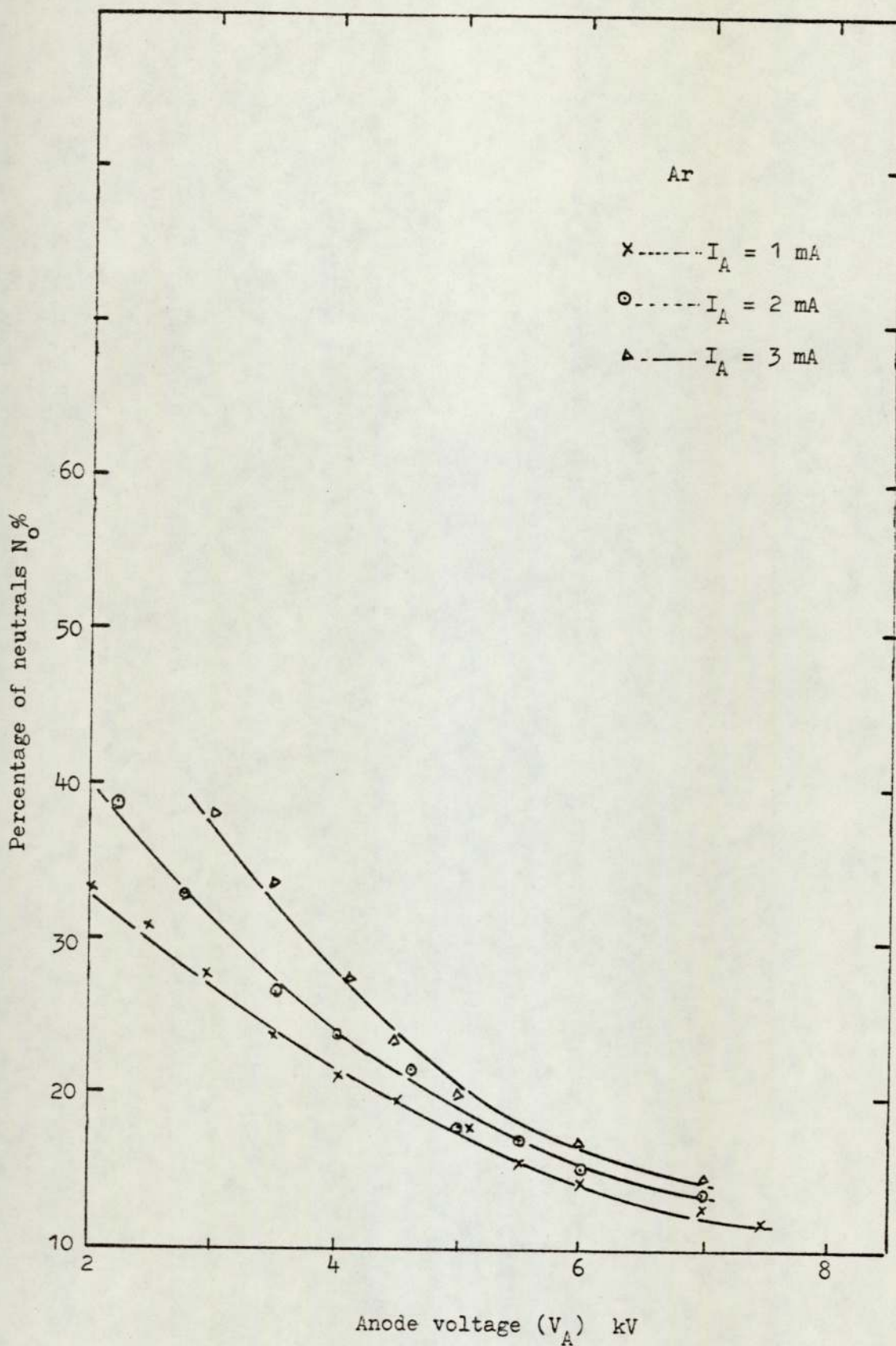


Figure 7.5. Percentage of neutrals against the anode voltage for the cylindrical source using argon.

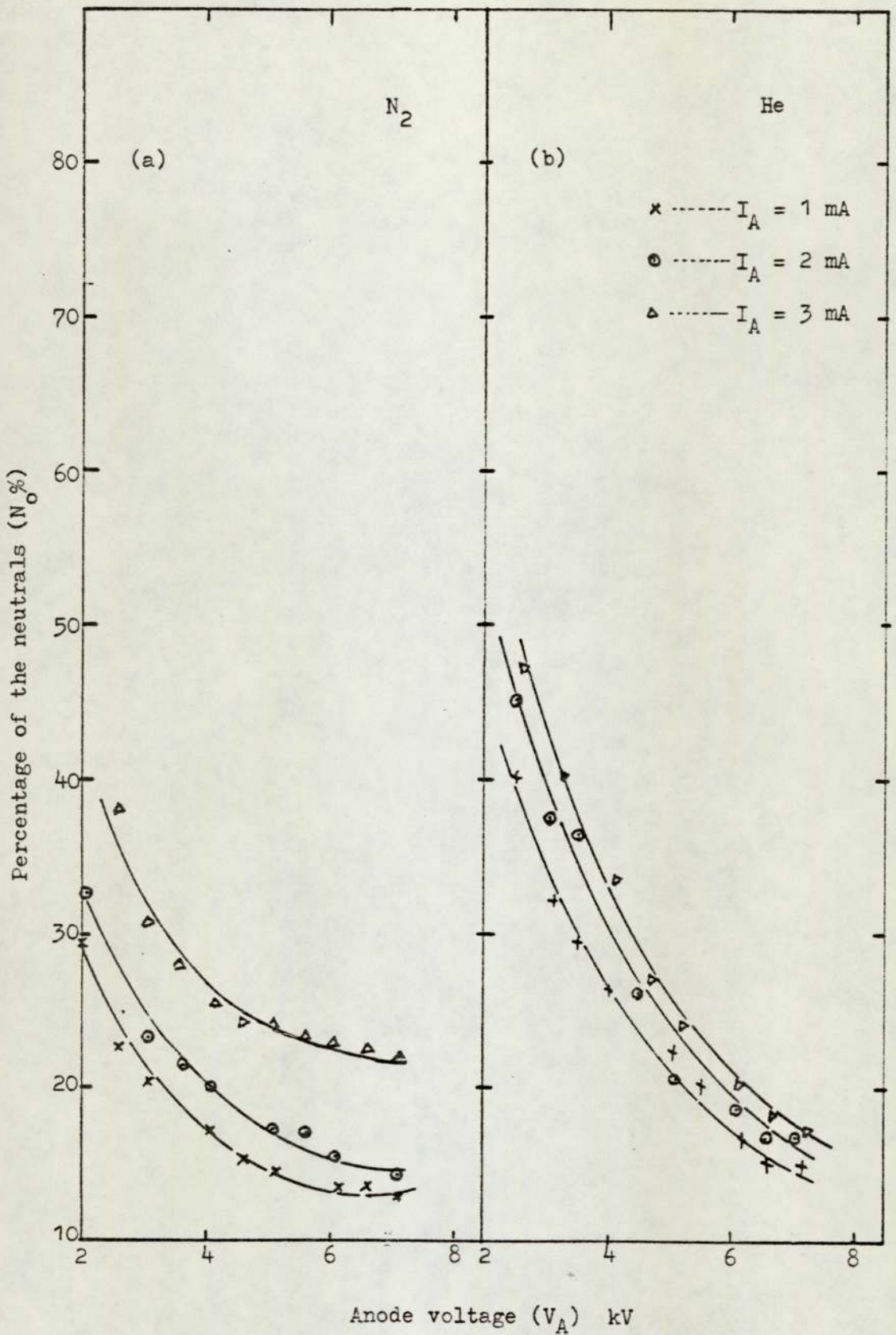


Figure 7.6. Variation of percentage of neutrals with anode voltage for the cylindrical source using nitrogen and helium.

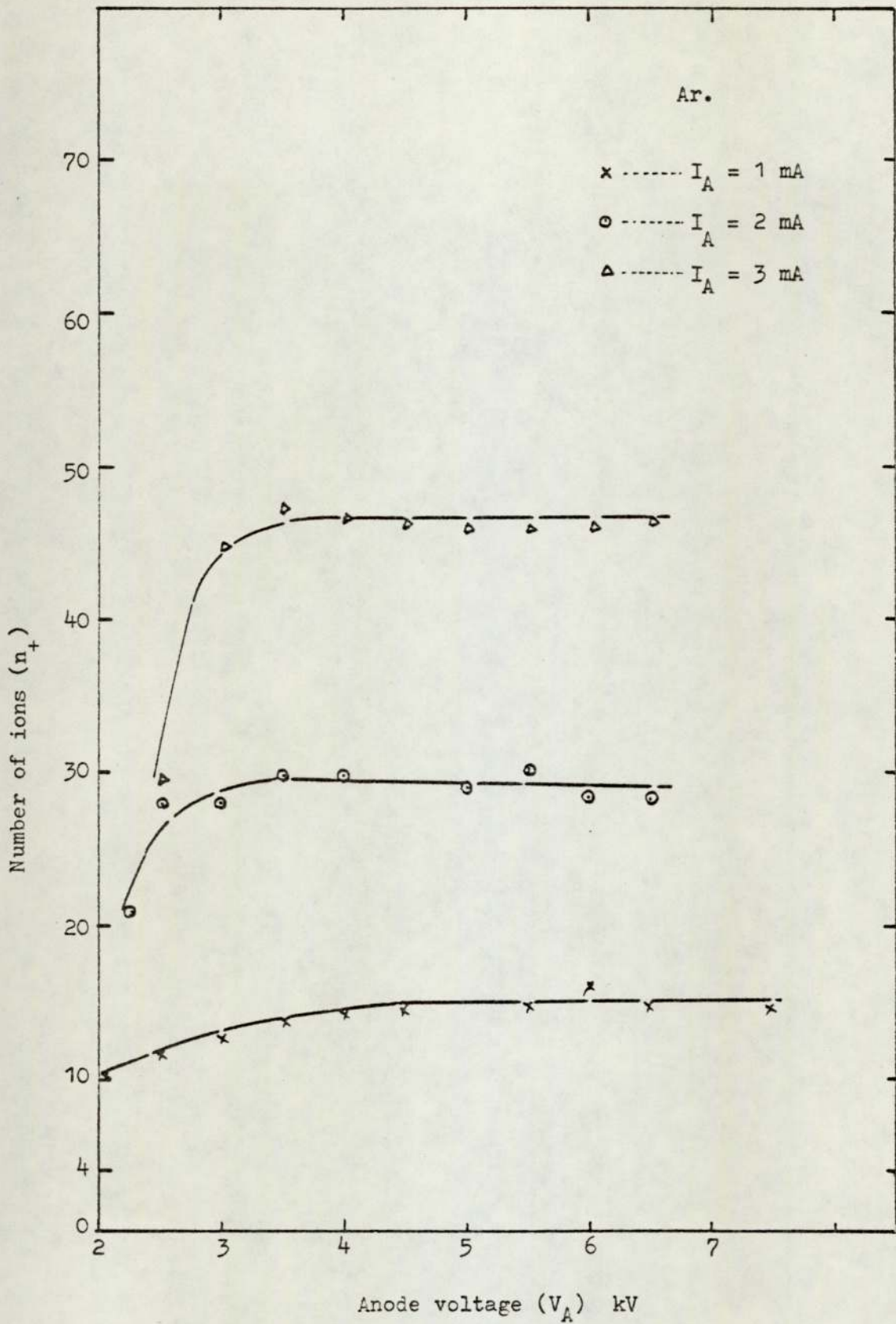


Figure 7.7. Variation of number of ions with anode voltage for the cylindrical source using argon.

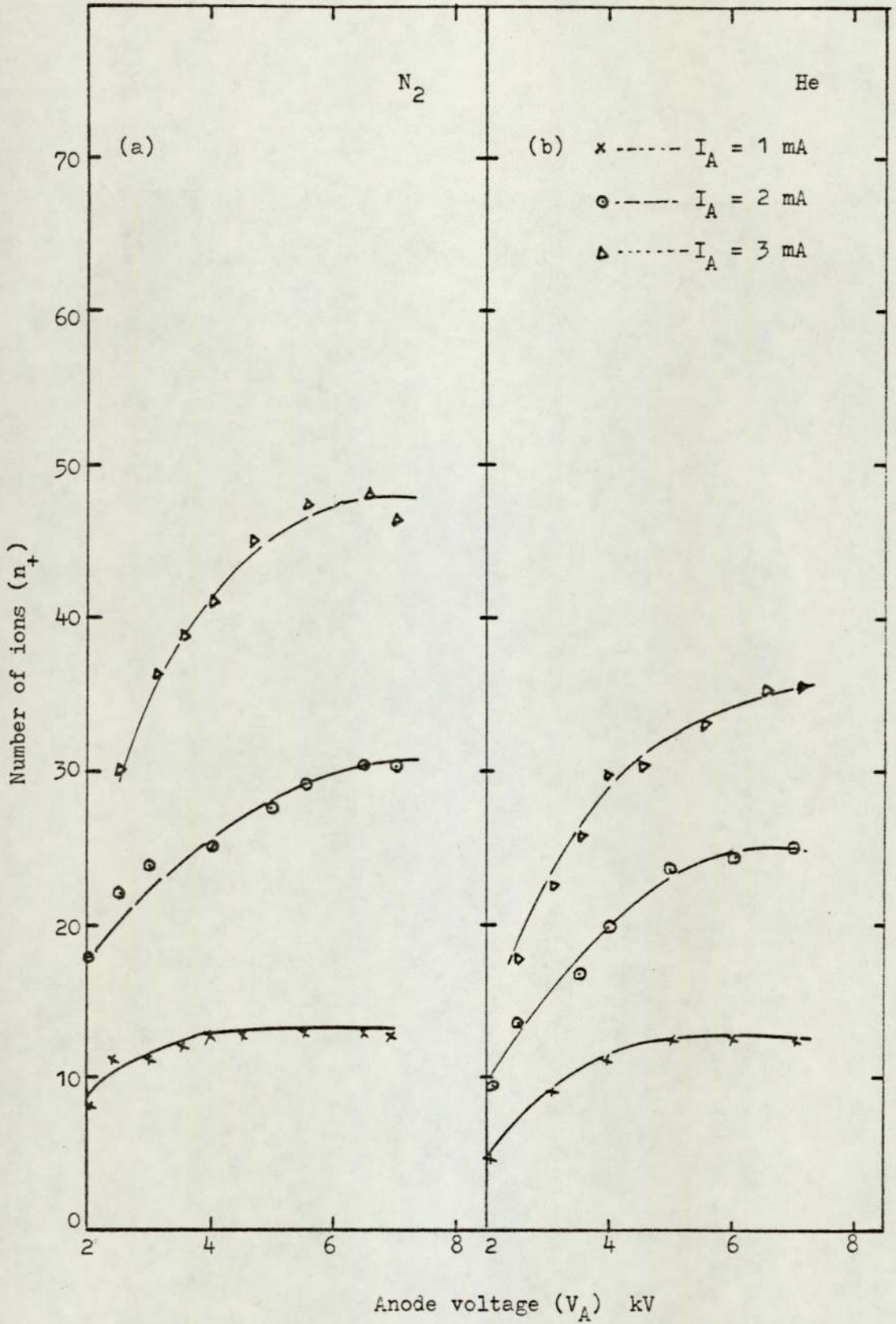


Figure 7.8. Number of ions with anode voltage for the cylindrical source using nitrogen and helium.

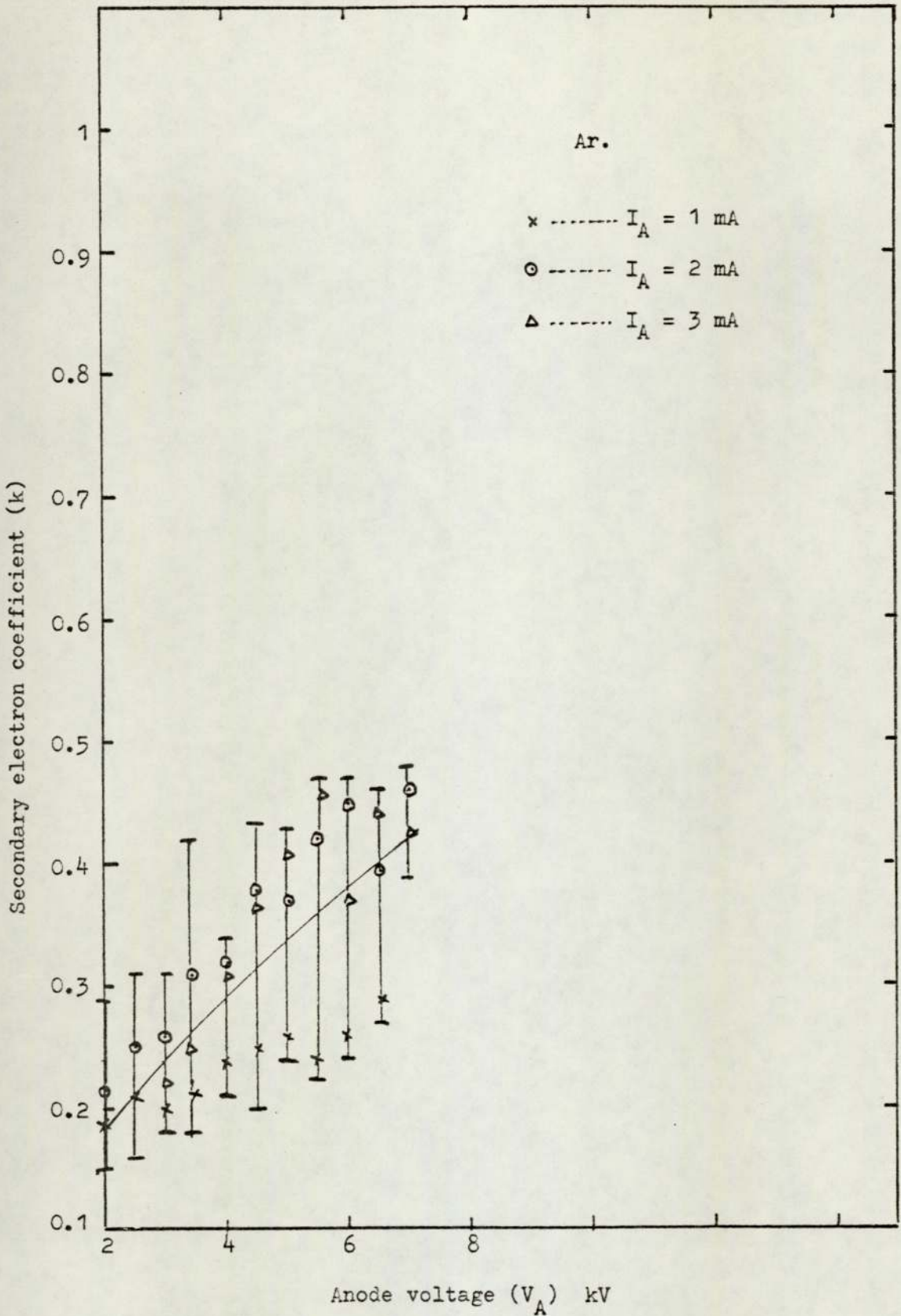


Figure 7.9. Variation of secondary electron coefficient with anode voltage for the spherical source using argon.

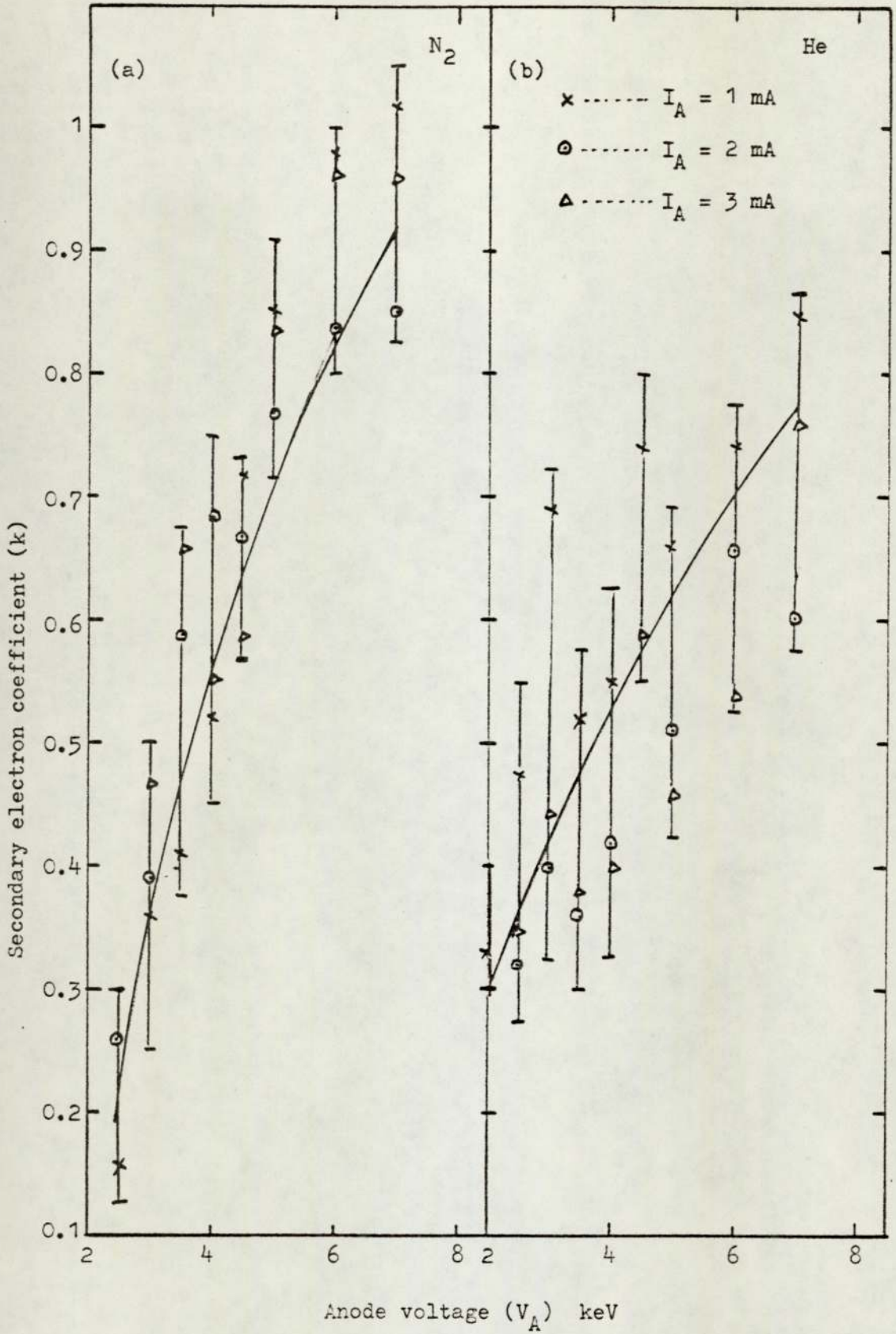


Figure 7.10. Variation of the secondary electron coefficient with anode voltage for the spherical source using nitrogen and helium.

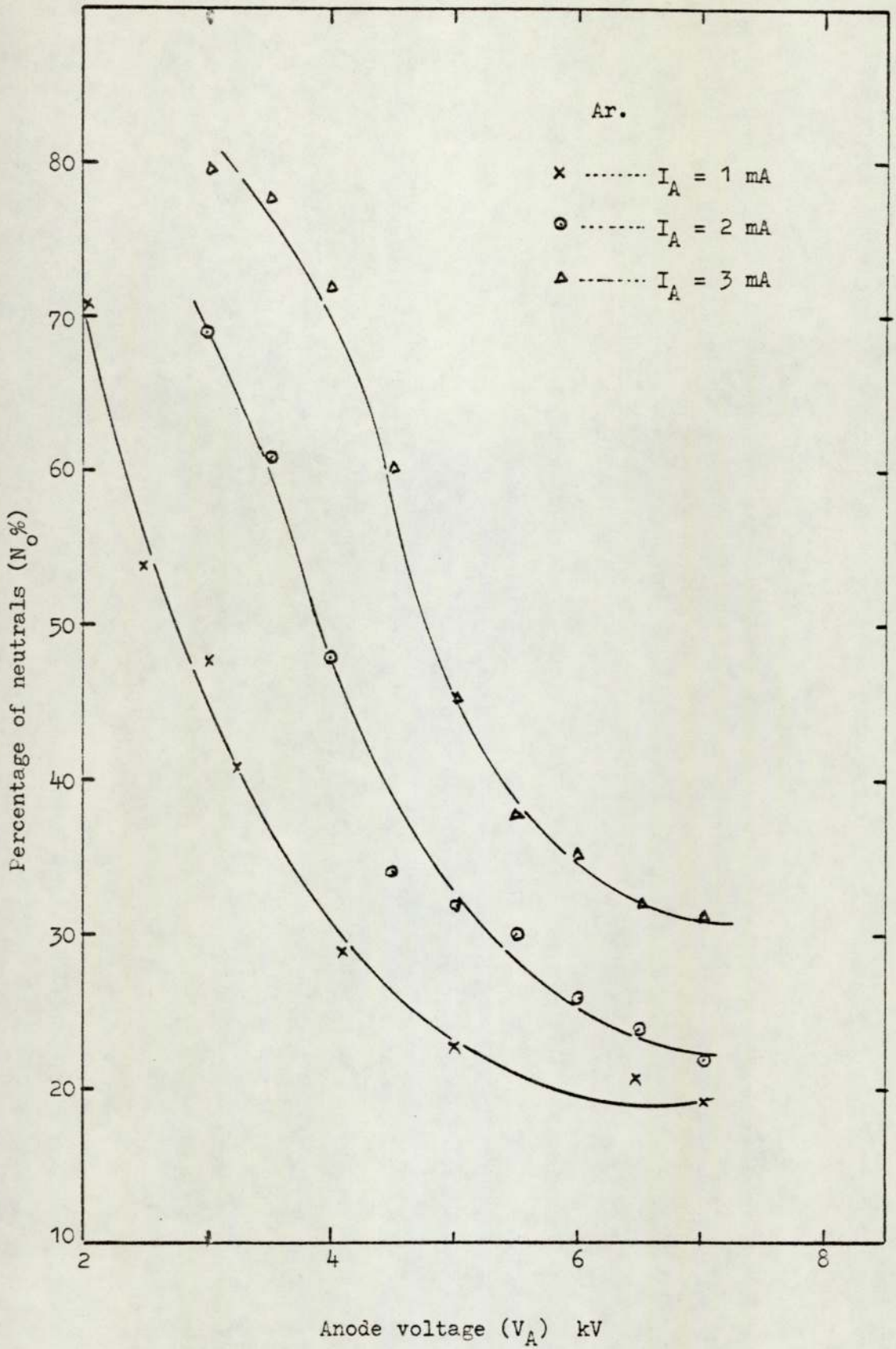


Figure 7.11. Percentage of neutrals against the anode voltage for the spherical source using argon.

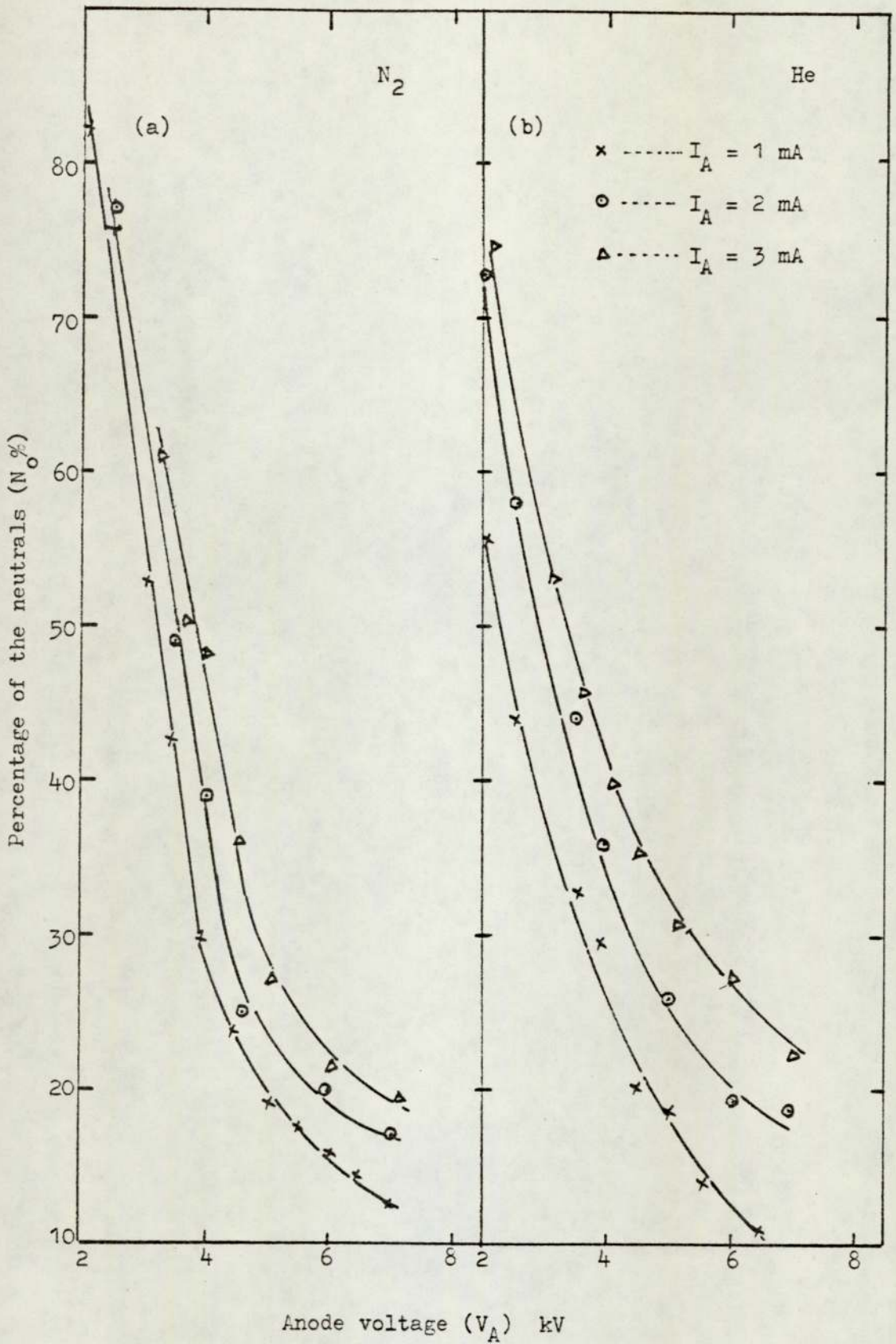


Figure 7.12. Percentage of neutrals with anode voltage for the spherical source using nitrogen and helium.

Figures 7.13 and 7.14a and b show variation of number of ions with V_A using argon, nitrogen and helium. These curves show a rapid increase in n_+ at low values of V_A and then come to a constant value at higher ion energies. However the results indicate that n_+ and N_O both are dependent on I_A . Table 7.2 shows the variation of n_+ and N_O with V_A and P_c for argon, nitrogen and helium when $I_A = 3$ mA using the spherical source.

7.4 Etching of thin films by energetic neutrals

In order to show the effect of the energetic neutrals and verify the previous results, the spherical source was used to etch a few thin films of copper using different anode voltages which correspond to various ratio of neutrals and ions with V_1 and V_2 just sufficient to separate the ions and neutrals. The time required to etch a copper film evaporated onto a glass plate was recorded for the ions (t_+) and neutrals (t_o) using argon with $V_A = 2$ to 6.5 kV and $I_A = 2$ mA.

A photograph of the etched film for various ion energies is shown in figure 7.16, and the variation of the ration $R = \frac{t_+}{t_o}$ with V_A is given in Figure 7.15 which clearly follows the same variation as N_O does with V_A as is shown in Figure 7.11. For example for $V_A = 3$ kV and $I_A = 2$ mA when $N_O = 70\%$ the required etching time is about 3 times less than the etching time for the ions. On the other hand when $V_A = 4$ kV and $R \approx 1$ the corresponding value of N_O is nearly 50%.

This overall agreement between N_O and R is as good as could be expected, taking into account the likely uncertainty in the values of N_O and R in the two different types of experiments.

7.5 Discussion

The range of variation of the secondary electron coefficient, k , from 0.2 to about 0.95 found for ion energies from 2 to 7 keV with all gases are in reasonable agreement with the published literature

Gas	$P \times 10^{-4}$ Torr	V_A kV	k	N_o	n_+
Ar	2.4	3	.22	80.5	6.0
	2.2	3.5	.24	78	7.6
	1.3	4	.27	72	14
	.52	4.5	.31	60	26
	.32	5	.37	41	43
	.25	6	.37	37	52.5
	0.20	7	.43	32	59
N ₂	2.6	3	.47	62	7.0
	1.9	3.5	.64	50	14.0
	1.4	4	.55	51	25
	0.7	4.6	.59	36	41
	0.45	5	.85	27.5	50
	0.32	6	1.0	21	58
	0.27	7	.96	19	62.5
H _e	0.8	3	.44	53	35
	.7	3.5	.38	48	41
	.6	4	.40	40	44
	.52	4.5	.61	36	45.5
	.44	5	.46	31	47
	.4	6	.54	28	51
	.35	7	.64	23	52

Table 7.2. Variation of k, N_o and n_+ with V_A and P_c using argon, nitrogen and helium for spherical source for $I_A = 3$ mA.

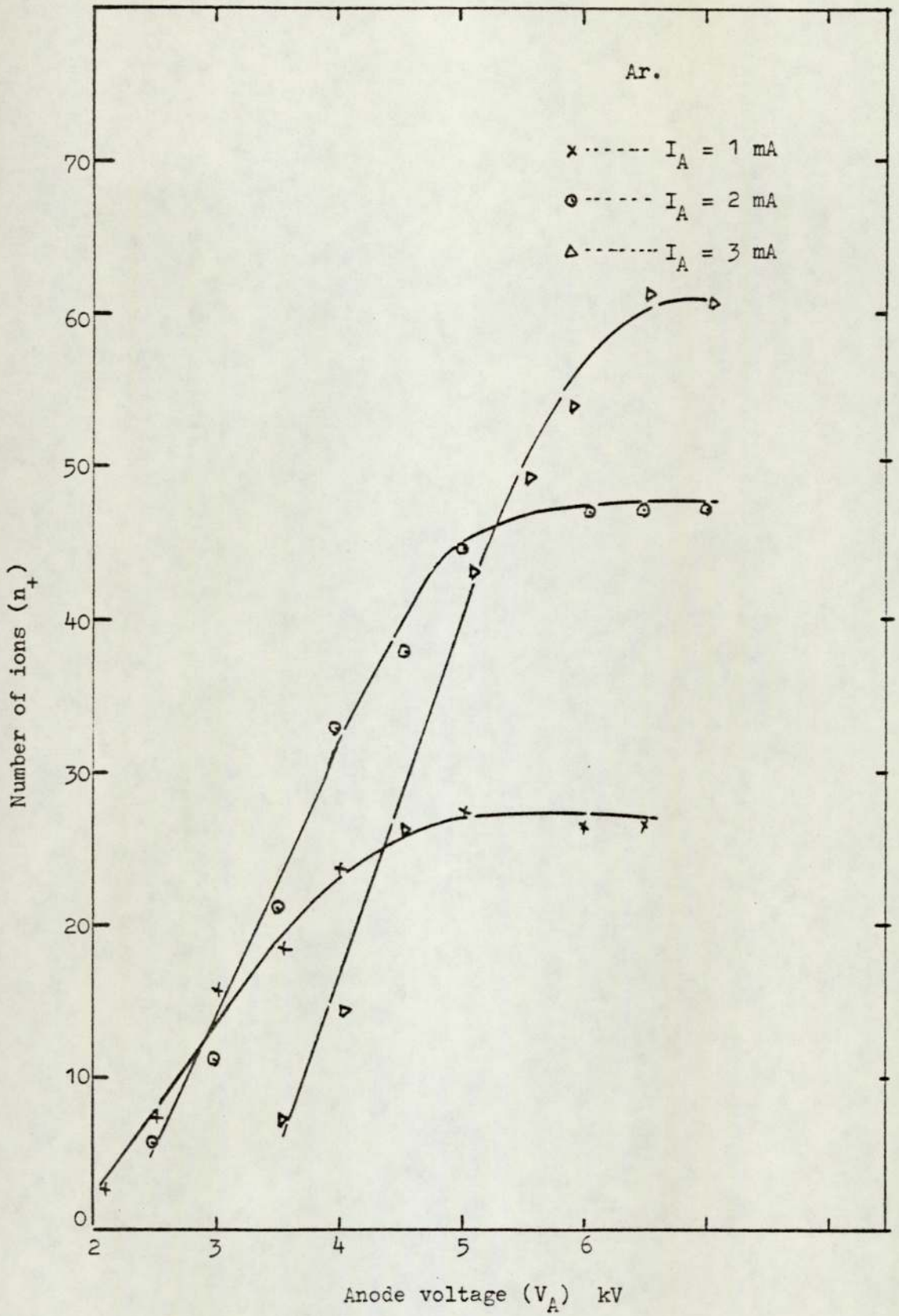


Figure 7.13. Number of ions against the anode voltage for the spherical source using argon.

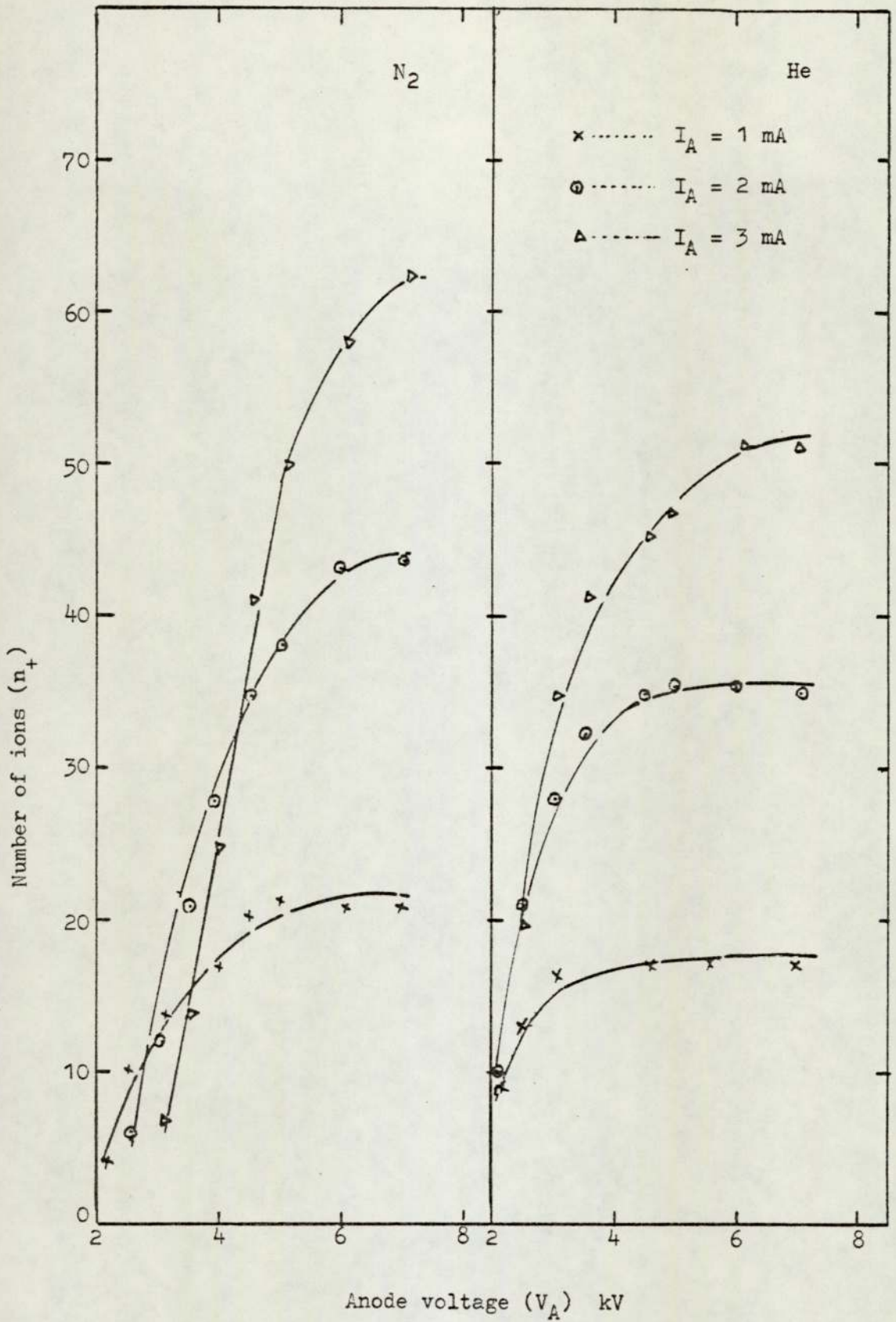


Figure 7.14. Variation of the number of ions with anode voltage for the spherical source using nitrogen and helium.

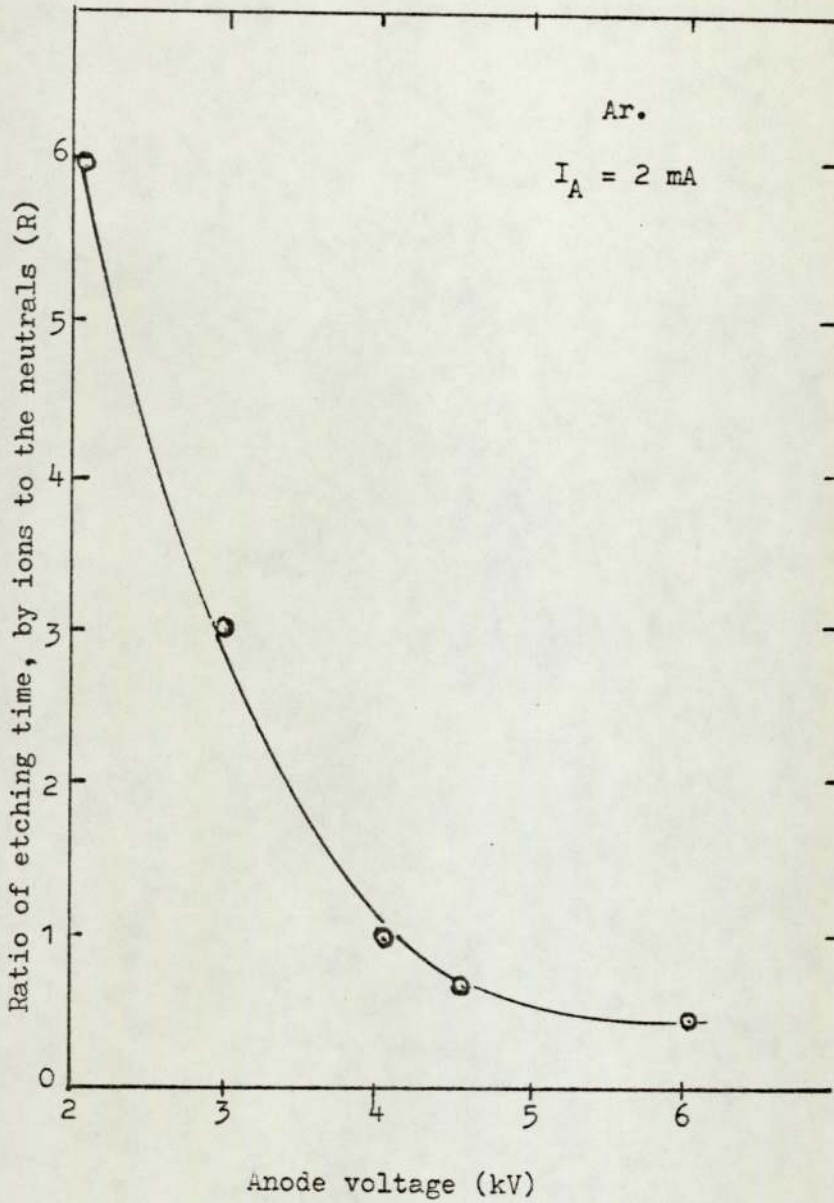


Figure 7.15. Variation of ratio of etching time by the ions to the etching time by neutrals with the spherical source using argon.

(Carter and Colligon)⁶⁷. It is realised that the experimental conditions in the present work are not suitable for very reliable and reproducible measurements, because of the type and nature of the

Etched thin film with

energetic ions and neutrals at:

$$V_A = 3 \text{ kV}$$

$$I_A = 2 \text{ mA}$$

Etched thin film with energetic ions

and neutrals at:

$$V_A = 4 \text{ kV}$$

$$I_A = 2 \text{ mA}$$

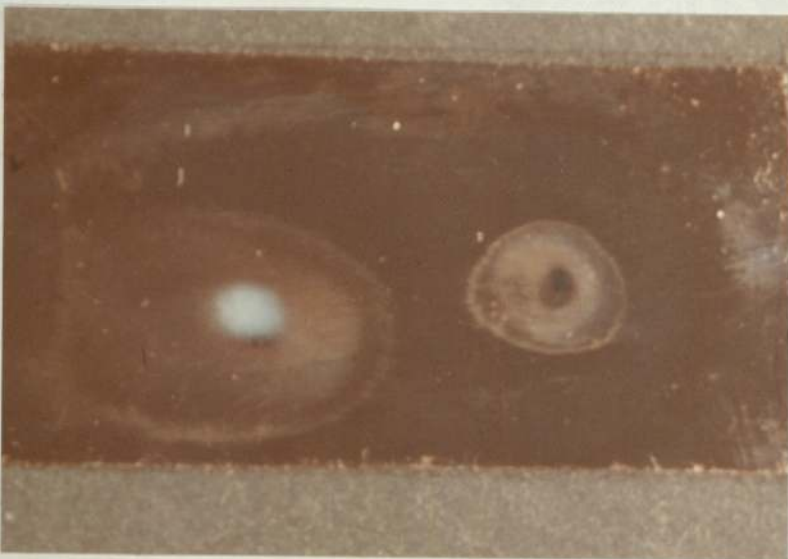
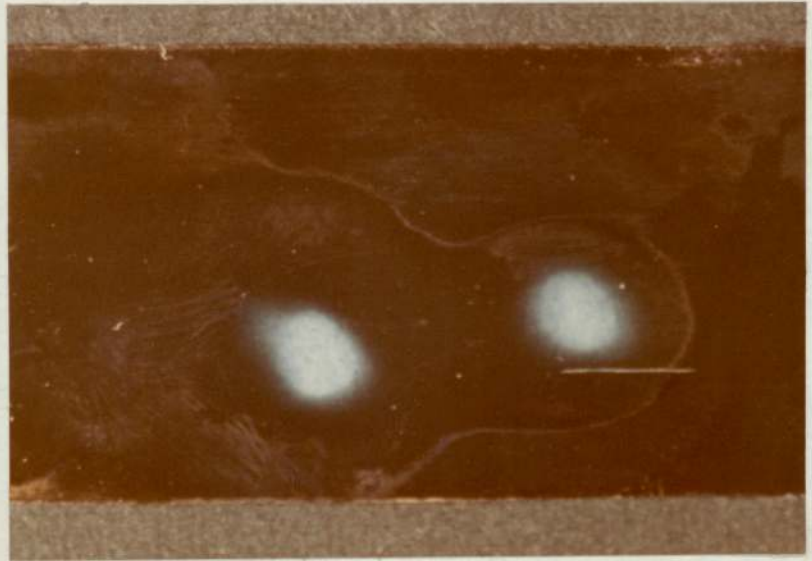
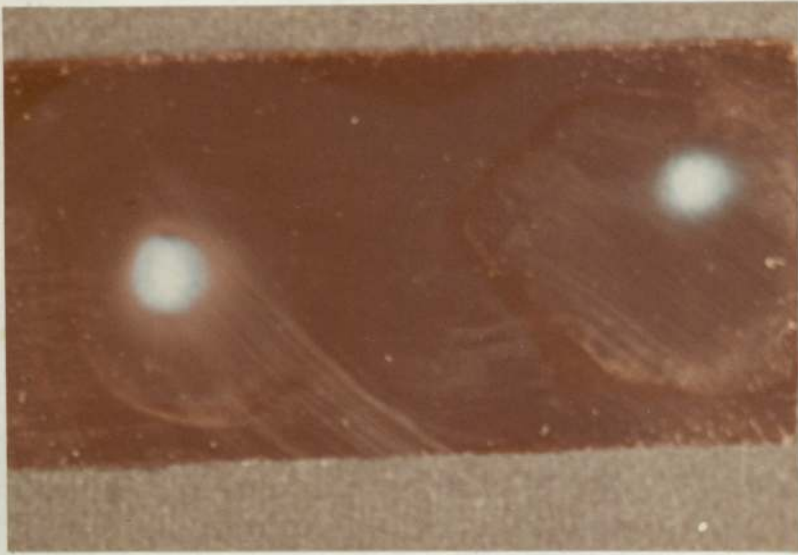
Etched thin film with energetic

ions and neutrals at:

$$V_A = 6 \text{ kV}$$

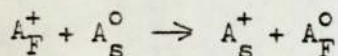
$$I_A = 2 \text{ mA}$$

Figure 7.16. Photographs of thin films etched with various ion and neutral energies.



collector surface and gas pressure. However the variation of k with V_A using both sources was found to be less with argon than nitrogen or helium. It is thought that this is due to the production of a significant proportion of the doubly charged ions with argon⁴⁹. The Figures 7.3, 7.4, 7.9 and 7.10 also show that when V_A and hence the ion energy is low the k values for all gases obtained using the spherical source are less than with the cylindrical source. This is assumed to be due to the larger number of low energy ions at high source pressures when using the spherical source.

It is clear from the results that both sources produce a significant proportion of the energetic neutrals. In all cases the percentage of neutrals increases with decreasing V_A which corresponds to an increase in P_c . Furthermore Figures 7.5 to 7.8 show that at constant V_A , N_0 increases when I_A changes from 1 to 3 mA, because P_c is greater at the larger anode current. These results can be explained assuming a symmetric resonance charge exchange process occurring inside the source in which a fast ion and a slow neutral produce a slow ion and a fast neutral⁶⁸. This can be expressed for any ion A by the following equation



The probability of the charge exchange process (p) is given by:

$$p = \sigma \bar{l} n$$

where σ is the charge exchange cross section, \bar{l} is the average path length of the ions and n is the gas density inside the ion source. This can be illustrated using the results for the spherical source when $V_A = 5$ kV, $I_A = 2$ mA and $P = 3 \times 10^{-5}$ Torr⁶⁹. The effective speed of the diffusion pump was measured and found to be about 90 l s^{-1} . Thus assuming molecular flow, the total conductance of both apertures

is 0.4 ls^{-1} which gives a pressure inside the source of about 7.0×10^{-3} Torr when $P_c = 3 \times 10^{-5}$ Torr and the corresponding value of $n = 7 \times 10^{13} \text{ mol cm}^{-3}$. At 5 kV the average ion energy is about 4 keV⁶⁴ giving a value of σ for argon as $6 \times 10^{-15} \text{ cm}^2$. The radius of the spherical source is about 1.3 cm so that it can be assumed that \bar{l} is about 1 cm. These figures give a value of $p = 0.4$ and this is in reasonable agreement with the experimental value of N_o which is equivalent to about 0.3.

Figures showing the variation of N_o with V_A for either source show that at the same anode voltage N_o is larger for the spherical source. This arises from the fact that the source pressure is much higher in the spherical source due to the larger conductance of the aperture in the cylindrical source. This investigation has shown that with these sources it is possible to set the operating conditions to select the desired energetic neutral content in the beam. This is particularly important when the source is being used for etching insulating materials.

Furthermore it has been pointed out in the energy measurements described in Chapter 6, that at high pressure using both sources the initial part of the retarding characteristic curves is not flat indicating the presence of the very low energy ions even lower than the ionisation potential. This effect can be explained in terms of the energetic neutrals produced by the charge exchange process. Thus at high source pressure the production of a large percentage of energetic neutrals results in a high proportion of low energy ions as it is shown most clearly by the low energy background on the energy spectra of the spherical source.

Of course the results discussed in this Chapter refer to the escape of energetic neutrals from the source aperture, but

frequently in ion source design one is interested in the ratio of the number of ions to the total number of gas molecules emerging from the aperture, and this enables us to define the gas ionisation efficiency, ϵ_g , of the source. These efficiencies have been calculated for both sources and are shown in Table 7.3

Source	P_c Torr	V_A	Mode	$i_+^{\mu A}$	i^+/sec $\times 10^{12}$	mol/sec $\times 10^{16}$	$\epsilon_g \times 100\%$
Cylindrical	6×10^{-4}	6	O.M	115	670	5.5	1.2
	1.7×10^{-3}	2	T.M	4	24	150	0.0016
	2.5×10^{-3}	0.5	G.M	1	6	220	0.0003
Spherical	2×10^{-5}	6	O.M	57	340	1.8	1.9
	2.5×10^{-4}	2	T.M	7	40	22	0.018
	5×10^{-4}	1.5	G.M	2	12	45	0.0027

Table 7.3. Gas ionisation efficiency at different modes of operation for the cylindrical and spherical sources at $I_A = 3 \text{ mA}$ using argon.

The Table shows the number of ions produced per second which have been calculated from the ion beam current, in the three different modes of operation, and the number of molecules per second is calculated from a knowledge of the chamber pressure and pumping speed which is assumed to be 90 l s^{-1} .

These results for ϵ_g clearly demonstrate that the gas ionisation efficiency is much higher in the oscillating mode for both sources, and as expected with the more efficient spherical source, ϵ_g is larger than with the cylindrical source. The difference in ϵ_g from the glow mode to oscillating mode is of the order of a few thousand indicating that for a source of radius 1 cm, the electron path length

is greater than 10 m. This is consistent with the value of 5 km calculated by McIlraith³³ at a source pressure of 10^{-6} Torr.

Of course, if ϵ_g is calculated in terms of the total number of energetic particles produced - ions and neutrals - it will be much greater than the figure given in Table 7.3 for the glow mode, in particular, when the source is more efficient at producing energetic neutrals than energetic ions.

CHAPTER 8

CONCLUSIONS AND SUGGESTIONS FOR FUTURE WORK

Experiments have shown that these ion sources can produce high intensity ion beams and are simple in construction and easy to operate. Their size, particularly the spherical source, makes them useful in very small vacuum chambers. It is advantageous to use the cylindrical source with a 5 mm aperture for etching a large area due to the divergence of the beam and to use the spherical source when it is necessary to have high etching rates over a small area. Since both sources can produce two beams they are useful for studying comparative etching rates of different materials under the same conditions, or alternatively one beam can be monitored while the other beam is being used for a particular application.

It has been shown that for both sources there are three operational modes namely, the oscillating, transition and glow discharge modes. This has been explained in terms of the electron-molecule mean free path inside the source. Measurements showed that the ionisation efficiency increases by nearly 1000 times in the spherical source and about 4000 times in the cylindrical source in changing from the glow mode to the oscillating mode. This indicates that the average path length of the electron can be as much as 20 m.

The cylindrical source with a broad energy spread and the spherical source with a narrow energy spread give ions of energy ranging from a few electron volts up to energies equivalent to the region of the saddle point potential. Also the variation of energy for different positions of the aperture showed that these sources could be used as an energy selector. The energy spectra in both

sources are dominated by a high energy peak confined to the centre of the beam and the majority of the low energy ions are mainly confined to the edges of the beam.

It has also been established that these sources produce a significant proportion of energetic neutrals in the beam which varies from a little as about 10% to as much as 80% depending on the source pressure. These figures are in agreement with a charge exchange process taking place inside the ion source.

These studies have produced valuable information with regard to the various applications of the sources. Moreover the variation of ion energy, the proportion of ions and neutrals and also the gas ionisation efficiency in the different modes of operation determine the application of these sources. For example if a broad energy spread is required the cylindrical source is more suitable but when a narrow energy spread is essential the spherical source will be ideal. It also has been shown that the proportion of energetic of energetic neutrals can be controlled by adjusting the pressure and advantage may be taken of this for bombardment of different materials.

All measurements discussed in the previous chapters were done over a wide range of all the variable parameters to get a better understanding of these ion sources. However further investigations must still be made on the existing sources. The plasma characteristics involving measurements of the potential distribution, ion and electron density, ion distribution and plasma temperature inside the source are essential. This could be achieved by using a simple and very small Langmuir probe, but even small probes can disturb the discharge which can make interpretation of the measurements difficult. Some other plasma diagnostic techniques such as R.F. probes, which do not disturb the

plasma⁷⁰, may be an advantage.

In future developments of these devices a small source of either type, particularly the most efficient spherical source, could be made and used to advantage. For example if small spherical sources could be made efficient enough, it might be possible to overlap a few of these for ion bombarding large areas and still retain a fairly narrow energy spread.

The ion energy should also be measured by deflecting the ion beam in an electric or magnetic field to separate them with a slit system, or using a time of flight method. It has been reported that the retarding and deflecting analysers, particularly those using only electric fields, are the most straightforward and useful analysers⁶². Thus some useful ion beam parameters such as angular divergence and diameter of the ion beam, energy spread and the mean energy of the ions could be obtained.

It also might be possible to produce ions with multiply-charged states using these sources. It is important to note that for a higher degree of ionisation the main aspects to consider are the need for a very low source pressure to avoid charge exchange, a large electron path length, and a high containment time for the ions⁶³. It is assumed that the first two conditions can be obtained with these sources, but as the ions are accelerated over a small distance of only about 1 cm in a radial direction towards the cathode, the possibility of further ionisation is less likely. It is possible that this could be achieved by using a magnetic field to contain the ions, and water cooling the source to enable it to operate at lower pressures.

Finally, although considerable effort has been made to design and test an efficient ion beam collector, it is realised the one

used in the present work is not ideal and it would be valuable to repeat many of these measurements using an ion beam calorimeter in which the problem of secondary electron emission does not arise.

APPENDIX 4.2/1

MEASUREMENT OF THE EFFECTIVE SPEED OF THE DIFFUSION PUMP

The effective speed S_E of the pump can be calculated from the following equation:

$$S_E = \frac{V}{P} \cdot \frac{dP}{dt}$$

where V and P are the volume and equilibrium pressure of the experimental chamber respectively. The rate of rise of pressure is shown in Figure 4.2/1

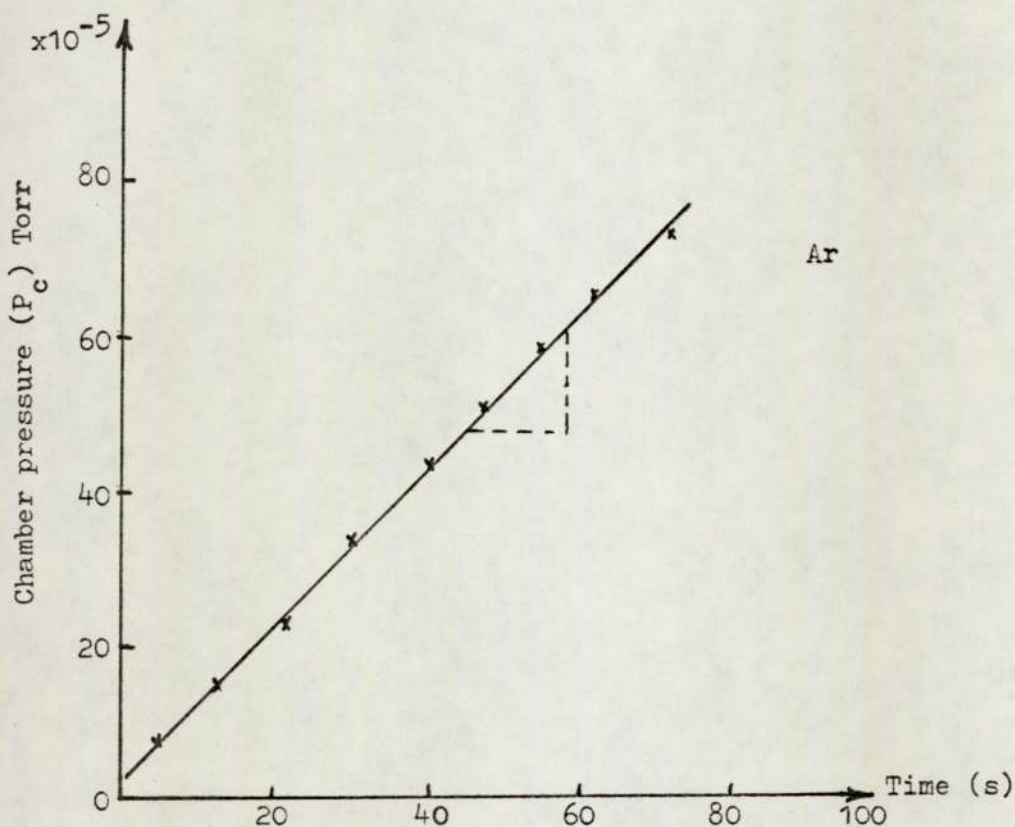


Figure 4.2/1. Variation of the chamber pressure with time

Thus the value of S_E was found to be about 90 l. sec^{-1} with $V = 35 \text{ l.}$
 $P = 4 \times 10^{-6} \text{ Torr}$ and $\frac{dP}{dt} = \frac{26}{25} \times 10^{-5} \text{ Torr.l.sec}^{-1}$. This compares with the rated speed of the un baffled diffusion pump of 400 l. sec^{-1} .

APPENDIX 4.2/2

MEASUREMENT OF THE SOURCE PRESSURE

The source pressure, P_s , can be calculated from following equation:

$$P_s = P_c \frac{(S_E + c)}{c}$$

where S_E is the effective speed of the pump, P_c is the chamber pressure in Torr and the conductance of the aperture, c , is given by:

$$c = \frac{62.5 \times A}{M^{\frac{1}{2}}} \frac{50 d_1^2}{M^{\frac{1}{2}}} \text{ l. sec}^{-1}$$

where A and d_1 are the area and diameter of the aperture respectively, and M is the molecular weight of the gas. Thus by using Ar, N_2 and H_e gases the source pressure was for example 4.6×10^{-3} , 4×10^{-3} and 1.5×10^{-3} Torr for the cylindrical source with 5 mm aperture and 2.6×10^{-2} , 2×10^{-2} , 9×10^{-3} Torr for the spherical source with two 1.5 mm apertures respectively for a chamber pressure of 1×10^{-4} Torr.

APPENDIX 5-2/3

Variation of ion beam current with input power of the cylindrical source with a 5 mm ion exit aperture using nitrogen.

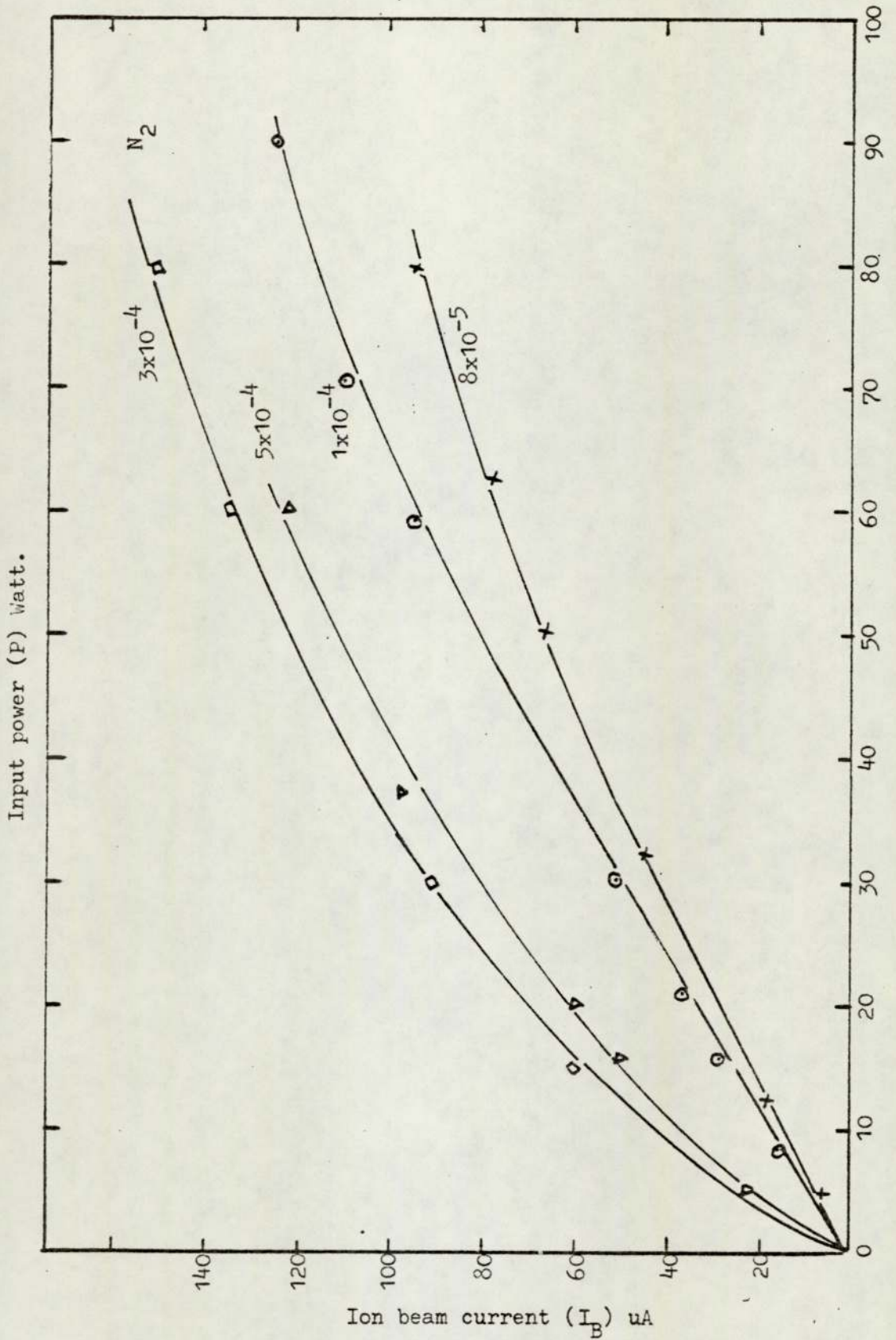


Figure 5.2/3. Ion beam current against the input power for the cylindrical source using nitrogen.

APPENDIX 5-2/4

The characteristics of the spherical source with two
1.5 mm apertures using nitrogen and helium.

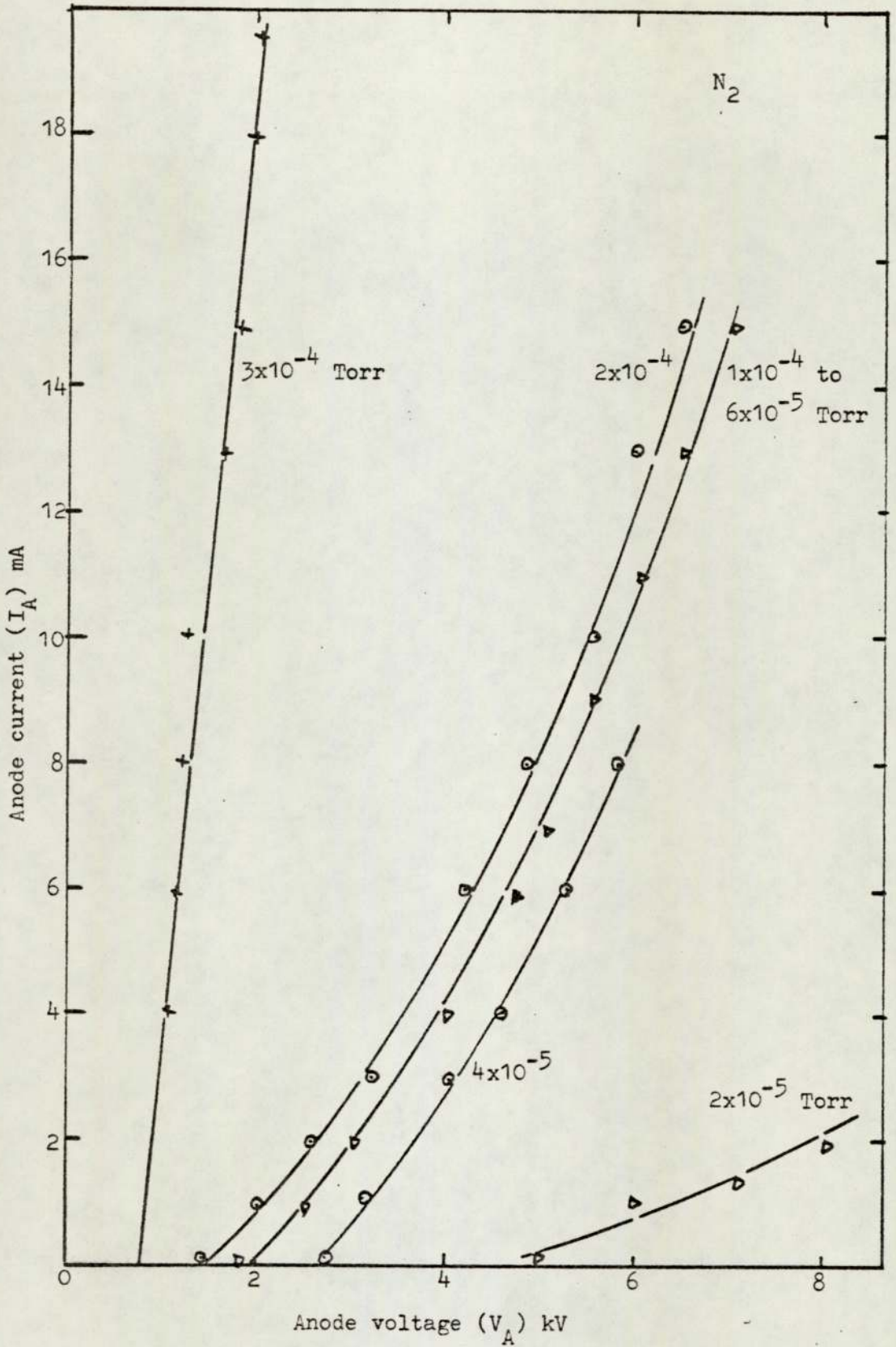


Figure 5.2/4. Anode current against anode voltage for the spherical source using nitrogen.

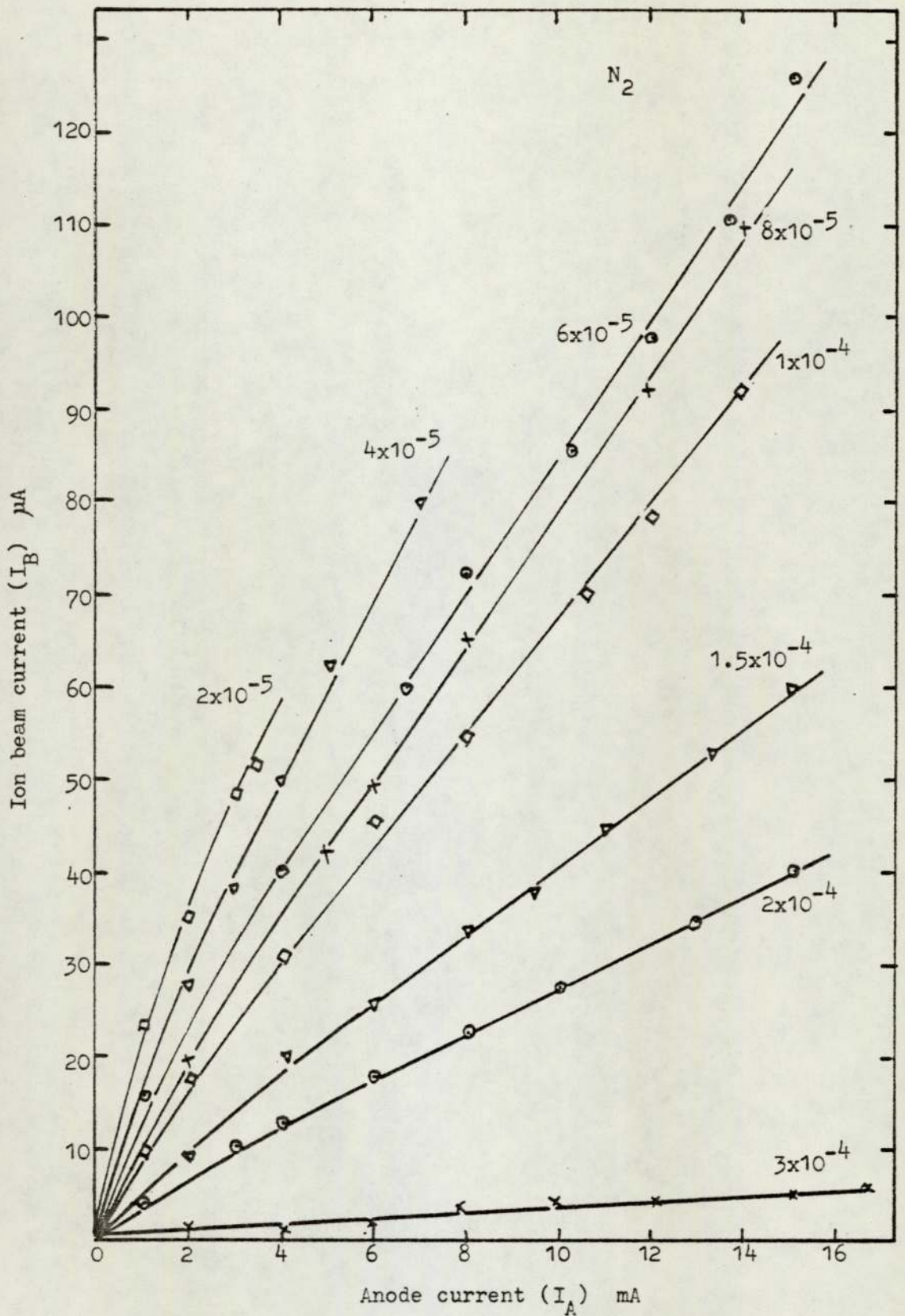


Figure 5.2/4. Variation of ion beam current with anode current for the spherical source using nitrogen.

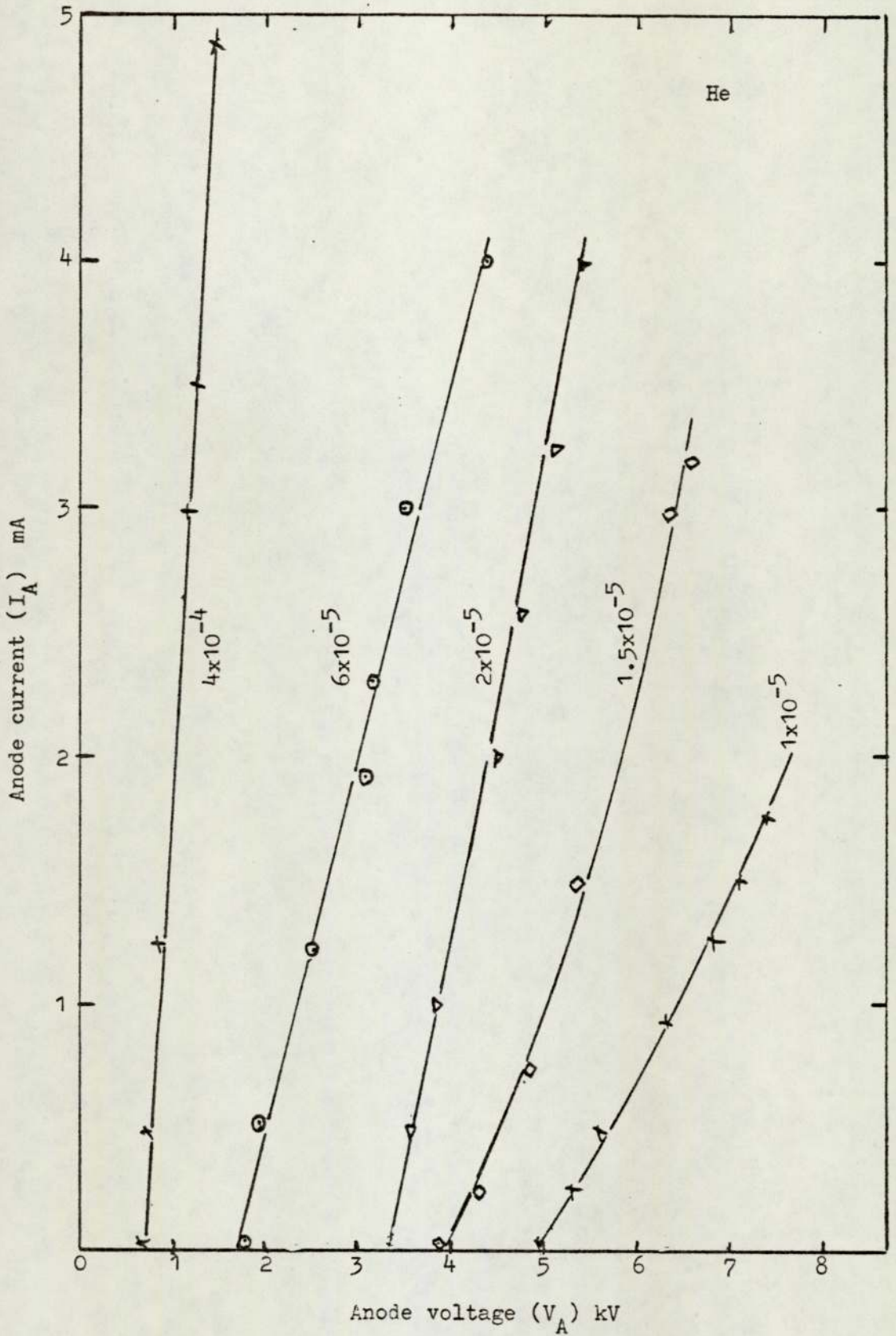


Figure 5.2/4. Anode current - voltage characteristic for the spherical source using helium.

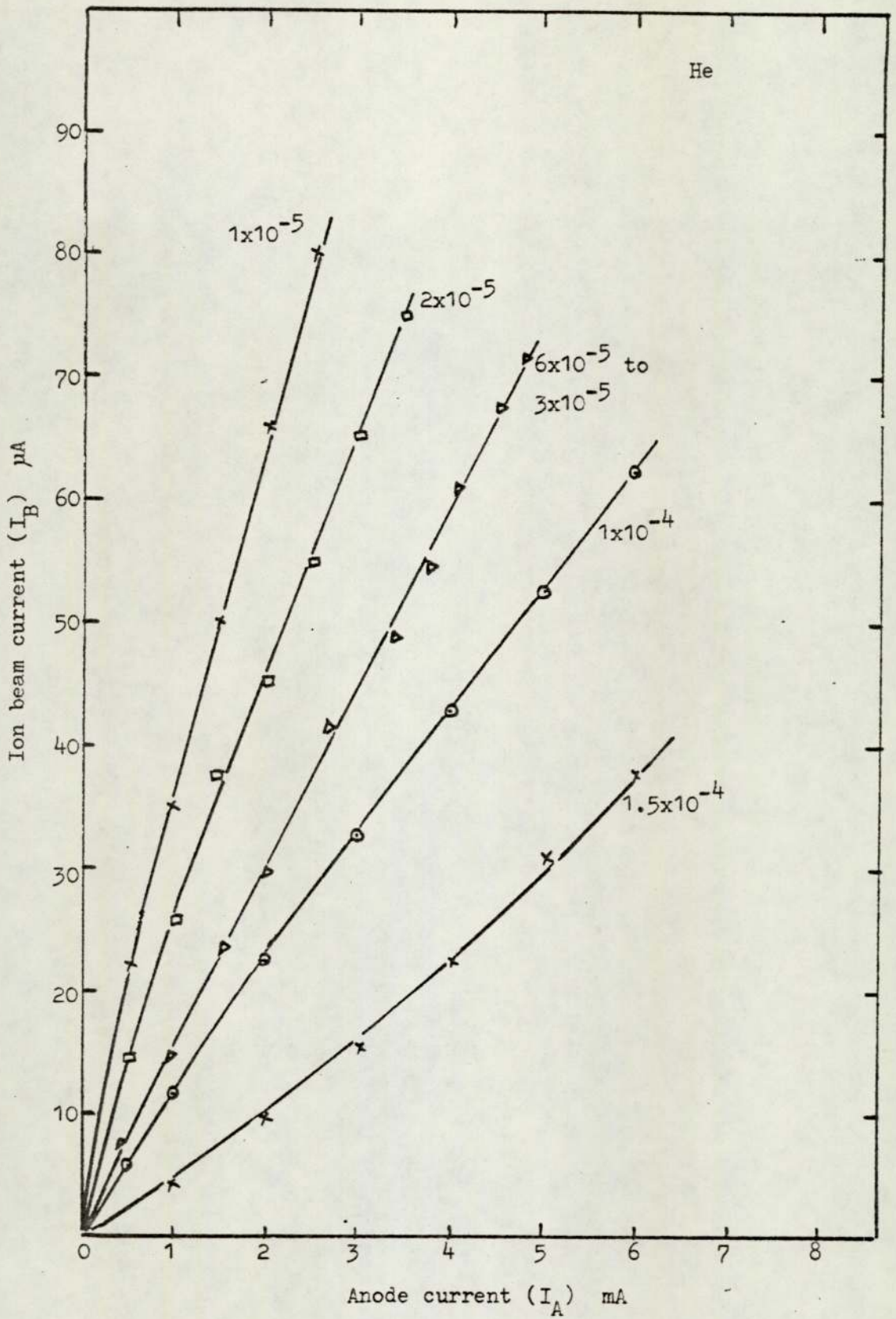


Figure 5.2/4. Ion beam current against anode current for the spherical source using helium.

APPENDIX 5-3/5

Modes of operation of the cylindrical source with
a 5 mm ion exit aperture using nitrogen and helium.

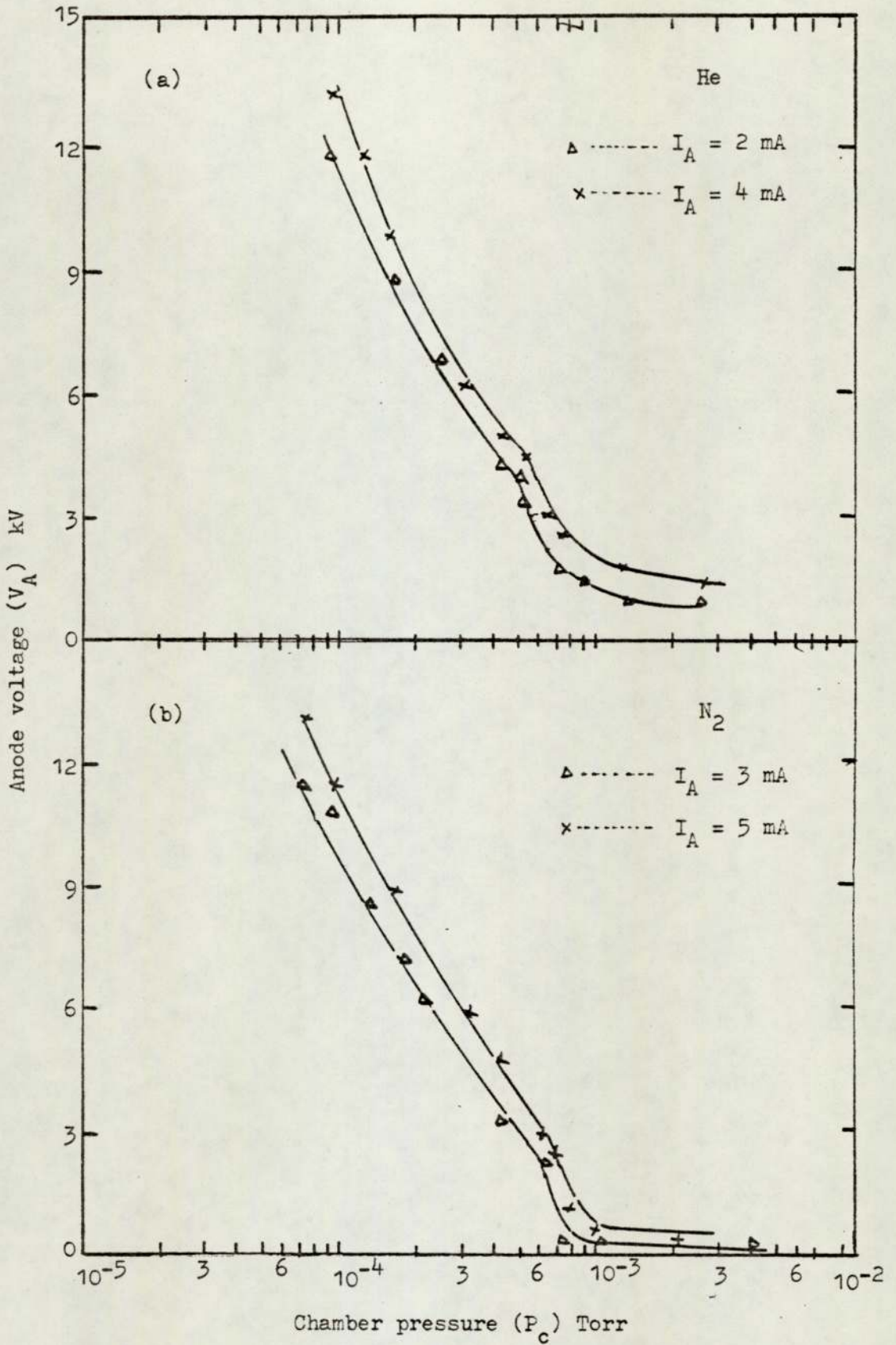


Figure 5.3/5. Variation of anode voltage due to the chamber pressure for the cylindrical source using nitrogen and helium.

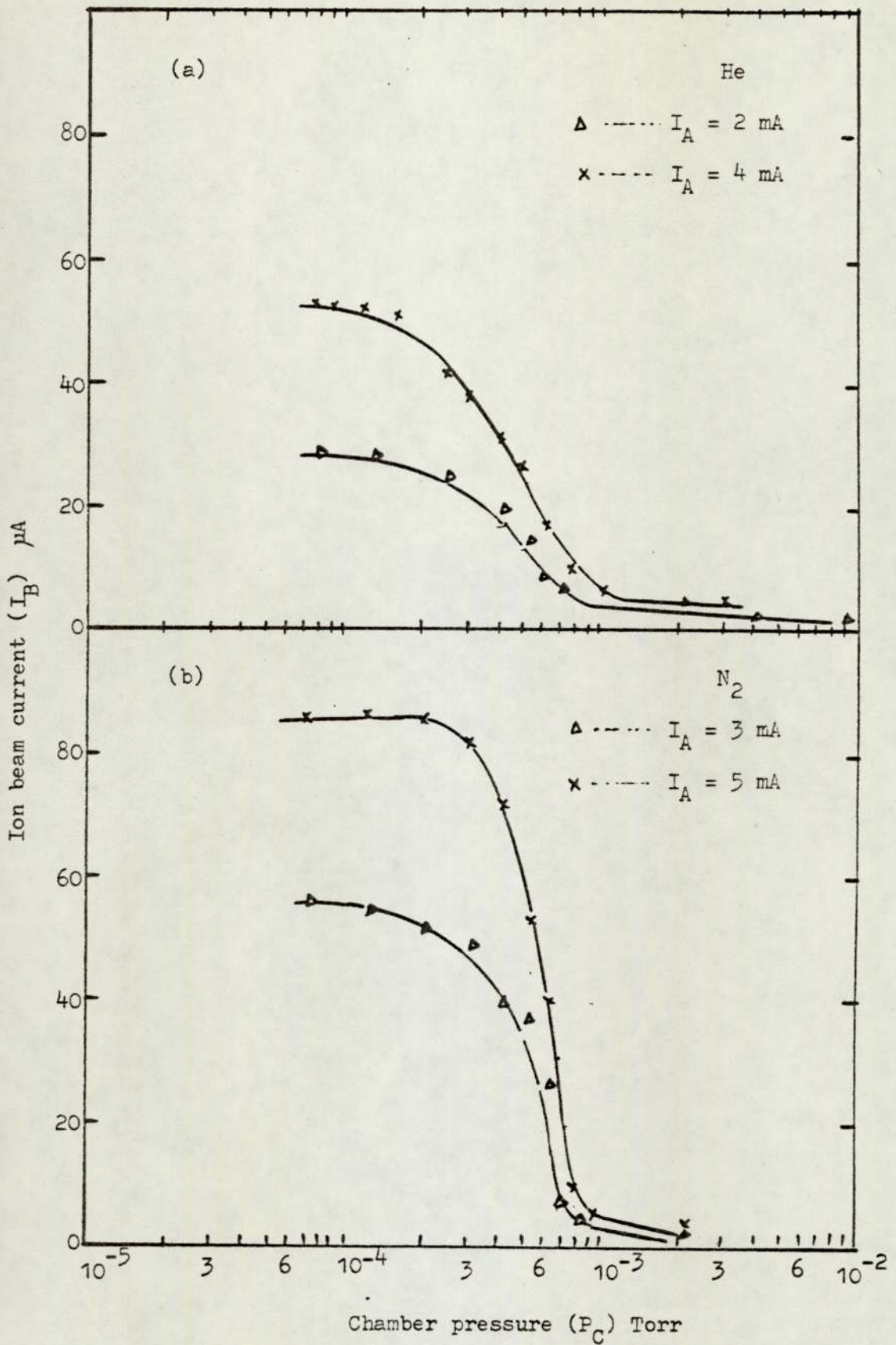


Figure 5.3/5. Modes of operation for the cylindrical source with 5 mm aperture using nitrogen and helium.

APPENDIX 5-3/6

Modes of operation of the spherical source with
two 1.5 mm ion exit apertures using helium.

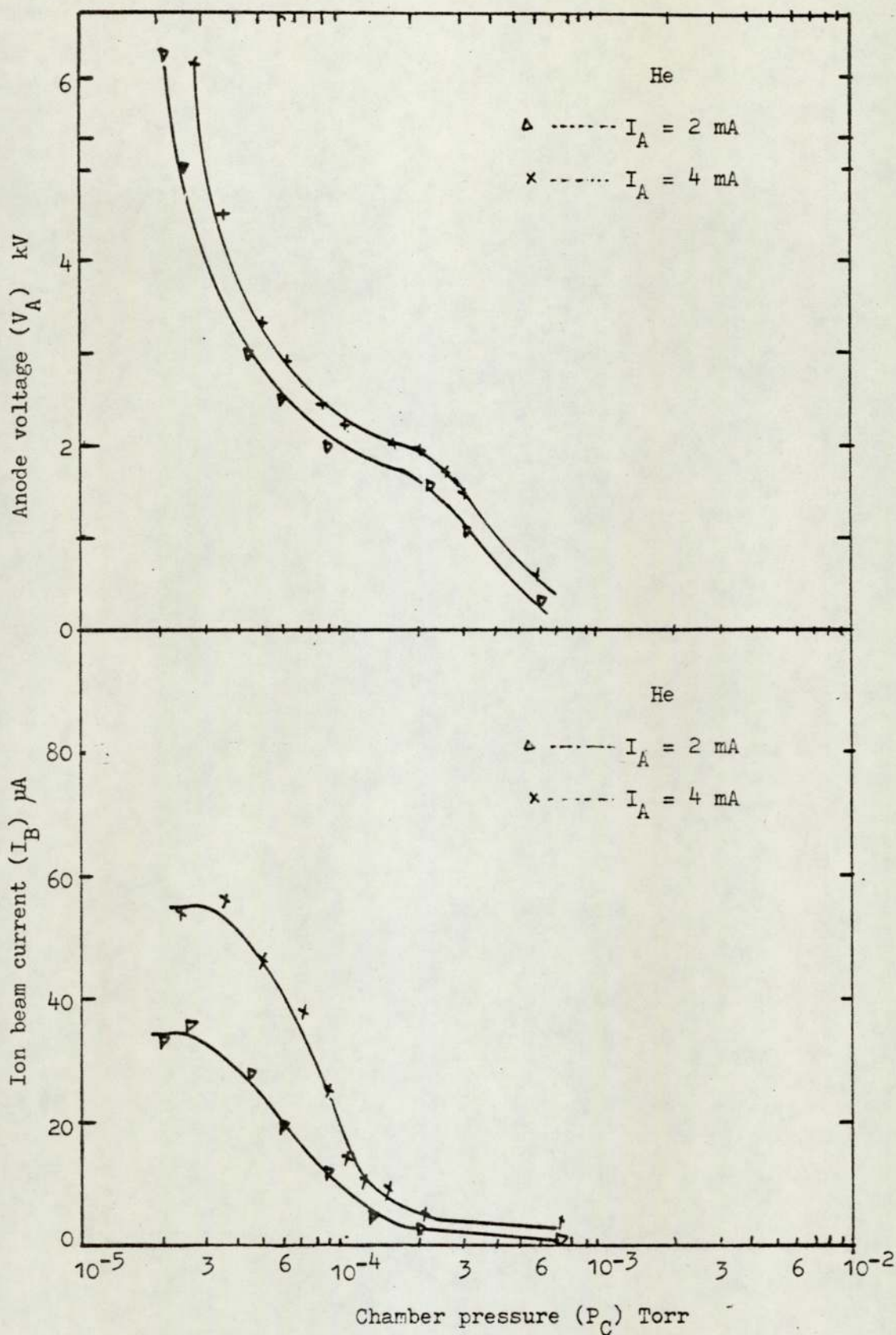


Figure 5.3/6. Modes of operation for the spherical source with two 1.5 mm apertures using helium.

APPENDIX 6-3/7

Energy distribution of the cylindrical ion source with a 5 mm aperture at 5 kV, 3 mA anode voltage and anode current respectively using nitrogen.

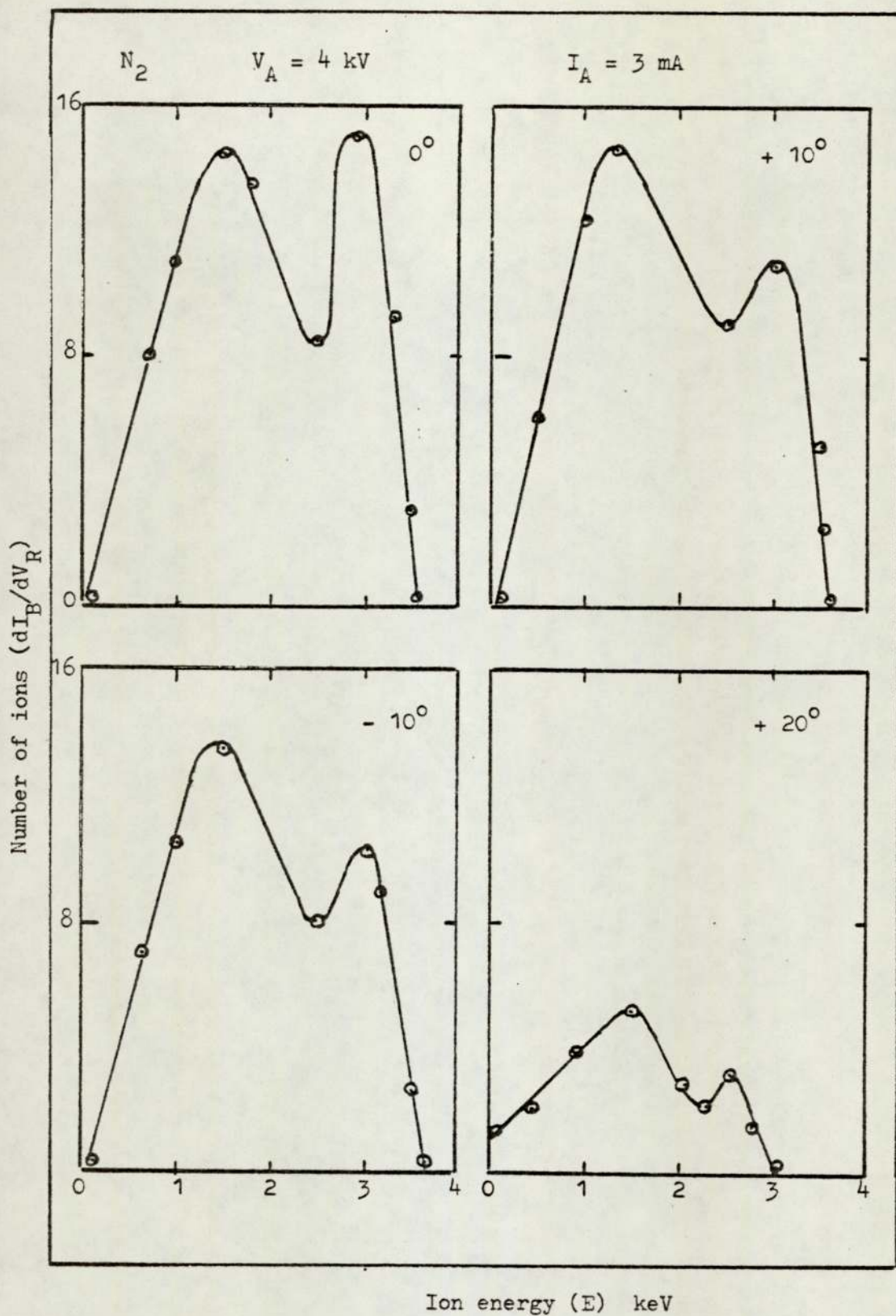


Figure 6.3/7. Ion energy spectrum for nitrogen with the cylindrical source using 5 mm aperture at different angular positions.

LIST OF FIGURES

<u>Figure No.</u>		<u>Page</u>
1.1	Schematic diagram of duoplasmatron	7
1.2	Schematic diagram of PIG-type ion source	9
1.3	Simple diagram of a high yield low pressure ion source	10
1.4	Diagram of low voltage arc source	11
1.5	Schematic diagram of the surface ionisation source	14
1.6	Typical ion beam system	16
1.7	Sputtering yield vs. angle of incidence	20
2.1	Examples of particle trajectories	22
2.2	Stable trajectory region	23
2.3	Stable and unstable trajectories	23
3.1	Ion current density vs. collector position	30
3.2	An example of cold cathode characteristics	31
3.3	Ion gun efficiency at different pressures	33
3.4	Ion beam density at different modes of operation (Previous work)	33
3.5	Modes of operation (Previous work)	34
3.6	Schematic diagram of two spherical ion sources	36
3.7	Ion energy spectrum obtained for a cylindrical source (Previous work)	38
4.1	Diagram of the cylindrical source	43
4.2	Diagram of rotating aperture ring	44
4.3	Equipotential distributions in the cylindrical source	45

<u>Figure No.</u>		<u>Page</u>
4.4	Simple diagram of spherical source	45
4.5	Potential distribution in the spherical source	47
4.6	Photograph of experimental ion sources	48
4.7	Photograph of the experimental system	49
4.8	Penning-McLeod gauge calibration curve	50
4.9	Electrical circuit of ion current measurements	52
4.10	Electron micrograph of carbon deposit on the ceramics and anodes of the cylindrical source	54
4.11	Electron micrograph of cathode and aperture in the spherical source	55
4.12	Simple diagrams of the ion collectors	57
5.1	V_A vs. I_A for the cylindrical source using argon	62
5.2	V_A vs. I_A for the cylindrical source using nitrogen	63
5.3	I_B vs. I_A for the cylindrical source using argon	64
5.4	I_B vs. I_A for the cylindrical source using nitrogen	65
5.5	Angular distribution of ion beam for the cylindrical source	66
5.6	Input power vs. I_B for the cylindrical source using argon	68
5.7	V_A vs. I_A for the spherical source using argon	69
5.8	I_B vs. I_A for the spherical source using argon	70
5.9	Angular distribution of the ion beam for the spherical source	71
5.10	Input power vs. I_B for the spherical source using argon	73
5.11	Variation of I_B with P_c for the cylindrical source using argon	75

<u>Figure No.</u>		<u>Page</u>
5.12	V_A vs. P_C for the cylindrical source using argon	76
5.13	Photograph of three different modes of operation	77
5.14	I_B vs. P_C for the spherical source using argon	79
5.15	Modes of operation of the spherical source using argon	80
5.16a	Ion beam efficiency vs. P_C for the cylindrical source	82
5.16b	Ion beam efficiency vs. P_C for the spherical source	83
5.17a	Power efficiency vs. P_C for the cylindrical source	84
5.17b	Power efficiency vs. P_C for the spherical source	85
5.18	Lines of force and equipotentials at the ion exit aperture	86
6.1	I_B vs. V_R for the monenergetic and divergent beam	91
6.2	Schematic diagram of the energy analyser	93
6.3	I_B vs. V_R , for the cylindrical source using argon	95
6.4	Ion energy spectrum for cylindrical source using argon at $V_A = 6$ kV	96
6.5	Ion energy spectrum for cylindrical source using argon at different V_A	97
6.6	Ion energy spectrum for the cylindrical source using nitrogen	100
6.7	Ion energy spectrum for the cylindrical source using helium	101

<u>Figure No.</u>		<u>Page</u>
6.8	Ion energy spectrum for the cylindrical source at different angular positions	102
6.9	Percentage of ions with energies greater than $0.6 V_A$	104
6.10	Ion energy spectrum for the cylindrical source from 2 mm ion exit aperture	105
6.11	I_B vs. V_R for the spherical source using argon	107
6.12	Ion energy spectrum for the spherical source using argon at $V_A = 6$ kV	108
6.13	Energy spectrum for the spherical source using argon at different voltages	109
6.14	Energy spectrum for the spherical source using nitrogen and helium	111
6.15	Energy spectrum for the spherical source at different angular positions	112
6.16	Percentage of ions with energies greater than $0.6 V_A$	110
6.17	Energy spectrum for the spherical source using different apertures	114
7.1	Diagram of basic ion deflecting system	118
7.2	Three arrangements of the analyser	120
7.3	Secondary electron coefficient (k) vs. V_A for the cylindrical source using argon	122
7.4	k vs. V_A for the cylindrical source using nitrogen and helium	123
7.5	Percentage of neutrals (N_0) vs. V_A for the cylindrical source using argon	126
7.6	N_0 vs. V_A for the cylindrical source using nitrogen and helium	127

<u>Figure No.</u>		<u>Page</u>
7.7	Number of ions (n_+) vs. V_A for the cylindrical source using argon	128
7.8	n_+ vs. V_A for the cylindrical source using nitrogen and helium	129
7.9	k vs. V_A for the spherical source using argon	130
7.10	k vs. V_A for the spherical source using nitrogen and helium	131
7.11	N_O vs. V_A for the spherical source using argon	132
7.12	N_O vs. V_A for the spherical source using nitrogen and helium	133
7.13	n_+ vs. V_A for the spherical source using argon	136
7.14	n_+ vs. V_A for the spherical source using nitrogen and helium	137
7.15	Etching rate (R) vs. time for energetic neutrals	138
7.16	Photographs of thin film etched by energetic neutrals and ions	139
4.2/1	Variation of P_c with time for measurement of pump speed	148
5.2/3	I_B vs. input power for the cylindrical source using nitrogen	151
5.2/4	Characteristic curves of the spherical source using nitrogen and helium	153
5.3/5	Modes of operation for cylindrical source using nitrogen and helium	158
5.3/6	Modes of operation for the spherical source using helium	161
6.3/7	Energy spectrum for cylindrical source at different angular positions using nitrogen	163

LIST OF SYMBOLS

A	Area of ion exit aperture
A_1, A_2	Symbol for the anodes of the cylindrical source
A^0	Symbol for the neutral
A_F^+	Symbol for the energetic (fast) ion
A_P^0	Symbol for the energetic neutral
A_S^+	Symbol for the low energy (slow) ion
A_S^0	Symbol for the slow neutral
A.E.S.	Auger Electron Spectroscopy
B^+	Symbol for a charged particle
c	Conductance of the ion exit aperture
d	Half distance between the anodes in the cylindrical source
d_1	Diameter of the ion exit aperture
d'	Half distance between the deflecting plates in the beam analyser
E	Kinetic energy of ions
E_x	Electric field component at the x axis
E_y	Electric field component at the y axis
E.S.C.A	Electron spectroscopy of chemical analysis
F.W.H.M or E	Full width of the energy peak at its half maximum height
G_R	Retarding grid

G_S	Shield grid
G.M.	Glow discharge mode
i_1	Ion current
i_2	Ion current and current equal to the secondary electron produced by energetic neutrals and ions
i_3	Current equivalent to the secondary electron produced by the energetic neutrals
I_A	Anode Current
I_B	Ion beam current
I_c	Collector current
I_e	Initial electron current
k	Secondary electron coefficient
\bar{l}	Average path length of ions
M	Molecular weight of the gas
MW	Maximum width of the energy peak
N_i	Pair of ions produced by electrons inside the ion source
$N(E)$	Number of ions with certain energy
n	Density of gas inside the source
n_+	Number of ions inside the source
n_o	Number of neutrals inside the source
N_o	Percentage of n_o inside the source

Osc.M.	Oscillating mode of operation
P	Charge exchange probability
P_e	Equilibrium pressure of the vacuum chamber
P_1	Symbol for deflector plate with negative voltage
P_2	Symbol for deflector plate with positive voltage
P_c	Experimental chamber pressure
P_s	Source pressure
P_{CT}	Chamber pressure at transition mode
P_{ST}	Source pressure at transition mode
g	Electron charge
R	Ratio of t_+ to t_o
S_E	Effective speed of the vacuum pumps
S.E.M.	Scanning electron microscope
t_o	Etching time of a thin film with energetic neutrals
t_+	Etching time of a thin film with the energetic ions
T.E.M.	Transition electron microscopy
Tr.M.	Transition mode of operations
V	Volume of the experimental chamber

V_A	Anode voltage
V_P	Potential of point A inside the source
V_R	Retarding voltage
V_D	Total deflecting voltage
V_1	Negative deflecting voltage
V_2	Positive deflecting voltage
x	Abscissa of Point A
x_p	Length of the deflector plate
y	Ordinate of the point A inside the source
y	Deflections of the ion beam by the analyser
α	Maximum total collision cross section of electron with molecule
σ	Charge exchange cross section
λ_e	Electron-molecule collision mean free path
ϵ_g	Gas ionisation efficiency or the ratio of number of ions into the total number of gas molecules emerging from the source
ϵ_i	Ion source efficiency or I_B/I_A
ϵ_p	Power efficiency or $i_1/\text{input power}$

REFERENCES

1. HAMILTON, G.W. Lawrence Livermore Laboratories, Livermore California. From Proceedings of the Symposium of ion sources and formation of the ion beams. Brookhaven National Laboratories, ENL, 50310 (1971)
2. BLEAKNEY, W. Phys.Rev. 34, 157 (1929)
3. NIER, A.O. Rev.Sci.Instr. 18, 398, (1947)
4. ARDENNE, M.V. Tabellen der Elektrone-Phys. Ionen-Physik und ubermikroskopie. Deutscher, Verlag der wissenschaften, Berline (1956)
5. ILLGEN, R. and KIRCHNER, J. Schutte der Baumen Geselleschaft for schmerien Darmastade, Germany, English Translation (1972)
6. MASIC, R., SAUTTER, J.M. and WARNEKE, R.J. Nucl.Inst. and Method , 71, 339. (1969)
7. WILSON, R.G. and BREWER, G.R. Ion beam. John Willey, New York, (1973)
8. BETHGE, K. and HEINISCHE, E. Nucl.Inst. and method, 30, 283 (1964)
9. BENNETT, I.R.I. and IEEE. Trans.Nucl.Sci. 19, 48, (1972)
10. BAUMANN, H. and BETHGE, K. Nucl.Inst. and method, 122, 517-525 (1974)
11. WINTER, H. and WOLF, B.H. Plasma Phys. 16, 791, (1974)
12. FREEMAN, J.H. Nucl.Inst. and method, 22, 306, (1963)
13. KORNELSEN, E.V. J.Vac.Sci.Technol, Vol.13, No.3, May/June (1976)

14. KOCH, J. Mass spectrometry in Phys. research, N.B.S. Circular No. 522, P 165 Washington (1953)
15. FETZ, H. Annual Phys. 37, 1, (1940)
16. STUART, R.V. Trans. 8th National vacuum symposium, Washington 1961. 1, 252 Pergamon Press (1962)
17. BARNETT, C.F., STIER, P.M. and EVANS, G.E. Rev.Sci.Instr. 24, 394 (1953)
18. COBIC, B., PEROVIC, B. and TOSIC, D. Rev.Sci.Instr. 36, 1844 (1965)
19. CROCKETT, C.G. Vacuum, Volume 23/No.1, 11-13 (1972)
20. THONEMANN, P.C., MOFFATT, J., ROOF, D. and SANDERS, J.H. Proc.Phys.Soc., London, 61, 483 (1948)
21. EUBANK, H.P., PECK, R.A. and TRUPELL, R. Rev.Sci.Instr. 25, 989 (1954)
22. HAGUE, C.A. and DONALSON, E.E. Rev.Sci.Instr. 34, 409, (1963)
23. DEMPSTER, A.J., Rev.Sci.Instr. 7, 46, (1936)
24. CRAIG, R.D., ERROCK, G.A. and WALDRON, J.D., Advances in Mass Spectrometry, P.136, Pergamon Press, London (1959)
25. TYRELL, A.C., ROBERTS, J.W. and RIDLEY, R.G. J.Sci.Instr. 42, 806, (1965)
26. HURLEY, R.E. Vacuum, Volume 25, No.4, Pergamon Press (1975)
27. TAYLOR, C.S., Proc. high energy accelerator conf. p.475-485, Dubna (1963)
28. HAWKINS, D.J. J.Vac.Sci.Technol, Vol.12, No.6, Nov/Dec. (1975)
29. GLÖERSEN, P.G. J.Vac.Sci. and Technol. 12, 28 (1975)

30. PLESHIVTSEV, N.V., PRIBORY, I. Tekhn Eksper, 5, 5. English Translation in Soviet Phys. Instrum. and experimental techniques 5, 929, (1964)
31. WHENER, G.K., J.Appl.Phys. 30, 1762 (1959)
32. TSONG, I.S.T. and BARBER, D.J. J. of Mat.Sci. 7, 682 (1972)
33. McILRAITH, A.H., Nature, 212, 1422 (1966)
34. MÖLLENSTEDT, G. Optik, 5, pp. 499-517 (1949)
35. FITCH, R.K. and G.J. RUSHTON, Vacuum, Vol.20, No.12, pp. 535-537 (1970)
36. ATKINSON, S.M., FITCH, R.K. and RUSHTON, G.J. Vacuum, Vol.22, No. 7, pp. 257-260 (1972)
37. PEGGS, G.N. and McILRAITH, A.H. J. of Phys.E.Scientific Instr. Vol. 8, pp. 420-422 (1975)
39. FITCH, R.K., MULVEY, T., THATCHER, W.J. and McILRAITH, A.H., J.Phys.D. Appl.Phys., Volume3, pp. 1399-1402 (1970)
40. MUKHERJEE, D.K. and BHATTACHERYA, R.S. Saha Institute of Nuclear Phys., Calcutta, pp. 471-475 (1971)
41. RUSHTON, G.J. and FITCH, R.K. Vacuum, Vol. 21, No.10, pp. 449-452 (1971)
42. FITCH, R.K. and RUSHTON, G.J. J. of Vac.Sci and Technol. Vol. 9, No.1, pp. 379-381 (1971)
43. FITCH, R.K., O'SHEA, K.R. and RUSHTON, G.J. J. of Phys.E: Scientific Instr. Vol.5, pp. 622-623 (1972)
44. DHARIWAL, R.S., Ph.D. Thesis, Dept. of Phys., University of Aston in Birmingham, (1976)

45. RUSHTON, G.J. Ph.D. Thesis, Dept. of Phys., University of Aston in Birmingham (1972)
46. RUSHTON, G.J., O'SHEA, K.R. and FITCH, R.K. J.Phys.D: Appl. Phys., Vol. 6, pp. 1167-1172 (1973)
47. GHANDER, A.M. Ph.D. Thesis, Dept. of Phys., University of Aston in Birmingham (1974)
48. RUSHTON, G.J. and FITCH, R.K., J. of Phys. E: Scientific Instr. Vol.7, pp. 313-315 (1974)
49. CLARK, R.K., FITCH, R.K., GHANDER, A.M. and SMITH, A.G. J.of Phys.E: Scientific Instr. Vol.7, pp. 566-568 (1974)
50. GHANDER, A.M. and FITCH, R.K. Vacuum, Vol.23, No. 8.
51. FRANKS, J. (Ion Tech. Ltd). British Patent Appl. No. 44718/78 (1973)
52. FRANKS, J. Proc. 2nd Instr.Conf. on ion sources, p.812 (1972)
53. FRANKS, J. and GHANDER, A.M. Vacuum, Vol. 24, No.10, pp. 489-491 (1974)
54. SWAMINATHAN, S. and VENKATASUBRAMANIAN, V.S., Private Communication (1974)
55. DHARIWAL, R.S., FITCH, R.K., LAVELLE, C.L.B. and JOHNSON, G.A., J.Anat. 122, 1, pp.133-140 (1976)
56. THOMPSON, M.W., Sussex University, Private Communication (1976)
57. MOHINDRA, S. and LATHAM, R.V., Private Communication (1977)
58. REHAL, A.S. and NEAL, W.E.J., Private Communication (1977)
59. ARIFOV, U.A. and RAKHIMOV, R.R. (1960). IZV Akad Nauk SSSR. ser fiz 24, 657. English translation in Bull.Acad.Sci. USSR Phys. Series 24, 666 (1961)

60. ARIFOV, U.A. and TASHKANOVA, D.A. IZV. Akad Nauk. SSSR ser.fiz.
24, 664. English translation in Bull.Acad.Sci. USSR.
Phys. Series 24-673 (1961)
61. MASSEY, E. and BURHOP, V.D. Electronic and Ionic impact
phenomena. Oxford University Press (1952)
62. STECKELMACHER, W. Journal of Phys.E: Scientific Instr.
Vol.6, 1061-1071 (1973)
63. SIMPSON, J. Anal. National bureau of standards, Washington D.C.,
Vol. 32, No. 12, 1283-1293 (1961)
64. KHORASSANY, M. and FITCH, R.K. Vacuum, Vol. 27, No.3, (1977)
65. SWAMINATHAN, S. and BHATTACHERYA, R.S., Saha Institute of
Nuclear Phys., Calcutta (1973)
66. DHARWAL, R.S. and FITCH, R.K. J.Mat.Sci. 12, 1225 (1977)
67. CARTER, G. and COLLIGON, J.S. Ion bombardment of solids.
Heinman Educational Books Ltd., London (1969)
68. SALZBORN. IEEE Trans. on Nuclear Science, 23, No. 2, 947, (1976)
69. FITCH, R.K., KHORASSANY, M., and MAWLOD, T.N. Proc. 7th
Inter.Congr. and 3rd Inter. Conf. Solid Surfaces,
Vienna (1977)
70. SWIFT, S. and SCHWAR, M. J. electrostatic probes for plasma
diagnostic, London, Iliffe (1970)

1.14 Energy distribution of the ions produced by saddle field ion sources

M. Khorossany* and R K Fitch, Department of Physics, University of Aston in Birmingham B47ET, England

A retarding field energy analyser has been used to measure the energy distribution of the ions produced by two forms of the saddle field ion source for argon, nitrogen and helium. It has been shown that with the cylindrical ion source the distribution is broad but always contains two distinct peaks at energies equivalent to about 35% and 75% of the anode potential. However, with the spherical source the ion energy spread is much narrower and most of the ions occur at an energy equivalent to about 75% of the anode potential with a peak half width of about 10% of the anode potential. It has also been found that the proportion of high energy ions in the beam decreases towards the edge of the beam for both sources.

Introduction

During the last few years there have been substantial developments in two forms of the saddle field ion source which originated from the idea of McIlraith¹ for an electrostatic charged particle oscillator. One of these is of cylindrical geometry and was first described by Fitch *et al.*² and subsequently in improved forms by Fitch and Rushton,³ Rushton *et al.*⁴ and Fitch *et al.*⁵ The other version was developed later by Franks⁶ and is of spherical geometry and the characteristics of this source are given in a paper by Franks and Ghander.⁷

These sources have now been used in a variety of applications. For example, preparation of specimens for electron microscopy by ion etching,⁸ preparation of field electron/ion emitters,⁹ and as a vacuum ultra violet source of line radiation of the rare gases for photoelectron spectroscopy.¹⁰ However, there has been little work reported on the energy distribution of the ions produced by these sources. Franks¹¹ used an electrostatic analyser with the cylindrical source and found that the energy spectra contains one main peak and several subsidiary peaks which varied with source geometry, nature and pressure of the gas and anode voltage. Ghander¹² used a simple retarding field energy analyser and found that the energy spectra were rather complex but Swaminathan and Venkatasubramanian¹³ found that there were two main peaks in the energy spectra of the ions produced by a cylindrical source incorporating thermionic electron injection.

The purpose of this paper is to report the results of the measurements of the ion energy spectra for both the cylindrical and spherical ion sources using an energy analyser developed from the one used by Ghander.¹²

Description of the ion source and the energy analyser

The cylindrical ion source consists essentially of a stainless steel cathode, 75 mm in length and 25 mm in diameter, surrounding two 1.5 mm diameter tungsten anodes symmetrically disposed about the axis of the cylinder at a separation of 5 mm. The

anodes are supported in stainless steel end-caps and insulated from them with ceramic bushes. Gas is admitted into the source through a stainless steel tube in the cathode wall. The diameter of the ion exit aperture could be varied from 1 to 5 mm and it was also possible to rotate the aperture from -10° to $+40^\circ$ with respect to the central position. In all cases the depth of the aperture was about the same as its diameter in order to minimize the field distortion.

The spherical source was purchased from Ion Tech Ltd and is normally provided with a cathode aluminium insert containing a 1.5 mm diameter aperture. This source was modified so that the size and position of the aperture could be varied in a similar manner to that described for the cylindrical source.

A schematic diagram of the cylindrical source and the ion energy analyser is given in Figure 1. It was necessary to design

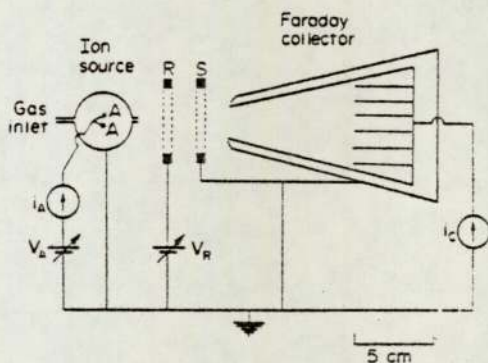


Figure 1. Schematic diagram of the ion source and retarding field energy analyser.

the Faraday collector to have a relatively large entrance aperture to admit the total ion beam at a distance of about 60 mm from the aperture yet still be efficient at retaining the secondary electrons. A number of designs were constructed and tested and the collector shown in Figure 1 was found to be the most satisfactory. The conical collector is made from nickel sheet, entrance aperture 27 mm and has an overall length of 125 mm and base diameter of 75 mm. Several nickel sheets, 40 mm in length are also attached to the base of the collector, as shown in the

* On leave from National University of Iran, Tehran.

figure, to improve its efficiency at retaining secondary electrons. The figure shows that the collector is also completely surrounded by an earthed copper screen to avoid collection of any reflected ions. Double grids were used to give a large transparency yet still produce a reasonably uniform field.¹⁴ They were made by winding 0.1 mm diameter tungsten wire round an aluminium frame such that the grids were 40 × 40 mm and with the wire spaced at a distance of 5 mm this should give a transparency of 98%. In practice due to some misalignment of the grid wires the transparency was found to be just greater than 90%. Grid R is the retarding field grid and grid S is the shield grid to shield the collector from the positive retarding field at R. The collector current, i_c , was recorded with a digital meter as a function of the retarding voltage V_R and the corresponding energy spectrum was obtained by differentiating this curve.

It is known that these sources produce a significant proportion of energetic neutrals which are, of course, unaffected by the retarding field but can still produce secondary electrons at the collector. Thus the efficiency of the collector at retaining the secondary electrons could be assessed by recording the collector current with V_R greater than the anode voltage, V_A . It was found that under these conditions the escape of secondary electrons contributed to always less than 3% of the collector current depending upon the source anode voltage.

The source was tested in a stainless steel chamber evacuated by a conventional rotary pump/diffusion pump system using Santovac 5' fluid in the diffusion pump. The pressure was measured with a Penning gauge situated in the chamber.

Operating modes and energy spectra of the ion sources

In an earlier publication⁴ it was reported that there are three principal modes of operation for the cylindrical source—namely the oscillating, transition and glow modes. In the present work the existence of these modes has been confirmed for both the cylindrical and spherical sources by monitoring the ion beam current with the Faraday collector shown in Figure 1. Figures 2a and b show how with Argon, V_A varies with pressure for the cylindrical and spherical sources using central ion exit apertures of 2 and 1.5 mm at anode currents, i_A , of 3 and 4 mA

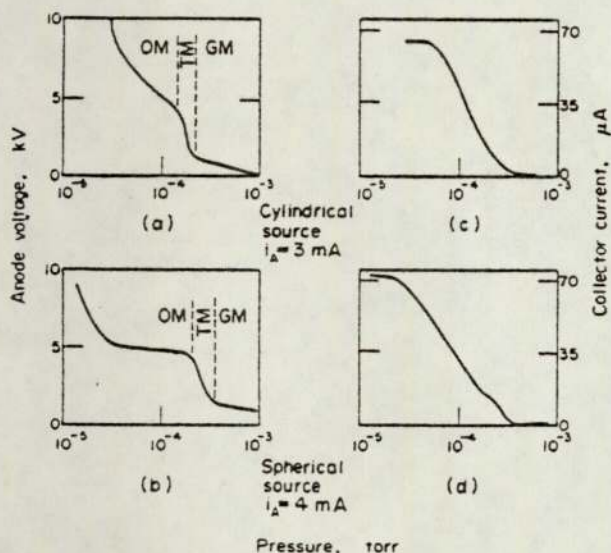


Figure 2. Modes of operation of the cylindrical ion source (a) and the spherical source (b).

respectively. It can be seen that when the pressure is high V_A is only about 500 V which corresponds to the normal glow mode. As the pressure is reduced there is a sudden rise of anode voltage during the transition mode. At still lower pressures the rate of rise of V_A decreases at the onset of the more efficient oscillating mode. This is much more apparent with the spherical source where it can be seen that the anode voltage is almost constant at 5 kV between pressures of 3.5×10^{-5} and 1.5×10^{-4} torr. Figures 2c and d show the corresponding variation of i_c with pressure and it can be seen that the source efficiency—defined as the ratio i_c/i_a —increases to a maximum at pressure of 6×10^{-5} and 3×10^{-5} torr for the cylindrical and spherical sources respectively.

The variation of collector current, i_c , with retarding voltage, V_R , was recorded for both sources at various pressures for argon, nitrogen and helium. Figures 3a and 4a show two such typical curves for argon for the cylindrical and spherical sources respectively. The corresponding energy spectrum of $d i_c / d V_R$ against V_R are shown in Figures 3b and 4b. In Figure 3 the

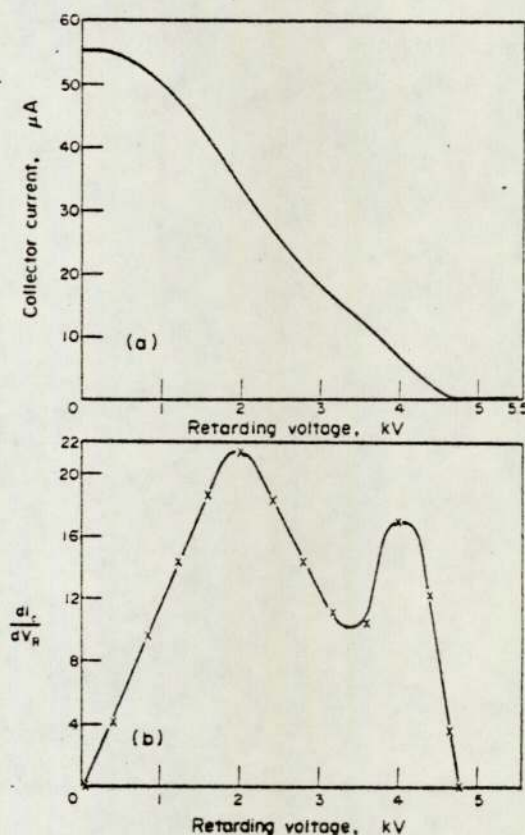


Figure 3. Collector current against retarding voltage (a) and ion energy spectrum (b) for the cylindrical source for Argon.

central ion exit aperture was 5 mm and the source was operated at $V_A = 5.5$ kV, $i_A = 3$ mA at a pressure of 3.8×10^{-4} torr. The corresponding values for the spherical source in Figure 4 are 1.5 mm, 6 kV, 2 mA and 1×10^{-4} torr. With the above conditions both sources were operating in the oscillating mode.

It is clear from Figures 3 and 4 that the ion energy spectra are very different for the two sources. In the case of the cylindrical source two distinct peaks occur at 2 keV and 4.1 keV which is equivalent to 36 and 75% of the anode potential. In fact it was found that for all pressures with argon, nitrogen and helium two similar peaks were always present and the low and high

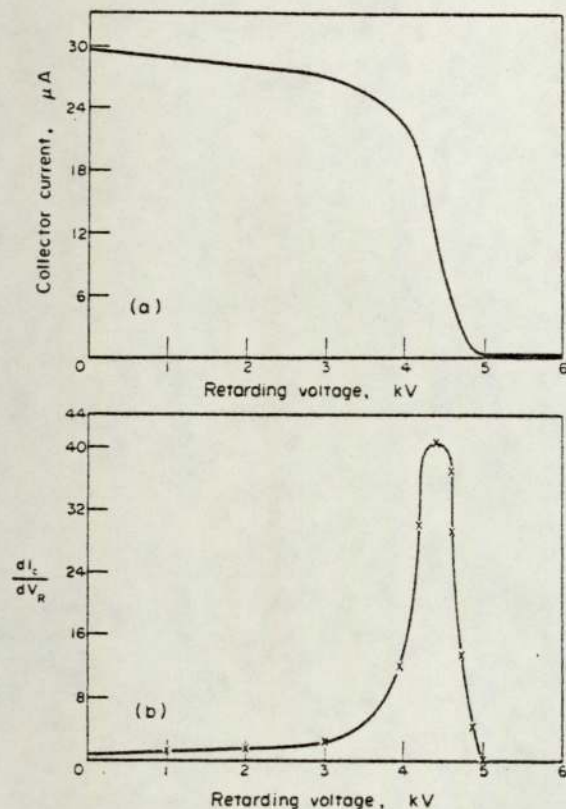


Figure 4. Collector current against retarding voltage (a) and ion energy spectrum (b) for the spherical source for Argon.

energy peaks always occurred in the range 35–40% and 70–80% of the anode voltage. This spread is no more than the uncertainty of $\pm 5\%$ in the determination of the position of the peaks. The mean value of $0.75 V_A$ for the high energy peak corresponds to the saddle point potential between the two anodes. For the spherical source the energy spectra shown in Figure 4 shows only one peak occurring at $0.73 V_A$ and is superimposed on a broad low energy background. Once again the position of this peak varied from only $0.7 V_A$ to $0.8 V_A$ for all pressures with argon, nitrogen and helium.

Figures 5a to 5f show the ion energy spectra for argon with the cylindrical source using a 5 m aperture at angular positions of -10° , 0° , $+10^\circ$, $+20^\circ$, $+30^\circ$ and $+40^\circ$ with respect to the central position at 0° . It is clear from the figures that proportion of high energy ions is much greater at the central position—shown in Figure 5b—and decreases when the aperture is moved either side of the central position. The similarity of Figures 5a (-10°) and 5c ($+10^\circ$) demonstrate that the aperture was correctly in the central position in Figure 5b.

This effect is also shown in Figure 6a in which the percentage of ions having energy greater than $0.6 V_A$ —estimated from the appropriate areas under the $i_c \rightarrow V_R$ curves—is plotted against the angular position of the aperture for $V_A = 4, 5$ and 6 kV. Similar observations were taken with the spherical source and are shown in Figure 6b but it can be seen the high energy ions are much more confined to the central portion of the ion beam than with the cylindrical source.

4. Discussion of results

The form of the energy spectrum for the cylindrical source has been found to be rather similar to that given by Swaminathan

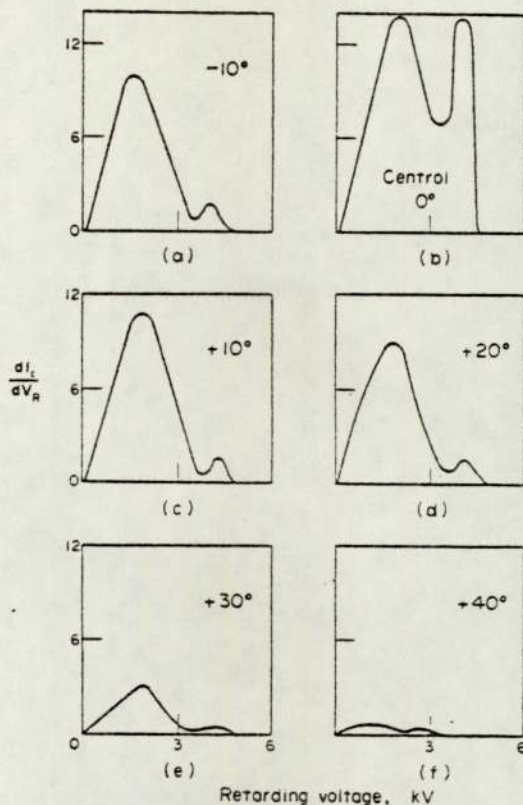


Figure 5. Ion energy spectrum for argon with the cylindrical source using different angular positions of the ion exit aperture.

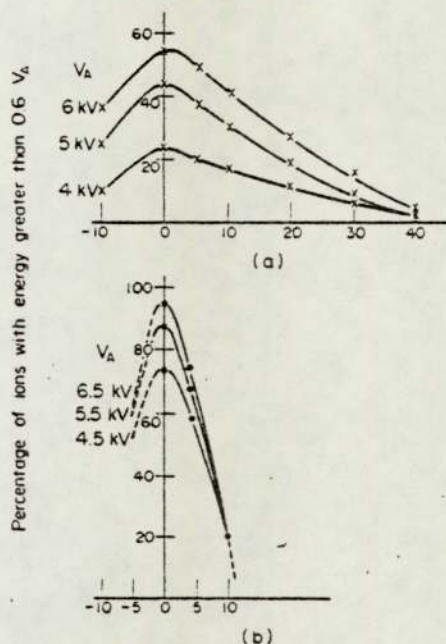


Figure 6. Percentage of ions having energy greater than $0.6 V_A$ for different angular positions of the ion exit aperture using the cylindrical source (a) and the spherical source (b) at various values of V_A .

and Venkatasubramanian¹³ but comparison is only partly justified as their measurements were made on a cylindrical source using a thermionic source of electrons whereas the present measurements were taken with the normal cold cathode

source. The energy spectrum for the spherical source is similar to that reported by Franks and Ghander⁷ but does not show any evidence of any additional low energy peaks. Furthermore in the present work the high energy peak always occurred at about $0.75 V_A$ with a peak half-width of 500 V whereas in the work of Franks and Ghander the corresponding values were $0.85 V_A$ and 250 V. It is thought that these differences are due to the more satisfactory design of the grids and Faraday collector used in the present work.

The difference in the energy spectra between the cylindrical and spherical source was not unexpected. This is due to the axial symmetry of the spherical source in which the end effects of the cylindrical design have been eliminated. It is thus proposed that the low energy peak at the edge of the ion beam produced by the cylindrical source arises from a potential gradient across the plasma inside the source which is in a direction transverse to the emerging ion beam. In future experiments it is hoped to be able to confirm this by measuring the potential inside the source using probe techniques.

Both designs of the saddle field ion source should continue to find new applications in various aspects of vacuum technology. In general the cylindrical source should be used if a wide ion beam with a broad energy spread is required but if a fine ion beam of much lower energy spread is necessary, then the spherical source is more suitable.

Acknowledgements

One of us (M K) would like to thank the National University of Iran for granting him study leave and both of us would like to acknowledge support from the Iran Ministry of Science (M K) and the University of Aston in Birmingham (R K F) to attend the symposium.

References

- ¹ A H McIlraith, *Nature, Lond*, **212**, 1966, 1422.
- ² R K Fitch, T Mulvey, W J Thatcher and A H McIlraith, *J Phys E*, **4**, 1971, 553.
- ³ R K Fitch and G J Rushton, *J Vac Sci Technol*, **9**, 1972, 379.
- ⁴ G J Rushton, K R O'Shea and R K Fitch, *J Phys D*, **6**, 1973, 1167.
- ⁵ R K Fitch, A M Ghander, G J Rushton and R Sing, *Jap J App Phys Suppl 2*, Pt 1, 1974, 411.
- ⁶ J Franks, British Patent No 44718/73 (1973).
- ⁷ J Franks and A M Ghander, *Vacuum*, **24**, 1974, 489.
- ⁸ R K Fitch, K R O'Shea and G J Rushton, *Proc Vth European Congress on Electron Microscopy*, 1972, 296.
- ⁹ J M Walls, H N Southworth and G J Rushton, *Vacuum*, **24**, 1974, 475.
- ¹⁰ F Burger and J P Maier, *J Phys E*, **8**, 1975, 420.
- ¹¹ J Franks, *Proc 2nd Int Conf on Ion Sources*, 1972, 812.
- ¹² A M Ghander, PhD thesis, University of Aston in Birmingham (1974).
- ¹³ S Swaminathan and V S Venkatasubramanian, Private Communication, 1974.
- ¹⁴ S Stephanakis and W H Bennett, *Rev Sci Instrum*, **39**, 1968, 1714.

THE PRODUCTION OF ENERGETIC NEUTRALS BY SADDLE FIELD ION SOURCES

R.K.Fitch, M.Khorassany* and T.N. Mawlood

Department of Physics, University of Aston in Birmingham, B4 7ET, U.K

Abstract: An electrostatic analyser has been developed to investigate the production of energetic neutrals by saddle field ion sources using helium, argon and nitrogen. It has been found that with both the cylindrical and the spherical source operating at constant source current, the percentage of energetic neutrals in the emerging beam increases from about 20% to 70% as the chamber pressure increases from 10^{-5} to 10^{-3} torr. This corresponds to a decrease in anode voltage from about 7 kV to 2 kV. Calculations have shown that these results can be explained in terms of a charge exchange process occurring inside the source. Advantage can be taken of this high neutral content when the source is used for ion etching insulating materials.

INTRODUCTION

The saddle field ion sources discussed in this paper are electrostatic devices which operate at low pressures without a magnetic field or thermionic filament. They originally arose from the idea of McIlraith /1/ for a charged particle oscillator which was similar to the energy analyser described by Mollenstedt /2/. Two forms of the ion source are now available, one employing cylindrical and the other spherical geometry. The former produces a wide ion beam with a fairly broad energy spread whereas the latter produces an intense fine beam of ions with a narrower energy spread /3/. The cylindrical source was first described by Fitch et al. /4/ and later in improved forms by Fitch and Rushton /5/ and Ghander and Fitch /6/. The spherical source was devised by Franks /7/ and the properties of this source are given by Franks and Ghander /8/.

These sources are particularly useful in high and ultra-high vacuum technology such as for ion cleaning of surfaces for surface analytical techniques. One particular application which has been in use for some time is for ion etching and thinning of materials for examination by transmission and scanning electron microscopy. In a recent paper Dhariwal and Fitch /9/ incorporated one of these sources into the specimen stage of a scanning electron microscope for in-situ ion etching and applied it to a variety of materials. They observed that the source could be used with electrically

* On leave from National University of Iran, Tehran.

insulating materials as well as with conductors and suggested that this was due to the presence of energetic neutrals in the emerging ion beam. The purpose of this paper is to report the results of an investigation undertaken to determine the neutral content as a function of pressure and anode voltage for helium, argon and nitrogen.

DESCRIPTION OF THE ANALYSER AND EXPERIMENTAL PROCEDURE

The cylindrical source used in this work consisted of a stainless steel cathode, diameter 25mm and length 75mm, enclosing two tungsten rod anodes, diameter 1.5mm, disposed symmetrically about the cylinder axis at a separation of 4mm. The ions emerged through a circular aperture, diameter 5mm, positioned midway along the cathode and normal to the plane of the anodes. The spherical source was purchased from Ion Tech Ltd. The effective diameter is about 25mm, the anode aperture is 5mm and the two ion exit apertures, diameter 1.5mm, are positioned at diametrically opposite points in the cathode. Schematic diagrams of the source and analyser are shown in figure (1). The Faraday collector, C entrance aperture 27mm, was first used in this laboratory for ion energy analysis /3/. The two flat plates V_1 and V_2 , were used when it was required to deflect the ions by applying potentials of $\pm \frac{1}{2}V_a$, where V_a is the source anode voltage. Three arrangements of the analyser are shown in the figure. In figure 1a, $V_1 = V_2 = 0$ and it is assumed that the current i_1 is

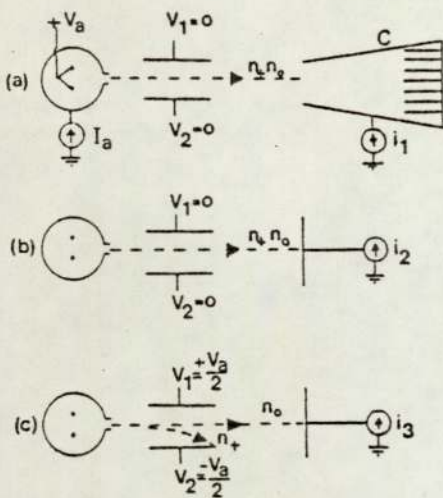


Fig. 1. Schematic diagram of the ion source and analyser.

proportional to the number of ions n_+ . In figure 1b, $V_1 = V_2 = 0$, but the Faraday collector has been replaced by a flat nickel collector and it is assumed that the current i_2 is proportional to n_+ and the secondary electrons produced by n_+ and the energetic neutrals n_0 . In figure 1c, $V_1 = +\frac{1}{2} V_a$ and $V_2 = -\frac{1}{2} V_a$ and the current i_3 is then only due to the secondary electrons produced by the energetic neutrals. These three situations can be represented by the following equations:

$$i_1 = n_+ e$$

$$i_2 = (n_+ + k n_+ + k n_0) e$$

$$i_3 = k n_0 e$$

where e is the electron charge and k is the secondary electron coefficient assumed to be equal for ions and neutrals of the same energy. Thus any determination of i_1, i_2 and i_3 makes it possible to measure k given by:

$$k = \frac{i_2 - i_1 - i_3}{i_1} \dots \dots \dots (1)$$

and hence n_+ and n_0 and thus the percentage of neutrals, N , in the beam where,

$$N = \frac{n_0}{n_0 + n_+} \times 100\%$$

The source and analyser were operated in a stainless steel chamber pumped by a conventional rotary pump/diffusion pump system, using an alumina trap in the fore line and "Santovac 5" fluid in the

diffusion pump. The pressure in the chamber, p_c , was measured with a Penning gauge calibrated for dry nitrogen.

EXPERIMENTAL RESULTS

Figure 2a shows the variation of k for helium as a function of V_a for anode currents I_a of 1mA and 3mA using the spherical source. The values of k vary from about 0.3 to 0.8 as V_a increases and hence as the average ion energy also increases. The uncertainty in k , indicated by the error bars have been estimated from equation (1) and show that the uncertainty in k increases with decreasing V_a . These large uncertainties were expected on account of the limitation of the method and likely variation of the condition of the collector surface during the measurements. The figure does however show that k is independent of I_a . Figure 2b gives the corresponding variation of N and shows that N increases with decreasing V_a , which corresponds to an increase in the chamber pressure. However for all values of V_a , N is greater for $I_a = 3mA$. It should also be noted that the uncertainties in N are less than the corresponding uncertainties for k . This arises from the fact that N is relatively insensitive to the uncertainty in k .

Figure 3 gives two curves of the variation of N with V_a for argon - one for the spherical source and the other for the cylindrical source for $I_a = 1mA$. Both curves again show that N increases with decreasing V_a but at all values of V_a , N is greater for the spherical source.

In order to verify these measurements of the percentage of neutrals at different values of V_a , the spherical source was set up as in figure 1c with V_1 and V_2 just sufficient to separate the ion and neutral beams. The times required to etch a copper film evaporated onto a glass plate were then recorded for the ions (t_+) and the neutrals (t_0) using argon. The variation of the ratio $R = t_+/t_0$ with V_a is given in figure 4 and clearly follows the same variation as N does with V_a as given in figures 2b and 3. For example, for $V_a = 4 kV$, R is about unity and the corresponding value of N is about 40%. This agreement is as well as can be expected taking into consideration the various uncertainties in both experiments.

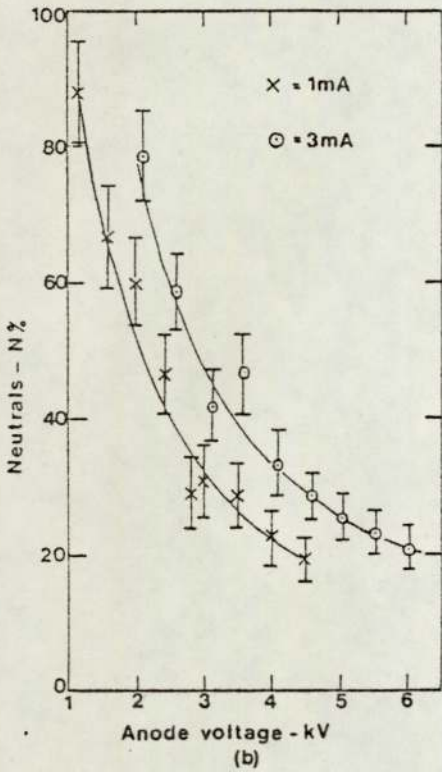
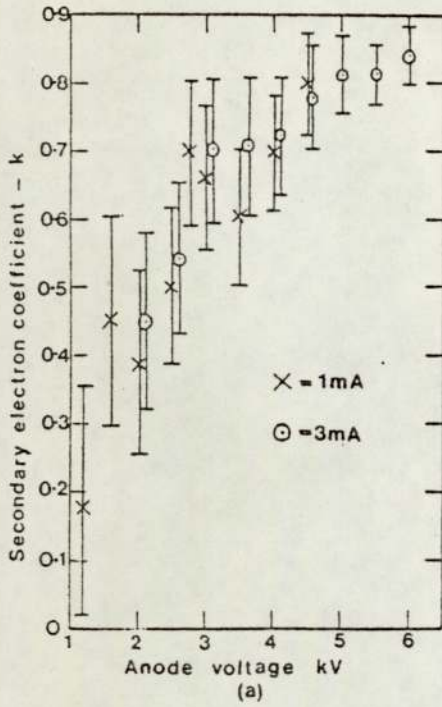


Fig. 2. The variation with anode voltage of (a) the secondary electron coefficient and (b) the percentage of energetic neutrals, using the spherical source with helium for I_a equal to 1mA and 3mA.

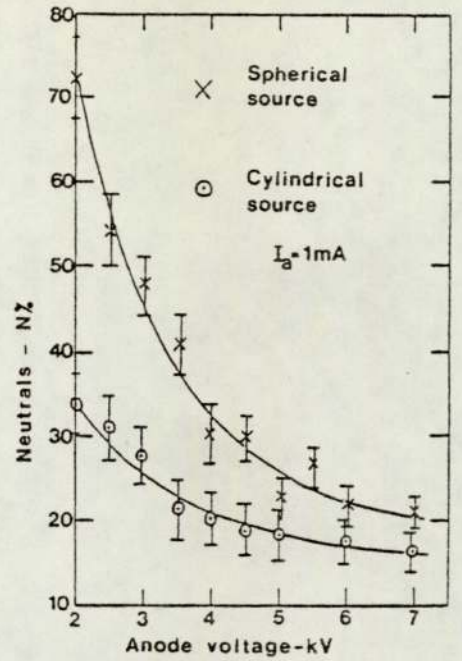


Fig. 3. The variation of the percentage of energetic neutrals for both sources using argon for $I_a = 1mA$.

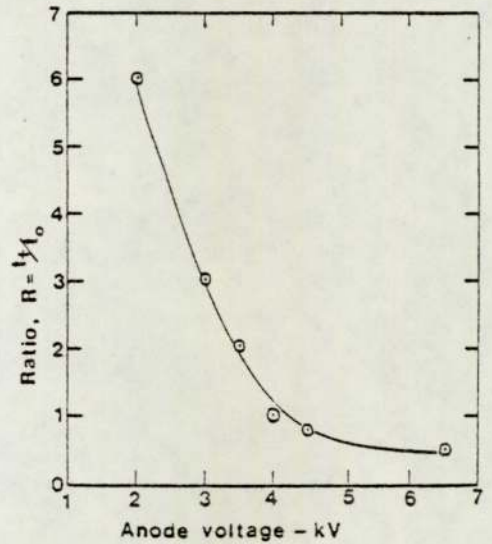


Fig. 4. The ratio of the etching times for ions and neutrals as a function of anode voltage using the spherical source with argon.

DISCUSSION AND CONCLUSIONS

It is clear from the results for helium and argon shown in figures 2 and 3 that both sources produce a significant proportion of energetic neutrals. Similar results have also been obtained for nitrogen. In all cases the percentage of neutrals increases with decreasing anode voltage which corresponds to an increase in chamber pressure, p_c . Furthermore figure 2b shows that at constant V the neutral content increases as I_a changes from 1mA to 3mA, because p_c is greater when $I_a = 3mA$. These results can be explained assuming a symmetric resonance charge exchange process occurring inside the source, in which a fast ion and a slow neutral produce a slow ion and a fast neutral. The probability of the charge exchange process, P , is given by:

$$P = \sigma \lambda n$$

where σ = charge exchange cross section, λ average path length of the ions and n is the gas density.

This can be illustrated using the results for the spherical source with argon when $V = 4kV$, $I_a = 2mA$ and $p_c = 7 \times 10^{-5}$ torr. The effective speed c of the diffusion pump was measured and found to be about 100 ls^{-1} . Thus assuming molecular flow the total conductance of both apertures is 0.35 ls^{-1} which gives a pressure inside the source of 2×10^{-2} torr when $p_c = 7 \times 10^{-5}$ torr, and the corresponding value of $n = 2 \times 10^{14} \text{ mol.cm}^{-3}$. At $4kV$ the average ion energy is about $3keV/3$ giving a value of σ for argon as $14.5 \times 10^{-16} \text{ cm}^2 / 10$. The radius of the spherical source is 1.3 cm so that it can be assumed that λ is about 1 cm. These figures give a value of $P = 0.3$ which is in reasonable agreement with the experimental value of N which is equivalent to about 0.4. Figures 3a and 3b show that at the same anode voltage N is larger for the spherical source. This arises from the fact that although λ is greater in the larger diameter cylindrical source, the source pressure is much higher in the spherical source due to the larger conductance of the aperture in the cylindrical source. This investigation has shown that with these sources it is possible to set the operating conditions to select the desired neutral content in the beam. This is particularly important when the source is being used for etching insulating materials. In one particular experiment the spherical source was used to etch a

sample of P.T.F.E. using argon with the anode voltage selected to provide 50% neutrals and 50% ions at an anode current of 2mA. The etched specimen was examined in a scanning electron microscope and it was found that the etching rate of the neutrals was about $7 \mu\text{m hr}^{-1}$ whereas the etching rate of the ions was only about $1.5 \mu\text{m hr}^{-1}$.

ACKNOWLEDGEMENTS

One of us (M.K.) would like to thank the National University of Iran for granting him study leave. Two of us would like to acknowledge support from the Iran Ministry of Science (M.K.) and the Royal Society and the University of Aston in Birmingham (R.K.F.) to attend the Congress.

REFERENCES

- /1/ A.H.McIlraith: Nature, Lond., 212 (1966) 1422.
- /2/ G.Mollenstedt: Optik.5 (1949) 499.
- /3/ R.K.Fitch and M.Khorassany: Vacuum 27 (1977).
- /4/ R.K.Fitch, T.Mulvey, A.H.McIlraith, and W.J.Thatcher: J.Phys.D, 3 (1970) 1399.
- /5/ R.K.Fitch and G.J.Rushton: J.Vac. Sci. and Tech. 9 (1972) 379.
- /6/ A.M. Ghander and R.K.Fitch: Vacuum 24 (1974) 483.
- /7/ J.Franks: British Patent No.44718/73 (1973).
- /8/ J.Franks and A.M.Ghander: Vacuum 24 (1974) 489.
- /9/ R.S.Dhariwal and R.K.Fitch: J.Mat. Sci. 12 (1977) 1225.
- /10/ E.Salzborn: IEEE Trans. on Nuclear Science 23 (1976) 947.